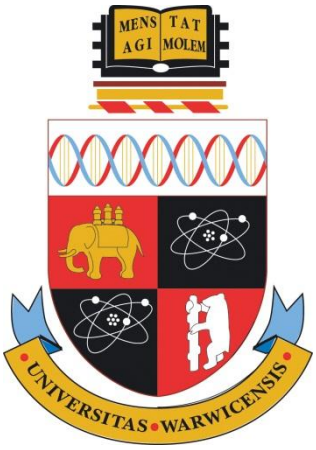

Characterisation of host-range determinants in Chandipura virus

by

Emily Louise Stock

Thesis

Submitted for the degree of Doctor of Philosophy

The University of Warwick

School of Life Sciences

June 2014

Contents

List of tables

List of figures

ACKNOWLEDGEMENTS

Firstly, I would like to thank my supervisor Professor Andrew Easton for all your guidance during my PhD. I could not have asked for a better supervisor, your fascination for everything virology and your constant optimism when 'things were not working' made the three (and a bit!) years really enjoyable. Your door was always open and you were always prepared to talk through my work and answer my many questions, for which I am very grateful.

I would also like to thank Dr Philip Gould for all your assistance in the laboratory and not laughing too much if I did something stupid! It has been great sharing a lab with you. I would like to thank all current and past members of the PVL laboratory, everyone has been so helpful and friendly.

Thank you also to Dr Daniel Fulton, without whom half of my project would not have been possible. You we always ready to show me new techniques and talk over my results with a neurobiologist's perspective.

Lastly, I would like to thank our collaborators at the Pirbright Institute, Dr Rennos Fragkoudis and Professor John Fazakerley and at the University of Liverpool for their assistance.

DECLARATION

This thesis is submitted to the University of Warwick for the degree of PhD. I declare that all of the work presented in this thesis was original work performed by myself, except where specifically stated. None of this work has been previously submitted for any other degree.

Abbreviations

ACSF	Low sodium Artificial Cerebrospinal Fluid
CE	Chick embryo
CEF	Chick embryonic fibroblasts
CHPV	Chandipura virus
CNS	Central nervous system
CPE	Cytopathic effects
CSF	Cerebrospinal fluid
E.O.P.	Efficiency of plating
ESCRT	Endosomal Sorting Complexes Required for Transport
FBS	Foetal bovine serum
G	Glycoprotein
GDP	Guanosine 5'-diphosphate
GFP	Green fluorescent protein
GMEM	Glasgow Modified Eagle's Medium
GMP	Guanosine 5'-monophosphate
GTP	Guanosine 5'-triphosphate
*hr*CE	Host restricted mutants
HSP	Heat shock protein
I.p.	Intraperitoneal
IFHV	Isfahan virus
JEV	Japanese encephalitis virus
L	Large protein
LBPA	Late endosomal lipid lysobisphophatidic acid
LDLR	Low density lipoprotein receptor
M	Matrix
M.O.I.	Multiplicity of infection
MAPK	Mitogen-activated protein kinase
MTase	Methyltransferase
N	Nucleocapsid
NKT	Natural killer T
NNS	Nonsegmented negative sense
P	Phosphoprotein
PCBP	Poly(C) binding protein
PH	Pleckstrin homology
PRNTase	Polyribonucleotidyltransferase
RdRp	RNA dependent RNA polymerase
RFP	Red fluorescent protein
RNP	Ribonucleoprotein
RSV	Respiratory syncytial virus
TBP	TATA-binding protein
*Td*CE	Temperature-dependent host range
TLR4	Toll-like receptor 4
TNP	Transcribing nucleoprotein complexes
VS	Vesicular stomatitis
VSV	Vesicular stomatitis virus
WNV	West Nile virus

Summary

The emerging arbovirus, Chandipura virus (CHPV) has been implicated in epidemics of acute encephalitis in India with mortality rates in hospitalised children of over 50%. CHPV is a member of the *Vesiculovirus* genus of the *Rhabdoviridae* family.

Viruses are dependent on the host cell at every stage of their lifecycle. The isolation of temperature-dependent host range (*td*CE) mutants, which are characterised by growth impairment at 39°C in chick embryo (CE) cells but not in monkey cells, highlights a dependence of CHPV on undetermined host factors. The characterisation of three *td*CE mutants was carried out. Each of the mutants contain one or more coding mutations in the RNA polymerase gene and two contain additional mutations in the attachment protein gene. Using a reverse genetics system of CHPV recombinant viruses containing the specific mutations were generated. This demonstrated that a single amino acid change in the virus RNA polymerase of each mutant, located either between domains III and IV or within domain IV or VI was responsible for host range specificity, the *td*CE phenomenon. In CE cells at 39°C the *td*CE lesions were shown to disrupt the assembly of cytoplasmic replication complexes.

A recombinant virus with a Flag tag attached to the L protein was generated and used to infect mammalian and avian cells. Potential L/Flag interacting partners were co-immunoprecipitated and analysed by mass spectrometry. The predominant cellular functions of the identified proteins were in gene expression and the cytoskeleton.

To investigate the neuropathogenisis and cell tropism of CHPV *in vivo* and *ex vivo* models of CHPV disease were established. The virus was shown to principally localise to the cerebellum in the mouse brain with the virus targeting immature neurons, granule cells and microglia. Mature neurons, oligodendrocytes and astrocytes were permissive to infection with CHPV but their infection occurred infrequently.

CHAPTER 1

1 Introduction

1.1. Emerging viruses

In an increasingly interconnected, globalised society emerging viruses pose a substantial threat to public health at a local, national and global scale. Human population growth and the transformation of environments and ecosystems by people throughout the world has provided and will continue to provide opportunities for the emergence of new viruses, the spread of existing viruses into new geographical locations or expansion of their host range.

Recently emerged viruses belong to a wide range of virus families including *Bunyaviridae, Coronaviridae, Filoviridae, Flaviviridae, Orthomyxoviridae, Paramyxoviridae and Rhabdoviridae.* Many emerging viruses are zoonoses that are unable to transmit efficiently from human to human, examples of which include Ebola, Marburg, Hantaan, Nipah and Hendra viruses. The Filoviruses Ebola and Marburg are the causative agents of sporadic cases of severe haemorrhagic fever in humans and non-human primates in central Africa with high case fatality rates ranging from 25-90% and 25-80% respectively (MacNeil & Rollin, 2012). Fruit bats have been implicated as the natural reservoir of both viruses (Leroy *et al.*, 2005; Towner *et al.*, 2007). Bats have also been identified as the reservoirs of the emerging Paramyxoviruses Hendra and Nipah. Hendra virus has caused outbreaks of severe acute respiratory disease in horses and humans in Australia since 1994 and has also been frequently isolated from pteropid bats, the natural host of the virus (Halpin *et al.*, 2000). Nipah virus first emerged in Malaysia in 1998 and has been

responsible for 12 outbreaks of acute febrile encephalitis in humans and pigs in South-East Asia (Aljofan, 2013).

Other examples of zoonotic emerging virus are the Hantaviruses. Over 20 New world hantaviruses, family *Bunyaviridae,* have been isolated in the Americas, 13 of which are associated with Hantavirus Pulmonary Syndrome (HPS) in humans and each of which have a different rodent host (Macneil *et al.*, 2011). HPS was first reported in 1993 in the southwestern United States and the etiological agent was identified as the novel hantavirus Sin Nombre virus. Increased human contact with the natural host species of Sin Nombre virus, the deer mouse (*Peromyscus maniculatus)* is considered the overriding factor in the emergence of this virus. This increased contact was brought about by a rise in the mouse population because of an abundance of food which has been linked to increased rainfall during the 1992-1993 El Niño (Engelthaler *et al.*, 1999).

Severe acute respiratory syndrome coronavirus (SARS-CoV) is an example of a recently emerged zoonotic virus which had adapted for highly efficient person to person transmission. SARS-CoV originated in Guangdong province in southern China in late 2002 and subsequently spread rapidly around the world due to international air travel, resulting in a global outbreak of severe atypical pneumonia. By September 2003 8,098 people had been infected and 774 people died as a result, a case fatality rate of 9.6% (Graham *et al.*, 2013). The animal reservoirs of SARS-CoV are *Rhinolophus (*horseshoe) bats but the virus has also been isolated from palm civets in live animal markets, which facilitated transmission of the virus to humans (Li *et al.*, 2005b). Virus isolates from the epidemic contained mutations in the receptor-binding domain of the spike glycoprotein which greatly enhanced the viruses affinity for human angiotensin-converting enzyme 2 (ACE2), the receptor of

SARS-CoV (Li *et al.*, 2005a). Since the epidemic of SARS-CoV many more novel bat coronaviruses have been isolated, highlighting the large potential for human disease within this virus family. Another coronavirus, Middle East respiratory syndrome coronavirus (MERS-CoV) emerged in 2012. The index human case occurred in Saudi Arabia and there have been a further 16 cases in the Arabian Peninsula and the UK with a case fatality rate of 50% of people who were hospitalised (Graham *et al.*, 2013). Bats have been implicated as the natural host of MERS-CoV (Zaki *et al.*, 2012).

Unlike the epidemic of SARS-CoV, which despite being readily transmissible was controlled within 4 months, newly emerged influenza A virus H1N1 quickly spread to over 214 countries, becoming the first pandemic of the 21st century (van Doremalen *et al.*, 2011). Influenza H1N1 emerged from Mexico and the United States in 2009 due to a gene reassortment event between the classical swine H1N1, Eurasian swine H1N1 and the triple-reassortment influenza viruses (Garten *et al.*, 2009). The natural host of influenza A viruses is aquatic birds although pigs are also thought to play an important role in the transmission of novel influenza viruses to humans (Moncorge *et al.*, 2013).

Many emerging viruses are arthropod-borne such as West Nile virus (WNV), dengue, chikungunya and bluetongue viruses, all of which have recently emerged in new regions of the world as the geographical range of their vectors have expanded. The dengue viruses (serotypes 1-4), members of the *Flaviviridae* family, are the causative agents of dengue fever and the more serious clinical manifestation of the virus dengue haemorrhagic fever in tropical and sub-tropical regions of the world. Dengue viruses account for the largest number of arbovirus infections worldwide and have spread considerably in recent years with prolonged transmission of the virus in

Europe now threatening (Mackenzie & Jeggo, 2013). This expansion of geographical range occurred due to the continued establishment of *Aedes aegypti* mosquitoes (the principle vector of the virus) in expanding urban areas and also the spread of *Aedes albopictus* mosquitoes into North America and Europe (Mackenzie & Jeggo, 2013). The spread of *Aedes aegypti* mosquitoes into new habitats is also responsible for the increase in range and incidence of chikungunya virus infections. Indian Ocean epidemic isolates of the virus frequently contain an A226V amino acid mutation in the envelope glycoprotein which enhances transmissibility by *Aedes albopictus* mosquitoes and thus there is potential for the virus to become endemic in Southern Europe and the Americas (Tsetsarkin *et al.*, 2007). This possibility was highlighted when a localised outbreak of chikungunya occurred in Italy in 2007 infecting 254 people (Burt *et al.*, 2012; Mackenzie & Jeggo, 2013).

The lesser-known emerging arbovirus Chandipura virus was the focus of this investigation. This Rhabdovirus is transmitted by *Phlebotomus* sandflies and is the causative agent of a number of outbreaks of encephalitis in children in central states in India since 2003 (Chadha *et al.*, 2005; Gurav *et al.*, 2010; Tandale *et al.*, 2008). The virus has also been isolated from sand flies in the northern region of Senegal (Traore-Lamizana *et al.*, 2001) and in a pygmy hedgehog in Nigeria (Fontenille *et al.*, 1994), indicating the presence of the virus and thus the potential for human disease outside of India. The nature of CHPV disease is discussed in section 1.5.

1.2. Chandipura virus (CHPV) classification

1.2.1. **Order *Mononegavirales***

CHPV is a non-segmented, negative stranded RNA virus belonging to group V (negative sense ssRNA viruses) in the Baltimore classification system. CHPV is

classified within the order *Mononegavirales*, family *Rhabdoviridae* and genus *vesiculovirus*. The order *Mononegavirales* is comprised of four virus families: *Bornaviridae, Filoviridae, Paramyxoviridae and Rhabdoviridae* and contains a large number of viruses of public health, veterinary and economic significance such as Marburg and Ebola viruses (*Filoviridae*), measles and respiratory syncytial virus (RSV) (*Paramyxoviridae*), rabies and vesicular stomatitis virus (VSV) (*Rhabdoviridae*). The phylogenetic relationships between the members of the *Mononegavirales* are depicted in Figure 1.1.

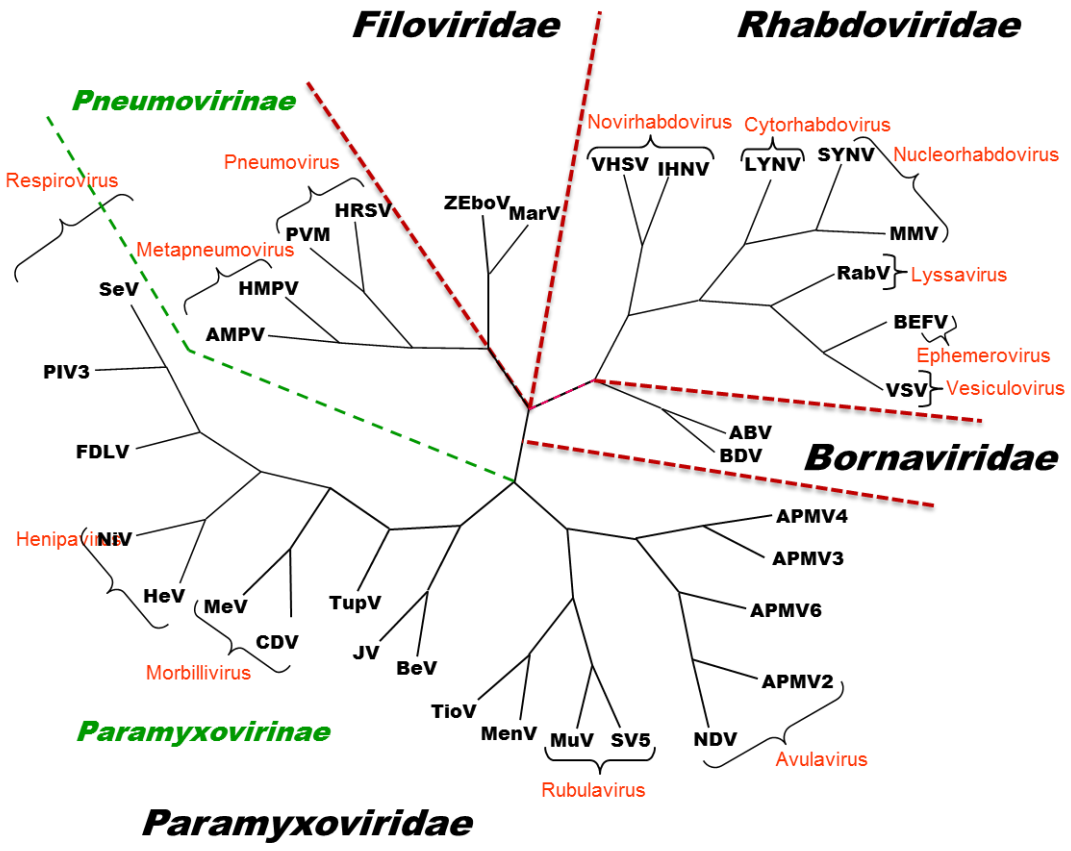

Figure 1.1| **Unrooted phylogenetic tree of the *Mononegavirales* based on L gene alignment** (obtained from the Ninth report of the International Committee on Taxonomy of Viruses)

1.2.2. **Family *Rhabdoviridae***

Rhabdoviruses have a wide host range and greater than 200 rhabdoviruses have been isolated to date from plants, invertebrates and vertebrates (Walker *et al.*, 2011) with some members of the family able to replicate in both plants and invertebrates and others in invertebrates and vertebrates (Easton & Pringle, 2011). There are nine genera within the family *Rhabdoviridae*, six are composed of animal viruses: *Vesiculovirus, Lyssavirus, Ephemerovirus, Tibrovirus, Perhabdovirus* (fish viruses) and *Novirhabdovirus* (fish viruses), two contain plant viruses: *Cytorhabdovirus* and *Nucleorhabdovirus* and the *Sigmavirus* genus is comprised of viruses which infect dipterans (Dietzgen *et al.*, 2011). Members of the family *Rhabdoviridae* are listed in Table 1.1 and the phylogenetic relationships between them are illustrated in Figure 1.2. Recently, several novel rhabdoviruses have been characterised, emphasising the likelihood that there are many more unidentified rhabdoviruses and that the full diversity of this virus family is yet to be exposed. Examples of such viruses include Niakha virus, which was isolated from phlebotomine sandflies in Senegal (Vasilakis *et al.*, 2013a). Also, the recently identified and highly divergent Bas Congo Rhabdovirus was associated with a small outbreak of acute hemorrhagic fever in humans in the Democratic Republic of Congo in 2009 (Grard *et al.*, 2012).

Genus	Type virus	Other viruses	Host(s)
Cytorhabdovirus	Lettuce necrotic yellow virus	Barley yellow striate mosaic virus Broccoli necrotic yellows virus Festuca leaf streak virus Lettuce yellow mottle virus Northern cereal mosaic virus Sonchus virus Strawberry crinkle virus Wheat American striate mosaic virus	Plants, insect vectors (aphids, leafhoppers, planthoppers)
Ephemerovirus	Bovine ephemeral fever virus	Adelaide River virus Berrimah virus	Cattle, mosquitoes
Lyssavirus	Rabies virus	Aravan virus Australian bat lyssavirus Duvenhage virus European bat lyssavirus 1 European bat lyssavirus 2 Irkut virus Khujand virus Lagos bat virus Mokola virus Shimoni bat virus West Caucasian bat virus	Mammals
Novirhabdovirus	Infectious hematopoietic necrosis virus	Hirame rhabdovirus Snakehead virus Viral hemorrhagic septicemia virus	Fish
Nucleorhabdovirus	Potato yellow dwarf virus	Datura yellow vein virus Eggplant mottled dwarf virus Maize fine streak virus Maize Iranian mosaic virus Maize mosaic virus Rice yellow stunt virus Sonchus yellow net virus Sowthistle yellow vein virus Taro vein chlorosis virus	Plants, insect vectors
Perhabdovirus	Perch rhabdovirus	Anguillid rhabdovirus Sea trout rhabdovirus	Fish
Sigmavirus	Drosophila melanogaster sigmavirus	Drosophila affinis sigmavirus Drosophila ananassae sigmavirus Drosophila immigrans sigmavirus Drosophila obscura sigmavirus Drosophila tristis sigmavirus Muscina stabulans sigmavirus	Dipterans
Tibrovirus	Tibrogargan virus	Coastal Plains virus	Cattle, midges
Vesiculovirus	Vesicular stomatitis Indiana virus	Carajas virus Chandipura virus Cocal virus Isfahan virus Maraba virus Piry virus Spring viraemia of carp virus Vesicular stomatitis Alagoas virus Vesicular stomatitis New Jersey virus	Humans, cattle, horses, swine, sand flies, black flies, mosquitoes

Table 1.1| **Members of the *Rhabdoviridae* family**

Species belonging to each of the nine genera of the *Rhabdoviridae* family are listed. The prototype viruses and the host(s) are also shown.

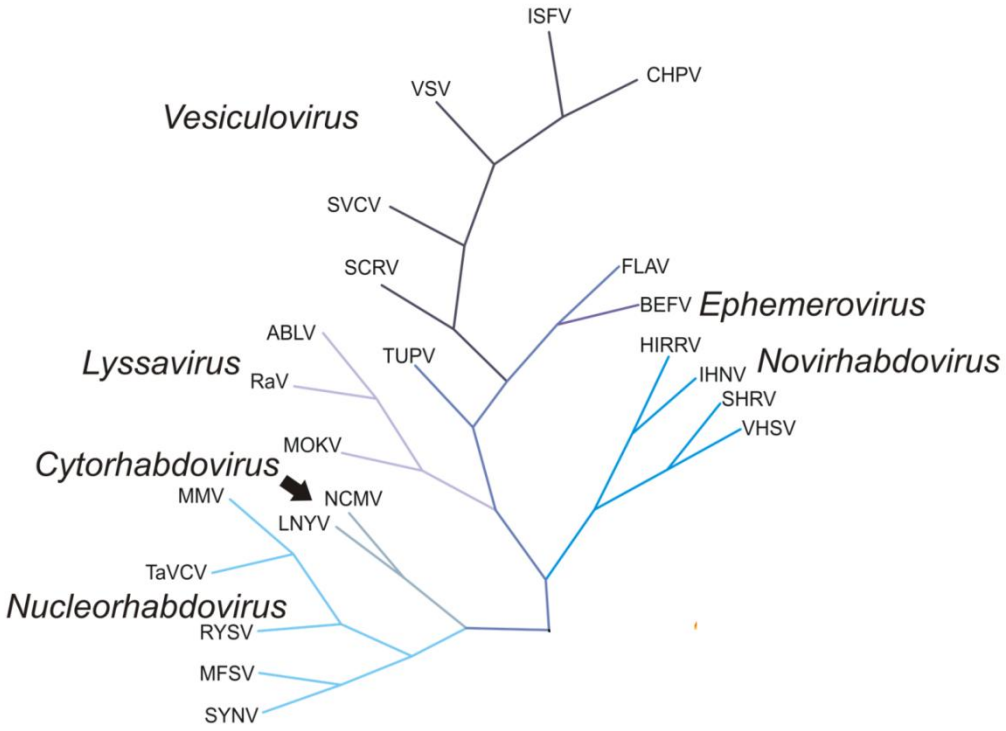

Figure 1.2| **Unrooted phylogenetic tree of the *Rhabdoviridae* based on L gene alignment**

1.2.3. **Genus *Vesiculovirus***

Currently, ten virus species are assigned to the vesiculovirus genus and there is evidence to suggest that several other viruses should also be members (Table 1.2). This genus contains predominantly zoonotic viruses which are capable of causing a diverse range of clinical manifestations including flu-like and encephalitic illnesses in humans, vesicular disease in livestock, persistent infections in insects and hemorrhagic disease in fish.

	Virus
Vesiculovirus	Carajas virus
	Chandipura virus
	Cocal virus
	Isfahan virus
	Maraba virus
	Piry virus
	Spring viraemia of carp virus
	Vesicular stomatitis Alagoas virus
	Vesicular stomatitis Indiana virus
	Vesicular stomatitis New Jersey virus
Tentative *vesiculovirus*	Boteke virus
	Farmington virus
	Gray Lodge virus
	Jug Bogdanovac virus
	Jurona virus
	Keuraliba virus
	Klamath virus
	Kwatta virus
	La Joya virus
	Malpais spring virus
	Perinet virus
	Porton virus
	Radi virus

Table 1.2| **Confirmed and putative vesiculoviruses**
Members of the vesiculovirus genus, as confirmed by the ICTV and species currently being considered for assignment to this genus (Vasilakis *et al.*, 2013b). Highlighted viruses have been shown to cause flu-like illness in humans (green), encephalitis in humans (red) and hemorrhagic disease in fish (blue).

The type species, the arbovirus vesicular stomatitis virus (VSV) is the causative agent of vesicular stomatitis (VS), a disease of ruminants, pigs and several other wildlife species found in large areas of the Americas. The clinical presentations in domestic animals resemble those of foot-and-mouth disease with vesicular lesions on the mouth, tongue, hooves and teats and this has significant economic consequences as well as being a welfare concern (Perez *et al.*, 2010). Putative biological vectors of VSV include black flies, sand flies (*Lutzomyia* spp) and biting midges. However, transmission by direct contact and infected fomites has also been demonstrated (Perez *et al.*, 2010).

VSV is endemic from northern South America to southern Mexico whereas disease presentations have occurred in approximately 10 year cycles in the southwestern United States and sporadically since the mid 1970's (only in wildlife species) in southeastern states (Rodriguez, 2002). The regular re-emergence of VSV in the southwestern US is due to the novel introduction of the virus from the endemic regions of Mexico and these events have been associated with high precipitation levels in the months preceding an outbreak, although there are likely to be a range of contributing factors which are not fully understood (Rainwater-Lovett *et al.*, 2007). VSV has also been shown to over-winter, thus causing incidences of disease for a few years after the first reported case (Perez *et al.*, 2010). Of the two serotypes of VSV (VSV New Jersey and VSV Indiana) VSV New Jersey accounts for the majority of infections in the US.

Two other vesiculoviruses, Cocal and Alagoas are responsible for the periodic incidences of vesicular disease in Brazil and Argentina (Rodriguez, 2002). The geographical distribution of these and other vesiculoviruses is shown in Figure 1.3. The mosquito-borne Malpais spring virus was first isolated in New Mexico in 1985 (Clark *et al.*, 1988) and a recent genetic analysis strongly indicated that it should be assigned to the *Vesiculovirus* genus (Vasilakis *et al.*, 2013b). This virus infects deer and horses and there is a high seroprevalence of Malpais spring virus antibodies among ungulates throughout New Mexico (Vasilakis *et al.*, 2013b).

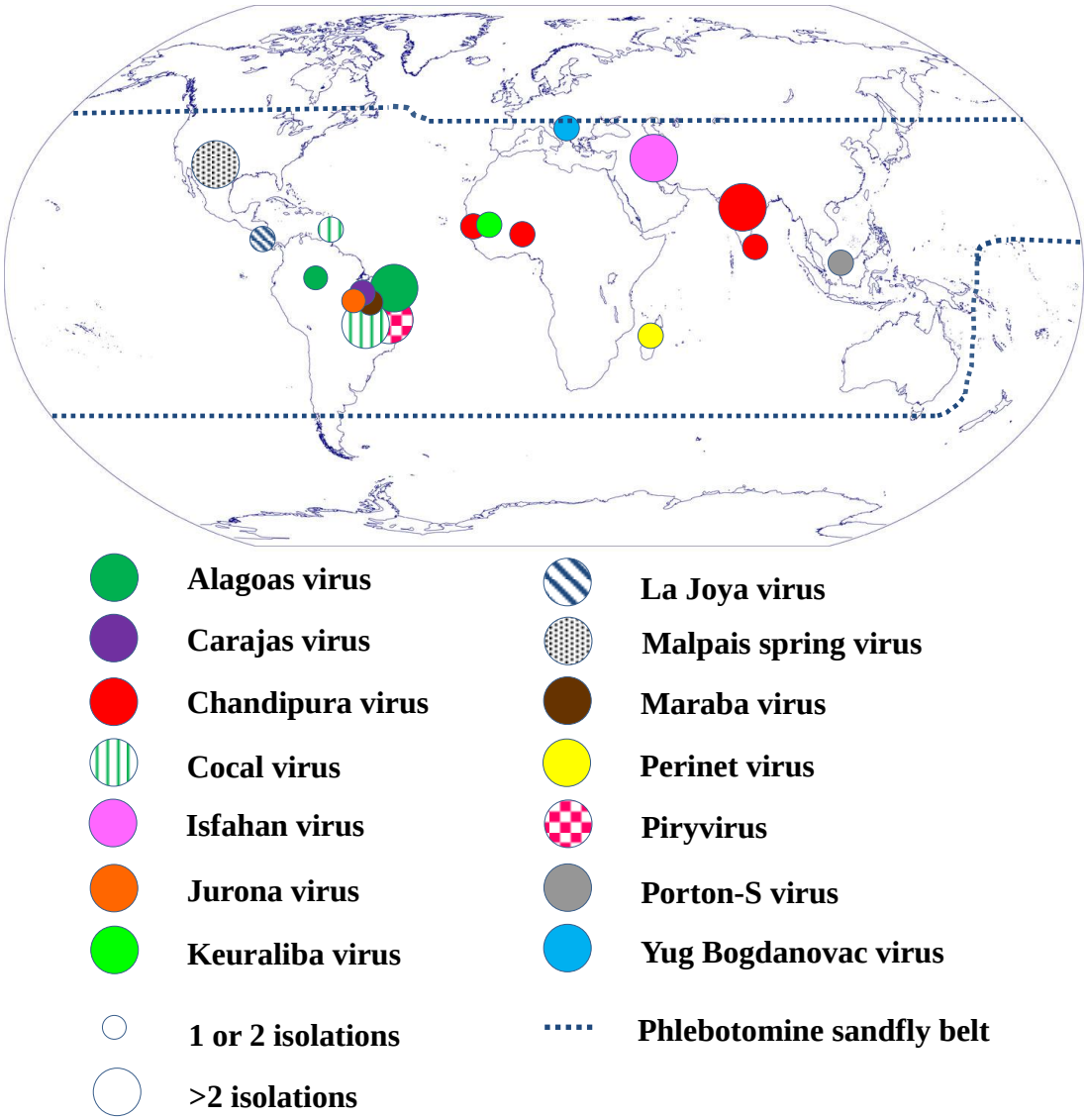

Figure 1.3| **Geographical distribution of vesiculoviruses**
The approximate locations of virus isolations are shown. The large circles represent >2 isolations and the smaller circles represent 1 or 2 isolations of virus. VSV New Jersey and VSV Indiana are not included because of their large geographical spread throughout North, Central and South America. The distribution of phlebotomine sandflies is shown by a dotted line.

CHPV replicates within, and is transmitted by, phlebotomine sand flies, the geographical distribution of which is shown in Figure 1.3. However, the virus has only been isolated in India where it has caused several human epidemics of acute encephalitis and in West Africa from the vector (Traore-Lamizana *et al.*, 2001) and one other non-human isolation (Fontenille *et al.*, 1994). The vesiculovirus most

closely related to CHPV, Isfahan virus (IFHV), was isolated from phlebotomine sand flies in Iran in 1975 (Tesh *et al.*, 1977). While there have been no documented outbreaks of IFHV-associated disease in humans it has been associated with a small number of sporadic cases of febrile illness.

1.3. CHPV structure and lifecycle

Although first isolated in 1965 there has been limited research into CHPV, especially until the recent epidemics, with much of our understanding of the molecular aspects of replication shaped by analogy with the extensively studied VSV, the prototype *vesiculovirus.*

1.3.1. **CHPV structure**

CHPV is an enveloped, bullet-shaped, helical virus containing 11,119 nucleotides of non-segmented single-stranded, negative sense RNA (Marriott, 2005) (Figure 1.4). By analogy with VSV, the CHPV genome is encapsidated by approximately 1,200 molecules of the 48kDa nucleocapsid (N) protein to generate the core ribonucleoprotein (RNP) complex, functioning as the template for CHPV RNA synthesis (Figure 1.4a). In addition, the two constituents of the viral RNA dependent RNA polymerase (RdRp); the 238.5 kDa large (L) protein (the catalytic subunit) and the phosphorylated form of 32.6 kDa phosphoprotein (P) (the cofactor) are closely associated with the RNP in mature virus particles (Basak *et al.*, 2007; Mondal *et al.*, 2010). The RNP is the minimal unit required for rhabdovirus infection (Thornton *et al.*, 1983). The 26kDa matrix (M) protein covers the inner membrane of the virus and attaches the RNP particle to the envelope. The attachment and fusion

glycoprotein (G) is embedded in and protrudes from the envelope of the virion. These can be clearly seen coating the surface of the virus particle in electron micrographs of the virus (Figure 1.4b).

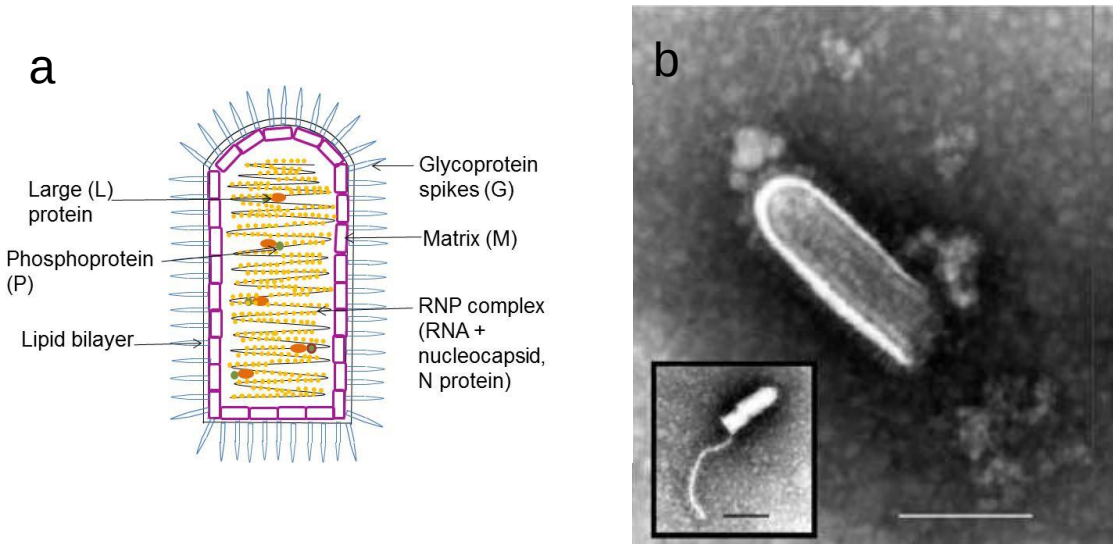

Figure 1.4| **Structure of CHPV**
A. Diagram of a CHPV particle
B. Transmission electron micrograph of CHPV (Rao *et al.*, 2004). Scale bar is 100 nm. A released RNP particle is shown in the insert.

1.3.2. **Genome organisation**

The CHPV genome contains (from 3' to 5'): a 49 nucleotide untranslated, non-capped, non-polyadenylated leader RNA, 5 genes encoding the five structural proteins of the virus; N, P, M, G, L proteins, each of which is separated by a conserved (G/CA) dinucleotide intergenic sequence, and a 46 nucleotide trailer sequence (Basak *et al.*, 2004) (Figure 1.5). Each gene also has cis-acting stop sequences at the 5' terminus and 3' start sequences, which are required for mRNA synthesis.

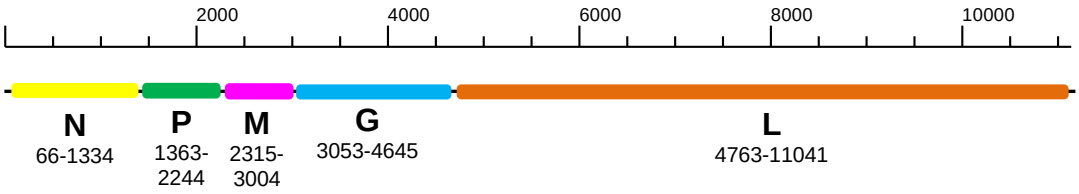

Figure 1.5| **CHPV genome**
The nucleotide positions within the 11,119 nt CHPV genome are indicated. The locations of the genes encoding the 5 virus proteins are indicated.

1.3.3. **Replication cycle**

The life cycle of all vesiculoviruses is entirely cytoplasmic and is the product of an intimate association with numerous host cell proteins, which act as both positive and negative regulators of viral replication. There is limited information about these cellular factors, however, a recent RNAi screen identified 72 mammalian genes as essential for VSV infection (Panda *et al.*, 2011) A summary of the vesiculovirus replication cycle with the names of host cell proteins known to be involved at each stage is shown in Figure 1.6. Table 1.3 gives details of the cellular proteins shown to be involved in vesiculovirus replication.

Following adsorption and entry into the cell by clathrin-mediated endocytosis (step 1, Figure 1.6), a low pH-triggered fusion event takes place between the G spike proteins protruding from the vesiculovirus envelope and the membranes of acidified endosomes, resulting in the liberation of virion constituents into the cytoplasm (Basak *et al.*, 2007) (step 2, Figure 1.6). Delivery of the nucleocapsid into the cytoplasm marks the initiation of vesiculovirus infection.

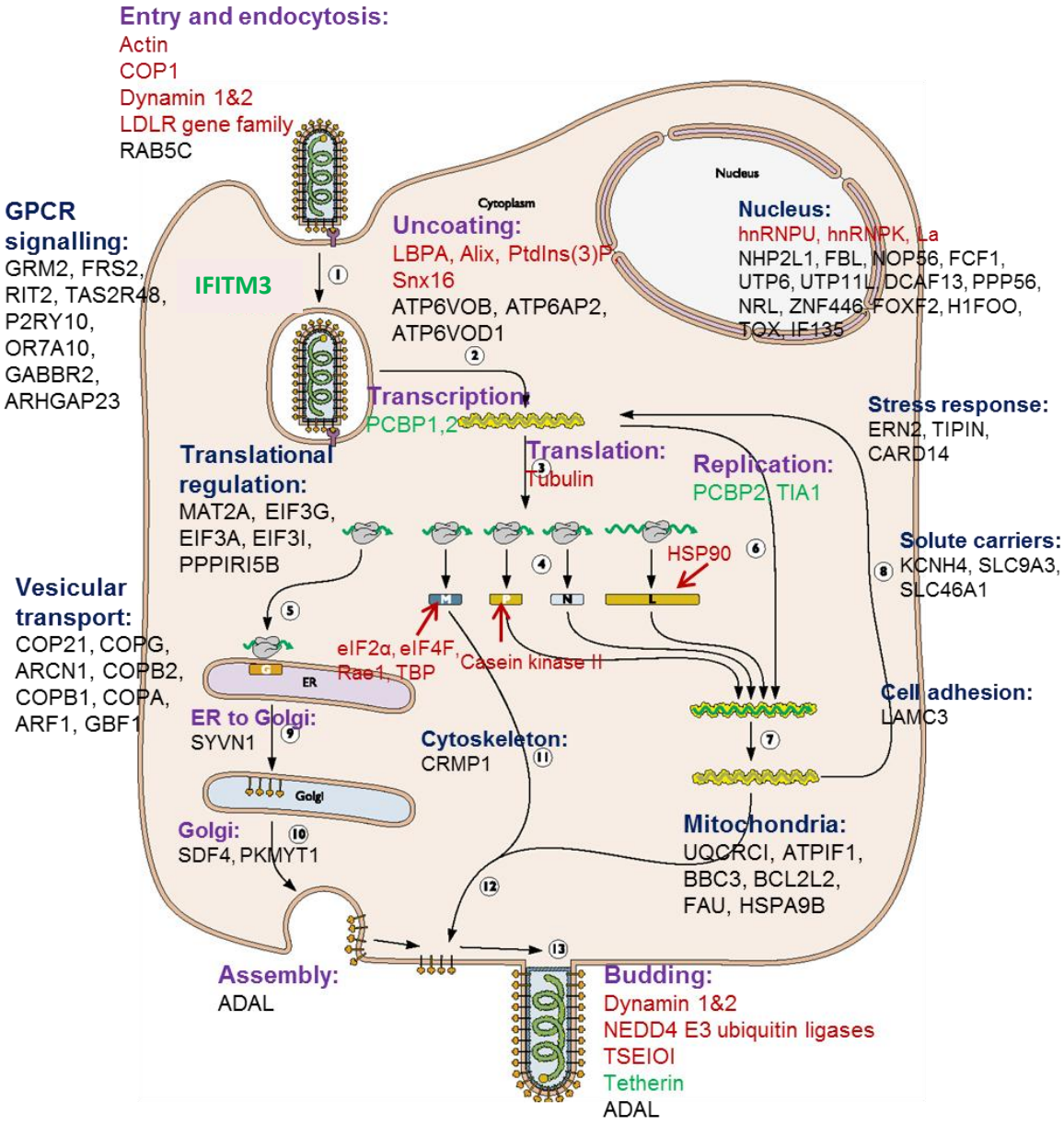

Figure 1.6| **Replication cycle of VSV** (adapted from Flint *et al.*, 2009)
Stages of the VSV replication (purple): entry and endocytosis (1), uncoating (2), primary transcription (3), translation (4), ER membrane-associated translation of the G protein (5), replication (6), secondary transcription and replication (7, 8), transport of the G protein through the secretory pathway (9, 10), assembly (11, 12) and budding of the virion from the host cell (13). Cellular processes involved in the vesiculovirus life cycle are shown in blue. Specific host proteins which have been shown to be vital for or support virus replication are in red and those shown to suppress virus growth are in green. Cellular genes whose expression has been demonstrated to be required for VSV replication by RNAi screening (Panda *et al.*, 2011) are given in black.

Cellular factors	Interactions with virus	Roles
Actin	ND	Entry into cells (Cureton *et al.*, 2009)
Actin-related protein 3 (APR3)	ND	
Alanine deamininase like (ADAL)	ND	Assembly and budding of nascent VSV virions (Panda *et al.*, 2011)
ARF1	ND	Activator of COP1 (Panda *et al.*, 2011)
ATPIF1 gene	ND	ATPIF1 encodes a mitochondrial ATPase inhibitor, shown to be required for VSV infection (Panda *et al.*, 2011)
BBC3 gene, encodes Bcl2 binding component 3	ND	Required for VSV infection (Panda *et al.*, 2011). Cellular function is to induce apoptosis through the mitochondrial apoptotic pathway
BCL2L2 gene, encodes Bcl-2-like protein2	ND	Required for VSV infection (Panda *et al.*, 2011). Pro-apoptotic cellular factor.
CEACAM7	ND	
Casein kinase II	Phosphoprotein	Modulate the activity of VSV and CHPV P (Chattopadhyay & Banerjee, 1987; Chattopadhyay & Raha, 1997)
Coatomer complex (COP) 1	ND	COPZ1, COPG, COPB2, COPB1, COPA and ARCN1 gene expression is required for VSV infection. Facilitates the processing of VSVG through its involvement in its transport through the secretory pathway (from the Goli to the ER) and also plays important roles in VSV gene expression (Panda *et al.*, 2011). Expression of COP1 is required for VSV internalisation (Cureton *et al.*, 2012).
Collapsin response mediator protein I (CRMPI)	ND	CRMP1 is involved in cytoskeleton remodelling and was found to be required for VSV infection during RNAi screening (Panda *et al.*, 2011)
C-terminal Src kinase	Phosphoprotein	? (Dinh *et al.*, 2011)
Cyclophilin A	Nucleoprotein	Essential for primary transcription of VSV New Jersey but not VSV Indiana (Bose *et al.*, 2003)
Dynamin 1 and 2	Matrix protein	Modulates clathrin-mediated endocytosis and is required for efficient progeny virus egress (Raux *et al.*, 2010)
eIF2α and the eIF4F complex	Matrix and (ND)	Alters the phosphorylation state of the eIF2α and the eIF4F complexes, impairing host cell translation (Connor & Lyles, 2002)
EIF3 subunits A, G, I	ND	Shown to be essential for VSV infection during RNAi screening (Panda *et al.*, 2011)
G protein couples receptor (GPCR) signalling proteins	ND	The following proteins involved in signalling from GPCRs were found to be upregulated during VSV-infection (GRM2, FRS2, RIT2, TAS2R48, P2RY10, OR7A10, GABBR2, ARHGAP23)

		(Panda *et al.*, 2011)
GBF1	ND	An activator of COP1 (Panda *et al.*, 2011)
Genes involved in regulating transcription	ND	NRL, ZNF446, FOXF2, HIFOO, TOX, IFI35 genes were shown to be required for VSV infection. Their precise involvement in infection has not been established (Panda *et al.*, 2011)
Genes involved in RNA processing	ND	NHP2L1, FBL, HNRPK, NOP56, FCF1, UTP6, UTP11L, DCAF13, PPP56 genes were shown to be required for VSV infection. (Panda *et al.*, 2011)
Cellular stress response genes	ND	GRN2, TIPIN, CARD14 genes were shown to be required for VSV infection (Panda *et al.*, 2011)
Heat shock protein (HSP)	Nucleoprotein	HSP90 was shown to be involved in VSV replication and maintaining L protein stability (Connor *et al.*, 2007)
hnRNP K	ND	Required for VSV infection by inhibiting apoptosis, enhancing virus replication and release by modulating the expression of several host cell proteins including the upregulation of alanine deaminase like (ADAL), ARF1, Bcl-Xl, Bcl-2 and BagI and downregulation of Bcl-Xs and Bik (pro-apoptotic factors) (Dinh *et al.*, 2013b)
hnRNPU proteins	Leader RNA	Postulated to inhibit cellular mRNA synthesis (Gupta *et al.*, 1998a)
HSPA9B gene (HSP9)	ND	Required for VSV infection (Panda *et al.*, 2011). Cellular function is to modulate cell proliferation
IFN-induced transmembrane family (IFITM) 3	ND	Negatively regulates VSV at an early stage of the virus lifecycle, prior to primary transcription but after endocytosis (Weidner *et al.*, 2010)
La	Leader RNA	VSV leader RNA interacts with La in the nucleus to inhibit RNA polymerase III transcription (Kurilla & Keene, 1983)
Laminin gamma 3 (LAMC3)	ND	Involved in cellular adhesion
LBPA, Alix, phosphatidylinositol-3-phosphate and Snx16	ND	Release of nucleocapsids from multivesicular bodies into the cytoplasm (Le Blanc *et al.*, 2005)
LDLR gene family	Glycoprotein	Cellular receptor (Finkelshtein *et al.*, 2013)
MAPK	Matrix protein	Activates MAPK preventing CD1d antigen presentation to NKT cells (Renukaradhya *et al.*, 2008)
MAT2A	ND	Required for VSV gene expression (Panda *et al.*, 2011)
NEDD4 E3 ubiquitin ligases	Matrix protein	Budding of mature virus particles (Harty *et al.*, 1999)
PKMYT1 gene, encodes a serine/threonine protein kinase	ND	RNAi screening identified a requirement for this kinase in VSV infection (Panda *et al.*, 2011). This kinase inhibits the G2/M transition of the cell cycle.
Poly(C)binding protein 1 (PCBP1)	Phosphoprotein	Inhibits primary viral transcription (Dinh *et al.*, 2011)
Poly(C)binding protein 2 (PCBP2)	Phosphoprotein	Associates with VSV P to inhibit viral transcription and replication (Dinh *et al.*, 2011)
Ppp1r15b gene which encodes	ND	RNAi screening identified a requirement for CReP in VSV infection (Panda *et al.*, 2011). CReP

CReP		triggers dephosphorylation of eIF2(αP) by modulating the activity of protein phosphatases.
RAB5C	ND	This GTPase was shown to be necessary for VSV infection (Panda *et al.*, 2011)
RaeI	Matrix protein	Targets the nucleoporin Nup98 to inhibit the nuclear-cytoplasmic trafficking of host cell macromolecules in a Ran-TC4 GTPase-dependant manner (Rajani *et al.*, 2012)
Solute transporters SLC46A1 (PCFT), KCNH4, SLC9A3	ND	The SLC46A1 solute transporter was shown to be required at the entry and/or uncoating stage of VSV infection (Panda *et al.*, 2011)
Stromal cell derived factor (SDF) 4	ND	
SYVN1 gene, encodes the E3 ubiquitin ligase synoviolin	ND	RNAi screening identified a requirement for SYVN1 expression in VSV infection (Panda *et al.*, 2011). The cellular function of synoviolin is to remove proteins from the ER to the cytoplasm.
TATA-binding protein (TBP)	Matrix protein	Inhibits TBP activity which contributes to viral inhibition of cellular transcription (Ahmed & Lyles, 1998)
T-cell-restricted intracellular antigen 1 (TIA1)	ND	Suppresses VSV replication in conjunction with PCBP2 within stress granule-like complexes induced by VSV infection (Dinh *et al.*, 2013a).
Tetherin	ND	Blocks VSV virion egress (Weidner *et al.*, 2010)
TSEIOI (ESCRT complex)	Matrix protein	Budding of mature virus particles (Raux *et al.*, 2010)
Tubulin	Matrix protein	Stimulates cell rounding (Melki *et al.*, 1994) and required for virus transcription (Moyer *et al.*, 1986) Microtubules are required to transport the viral mRNA from replication complexes to the cell membrane and this is essential for efficient translation (Heinrich *et al.*, 2010)
UQCRC1 gene, encodes a subunit of ubiquitinol cytochrome c reductase	ND	Demonstrated to be essential for VSV infection from RNAi screening (Panda *et al.*, 2011)
Vaculolar-type H^+-ATPase (V-ATPase) subunits	ND	ATP6VOB, ATP6AP2 and ATP6VOD1 V-ATPase subunits were shown to be required for VSV infection (Panda *et al.*, 2011)

Table 1.3| **Cellular factors influencing vesiculovirus replication**
Known cellular interactions with virus RNA or proteins and details of the effects of such interactions are given. The majority of the virus-host interactions above have been demonstrated only in VSV. ND denotes not determined.

The current model for CHPV transcription is based on analogy with that for VSV in which the virus encoded RNA dependent RNA polymerase (RdRp) sequentially transcribes the virus genome, beginning at the 3' end, by a stop-start mechanism to generate a gradient of capped and polyadenylated mRNA transcripts whereby the most abundant mRNA is that encoding the N protein (as it is nearest to the 3' end) (steps 3,4,5 Figure 1.6). This progressive attenuation of transcription is a consequence of the reduced capacity of RdRp to reinitiate transcription at each downstream intergenic sequence. The levels of protein are believed to reflect the levels of each mRNA. VSV primary transcription has been shown to take place throughout the cytoplasm but protein expression triggers a shift in the principal site of mRNA synthesis to cytoplasmic inclusions as the infection progresses (Heinrich *et al.*, 2010). Microtubules are utilised to transport viral mRNA from replication complexes to the cell membrane and this was demonstrated to be essential for efficient translation (Heinrich *et al*., 2010). VSV infection induces the formation of stress granule-like complexes which are comprised of viral RNA, replicative proteins and several cellular antiviral proteins. This has led to the suggestion that the generation of inclusions is host-cell mediated and that they are in fact the replication complexes described previously (Dinh *et al.*, 2013a).

Read-though of the termination signals at gene junctions by the same RdRp that carries out mRNA transcription produces full-length anti-genomic RNA, which subsequently serves as templates for progeny genomes (Bhattacharya *et al.*, 2006) (step 6, Figure 1.6). The precise explanation for the switch in polymerase function from transcription to replication remains elusive, although proposed mechanisms include the suppression of mRNA synthesis due to the accumulation of N protein on

nascent genomic RNA. Formation of complexes of CHPV leader RNA and underphosphorylated P protein dimers has also been implicated in anti-termination at gene junctions and therefore replicative phase initiation (Basak *et al.*, 2004; Mukhopadhyay *et al.*, 2010). Progeny genomes are then used as templates for secondary transcription or replication (steps 7 & 8, Figure 1.6) or are assembled into progeny virions by budding from host plasma membrane (steps 12 & 13, Figure 1.6).

The sections below give a more detailed discussion about the current understanding of the roles of each of the viral proteins and the involvement of host cell proteins at each stage of the vesiculovirus lifecycle.

1.3.4. **Attachment and fusion mediated by the G protein**

The G envelope glycoprotein of CHPV is crucial in the initial phases of infection and is responsible for mediating both the attachment and fusion processes, as is the case for all Rhabdoviruses and many other enveloped viruses. This dual function is made possible through the ability of the glycoprotein to exist in three forms and to undergo large scale reversible structural rearrangements to transition between them (Roche *et al.*, 2008). Mature Rhabdovirus G proteins are embedded on the virion surface as trimers with each monomer composed of three domains: an N-terminal ectodomain, a transmembrane domain (which functions to anchor the protein into the virion membrane) and a C-terminal cytoplasmic tail (Masters *et al.*, 1989). The ectodomain contains a cleavable signal peptide and two glycosylation sites and forms the external portion of the protein and as such is the major target of neutralising antibodies during infection.

Recently, research has shown that the cellular receptor of VSV is the ubiquitously expressed low density lipoprotein receptor (LDLR) with other members of the LDLR gene family also acting as receptors but at lower frequency (Finkelshtein *et al.*, 2013). This is consistent with the broad tropism and pantropic nature of VSV. It is this characteristic which has been harnessed to generate recombinant viral vectors for gene therapy, vaccination and viral oncolysis (Finkelshtein *et al.*, 2013). Soluble LDLR is able to prevent VSV infection by binding to receptors, thus making them unavailable for virus attachment in all cell types tested except in SF6 insect cells (Finkelshtein *et al.*, 2013). This indicates that the virus uses another receptor in insect cells and is interesting because of the markedly different manifestation of VSV infection in insect cells (non-cytopathic) compared to other cell types (highly cytopathic). Currently, it is not known whether the other vesiculoviruses such as CHPV also use LDLR to gain entry into host cells.

Following receptor recognition, the virus is able to hijack cellular trafficking pathways and is taken up by the cell by clathrin-mediated endocytosis. Entry of VSV into cells occurs in vesicles only partially covered by clathrin and requires actin (Cureton *et al.*, 2009) and dynamin-2 (Johannsdottir *et al.*, 2009). LDLR family proteins serve as ideal viral receptors as they are regularly endocytosed and recycled back to the plasma membrane even when a ligand is not bound (Finkelshtein *et al.*, 2013).

The fusion peptides of the VSV G and CHPV G glycoproteins are distinct from the well-defined class I (e.g. HA of influenza) and class II (e.g. E1 protein of Semliki Forest virus) viral fusion glycoproteins and have recently been grouped into a third class together with the spike protein of other Rhabdoviruses, including rabies virus, and the orthologous gB of herpesviruses (Roche *et al.*, 2006). Crystal structures of

VSV G (Roche *et al.*, 2006) and recently CHPV G proteins (Baquero *et al.*, 2012) have been solved, providing further information about the three forms of G protein during the fusion process.

The low pH of the endosomal lumen triggers a major conformational change in the G glycoprotein from the pre-fusion trimer (occurring above pH7) to the post-fusion trimeric conformation via a monomeric hydrophobic intermediate, resulting in the fusion of the viral envelope with endosomal membranes (at an optimum of pH 6) and releasing the nucleocapsid into intra-endosomal vesicles (Baquero *et al.*, 2012; Le Blanc *et al.*, 2005; Roche *et al.*, 2006). In contrast with class I or II fusion proteins, the G proteins of these vesiculoviruses transition through the three states in a completely reversible manner as the pre- and post-fusion conformations are in a pH-dependent dynamic equilibrium in which the latter is favoured at low pH (Albertini *et al.*, 2012). This is crucial for the protein to exist in the native form on the virion envelope following transport through the low pH environment of the Golgi apparatus (Roche *et al.*, 2008; Yao *et al.*, 2003). Therefore, the pre- and post-fusion trimers of vesiculovirus G proteins are equally stable, unlike the metastable pre-fusion form of the class I and II glycoproteins (Yao *et al.*, 2003).

Furthermore, it has been demonstrated that VSV G protein is also involved in the late stages of the infectious cycle assembling 100 to 150 nm G protein microdomains in the plasma membrane of infected cells that act as sites of progeny particle assembly (Brown & Lyles, 2003). VSV G protein also promotes budding, a characteristic residing in the extracellular membrane proximal stem of the protein (Robison & Whitt, 2000; Rolls *et al.*, 1994).

1.3.5. **Transport of viral nucleocapsids through the endocytic pathway**

VSV has been shown to hijack the endocytic pathway, enabling the transport of viral nucleocapsids within vesicles of multivesicular bodies to late endosomes (via microtubules) and following fusion of the RNP-containing vesicle with the membrane of the endosome, release into perinuclear regions of the cytoplasm (Le Blanc *et al.*, 2005). The cargo contained within internal vesicles of multivesicular bodies is usually destined for degradation in lysosomes and thus VSV has evolved a mechanism to facilitate nucleocapsid release into the cytoplasm (and hence initiate infection) prior to encountering any lysosomes. The precise mechanism has yet to be elucidated, although results show that the process is dependent on the cellular factors late endosomal lipid lysobisphophatidic acid (LBPA), Alix, phosphatidylinositol-3-phosphate and Snx16, which are required for membrane fusion within late endosomes (Le Blanc *et al.*, 2005).

1.3.6. **Replication complex proteins**

1.3.6.1. **Nucleocapsid (N) protein**

In VSV the viral RNA lies in a positively charged groove within consecutive N protein monomers, encapsidating the genome and forming the template for RNA synthesis (Green & Luo, 2006). N protein monomers associate with the 3' end of the viral RNA upon recognition of specific sequences at the start of the leader RNA (Bhattacharya *et al.*, 2006). Subsequently, additional N proteins bind and this has been hypothesised to trigger a structural change in the N protein which reduces the template specificity of the protein and thus promotes further N polymerisation (Basak *et al.*, 2007). The N protein contains two domains which serve as docking sites for the P protein. The monomeric form of N protein is retained when the P

protein binds at the N-terminal domain of N (by partially blocking the oligomerisation domain) whereas interaction of the P and N proteins in the nucleoprotein complex occurs at the C-terminal domain and leads to recruitment of the L polymerase (Mondal *et al.*, 2012).

1.3.6.2. **Phosphoprotein (P)**

The VSV P protein is indispensable for viral transcription. It has a highly flexible structure comprised of 3 domains; an N-terminal portion which binds L and N proteins that are not attached to the RNA, a central oligomerisation domain and an N-RNA-binding domain at the C-terminus (Green & Luo, 2009). The modules are linked together by long flexible disordered regions, which are thought to be intrinsic in enabling the protein to carry out its functions. Also, phosphorylation of the P protein at specific sites by casein kinase II has been postulated to regulate P activities (Chattopadhyay & Banerjee, 1987; Chattopadhyay & Raha, 1997). P protein dimers simultaneously bind to the N-RNA and the L protein, bringing the RNA template into contact with and at the correct orientation with the catalytic subunit of the polymerase to facilitate RNA polymerisation. Studies have shown that P protein homodimers engage with every 5 N protein monomers along the N-RNA and the dynamic nature of the P protein supports uninterrupted transcription or replication as the downstream P protein is able to reach the approaching polymerase complex as it travels along the template (Leyrat *et al.*, 2012; Morin *et al.*, 2012).

The P protein also has a role as an N protein chaperone by blocking N aggregation, modulating the addition of N protein to genomic RNA and inhibiting the aberrant binding of N to host cell RNA (Majumdar *et al.*, 2004). Moreover, there is evidence which indicates that the phosphoprotein stimulates the transient dissociation of N

protein from the RNA within the polymerase complex and thus enable RNA synthesis (Leyrat *et al.*, 2012). Recently, another key function of the P protein has been demonstrated; inducing the L protein into a more compact conformation, which is required for triggering RNA synthesis (Rahmeh *et al.*, 2012). It has also been found to be crucial in the assembly of infectious VSV particles (Das & Pattnaik, 2005).

Poly(C) binding protein (PCBP) 1 and 2 associate with VSV P protein to inhibit primary transcription (PCBP1) or both gene expression and replication (PCBP2) (Dinh *et al.*, 2011).

1.3.6.3. **Large (L) protein**

The large (L) protein of non-segmented RNA viruses are multifunctional and the rhabdovirus L proteins have been described as containing 6 functional domains of greater amino acid conservation and highly variable intra domains (Poch *et al.*, 1990). The positions of the 6 domains within the CHPV amino acid sequence are given in Figure 1.7. The more distantly related L proteins of the *Morbillivirus* genus have 3 conserved domains separated by 2 highly variable hinge regions. The insertion of the eGFP gene within hinge region 2 of the measles virus genome (corresponding to a region between blocks V and VI in rhabdoviruses) resulted in a functional virus with only slightly attenuated polymerase activity, suggestive of some conformational independence between the domains (Duprex *et al.*, 2002). A recombinant VSV in which the eGFP ORF was inserted at a comparable position in the genome exhibited a temperature sensitive phenotype (Ruedas & Perrault, 2009).

The L protein of non-segmented negative stranded RNA viruses contains all the enzymatic activities for RNA polymerisation, capping and polyadenylation. The

molecular interrelationship between the domains in the VSV L protein have also been established with conserved blocks I-IV arranged into a ring structure containing the RNA polymerase activity and a flexibly linked appendage of domains V and VI responsible for capping (polyribonucleotidyltransferase, PRNTase) and methylation (methyltransferase, MTase) respectively (Rahmeh *et al.*, 2010). The viral RNA is thought to pass through the ring of the L protein during polymerisation.

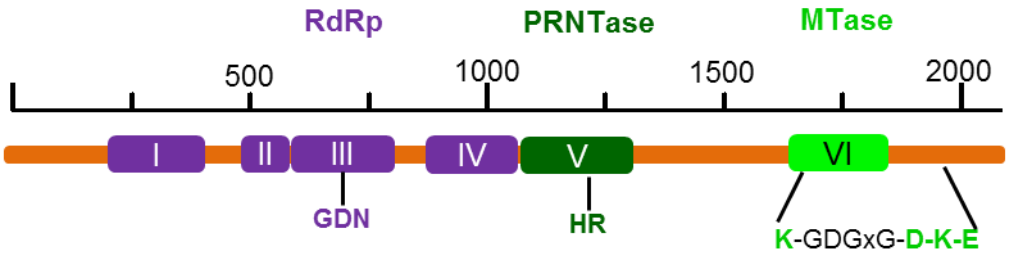

Figure 1.7| **Domain structure of the CHPV L protein**
The location of highly conserved domains I to VI within the L protein are given. The amino acid positions within the L protein are indicated. Domains I-IV form the core polymerase ring (purple) and V and VI are the viral polyribonucleotidyltransferase (PRNTase) and methyltransferase (MTase) respectively, together comprising the appendage (green). Essential motifs are also shown.

Domain III was found to confer the RNA dependent RNA polymerase (RdRp) activity of the L protein and the GDN motif, which is highly conserved in the domain III of non-segmented negative sense (NNS) RNA viruses and related to other viral RdRps, was shown to be essential for RNA synthesis (Sleat & Banerjee, 1993). An analogous region to another well conserved motif, designated the pre-A motif, located upstream of the GDN sequence within block III of NNS RNA viruses has been suggested to be involved in template engagement in the segmented negative sense RNA Phlebovirus Rift Valley fever virus (Muller *et al.*, 1994). The

rhabdovirus L protein is a dynamic structure that undergoes substantial reorganisation of its functional domains upon P protein binding, bringing the appendage into closer proximity of the RNA polymerase ring (Rahmeh *et al.*, 2010). It has been postulated that this arrangement is more conducive for transcription and thus these structural changes may serve to coordinate RNA synthesis and capping. Dimeric L-P protein complexes have also been observed (Rahmeh *et al.*, 2010). It has recently been shown that the L protein is capable of initiating RNA synthesis without both the N and P proteins but that the latter are needed in a modulatory capacity (Morin *et al.*, 2012).

The NNS RNA viruses have a unique capping mechanism provided by the viral PRNTase. In contrast with the conventional capping enzymes of eukaryotes and DNA viruses, the VSV PRNTase (following the hydrolysis of GTP to GDP by the GTPase activity of the L protein) catalyses the transfer of newly synthesised 5'-monophosphorylated mRNA with the conserved AACAG mRNA start sequence onto GDP (instead of GMP) to produce a GpppN cap via a covalent L-pRNA intermediate (Ogino & Banerjee, 2007; 2010). The strikingly conserved histidine-arginine (HR) motif located within domain V of the VSV L protein (H1217, R1218 in CHPV and H1227, R1228 in VSV) was shown to be critical for this process with the active site histidine residue required to bind through a phosphoamide linkage to the viral RNA start sequence (Ogino *et al.*, 2010). An arginine residue positioned slightly upstream of the HR motif (R1211 in CHPV and R1221 in VSV) is also essential for 5' cap addition in rhabdoviruses (Ogino *et al.*, 2010). The highly conserved GxxT(n)HR motif , which incorporates the upstream residues G1154 and T1157 in the VSV L protein and the HR sequence was also found to be essential for VSV capping (Li *et*

al., 2008), as well as for 3' polyadenylation and the efficient transcription of downstream genes (Li *et al.*, 2009).

Following the addition of a 5' cap to nascent viral mRNA, the VSV encoded MTase (containing the catalytic tetrad K-D-K-E at the C-terminus of L) methylates the structure by a unique mechanism distinct to that of eukaryotes and other viral MTases. The VSV MTase catalyses modification of the ribose 2'-O position which in turn leads to methylation at guanine N-7 resulting in the generation of 7mGpppNpmNp (Li *et al.*, 2006; Rahmeh *et al.*, 2009). Both methylation activities utilise the same S-adenosyl-L-methionine-binding site (GxGxG motif) within domain VI (Rahmeh *et al.*, 2009).

Another role of the L protein is to polyadenylate the viral mRNA on recognition of the 3'-AUACUUUUUUU-5' sequence, thus triggering the termination of mRNA synthesis (Rahmeh *et al.*, 2009). A protein kinase activity was also shown to reside within the VSV L protein (Banerjee, 1987). The cellular protein heat shock protein (HSP) 90 is required to maintain L protein stability (Connor *et al.*, 2007).

1.3.7. **Matrix (M) protein**

The rhabdovirus matrix (M) protein is multifunctional and this is achieved through multiple interactions with other virion and host cell proteins. The crystal structure of a thermolysin cleaved VSV Indiana Orsay strain M protein has been described (Gaudier *et al.*, 2002) and despite low amino acid sequence conservation among the vesiculoviruses (28% identity with CHPV) the protein structure and functions are thought to be highly similar (Taylor *et al.*, 1999). The M protein is an important structural constituent of mature rhabdovirus particles, being responsible for: condensing RNP complexes into coiled helices (Newcomb & Brown, 1981), linking

them to the phospholipid bilayer of the virion via a positively charged N-terminus containing eight lysine residues (Ogden *et al.*, 1986; Rose & Gallione, 1981) and associating with the cytoplasmic portions of the G protein.

Assembly of progeny particles and budding out of host cells are both directed by the M protein, and a flexible structure between the membrane binding domain and the rest of the protein, which is also present in other negative sense RNA viruses and the Gag protein in retroviruses, is essential for these processes (Gaudier *et al.*, 2002). The M protein interacts with, and recruits, RNP complexes to the membrane for assembly and induces the budding of mature virus particles. The latter has been shown to be facilitated through the association of host cell proteins with two late domains (PPXY and P(S/T)AP) in the flexible N-terminal structure of the VSV M protein (Raux *et al.*, 2010). The PPXY amino acid sequence binds the WW domain of the cellular proteins NEDD4 E3 ubiquitin ligases, which interact with cellular endosomal sorting complexes required for transport (ESCRT) complexes involved in vesicle biogenesis (Harty *et al.*, 1999). The second late domain of the M protein, containing the P(S/T)AP motif has been found to interact with the ESCRT constituent TSG1O1 (Raux *et al.*, 2010). Mutations in the late domains of VSV M protein disable release of fully-formed progeny particles and result in their accumulation at the plasma membrane (Jayakar *et al.*, 2000). The N-terminus of VSV M protein also binds dynamin 1 and 2 at the pleckstrin homology (PH) domain, an interaction which interferes with clathrin-mediated endocytosis and has been shown to be essential for efficient progeny virus egress (Raux *et al.*, 2010).

Another important role of vesiculovirus M proteins is the induction of a number of cytopathic effects including inhibiting host transcription, nuclear-cytoplasmic transport and translation. Induction of apoptosis via the mitochondrial pathway also

occurs due to the depression of host cell gene expression (Gaddy & Lyles, 2005). Inhibition of host cell transcription has been demonstrated for VSV with cellular RNA polymerases I, II and III (Ahmed & Lyles, 1998; Black & Lyles, 1992) and CHPV with RNA polymerase II (Taylor *et al.*, 1999). This is thought to be facilitated by the M protein entering the nucleus and the VSV M protein has been identified in the nucleus (Lyles *et al.*, 1988). The mechanism for inhibition has yet to be fully worked out, however there is some data to suggest the M protein impairs the activity of TATA-binding protein (TBP) (Ahmed & Lyles, 1998). M protein inhibits the nuclear-cytoplasmic trafficking of host cell macromolecules in a Ran-TC4 GTPase-dependent manner (Her *et al.*, 1997) by directly binding to the cellular export factor RaeI, which targets the nucleoporin Nup98 (Rajani *et al.*, 2012; von Kobbe *et al.*, 2000). However, many other host cell proteins are thought to play a role in this process (Rajani *et al.*, 2012). The M protein of CHPV blocks nuclear transport by the greatest extent compared to other host cell proteins (Petersen *et al.*, 2001). Moreover, VSV M specifically impairs host translation by altering the phosphorylation state of eIF2α and the eIF4F complex in addition to the decrease of host polypeptides attributed to the reduction in host mRNA as a consequence of virus-mediated depressed transcription (Connor & Lyles, 2002). There is evidence to suggest that the M protein is involved in modulating translation in this way but that another viral protein is primarily responsible (Connor & Lyles, 2002).

One study has found the $_{37}$PSAP$_{40}$ motif in the M protein of VSV to be an important determinant of species specific pathogenicity. Recombinant viruses in which the motif was changed to four alanines exhibited significantly reduced pathogenicity in mice but enhanced cytopathogenicity in insect C6/36 cells, indicating a role for the PSAP sequence in persistence (Irie *et al.*, 2012). The VSV M protein has also been

shown to supress host antiviral responses by downregulating interferon β gene expression (Ahmed *et al.*, 2003) and depressing the natural killer T (NKT) cell response. The latter is achieved by inhibiting CD1d antigen presentation to NKT cells through p38 mitogen-activated protein kinase (MAPK) activation (Renukaradhya *et al.*, 2008). VSV M protein stimulates cell rounding (Blondel *et al.*, 1990) through an interaction with tubulin (Melki *et al.*, 1994), an association which has been demonstrated to be essential for virus transcription (Moyer *et al.*, 1986).

1.3.8. **Leader RNA**

The major function established for the leader RNA is in containing the sequence required to initiate encapsidation of template RNA by the N protein (Bhattacharya *et al.*, 2006). It has been postulated that the leader RNA is also present in the nucleus of infected cells where it associates with the cellular protein La to modulate transcription by RNA polymerase III (Kurilla & Keene, 1983). An interaction between VSV-leader RNA and hnRNPU proteins in the nucleus has also been demonstrated, indicating a further role for this transcript in regulating cellular DNA synthesis (Gupta *et al*., 1998a).

1.4. Host range (*hr*) and temperature-dependent host range (*td*CE) mutants

Viruses are obligate intracellular parasites with host cell factors intrinsic to their lifecycles. These host factors can therefore determine the outcome of an infection in a cell. Essential host factors for CHPV are largely unknown. Section 1.3 and Table 1.3 gives details of host cell proteins involved in VSV replication. The critical

involvement of host factors in the replication of vesiculoviruses was highlighted by the isolation of VSV Indiana, VSV New Jersey and CHPV temperature-dependent host range (*td*CE) mutants by mutagenesis using 50-200 µg/ml 5-fluorouracil (Gadkari & Pringle, 1980; Pringle, 1978; Rasool & Pringle, 1986). These mutants are characterised by their ability to grow at both 31ºC (the permissive temperature) and the restrictive temperature of 39ºC in BSC-1 or BHK-21 cells (the permissive host) to comparable titres to wild-type virus yet display temperature sensitivity in primary avian cells (chick embryonic fibroblasts, CE). The *td*CE mutant phenotype has been defined as viruses with an efficiency of plating (E.O.P.) in BSC-1 cells of <0.7 and in CE cells of >2, where E.O.P. is calculated as $\log_{10}$ $PFU^{39ºC}$ subtracted from $\log_{10}$ $PFU^{31ºC}$. These E.O.P. values were selected arbitrarily to reflect significant growth impairment in CE cells compared to BSC-1 cells. This phenotype demonstrates a dependence of these *vesiculoviruses* on undetermined host factors (Gadkari & Pringle, 1980; Rasool & Pringle, 1986). All the CHPV *td*CE mutants isolated and a summary of important characteristics are given in Table 1.4.

Mutant	Additional host restriction(s)	Efficiency of plating		Transcriptase efficiency at 39°C determined by the plateau method (%of wt) (Rasool and Pringle, 1986)	Transcriptase efficiency at 39°C determined by the initial rate method (%of wt) (Rasool and Pringle, 1986)
		BSC-1	CE		
CH4[2]	ND	0.67	3.18	15	48
CH63[2] (re-cloned from CH859)	ND	0.36	2.09	28	53
CH72[2] (re-cloned from CH565)	ND	0.08	2.60	72	93
CH90[2] (re-cloned from CH530)	ND	0.09	2.15	110	109
CH112[2] (re-cloned from CH514)	ND	0.57	5.20	14	51
CH151[2]	ND	0.00	2.91	11	41
CH157[2]	ND	0.54	3.54	56	67
CH194[2]	ND	0.12	3.45	91	113
CH245[2]	ND	0.04	3.77	70	85
CH256[2]	ND	0.15	4.37	37	29
CH354[2]	ND	0.00	3.30	83	62
CH380[2]	ND	0.06	3.05	23	40
CH514[1]	None	0.40	3.18	X	X
CH516[1]	None	0.70	3.70	X	X
CH525[1]	None	0.78	5.00	X	X
CH530[1]	HE, RE, FEA, BEK, NIH/3T3, L929	1.18	5.00	X	X
CH565[1]	BEK	1.18	3.00	X	X
CH859[1]	RE, BEK, NIH/3T3, L929	0.60	3.18	X	X

Table 1.4| **Characteristics of CHPV *td*CE mutants**

[1]Denotes mutants isolated by Gadkari and Pringle (1980) and [2] isolated by Rasool and Pringle (1986). Mutants highlighted in blue have been selected to analyse the *td*CE phenotype in this study. Impaired growth at the restrictive temperature in chick embryo (CE), hamster embryo (HE), rat embryo (RE), feline embryo (FEA), bovine embryo kidney (BEK), mouse embryo (NIH/3T3), mouse (L929) cells are noted for several of the mutants. ND denotes not determined.

Two out of four of the VSV New Jersey *td*CE mutants studied synthesised RNA to comparable levels as the wild type virus at 31°C and 39°C whereas the RNA transcriptases of the remaining mutants were shown to be severely disabled at the restrictive temperature in BHK-21 and CE cells in *in vitro* transcription assays (Szilagyi & Pringle, 1975). Experiments in which transcribing nucleoprotein complexes (TNP) of the wild type and mutant viruses were dissociated and then reconstituted in various combinations suggested that the L protein contained the host range lesion (Szilagyi *et al.*, 1977). It was postulated that a host cell factor is required to counteract the thermoliability of the viral polymerase in *td*CE mutants found to have depressed RNA transcriptase activity whereas mutants displaying normal RNA synthesis have a defect at a different (later) stage in the viral life cycle (Szilagyi & Pringle, 1975).

Mutants that were unable to grow in CE and bovine kidney (MDBK) cells at any temperature, designated host restricted (*hr*CE) mutants, were also isolated from VSV New Jersey but not VSV Indiana or CHPV (Pringle, 1978; Rasool & Pringle, 1986). These mutants have provided a powerful tool for dissecting vesiculovirus replication. For *hr*CE and *td*CE mutants of VSV, increasing the incubation temperature from 31°C to 39°C after two hours post-inoculation was shown to have limited effect on VSV viral titre, whereas raising the temperature at an earlier time point severely disrupted virus replication, implying host restriction occurs at an early stage in viral replication (Pringle, 1978). However, involvement of the attachment protein was discounted when pseudotyped virions expressing the G protein from the *td*CE or *hr*CE VSV mutants grew to titres comparable with the wild type virus in CE cells. Together, these results added weight to the hypothesis that the host range phenotype

is caused by a genetic lesion in the virus polymerase which affects its association with host factor(s) that are not present in CE cells and are required to hold the polymerase in an active conformation at 39°C (Pringle, 1978).

As well as differences in mRNA synthesis, mutants also differed in their host restriction (Pringle, 1978). This is thought to highlight their unique characteristics and is suggestive of a range of mutational events and the involvement of more than one host cell factor. CHPV mutants with additional host cell restrictions are detailed in Table 1.4. A study of VSV *td*CE mutants found no link between certain cell types and properties, for example morphology, and conditional growth mutants, except that embryonic cells appeared to be more conducive to temperature-sensitivity and restrictiveness of murine embryonal carcinoma cells decreased after differentiation (Pringle, 1978).

Upon further investigation, the *td*CE mutants of VSV and CHPV were shown to have important intrinsic differences regarding the *in vitro* heat sensitivity of their viral RNA transcriptase. Reduced RNA transcriptase activity *in vitro* at 39ºC resulting in significantly lower amounts of viral RNA synthesised was observed in 10 out of 12 of CHPV *td*CE mutants compared to wild-type virus and a gradient of this activity ranging from 11% of the wild-type to greater than wild-type were determined across the mutants studied (Rasool & Pringle, 1986). This is in contrast with the severe impairment or wild type level RNA synthesis reported in the case of VSV *td*CE mutants. Moreover, viral protein synthesis was also found to be either considerably depressed or non-existent in all the transcriptionally deficient CHPV *td*CE mutants grown in CE cells at the restrictive temperature, leading to the postulation that the

growth restriction is caused by diminished RNA synthesis which in turn results in decreased production of viral polypeptides (Rasool & Pringle, 1986). In support of this, intracellular viral protein synthesis increased to wild-type levels when *td*CE mutants reverted to a non-temperature sensitive phenotype (Rasool & Pringle, 1986). Furthermore, *in vitro* RNA methylation activity of the virus RNA dependent RNA polymerase and heat shock protein induction were found to occur at similar levels as the wild type virus in all *td*CE mutants (Rasool & Pringle, 1986).

VSV Indiana dual ts/hr mutants have also been isolated (Simpson & Obijeski, 1974). These mutants are restricted in many human cell lines including Hep-2 and display temperature sensitivity in CE and BHK cells. One of these mutants, *hr1* contains a D1671V amino acid substitution in the MTase domain VI of the VSV L protein (within a predicted S-adenosyl-L-methionine-binding motif) rendering the mutant completely incapable of catalysing the methylation of 5' mRNA caps at both guanine-N7 and 2'-O-adenosine (Grdzelishvili *et al.*, 2005; 2006; Hercyk *et al.*, 1988; Horikami & Moyer, 1982). In contrast to *hr1* mutant *hr8* retained low levels of MTase activity at 2'-O-adenosine (but not at the guanine-N7 position). This phenotype was shown to be the consequence of a G1481R amino acid substitution located between domains V and VI in the L protein in a region of 31 amino acids subsequently identified as essential for VSV MTase activities (Grdzelishvili *et al.*, 2006).

1.5. Vesiculovirus disease: infection of the central nervous system

CHPV has been associated with central nervous system (CNS) disease in several outbreaks in India. There are over 100 neurotropic viruses, capable of infecting the CNS and giving rise to neurological disease. The most frequent clinical manifestations of such infections are viral meningitis and viral encephalitis, caused by inflammation of the meninges and brain parenchyma, respectively. The key characteristic clinical symptoms of acute viral encephalitis are fever, headache and altered sensorium (Whitley & Gnann, 2002), although the precise range of symptoms experienced depends on the regions of the brain that are affected. Areas of hyperintensity (a consequence of cerebral edema) and foci of intercerebral haemorrhage are often observed in the brains of patients with viral encephalitis using Magnetic Resonance Imaging (MRI). Determining the specific regions of the brain affected by inflammation is often important in deducing the aetiological agent because some viruses have predilections for certain parts of the brain. For example, abnormalities in the medial temporal lobes are suggestive of herpes simplex virus-induced encephalitis (Solomon *et al.*, 2012). Viral encephalitis results in tissue necrosis, necrotising vasculitis, eosinophilic inclusions within glial cells and neurons and perivascular infiltration of lymphocytes, which can be observed by microscopy. Viral encephalitis is potentially life-threatening as severe cerebral edema places pressure on the brainstem, which controls heartbeat and respiration.

1.5.1. **Causative agents of viral encephalitis**

Viral infections are responsible for the majority of encephalitis cases, with a global incidence of 7.4 per 100,000 people per year, although developing countries have a disproportionately higher disease burden (Griffin, 2010). Table 1.5 lists the viruses

known to cause CNS disease. Some of these viruses are ubiquitous in the global population but rarely cause neurological disease, such as the herpes simplex viruses which are the most common sporadic cause of viral encephalitis. Other viruses rarely infect humans but when infection does occur it always manifests with CNS involvement, for example rabies virus (Whitley & Gnann, 2002).

Class	Virus family	Virus
1 (double stranded DNA)	Herpesviridae	Herpes simplex virus
		Varicella-zoster virus
		Cytomegalovirus
		Epstein-Barr virus
		Human herpesvirus 6
		B virus
	Adenoviridae	Adenovirus
	Polyomaviridae	JC virus
III (double stranded RNA)	Reoviridae	Colorado tick fever virus
IV (positive sense single stranded RNA)	Picornaviridae	Echovirus
		Coxsackievirus
		Poliovirus
		Enterovirus
	Togaviridae	Eastern equine encephalitis virus
		Western equine encephalitis virus
		Venezuelan equine encephalitis virus
		Rubella virus
	Flaviviridae	St. Louis encephalitis virus
		Japanese encephalitis virus
		Murray valley encephalitis
		Ilheus virus
		Rocio virus
		Tick-borne encephalitis virus
		Far eastern
		Central European
		Kyasanur forest
		Louping ill virus
		Negishi
		West Nile virus
		Dengue virus
		Powassan virus
V (negative sense single stranded RNA)	Arenaviridae	Lymphocytic choriomeningitis virus
	Orthomyxoviridae	Influenza virus
	Paramyxoviridae	Measles virus
		Mumps virus
		Nipah virus
	Bunyaviridae	Californian encephalitis virus
		La Crosse virus
		Jamestown Canyon virus
		Snowshoe hare virus
		Tahyna virus
		Inkoo virus
		Rift valley virus
	Rhabdoviridae	Rabies virus
		Chandipura virus
VI	Retroviridae	Human immunodeficiency virus type I

Table 1.5| **Viruses known to cause CNS disease**

Many important viral encephalitides are arboviruses and these are therefore restricted to the geographical range of their vectors. Arboviruses that cause encephalitis are shown in Table 1.6. Recently, there has been a concern about the increased spread of viruses associated with CNS infections, many of which are arboviruses, and this poses a significant public health threat. Japanese encephalitis virus (JEV), transmitted by *Culex* mosquitoes, is responsible for the largest number of cases of arthropod-borne viral encephalitis per year with approximately 50,000 cases (mainly children) and 15,000 deaths annually (Solomon *et al.*, 2003). JE emerged in Japan in the 1870s, with the virus first isolated in Japan in 1935, and has since spread throughout Asia and Northern Australia (Misra & Kalita, 2010). The geographical range of the closely related flavivirus West Nile virus (WNV) considerably expanded from Africa and the Middle East into Southern Europe in 1996 and the East coast of the USA in 1999 (Whitley & Gnann, 2002) with enhanced avian virulence, neuroinvasiveness in humans and epidemic potential (Gubler, 2007). The virus has become established in the Americas, spreading westwards in the USA from 1999 to 2004 and then reached countries in Central and Southern America in 2003 and 2004 respectively (Gubler, 2007).

Virus family	Virus	Vector	Geographical location
Reoviridae	Colorado tick fever virus	Ticks (Dermacentor)	Rocky mountain, USA
Togaviridae	Eastern equine encephalitis virus	Mosquitos (Culiseta, Aedes)	Eastern and gulf coasts of USA, Caribbean, South America
	Western equine encephalitis virus	Mosquitos (Culiseta, Culex)	Western USA, Canada
	Venezuelan equine encephalitis virus	Mosquitos (Aedes, Culex and others)	South and Central America, Florida, Southwest USA
Flaviviridae West Nile complex	St Louis encephalitis virus	Mosquitoes (Culex)	USA
	Japanese encephalitis virus	Mosquitoes (Culex)	Japan, China, SE Asia, India
	Murray valley encephalitis virus	Mosquitoes (Culex)	Australia, New Guinea
	West Nile virus	Mosquitoes (Culex)	USA, Africa, Europe, Middle East, Asia
	Ilheus virus	Mosquitoes (Psorophora)	South and Central America
	Rocio virus	Mosquitoes (?)	Brazil
Tick-borne complex	Far Eastern virus	Ticks (Ixodes)	Eastern Russia
	Central European virus	Ticks (Ixodes)	Central Europe
	Kyassanur Forest virus	Ticks (Haemophysalis)	India
	Louping-ill virus	Ticks (Ixodes)	England, Scotland, N. Ireland
	Powassan virus	Ticks (Ixodes)	Canada, N. USA
	Negishi virus	Ticks (?)	Japan
Bunyaviridae	Californian encephalitis virus	Mosquitoes (Aedes)	W. USA
	La Crosse virus	Mosquitoes (Aedes)	C. and E. USA
	Jamestown Canyon virus	Mosquitoes (Culiseta)	USA, Alaska
	Snowshoe Hare virus	Mosquitoes (Culiseta)	Canada, Alaska, N. USA
	Tahyna virus	Mosquitoes (Aedes, Culiseta)	E. Europe
	Inkoo virus	Mosquitoes (?)	Finland
	Rift Valley virus	Mosquitoes (Culex, Aedes)	E. Africa
Rhabdoviridae	Chandipura virus	Sand flies (Phlebotomus)	India, W. Africa

Table 1.6| **Arboviruses that cause encephalitis**

1.5.2. **Viral encephalitis in India**

India has a high incidence of viral encephalitis and, as in the rest of Asia, the majority of cases were historically attributed to JEV. However a recent analysis of outbreak and surveillance studies indicated a possible shift in the aetiology of viral encephalitis in India with Chandipura virus (CHPV) and enteroviruses accounting for the largest proportion of outbreaks after 2000, whereas JEV was identified as the major agent of acute viral encephalitis from 1975 to 1999 (Joshi *et al.*, 2012). Possible explanations for this alteration in incidence include the high coverage JEV vaccination programme in endemic regions of India allowing the detection of non-JEV causes of acute viral encephalitis with considerably lower incidences and the expansion of diagnostic testing for other causes (Joshi *et al.*, 2012). Highlighting this, there were a number of outbreaks of unconfirmed aetiology that produced encephalitic symptoms between 1954 and 2002 in India in which chikungunya virus, JEV, dengue virus, measles and Reye's syndrome have been tentatively implicated (Rao *et al.*, 2004). These encephalitis outbreaks had clinically identical symptoms to the human epidemics of CHPV encephalitis identified from 2003 onwards and therefore may have also been caused by CHPV (Rao *et al.*, 2004).

There is a temporal difference between CHPV and JEV activity in India, with the majority of CHPV encephalitis cases occurring in late summer and the early monsoon season (June to August) while outbreaks of JEV typically occur late in the monsoon season (from mid-September) (Tandale *et al.*, 2008).

1.5.3. **Human epidemics of Chandipura virus encephalitis**

CHPV was first isolated in 1965 from two adults presenting with febrile illness in Nagpur district, Maharashtra state, India during screening for dengue and

chickungunya viruses (Bhatt & Rodrigues, 1967) and was later isolated from a patient suffering from encephalopathy syndrome in Madhya Pradesh in 1980 (Rodrigues *et al.*, 1983). Following these initial isolations there were no further confirmed human cases of CHPV infections until epidemics of acute encephalitis in children occurred in Andhra Pradesh and Maharashtra in 2003, Gujarat state in 2004 and Maharashtra in 2005 and 2007 (Chadha *et al.*, 2005; Gurav *et al.*, 2010; Tandale *et al.*, 2008). Thus, from 1965 until now the virus has been detected in four adjoining, predominantly rural, central Indian states: Madhya Pradesh, Andhra Pradesh, Maharashtra and Gujarat. The locations of the outbreaks are shown in Figure 1.8. The epidemic case fatality rates were high: 41% in Maharashtra in 2003, 55.6% (183 out of 329 cases) in Andhra Pradesh in 2003, 78.3% (18 out of 23 cases) in Gujarat in 2004 and 44% (34 out of 78 cases) in Maharashtra in 2007 (Chadha *et al.*, 2005; Gurav *et al.*, 2010), giving an average of 54.8%. Additionally, a hospital surveillance study carried out in Telangana district in Andhra Pradesh reported 90 cases of encephalitis from May 2005 to April 2006 with a case fatality rate of 54% (49 out of 90 cases) (Tandale *et al.*, 2008). In 52 of these cases of acute viral encephalitis, CHPV aetiology was confirmed in 25 (by either viral RNA isolation or presence of IgM antibodies against CHPV), JEV aetiology in 5 cases and 22 cases of unknown aetiology (Tandale *et al.*, 2008).

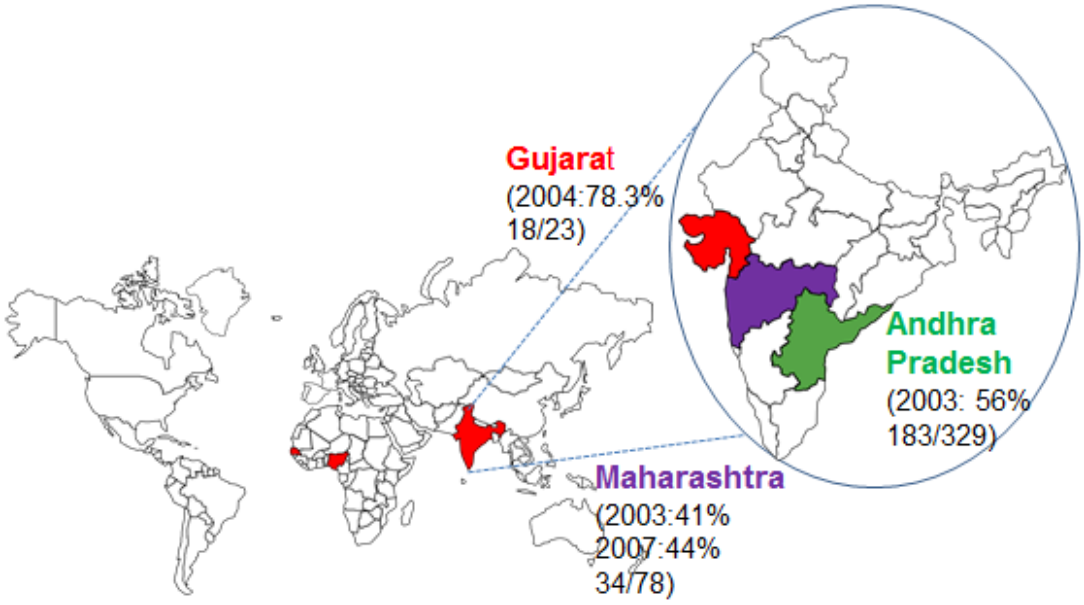

Figure 1.8| **Geographical distribution of CHPV**
Human epidemics have occurred in India and the virus has also been isolated from a pygmy hedgehog in Nigeria and from *Phlebotomus* sandflies in Senegal. The year of each human epidemic and case fatality rate in percentage with the actual values is shown in brackets. There are no figures available for the 2003 Maharashtra outbreak.

The true case fatality rates are likely to have been considerably lower as the figures only include hospital admissions. Added to this, serological studies have shown the virus is widespread in India with 94% (adult non-contacts) to 97% (adult contacts) seropositivity in Andhra Pradesh during 2005 and 2006 (Tandale *et al.*, 2008). The same surveillance study also reported a lower anti-CHPV N antibody seroprevalence in children (70.6% of child non-contacts 73.3% of contacts), indicative of an endemic infection. Isolation of anti-CHPV IgM antibodies from patients with fever but without CNS involvement and family contacts of a CHPV-confirmed case provided evidence of a disease continuum where infection with CHPV does not always result in the most severe manifestation of encephalitis but instead produces mild febrile symptoms or is asymptomatic (Rao *et al.*, 2004). Moreover, during all

of the documented outbreaks encephalitis only occurred in children (Chadha *et al.*, 2005; Rao *et al.*, 2004).

There is a great degree of variation in the quality of available data about the Indian CHPV outbreaks and those for which clear data are available are shown in Table 1.7. The documented clinical manifestations are consistent between the epidemics with all patients studied reporting a fever of rapid onset, which was of less than three days duration on admittance to hospital in 85% of patients in the 2007 outbreak in Maharashtra state (Gurav *et al.*, 2010). In contrast with JEV, a large proportion of patients also reported additional symptoms of vomiting and abdominal cramps (Van Ranst, 2004). The majority of CHPV patients experienced convulsions, altered sensorium and diarrhoea. No neurological sequelae was reported by survivors of any of the CHPV outbreaks (Chadha *et al.*, 2005).

	2003 Andhra Pradesh	**2003 Maharashtra (Nagpur division)**	**2004 Gujarat (Vadodara and Panchmahal)**	**2005- 2006 Andhra Pradesh** Mahatma Gandhi Memorial (MGM) Hospital, Warangal, north Telangana	**2007 Maharashtra (Nagpur division)**
Months	June to September		9th June to 14th July	May 2005 to April 2006	June to September
Case fatality rate	55.6% (183/329)	41% 33 cases	78.3% (18/23)	54.4% (49/90)	43.6% (34/78)
Confirmed cases (presence of virus, viral RNA, IgM antibodies)	50.9% (28 out of 55 cases investigated)		55% (11 out of 19 cases investigated)	48.1% (25 out of 52 cases investigated)	50% (39 out of 78 cases investigated)
Ages of cases	9 months to 14 years		2-16 years (mean age 6.03 years)	9 months-13 years	
Male to female ratio	1: 0.77		1: 1	1: 2	1:1.2
Reported symptoms	Fever (100%), vomiting (54%), altered sensorium (89%), convulsions (82%), diarrhoea (18%), neurological defect (14%), meningeal irritation (7%)		Fever (100%), altered sensorium (100%), convulsions (89%), vomiting (68%) diarrhoea (53%), chills preceding fever in (16%), cough (16%) (details for 19 patients)	Acute onset fever (94%), altered consciousness (90%), convulsions (78%), vomiting (44%), diarrhoea (16%)	Fever (100%), convulsions (76%), altered sensorium (34%), headache (24%), vomiting (45%), diarrhoea (24%) (details for 38 patients)
% deaths within 24 hours of hospitalisation			72.2%		60%
% deaths within 48 hours of hospitalisation				76%	
% identity to the 1965 strain	97% identical to 1965 strain				
Detected in sandflies	Yes, detected in a pool of sandflies in the house of a patient during the outbreak		No, tested 27 female and 54 male Sergentomyia sandflies between July 9 and 11 2004 from peridomestic habitats		In one of 2 pools of sandflies collected locally

Table 1.7| **Summary of CHPV outbreaks**

Key details of the Indian epidemics, including patient information (age, gender), clinical symptoms, case fatality rates, percentage of confirmed cases. Isolations of the virus from phlebotomine sand flies, the putative vector of CHPV are also given. The table is incomplete due to the variation in the data available for each outbreak.

There has been debate in the literature as to whether CHPV was directly responsible for the Indian epidemics of acute encephalitis (John, 2010). Some researchers have argued that a causal relationship has not been fully established, primarily due to the inability to detect the presence of the virus, viral RNA or IgM antibodies in 50% of probable cases. This has led to suggestions that CHPV is a passenger virus which despite being almost ubiquitous in the Indian population has no role in disease (Potharaju & Potharaju, 2006).

1.5.4. **Human clinical studies of CHPV infection**

The documented neurological manifestations of CHPV infection in humans includes abnormal plantar and deep tendon reflexes, slow pupillary reflexes, hypotonia (low muscle tone), hypertonia (increased rigidity of muscles), hemiparesis, facial nerve palsy and generalised convulsions (Chadha *et al.*, 2005; Gurav *et al.*, 2010; Rao *et al.*, 2004; Tandale *et al.*, 2008). However, neurological sequelae in survivors were uncommon. CSF analyses (colour, opening pressure, cell count, protein, glucose levels) were within the normal range in the majority of cases, although a clinical investigation of the 2005-2006 Andhra Pradesh outbreak reported increased intracranial pressure in 25% (13 out of 52) of patients (Tandale *et al.*, 2008). Diffuse edema of the brain parenchyma was observed by computerised tomography (CT) in 15% (8 out of 52) of cases during the 2005-2006 Andhra Pradesh epidemic (Tandale *et al.*, 2008).

1.5.5 **Non-human isolations of CHPV**

The only known natural route of transmission of CHPV is by female phlebotomine sand flies (Mavale *et al.*, 2007; Rao *et al.*, 2004) as is the situation for the majority of vesiculoviruses. However, transmission by *Aedes aegypti* mosquitos has also been

demonstrated in the laboratory (Mavale *et al.*, 2005). The virus has been isolated from pools of phlebotomine sandflies during the 2003 and 2007 (Gurav *et al.*, 2010) Indian epidemics, although the species of sandfly were unidentified. One study detected the virus in sandflies of the genus Sergentomyia which were collected in Andhra Pradesh following the 2005 outbreak (Geevarghese *et al.*, 2005). In the laboratory, vertical and venereal transmission of the virus by *Phlebotomus papatasi* (Mavale *et al.*, 2006; Tesh & Modi, 1983) and transmission by bite by *P. argentipes* (Mavale *et al.*, 2007), the predominant species in CHPV endemic areas, has also been demonstrated. No human to human transmission has been documented. Most of the human epidemics occurred during the monsoon period (July to December) when sandflies are present in their largest numbers (Rao *et al.*, 2004). CHPV seropositive animals have been detected in large parts of India demonstrating the widespread presence of CHPV infection (Jortner *et al.*, 1973) and also in domestic animals during the 2003 Indian epidemic (Joshi *et al.*, 2005).

CHPV has also been isolated in West Africa: from a pygmy hedgehog in northern Nigeria (Fontenille *et al.*, 1994) and from *Phlebotomus* sandflies in Senegal (Traore-Lamizana *et al.*, 2001), indicating the virus may be widespread in tropical regions (Figure 1.8). Low seroprevalence of CHPV antibodies in the torque macaque population in Sri Lanka has also been demonstrated (1.74%, 2 out of 115 tested) (Peiris *et al.*, 1993).

1.6. Experimental CHPV infection and disease

1.6.1. **CHPV infection in cultured cells**

As with VSV, CHPV has a wide host range and can replicate in avian, mammalian and insect cells in culture, although the cytopathic effects (CPE) seen following

infection differ markedly. The virus is highly cytopathic within a few hours in mammalian and CE cells and establishes a persistent infection with no CPE in insect cell lines despite the insect cells being highly susceptible to infection (Jadi *et al.*, 2010). Interestingly the recently characterised rhabdovirus Niakha virus, which is postulated to be transmitted by phlebotomine sandflies, produces CPE in mammalian cells and in the mosquito cell line C6/36 (*Aedes albopictus*) but not in sandfly PP-9 (*Phlebotomus papatasi*) cells (Vasilakis *et al.*, 2013a).

1.6.2. **Mouse model of CHPV pathogenesis**

Mice are susceptible to CHPV infection and inoculation into the brain results in fatal encephalitis (Rao *et al.*,2004). The virus has also been shown to cross the blood brain barrier to infect the CNS (after intraperitoneal or intravenous administration) resulting in a dose-dependent encephalitis (preceded by viremia) in young mice but not in adults (Balakrishan and Mishra, 2008). In adult mice infection leading to encephalitis is only achieved by direct intracranial inoculation into the brain (Sokhei & Obukhova, 1984), though a single report suggested that intranasal inoculation in adult mice may lead to infection and seroconversion. The mechanism of age-dependent susceptibility of CHPV-induced encephalitis has not been characterised, however, important contributory factors are likely to include an immature host immune response and immature nervous system in young mice (Balakrishnan & Mishra, 2008). A range of other neurotropic viruses have also been shown to produce age-related CNS disease including Japanese Encephalitis (JE), Yellow fever, St Louis Encephalitis, West Nile, Sindbis, measles, Semliki Forest and Herpes viruses (Oliver & Fazakerley, 1998).

Young mice infected with CHPV display a progressive paralysis prior to death. The first signs of encephalitis are uncoordinated movements and unilateral paralysis of the hind limb nearest the injection site at approximately three days post infection. Paralysis progresses rapidly: bilateral hind limb paralysis occurring 3-4 days after infection, forelimb paralysis at about day 4-5 after which the mice succumb to infection, although the precise timings are both strain- and dose-dependent (Jortner *et al.*, 1973).

In young mice inoculated with CHPV intraperitoneally, virus was detected in the blood, skeletal muscle, liver, lung, spleen and subsequently at high titres in the brain (Jortner *et al.*, 1973). These findings suggest that peripheral infection of CHPV in young mice produces plasma viraemia allowing the virus to be disseminated throughout the body via haematogenous spread. Also the higher brain viral titres indicate that the virus has a predilection for replication in the CNS or that virus is removed from the blood and other tissues due to the rapid production of anti-CHPV IgM antibodies (Balakrishnan & Mishra, 2008). A recent study detected rising levels of CHPV RNA in nervous tissue progressively further away from the site of inoculation during the course of infection, following inoculation of the virus into a hind footpad of suckling mice (Anukumar *et al.*, 2013). This indicates that CHPV may also disseminate to the brain by axonal transport following infection of peripheral nerves.

Pathology associated with CHPV infection is mainly restricted to the CNS with marked necrotic lesions in the cerebellum, hippocampus, olfactory bulb and spinal cord grey matter (Jortner *et al.*, 1973). Necrosis was not detected in the other tissues that were shown to contain virus (lungs, liver, spleen, skeletal muscle). Apoptotic cells, as determined by TUNEL staining, have been observed in the brains of young

mice 24 hours after intraperitoneal inoculation of the virus (Anukumar *et al.*, 2013). In addition, CHPV-infected neuronal cells were shown to undergo apoptosis via the Fas-dependent extrinsic apoptotic pathway (Ghosh *et al.*, 2013).

There is a small but growing literature on the immunology of CHPV infection. The innate immune response was shown to be intrinsic in infection outcomes. Experimentally infected mice had upregulated levels of proinflammatory cytokines and children who survived an infection with CHPV produced high levels of TNF-α (Balakrishnan & Mishra, 2008). Significantly fewer CD4, CD8 and CD19 positive cells were also present in infected mice (Balakrishnan & Mishra, 2008). Moreover, a role for Toll-like receptor 4 (TLR4) in CHPV pathogenesis was established. TLR4-mutant mice secreted significantly elevated levels of the cytokines MCP-1 and IFN-γ and had improved survival rates compared with the control mice which expressed wild type TLR4 (Anukumar & Shahir, 2012).

1.7. Aims

The aim of this project was to investigate the factors involved in CHPV host range. This had two principle objectives: to characterise the host range *td*CE phenotype of CHPV and to investigate the neuropathogenesis of the virus. The first objective involved determining the underlying molecular basis of host range specificity of three *td*CE mutants of CHPV. The effects of the specific mutations shown to affect host range on the formation of virus replication complexes in permissive and non-permissive cells were explored.

The second objective to investigate CHPV CNS disease involved establishing an *in vivo* model of CHPV-induced encephalitis. Using this model, the site of CHPV

replication in the mouse brain and the pattern of dissemination of the virus were identified.

CHAPTER 2

2 Materials and Methods

2.1. Cell lines and culture

2.1.1. Cell lines

The continuous African green monkey kidney cell line, BSC-1 and chick embryo fibroblasts (CE), prepared by previous members of the PVL laboratory were used to investigate the *td*CE mutant phenotype. The BSR-T7 cell line which was derived from the BHK-21 cell line and constitutively expresses the bacteriophage T7 RNA polymerase (Buchholz *et al.*, 1999) was used in all minigenome and full-length virus rescue transfections. BSC-1 cells were routinely maintained in Glasgow Modified Eagle's Medium (GMEM) supplemented with 10% foetal bovine serum (FBS), 0.2 mM L-glutamine and 100 µg/ml penicillin/streptomycin. BSR-T7 cells were also grown in complete GMEM (as described above) and every second pass in GMEM supplemented with 1 mg/ml G418, an aminoglycoside antibiotic that prevents polypeptide synthesis by irreversibly attaching to the 80S ribosomal subunit. G418 is required for the selection of cells stably transfected with a plasmid encoding the T7 polymerase and the neomycin-phosphotransferase gene which confers resistance to G418. Primary cultures of CE cells were maintained in medium 199 supplemented with 10% FBS, 0.2 mM L-glutamine and 100 µg/ml penicillin/streptomycin.

The mosquito (*Aedes albopictus*) cell line, C6/36 (Igarashi, 1978), was used to investigate the difference in cytopathic effect of CHPV in mammalian and insect cells. C6/36 cells were grown in Leibovitz's L-15 medium with 10% FBS, 0.2 mM L-glutamine and 100 µg/ml penicillin/streptomycin. The packaging cell line HEK

293T was used to generate lentivirus for pseudotyping experiments as they constitutively express the large T antigen of simian virus 40 (SV40). HEK 293T cells were grown in Dulbecco's Modified Eagle's Medium (DMEM) with 10% FBS, 0.2 mM L-glutamine and 100 µg/ml penicillin/streptomycin. The astrocytoma U373, human embryonic oligodendrocyte Oligo/TL, human rhabdomyosarcoma (RD) and hepatocellular carcinoma Hep-2 cell lines were also used in this investigation. U373 cells were cultivated in Eagle's Minimal Essential Medium (EMEM), while Oligo/TL, RD and Hep-2 cells were grown in DMEM, all supplemented with 10% FBS, 0.2 mM L-glutamine and 100 µg/ml penicillin/streptomycin.

2.1.2. Maintenance of cells in culture

Cultures of each of the cell lines were grown in 75 cm^2 tissue culture flasks with 20 ml of the appropriate medium and incubated at 37°C in 5% CO_2, except C6/36 cells which were incubated at 28°C without CO_2. Cells were passaged every 3-4 days in 1 in 4 (C6/36, U373) 1 in 6 (BSC-1, Hep-2 and CE) or 1 in 8 (BSR-T7, 293T, Oligo/TL and RD) dilutions. Confluent monolayers of cells were washed in 1:6 trypsin (0.25% (w/v) trypsin in PBS, pH 7.4 (137 mM NaCl, 2.7 mM KCl, 10 mM Na_2HPO_4, 1.8 mM KH_2PO_4) /versene (0.02% (w/v) EDTA and 0.002% (w/v) phenol red in PBS, pH 7.4) before incubation at 37°C (28°C for C6/36 cells) with trypsin until all the cells had detached from the flask surface, approximately 5-10 minutes. Growth medium was then added to inhibit trypsin activity and cells were resuspended to a homogenous suspension and an aliquot transferred to seed a new flask or roller bottle containing fresh medium or a tissue culture plate.

2.1.3. CHPV minigenome rescue

BSR-T7 cells were seeded into 12-well tissue culture plates 24 hours before transfection so that the cells were approximately 70% confluent when transfected. 0.6 µg pT7N, 0.1 µg pT7P, 0.1 µg pT7L and 0.2 µg mgT7NGFPL (a minigenome containing an eGFP reporter gene cloned between the N and L gene) were transfected using *Trans*IT®-LT1 transfection reagent (Mirus, USA). DNA was added to Opti-MEM® Reduced Serum Medium (Invitrogen Life Technologies, UK) and gently mixed before 3 µl of *Trans*IT®-LT1 transfection reagent was added to the diluted DNA. The *Trans*IT®-LT1 reagent: DNA complexes were gently mixed and incubated at room temperature for 15-30 minutes, after which the complexes were added dropwise to the cells and incubated at 37°C for 24 hours. The level of GFP expression was determined by fluorescence microscopy. The plasmids used in the minigenome rescue were all obtained from Dr A. C. Marriott (Marriott & Hornsey, 2011).

2.1.4. Rescue of infectious recombinant viruses

BSR-T7 cells grown to approximately 70% confluence were transfected with 0.8 µg pT7CV (the whole genome clone) and the support plasmids in the following proportions: 0.2 µg pT7N, 0.15 µg pT7P, 0.15 µg pT7L using 6 µl *Trans*IT®-LT1 transfection reagent, as described in section 2.1.3. 48 hours after transfection the supernatant (containing virus) was inoculated onto confluent monolayers of BSC-1 cells growing in complete GMEM with 2% FBS. The supernatant was harvested approximately 24 hours post infection.

2.1.5. Generation of CHPV-G glycoprotein pseudotyped lentivirus

The established HIV-1-based self-inactivating lentiviral vector system (Coleman *et al.*, 2003) was used to generated lentivirus pseudotyped with the CHPV G glycoprotein. The CHPV G gene was cloned into the pHEF-VSVG envelope plasmid (Addgene plasmid 22501) to give pHEF-CHPVG. HEK 293T cells grown to approximately 90% confluence in T75 cm^2 tissue culture flasks were transfected with 7.1 µg pNHP (Addgene plasmid 22500), 3.5 µg pTYF-1xSYN-EGFP (Addgene plasmid 19973) and 2.8 µg of either pHEF-VSVG or pHEF-CHPVG. Virus was harvested 24 hours and 48 hours post-transfection and pooled.

2.1.6. Cryopreservation of cell lines

Cells were treated with trypsin/versene as described in section 2.1.2. Following addition of complete growth medium, the cells were transferred into falcon tubes and centrifuged at 1,300 rpm in a benchtop centrifuge (Sorvall Legend) at 4°C for 5 minutes. The supernatant was then discarded and the cells resuspended in an appropriate volume (1 ml per T75 cm^2 tissue culture flask) of freezing medium, comprising of 90% FBS and 10% dimethyl sulfoxide (DMSO) (Sigma, USA). Aliquots were transferred into cryovials and placed in a Mr Frosty freezing container (Thermo Scientific, USA) which was immediately placed at -70°C. For long-term storage (>1 month), vials of cells were transferred to liquid nitrogen after 24 hours at -70°C.

2.2. Viruses and virus growth

2.2.1. Viruses

CHPV strain I653514 (GenBank accession number KF468775) and temperature sensitive derivatives from it (Gadkari & Pringle, 1980) (GenBank accession numbers KF468772, KF468773, KF468774 for *td*CE mutants CH112, CH157 and CH256 respectively) were obtained from Prof. A.J. Easton. Recombinant viruses CVeGFP (which contains the gene for enhanced green fluorescent protein inserted between the M and G genes of CHPV) and CVPRFP (in which the red fluorescent protein ORF mRFP1 (Campbell *et al.*, 2002) was fused in-frame within a putative hinge region of the CHPV phosphoprotein, between residues 213 and 214 of P) were made by Dr A.C. Marriott.

2.2.2. Growth of CHPV stocks

BSC-1 cells were grown to confluence in glass roller bottles and infected with CHPV at a M.O.I. of 0.01 pfu/cell in complete GMEM with 2% FBS. Cells were incubated at 37°C and virus harvested when all cells exhibited CPE, approximately 24-48 hours after infection. Sterile glass beads were used to break open any remaining cells that had not lysed. Cell debris was removed by low speed centrifugation and aliquots of the virus stocks were stored at -70°C.

2.2.3. Determination of virus titre by plaque assay

Cells were grown to 90-100% confluence in 6 well plates. Serial, 10-fold dilutions of virus were made up to the 10^{-9} dilution and 200 µl of the virus dilutions (or mock) were used to inoculate each well, with each dilution assayed in duplicate. The cells were incubated with the inoculum at the required temperature for 1 hour. Following

this, the inoculum was removed and 1% carboxymethyl cellulose (CMC)-GMEM (supplemented with 2% FBS, 0.2 mM L-glutamine and 100 µg/ml penicillin/streptomycin) overlay was added to each well. Cells were then incubated at the required temperature. Once plaques were clearly visible cells were fixed using 4% gluteraldehyde in PBS for 2 hours at room temperature followed by staining with crystal violet for 15 minutes. The plates were then washed, dried and plaques counted.

2.2.4. Microplaque assay

BSC-1 cells were grown to 90% confluence in 96 well tissue culture plates and infected in triplicate with 10-fold serial dilutions of wild-type CHPV for 1 hour at 37°C. Following this, the inoculum was replaced with complete GMEM with 2% FBS and incubated for 6 hours. The cells were then fixed with 1:1 acetone: methanol for 1 hour, washed once in TBS (50 mM Tris-HCl pH 7.5, 150 mM NaCl) and blocked in 1% (w/v) BSA in TBS for 1 hour at room temperature. Cells were washed once in TBS before being incubated with 50 µl of polyclonal sheep anti-CHPV antibody (diluted 1 in 100 in 1% BSA (w/v) in TBS) for 1 hour at room temperature. The cells were washed three times in TBS prior to incubation with 50 µl of donkey anti-sheep biotin (Amersham LS) diluted at 1 in 400 in 1% BSA (w/v) in TBS for 1 hour. After three washing steps, 50 µl of alkaline phosphatase-conjugated streptavidin at 1 in 3000 in 1% BSA (w/v) in TBS was added to the cells and incubated for 1 hour. The cells were washed three times in TBS and alkaline phosphatase activity was detected using the BCIP/NBT (5-bromo-4-chloro-3-indolyl-phosphate/nitro blue tetrazolium) detection system, according to the manufacturer's instructions (Sigma).

2.2.5. Virus growth curves

BSC-1 or CE cells were grown to 90-100% confluence in 6 well plates and infected with the appropriate virus at an M.O.I. of 10 pfu/cell. The inoculum was incubated at 33°C for 1 hour, after which the cells were washed three times in PBS and 3 ml of complete medium with 2% FBS was added. Medium was removed at 0, 1, 2, 3, 4, 5, 6, 7, and 8 hours post infection and the virus titre at each time point deduced by plaque assay (section 2.2.3). The assays were performed in duplicate.

2.2.6. Semi-purifying virus

Virus was underlaid with a 20% sucrose cushion in PBS and centrifuged at 120,000 x g for 45 minutes in a Beckman Coulter optima L-90K ultracentrifuge, SW50.1 rotor at 4°C. The pellet was resuspended in PBS.

2.3. Mice

All animal experiments were approved by the University of Warwick's Ethical Review Committee and the UK Home Office.

2.3.1. *In vivo* infection with CHPV

8 day old ICR (CD1) mice (bred in-house) of both sexes were used to investigate the neuropathogenesis of CHPV. Litters of 6 mice (housed with their mothers) were used in the study. Animals were kept at 19-23°C and 45-65% relative humidity. Mice were inoculated intraperitoneally with wild-type or recombinant CHPV at the required dose (or PBS as a control) in a volume of 50µl. After infection, mice were monitored, given a clinical score and each group of mice was weighed daily (or twice

daily for titration experiments, see section 2.3.2). The quantitative clinical scoring system used in all experiments required individual mice to be scored as follows: 1 point for healthy, 2 points for displaying the first signs of clinical disease (abnormal gait), 3 points for unilateral hind limb paralysis (at the side adjacent to the site of inoculation), 4 points for paralysis in two limbs or showing little activity, 5 points for dead. The animals were monitored for a maximum of 10 days. Any animals presenting with bilateral paralysis (score of 4) were immediately culled using a schedule 1 method. All surviving animals were culled using a schedule 1 method at the end of the 10 day observation period.

2.3.2. Titration of CHPV

In order to determine the dose of the strains of CHPV required to cause encephalitis groups of 3 animals were infected by the intraperitoneal route with various doses of CHPV, starting at a dose of 1.0×10^4 pfu (informed by an earlier study). If no disease was seen a further group of three mice was infected with 3.1×10^4 pfu of virus and observed. Conversely the dose was lowered if the disease onset was too rapid and a further group of three animals was tested. The process was repeated (increasing by half log increments or lowered appropriately) until a dose of virus was identified that caused observable disease in all three animals with bilateral paralysis seen on or near day three after infection. The animals were monitored twice daily from the time of infection for signs of disease and the weight of the group was measured daily.

2.3.3. Timecourse of infection with CHPV

Using the information from the procedure described in section 2.3.2. 5 groups of 6 mice were infected with a dose of wild type or mutant CHPV sufficient to cause

signs of clinical disease (as described in section 2.3.1.) and one group of 6 mice was inoculated with PBS. All infected and control mice were observed at daily intervals for signs of disease and the weight of the animals in each group was recorded. At daily intervals 1 mouse from each experimental group was sacrificed using a schedule 1 method. The process concluded when the remaining mice presented with bilateral paralysis or at ten days after infection, whichever was sooner, at which point all animals affected were sacrificed. The brains were removed from all of the sacrificed animals and divided into two (down the midsagittal plane). One half of each brain was fixed in 4% paraformaldehyde in PBS for pathological examination and the other frozen at -70°C (for storage).

2.3.4. Homogenising tissue

Brain samples (section 2.3.3.) were thawed and homogenised in 500 µl PBS using a 21 gauge needle. Lungs, kidneys, liver samples were homogenized with sterile sand in a pestle and mortar in 1 ml PBS and centrifuged to remove debris before titrating (section 2.2.3.).

2.3.5. Sectioning of fresh brain tissue

Immediately after harvesting, brains were transferred in ice-cold ACSF (low sodium Artificial Cerebrospinal Fluid; 1mM calcium chloride, 10mM D-glucose, 4mM potassium chloride, 5mM magnesium chloride, 26mM sodium bicarbonate, 246mM sucrose, pH 7.3) previously bubbled with carbogen (95% oxygen, 5% CO_2). 300 µM coronal sections or parasagittal cerebellar sections were then made using a vibrotome. The sections were fixed in 4% paraformaldedyde in PBS overnight, in preparation for immunohistochemistry (section 2.8.3.).

2.3.6. Deparaffinisation and rehydration of paraffin-embedded sections

Paraffin-embedded brain sections were incubated in clearene solvent, a xylene substitute (Leica Biosystems) and washed in decreasing concentrations of ethanol (100, 95, 70, 50 and 30%).

2.3.7. Heat-induced antigen retrieval

Brain sections were microwaved (750 W) in sodium citrate buffer (0.1M Citric acid monohydrate, 0.1M Tri-sodium citrate) for 12 minutes and allowed to cool for 20 minutes. The sections were incubated with 20 µg/ml proteinase K solution at 37°C in a humid chamber for 15 minutes. Immunohistochemical staining was then performed (section 2.8.3).

2.4. Organotypic mouse cerebellar slice cultures

2.4.1. Preparation and culture of cerebellar slice cultures

Immediately after harvesting, brains were transferred in ice-cold ACSF previously bubbled with carbogen (as above). The cerebellum was then sliced in parasagittal sections of 300 µM using a vibrotome and transferred to tissue culture plates containing culture plate inserts. The slices were cultured in 75% Minimum Essential Medium (MEM), 25% heat-inactivated horse serum, 25 mM HEPES, 1mM glutamine, 5mg/ml glucose, 100 µg/ml penicillin/streptomycin at 37°C in 5% CO_2.

2.4.2. Viral infection of cerebellar slice cultures

The slices were cultured (section 2.4.1.) for seven days before infection with 1 x 10^6 pfu of CVeGFP. The medium was replaced 90 minutes after infection. 24 hours

post-infection, the sections were fixed in 4% paraformaldehyde in PBS overnight. The fixed sections were used in immunohistochemistry to detect brain cell-specific markers (section 2.8.3.).

2.5. Bacterial culture

2.5.1. Bacterial culture

E.coli DH5α were streaked onto L-broth agar plates (1% (w/v) bacto-tryptone, 1% (w/v) sodium chloride, 0.5% (w/v) yeast extract and 2% (w/v) agar) containing 100 µg/ml ampicillin (if the bacteria carried plasmids conferring ampicillin resistance) and incubated overnight at 37°C. Single colonies from freshly streaked plates of bacteria were picked, placed into 5 ml L-broth (1% (w/v) bacto-tryptone, 1% (w/v) sodium chloride and 0.5% (w/v) yeast extract at pH7.5) containing, if required, 100 mg/ml ampicillin and incubated at 37°C with shaking (250 rpm) overnight.

2.5.2. Preparation of competent *E.coli* DH5α cells

Overnight cultures of *E.coli* DH5α (section 2.5.1.) were diluted 100-fold in pre-warmed L-broth and grown at 37°C with shaking (250 rpm) until the cells reached an optical density of 0.39 when measured at a wavelength of 600 nm. The cultures were immediately placed on ice for 5 minutes and then centrifuged at 2000 rpm for 15 minutes at 4°C in a benchtop centrifuge. The bacterial cell pellet was resuspended in 2/5 of the original culture volume of filter sterilised ice-cold TfbI buffer (30 mM potassium acetate, 100 mM rubidium chloride, 10 mM calcium chloride. 50 mM manganese chloride, 15% (v/v) glycerol at pH 5.8 adjusted with 0.2 M acetic acid) and left on ice for 1 hour. Following this, the cells were centrifuged

as before and the resultant pellet resuspended in 1/25 of the original culture volume in filter sterilised ice-cold TfbII buffer (10 mM 3-(N-Morpholino)propanesulfonic acid (MOPS), 75 mM calcium chloride, 10 mM rubidium chloride, 15% (v/v) glycerol at pH 6.5 with 1M potassium hydroxide) and left on ice for 2 hours. The competent cells were then aliquoted, snapped frozen in liquid nitrogen and stored at -70°C.

2.5.3. Transformation of competent cells and culture of transformants

100 ng of plasmid DNA was added to 100 µl of competent *E.coli* DH5α cells (section 2.5.2.), gently mixed and placed on ice for 20 minutes. The bacteria were then heat shocked at 42°C for 1 minute before being returned to ice for a further 2 minutes. Following the addition of 900 µl of pre-warmed L-broth, the cells were incubated at 37°C with shaking at 200 rpm for between 30 minutes and an hour. After this, 50 µl, 100 µl and 150 µl aliquots of the culture was spread out onto L-broth agar plates containing 100 mg/ml ampicillin and incubated overnight at 37°C. For blue/white screening to identify transformed bacteria containing the insert of interest L-broth agar plates supplemented with 40 mg/ml X-gal dissolved in dimethylformamide, 100 mg/ml isopropylthiogalactoside (IPTG) and 100 mg/ml ampicillin were used. Single colonies (white colonies if blue/white screening) were picked and then cultured as described in 2.5.1.

2.5.4. Preparation and recovery of glycerol stocks of bacteria

Bacteria containing plasmids of interest were stored in 30% glycerol at -70°C. The bacteria were recovered by streaking onto selective agar plates and incubating overnight at 37°C.

2.6. DNA techniques

2.6.1. Plasmid DNA purification from transformed *E.coli*

Overnight cultures of *E.coli* (2.5.1) were centrifuged at 3,000 x g for 10 minutes and the supernatant removed. The QIAGEN Plasmid Mini kit and Plasmid Maxi kit (QIAGEN, The Netherlands) were used, according to the manufacturer's protocols, for the small and large scale extraction of plasmid DNA from overnight cultures of *E.coli*. Alternatively, for small scale preparation of plasmid DNA, pelleted bacteria were resuspended in 200 µl solution 1 (50 mM EDTA, 50 mM glucose, 25 mM Tris-HCl pH8. 5 µg/ml RNase A), lysed with the addition of 200 µl solution 2 (0.2 M NaOH, 1% SDS) and then neutralised with the addition of 350 µl solution 3 (3 M KOAc, 2 M acetic acid). Samples were centrifuged at 13,000 rpm for 10 minutes in a bench top microfuge and a 1 x volume of isopropanol was added to the recovered supernatant. After mixing the mixture was centrifuged at 13,000 rpm for 20 minutes, as before, the supernatant was discarded and the pellet washed with 70% ethanol. The plasmid DNA was eluted from the pellet in an appropriate volume of sterile water (usually 50 µl). DNA concentration was subsequently determined using a Nanodrop spectrophotometer at 260 nm.

2.6.2. Polymerase Chain Reaction (PCR)

High-fidelity PCR using proof reading polymerases *Pfu* (Promega, USA) or *KOD* hot start DNA polymerase (Novagen, Germany) was carried out when downstream cloning and DNA sequencing was required. *Pfu* DNA polymerase was used for the amplification of DNA of up to 2 kb whereas *KOD* hot start DNA polymerase was employed when DNA fragments of over 2 kb were amplified.

For PCR reactions using *Pfu*: 1 x final concentration of *Pfu* DNA polymerase 10 x buffer with $MgSO_4$, 200 µM each dNTP (Fermentas) 0.5 µM forward primer, 0.5 µM reverse primer (Integrated DNA Technologies, refer to appendix for sequences), 6 ng DNA template, 1.25 U *Pfu* and nuclease-free water to a final volume of 50 µl were added to thin-walled PCR tubes. The standard PCR reaction mix using *KOD* hot start DNA polymerase contained 1 x buffer for *KOD* hot start DNA polymerase, 0.2 mM dNTPs, 1 mM $MgSO_4$, 6 ng template DNA, 0.3 µM forward primer, 0.3 µM reverse primer, 1 U/µl *KOD* in a total volume of 50 µl. All PCR mixtures were mixed and briefly centrifuged before being transferred to a thermal cycler. The standard reaction conditions were 94°C for 5 minutes, then 30 cycles of 94°C 20 seconds, 55 °C for 30 seconds and 72°C for 1 minute per kb of DNA to be amplified, followed by 72 °C for 10 minutes. Changes to the annealing temperature were sometimes required. PCR products were purified from primers, nucleotides and other impurities from the PCR reaction prior to downstream reactions using QIAquick PCR purification kit (Qiagen).

2.6.3. Quickchange site-directed mutagenesis

Quickchange site-directed mutagenesis was performed using *Pfu* DNA polymerase. The reactions contained 1 x final concentration of *Pfu* DNA polymerase 10 x buffer with $MgSO_4$, 100 ng DNA template, 100 ng forward primer, 100 ng reverse primer, 1 µl 10 mM dNTP mix, 1 µl *Pfu* and made up to 25 µl nuclease-free water. The mixtures were mixed, briefly centrifuged and placed in a thermal cycler programmed for 95°C for 1 minute, then 18 cycles of 95°C for 1 minute, 55°C for 1 minute and 65°C for 1 minute per kb of plasmid length.

2.6.4. Agarose gel electrophoresis

Agarose gels were made at the appropriate percentage required for the length of DNA fragments to be electrophoresed: from 0.7 to 2% (w/v) agarose in TBE buffer (89 mM Tris-HCl pH 7.5, 89 mM boric acid, 10 mM EDTA, altered to pH 8). 0.5 µg/ml ethidium bromide was added prior to the gel being poured. 1 x DNA loading buffer (0.25 % (w/v) bromophenol blue, 30% glycerol) was added to each DNA sample, after which they were loaded onto the gel alongside 5 µl Hyperladder 1 (Bioline) size marker. Agarose gels were run at 140 V for 30 minutes for 30 ml gels or 1 hour for 100 ml gels.

2.6.5. Extraction of DNA from agarose gels

Fragments of interest were excised from agarose gels using a clean scalpel and the DNA was extracted and purified from the gel using the QIAquick gel extraction kit (QIAGEN), following the manufacturer's instructions and eluting in 30 µl EB buffer.

2.6.6. Restriction digestion

Up to 1 µg DNA was digested using 1 unit of the required restriction endonuclease(s) (Fermentas, New England Biolabs) at the optimal incubation temperature for the enzyme (usually 37°C) for more than 1 hour. The reaction mixture contained the 1 x buffer recommended by the manufacturer and made up to a total volume of 20 µl with sterile water. FastDigest® restriction enzymes (Fermentas) were incubated in either FastDigest or FastDigest green buffer (for the direct loading of the digest on a gel) at the appropriate temperature for 5 minutes. All digestion mixtures were gently mixed and centrifuged briefly prior to incubation.

2.6.7. Ligation

Cohesive and blunt ended ligation of a single insert was performed at an insert: vector molar ratio of 3:1 using T4 DNA ligase (Fermentas). 100 ng of vector DNA, insert DNA (3:1 molar ratio over the vector DNA), 1 x T4 DNA ligase buffer and 1 unit of T4 DNA ligase were added together in total volumes of 20 µl, mixed and incubated at either 16°C overnight or for 1 hour at room temperature.

2.6.8. DNA sequencing

400 ng of purified plasmid DNA or 250 ng PCR product was added to 25 pmol of primer in 10 µl total volume. DNA sequencing was carried out by GATC, Germany.

2.7. RNA techniques

2.7.1. Viral RNA extraction

Virus RNA was isolated from virus stocks (cell supernatant) and homogenized tissue samples (2.3.4.) using TRIzol LS reagent® (Invitrogen Life technologies), according to the manufacturer's protocol. RNA concentration was determined using a Nanodrop spectrophotometer.

2.7.2. Reverse transcription

For each sample 1 x reaction buffer, 1 mM final concentration of dNTP mix, 100 pmol random hexamers (Fermentas) or specific primer, up to 2 µg RNA and 200 units of RevertAid™ Reverse Transcriptase (Fermentas) made up to 20 µl with RNase-free water was added to thin-walled PCR tubes. The samples were briefly

mixed and centrifuged. An automated PCR machine was then used to carry out sequential incubations of 42°C for 1 hour, followed by 70°C for 15 minutes.

2.8. Protein techniques

2.8.1. Antibodies

Antibody	Source	Dilution used
Anti gaba-a receptor α6	Merck Millipore (AB5610)	1:400
ANTI-FLAG® M2 magnetic beads	Sigma (M8823)	n/a
Blotting grade goat anti-mouse antibody	BioRad	1:3000
Blotting grade goat anti-rabbit antibody	BioRad	1:3000
Donkey anti-goat (Alexa Fluor®488	Abcam (ab150129)	1:1000
Fluorescein horse anti-mouse IgG antibody	Vector Labs (FI-2000)	1:200
Goat anti-GFP	Abcam (ab5450)	1:500
Goat anti-mouse (Alexa Fluor®568)	Abcam (175473)	1:1000
Goat anti-rabbit (Alexa Fluor®594)	Abcam (150080)	1:1000
Monoclonal ANTI-FLAG® M2 antibody produced in mouse	Sigma (F1804)	1:500
Mouse anti-bIII tubulin	Abcam (ab11314)	1:500
Mouse anti-calbindin	Abcam (ab82812)	1:1000
Mouse anti-cc1	Abcam (ab16794)	1:500
Mouse anti-MAP2	Abcam (ab28032)	1:500
Mouse anti-MBP	Abcam (ab62631)	1:500
Mouse anti-neuN	Abcam (ab104224)	1:200
Rabbit anti-cd11b	Abcam (ab133357)	1:200
Rabbit anti-GFAP	Abcam (ab7260)	1:500
Rabbit anti-NG2	Abcam (ab101807)	1:200
Rabbit anti-olig2	Abcam (ab81093)	1:500
RFP rabbit polyclonal antibody, purified	Invitrogen (R10367)	1:500
RFP-Trap® magnetic particles	Chromotek (rtm-20)	n/a

2.8.2. Immunofluorescence

Cells were grown on sterile glass coverslips in 12 well plates and infected with the appropriate virus. At the required time post-infection cells were firstly washed twice in PBS, fixed in 10% formaldehyde in PBS for 10 minutes at room temperature, then washed three times in PBS and permeabilised by incubation with 0.5% NP40 in PBS for 10 minutes. After a further three PBS washing steps, cells were blocked in 1% (w/v) BSA in PBS for 1 hour at room temperature. Following this, cells were washed once in PBS before being incubated with 250 µl primary antibody at the required dilution in 1% BSA (w/v) in PBS for 1 hour at room temperature. Anti-Flag M2 antibody (Sigma) was diluted 1 in 500. The cells were washed three times in PBS prior to incubation with the secondary antibody coupled to a fluorophore at the appropriate dilution in 1% BSA (w/v) in PBS for 45 minutes in the dark. A 1 in 200 dilution of horse anti-mouse FITC-conjugated secondary antibody (VectorLabs) was used. After this, the cells were washed three times in PBS and mounted onto glass slides using aqueous mounting medium containing DAPI. Fluorescence was visualised using the Leica SP5 confocal fluorescence microscope.

2.8.3. Immunohistochemistry

After fixing brain sections in 4% paraformaldehyde in PBS overnight, the slices were washed in PBS and left in blocking solution (PBS containing 10% Normal goat serum (NGS), 0.2% Triton x100) for 4-6 hours at room temperature. The blocking solution was then removed and primary antibody diluted in carrier solution (PBS containing 10% NGS, 0.05% triton) was added and incubated overnight at 4°C. After four washes in PBS the secondary antibody diluted in carrier solution was applied and the slices incubated for 4 hours at room temperature in the dark. The

slices were washed four times in PBS and mounted onto slides with coverslips with aqueous mounting medium.

2.8.4. Whole cell lysates

Cells were grown in T75 cm^2 tissue culture flasks and infected with virus. Cells were washed in PBS and harvested using a cell scraper before being transferred into a falcon tube. Cells were pelleted by centrifugation at 2,000 x g in a benchtop centrifuge at 4°C for 5 minutes. The supernatant was then discarded and the cell pellet (approximately $1x10^7$ cells) resuspended in 200 µl of lysis buffer (10 mM Tris/Cl pH7.5, 150 mM NaCl, 0.5 mM EDTA, 0.5% NP-40) and incubated on ice for 30 minutes. Cells were transferred to tubes and microfuged at maximum speed for 5 minutes after which lysates were removed and stored at -70°C.

2.8.5. Immunoprecipitation of Flag fusion proteins using ANTI-FLAG® M2 magnetic beads

The anti-flag® M2 magnetic beads (Sigma) were used according to the manufacturer's instructions. 200 µl cell lysate (2.8.4.) obtained from approximately $1x10^7$ cells and 20 µl of packed beads were used in each immunoprecipitation reaction. The cell lysate and beads were incubated together overnight. Flag fusion proteins were eluted with 0.1M glycine HCl, pH 3 and neutralised with 0.5 M Tris/HCl pH 7.4, 1.5 M NaCl.

2.8.6. SDS-PAGE

2x SDS-sample buffer was added to each sample and the mixture was heated at 95°C for 5 minutes. Samples were then loaded alongside the PageRuler™ Prestained protein ladder (Fermentas) on a SDS-PAGE gel. This comprised of a 3.9% (w/v)

stacking gel (2.5 ml 30% acrylamide/bisacrylamide, 3.75 ml 0.5 M Tris-HCl pH 6.8, 0.15 ml 10% SDS, 8.45 ml dH_2O, 0.15 ml 10% ammonium persulphate and 0.006 ml TEMED) and a resolving gel at the required percentage (3 ml 30% acrylamide/bis, 4 ml 0.5 M Tris HCl pH 6.8, 2.8 ml dH_2O, 0.1 ml 10% SDS, 0.1 ml 10% ammonium persulphate, 0.004 ml TEMED for a 10% gel). Samples were run in 1 x running buffer (15g/l Tris, 72g/l glycine, 5g/l SDS pH 8.3 for 5 x).

2.8.7. Coomassie staining and destaining

To visualise proteins on a SDS-PAGE gel following electrophoresis, gels were stained in coomassie stain (0.1% coomassie brilliant blue R250, 10% glacial acetic acid, 40% methanol) for 30 minutes with constant shaking. Gels were subsequently destained in destain solution (20% methanol, 10% glacial acetic acid) for approximately 2 hours, replacing with fresh destain solution frequently.

2.8.8. Western blotting

Proteins were transferred to nitrocellulose membrane in transfer buffer (192 mM glycine, 25 mM Tris, 20% (v/v) methanol) at 70 V for 2 hours, after which the membrane was placed in blocking solution of 3-5% non-fat milk powder in PBS-T (500 ml PBS containing 500 µl Tween20) for an hour with shaking. The membrane was then placed in 3-5% non-fat milk in PBS-T containing the required dilution of primary antibody and incubated overnight at 4°C with constant shaking. Following 3 x 10 minutes washes with PBS-T, the membrane was transferred to 5% milk powder in PBS-T containing horseradish peroxidase (HRP) secondary antibody (BioRad blotting grade antibody at 1:3000) and incubated on a shaker at room temperature for an hour. Membranes were washed as before and equal volumes of detection reagent

1 peroxidase and detection reagent 2 luminol enhancer solutions (Roche) were added for 5 minutes before exposure to film.

2.8.9. Plaque reduction assay

Serum samples (diluted 1 in 5 in 1% BSA (w/v) in TBS) or polyclonal sheep anti-CHPV as a control were incubated with wild-type CHPV at a M.O.I of 0.01 pfu/cell for 1 hour and then inoculated onto confluent monolayers of BSC-1 cells. After 1 hour at 37°C, the inoculum was removed and 1% carboxymethyl cellulose (CMC)-GMEM (supplemented with 2% FBS, 0.2 mM L-glutamine and 100 µg/ml penicillin/streptomycin) overlay was added to each well. Cells were then incubated at 37°C. The cells were fixed using 4% gluteraldehyde in PBS for 2 hours at room temperature once plaques were clearly visible followed by staining with crystal violet for 15 minutes. The plates were then washed, dried and plaques counted using a binocular microscope. Each serum sample was assayed in triplicate.

CHAPTER 3

Chapter 3: The host range *td*CE phenotype of Chandipura virus is determined by mutations in the polymerase gene

3.1 Introduction

The central requirement of host cell factors in the replication of vesiculoviruses was highlighted by the isolation of eighteen temperature-dependent host range (*td*CE) mutants of CHPV (Gadkari & Pringle, 1980; Rasool & Pringle, 1986). These mutants were characterised by their ability to grow at both 31ºC (the permissive temperature) and the restrictive temperature of 39ºC in BSC-1 cells (the permissive host) to comparable titres to wild-type virus yet display temperature sensitivity in primary avian cells (chick embryonic fibroblasts, CE). This phenotype demonstrates a dependence of CHPV on undetermined host factors. During the initial characterisation, analysis of *in vitro* transcription assays showed decreased RNA transcriptase activity resulting in significantly lower amounts of viral RNA synthesised by the *td*CE mutants prepared in avian cells at the restrictive temperature. Synthesis of viral proteins was also found to be either considerably diminished or absent in all *td*CE mutants grown in avian cells at the restrictive temperature (Rasool & Pringle, 1986). This led to the suggestion that the growth impairment is caused by reduced RNA synthesis which in turn results in decreased generation of viral polypeptides.

Due to the nature of the host range mutants studying them offered a unique approach to uncouple the specific roles of host cell and virus proteins in the replication of this vesiculovirus. Investigation of similar mutants of VSV by others has provided a

powerful tool to enhance understanding of vesiculovirus replication, shedding light on several critical amino acid residues required for the methyltransferase, MTase activity of the viral RNA dependent RNA polymerase (Grdzelishvili *et al.*, 2005; 2006; Simpson & Obijeski, 1974). This chapter reports on the investigation of the underlying molecular basis of host range specificity, the CHPV *td*CE phenomenon using a reverse genetics approach.

3.2 Identifying CHPV gene(s) associated with *td*CE mutant phenotype

3.2.1 Characteristics of CHPV *td*CE mutants

CHPV strain I653514 (GenBank accession number KF468775) and temperature sensitive derivatives from it (Gadkari & Pringle, 1980; Rasool & Pringle, 1986) were used in this study. Out of eighteen CHPV *td*CE mutants isolated three were selected for analysis of the *td*CE phenotype; namely CH112, CH157 and CH256. The *td*CE mutant phenotype has been defined as viruses with an efficiency of plating (E.O.P.) in BSC-1 cells of <0.7 and in CE cells of >2, where E.O.P. is calculated as $\log_{10}$ $PFU^{39ºC}$ subtracted from $\log_{10}$ $PFU^{31ºC}$. These E.O.P. values were selected arbitrarily to reflect significant growth impairment in CE cells compared to BSC-1 cells. The three *td*CE mutants were chosen for further characterisation during this investigation on the basis of their previously established range of E.O.P. values in CE cells (Gadkari & Pringle, 1980; Rasool & Pringle, 1986) and viability.

Wild-type and *td*CE mutant CHPV titres were determined by standard plaque assay in permissive (BSC-1 monkey kidney cells) and conditionally permissive (primary cultures of chick embryo (CE) fibroblasts) at 31°C and 39°C. Table 3.1 shows these

titres alongside the E.O.P scores obtained in the original studies when the mutants were first isolated. Attempts were made to utilise the permanent chicken cell line DF-1 as the avian host cell line, however the virus was non-cytopathic in these cells, possibly due to host restriction factors.

The titres confirmed that the three mutants: CH112, CH157 and CH256 displayed the *td*CE phenotype, i.e. all three mutants grew to a titre that was greater than 100-fold less at 39°C than at 31°C in CE cells. The E.O.P. scores of the three mutants in CE cells were comparable with those described following the original characterisation, though slightly reduced by an average of approximately 15%. Mutant CH157 had an E.O.P. of 0.83 in BSC-1 cells which was outside of the desired range of an E.O.P in BSC-1 cells of <0.7 and in CE cells of >2 (Gadkari & Pringle, 1980; Rasool & Pringle, 1986). However, this was not considered a problem because the E.O.P. values of the mutant in the two cell types were vastly different, clearly demonstrating a significant difference in the growth of the mutant in avian and mammalian cells.

	Titre in BSC-1 (PFU/ml)		Titre in CE (PFU/ml)		Efficiency of plating (E.O.P.)		E.O.P. original characterisation	
	31°C	**39°C**	**31°C**	**39°C**	**BSC-1**	**CE**	**BSC-1**	**CE**
wtCHPV	$5.5x10^9$	$5.1x10^9$	$8.9x10^8$	$6.2x10^8$	0.03	0.16		
CH112	$9.2x10^8$	$2.9x10^8$	$4.6x10^7$	$2.3x10^3$	0.50	**4.30**	0.57	**5.20**
CH157	$2.0x10^9$	$3.0x10^8$	$4.5x10^7$	$1.1x10^5$	0.83	**2.61**	0.54	**3.54**
CH256	$1.3x10^9$	$7.0x10^8$	$1.4x10^7$	$2.0x10^3$	0.27	**3.85**	0.15	**4.37**

Table 3.1| **Efficiencies of plating of wild type CHPV (wtCHPV) and *td*CE mutants CH112, CH157 and CH256 in permissive (BSC-1) and conditionally permissive (CE) cells at 31°C and 39°C.**
E.O.P was calculated as $\log_{10}$ PFU$^{31°C}$ - $\log_{10}$ PFU$^{39°C}$. The *td*CE phenotype is defined as clones with an E.O.P in BSC-1 cells of <0.7 and in CE cells of >2. E.O.P. values in CE cells of >2 are shown in red. Virus titres and E.O.P. values are the average from triplicate repeats. The last column (shaded) contains the E.O.P. scores obtained in the original characterisation (Rasool & Pringle, 1986).

3.2.1.1. Growth of tdCE mutant viruses in a range of cultured cells

During the initial characterisation of CHPV *td*CE mutants several mutants were shown to have additional host cell restrictions in one or a number of the following cell types: hamster embryo (HE), rat embryo (RE), feline embryo (FEA), bovine embryo kidney (BEK), mouse embryo (NIH/3T3), mouse (L929) cells (Gadkari & Pringle, 1980). Additional host cell restrictions were not investigated for CH112, CH157 and CH256, the mutants chosen for analysis in this study. Therefore, wild-type and *td*CE mutant (CH112, CH157 and CH256) viruses were titrated at 31°C and 39°C in a number of available cells types: astrocytoma U373, human embryonic oligodendrocyte Oligo/TL, human rhabdomyosarcoma (RD), hepatocellular carcinoma Hep-2 and BSR-T7 cell lines, and E.O.P. values calculated. The results are shown in Table 3.2. Viral titres in human RD cells at the two temperatures were determined because these cells have previously been used to study the growth

kinetics of CHPV (Jadi *et al.*, 2010). Also, due to the neuropathogenesis of CHPV investigation of *td*CE mutant growth in two brain cell lines (astrocytoma U373 and human embryonic oligodendrocyte Oligo/TL) was also carried out.

	Titre in U373 (PFU/ml)		Titre in RD (PFU/ml)		Titre in Hep-2 (PFU/ml)		Titre in BSR-T7 (PFU/ml)		Titre in Oligo/TL (PFU/ml)		Efficiency of plating (E.O.P.)				
	31°C	**39°C**	**31°C**	**39°C**	**31°C**	**39°C**	**31°C**	**39°C**	**31°C**	**39°C**	**U373**	**RD**	**Hep-2**	**BSR-T7**	**Oligo/TL**
wtCHPV	$4.6x10^8$	$9.2x10^7$	$1.1x10^9$	$3.7x10^8$	$2.2x10^9$	$9.6x10^8$	$5.3x10^9$	$4.8x10^9$	$4.8x10^9$	$2.6x10^9$	0.70	0.47	0.36	0.04	0.27
CH112	$2.1x10^7$	$6.9x10^6$	$3.8x10^8$	$2.2x10^7$	$9.4x10^8$	$3.2x10^8$	$8.9x10^8$	$3.0x10^8$	$5.1x10^8$	$1.6x10^8$	0.48	**1.24**	0.46	0.47	0.50
CH157	$3.3x10^7$	$8.4x10^6$	$2.1x10^8$	$3.4x10^7$	$9.7x10^8$	$2.3x10^8$	$1.7x10^9$	$8.7x10^8$	$6.7x10^8$	$9.4x10^7$	0.59	**0.79**	0.63	0.29	**0.85**
CH256	$1.2x10^7$	$2.8x10^6$	$6.5x10^8$	$7.8x10^7$	$1.0x10^9$	$3.5x10^8$	$9.9x10^8$	$2.4x10^8$	$7.1x10^8$	$2.1x10^8$	0.63	**0.92**	0.46	0.62	0.53

Table 3.2| **Efficiencies of plating of wild-type CHPV (wtCHPV) and *td*CE mutants in U373, RD, Hep-2, BSR-T7 and Oligo/TL cells at 31°C and 39°C.** E.O.P was calculated as $\log_{10} PFU^{31°C}$ - $\log_{10} PFU^{39°C}$. Virus titres and E.O.P. values are the average from duplicate repeats. E.O.P. scores above 0.7 are highlighted in red.

None of the three *td*CE mutant viruses exhibited additional host restrictions in any of the cell types tested as shown by E.O.P scores of less than 2 for each. Infection of U373, Hep-2, BSR-T7 and Oligo/TL cells with the *td*CE mutants produced viral titres and thus E.O.P values similar to those obtained in BSC-1 cells (all had E.O.P. values of less than 0.7, except for CH157 which had an E.O.P of 0.85 in Oligo/TL cells). However, the E.O.P. scores of the three mutants in human RD cells were outside of the desired range of an E.O.P of <0.7 in permissive cells.

3.2.2 Sequencing wild-type CHPV and *td*CE mutant genomes

To identify the genetic lesions responsible for, and therefore the virus gene(s) associated with, host range requirements, the entire genome of each mutant was sequenced. The wild-type virus was also sequenced because the only available sequence at the time was assembled from several different sources. Firstly, RNA was extracted from wild-type and mutant CHPV stocks and then reverse transcribed to generate full length cDNA using random hexanucleotide primers. Seven PCR products of approximately 2 kb, which overlapped with each other by 200-400 bp were amplified by PCR from the full length cDNA using a high-fidelity DNA polymerase, as detailed in Figure 3.1a. PCR products were separated on agarose gels (Figure 3.1b) and the correct size fragment of each reaction was purified, to eliminate the minor products generated as a consequence of non-specific primer binding. The sequences of primers which were used to construct PCR products 1-7 are shown in Appendix 1.

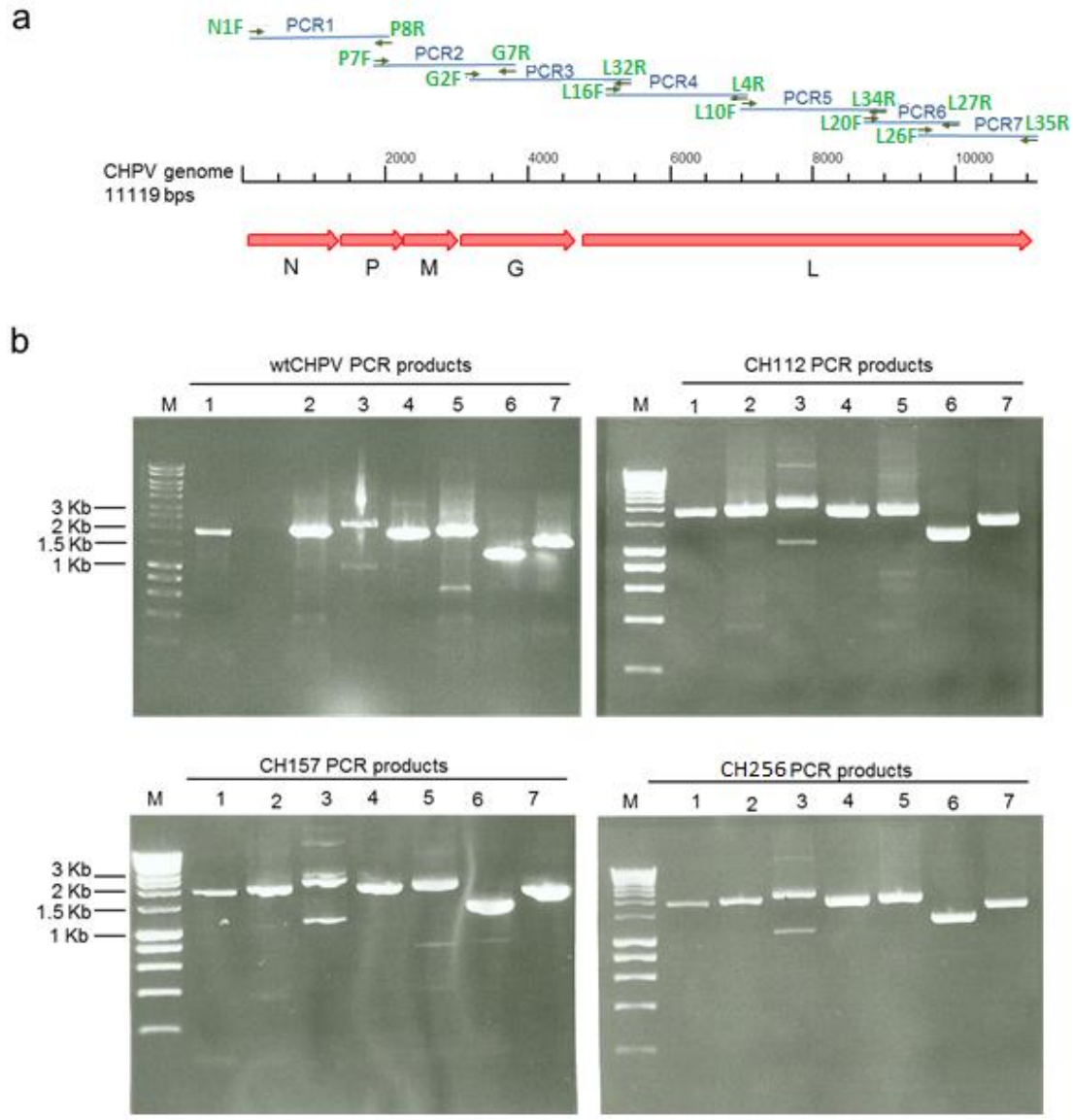

Figure 3.1| **Generation of PCR products for DNA sequencing wtCHPV and mutant genomes**

A. The positions of the amplified PCR products along the genome are shown in blue. The forward and reverse primer used to amplify each of the PCR products are shown in green. B. Agarose gel (0.7%) electrophoresis of PCR products 1 to 7 (1901, 2039, 2347, 2000, 2074, 1352 and 1708 bp, respectively) amplified from wtCHPV, CH112, CH157 and CH256. The position of size markers are shown on the left. The gels were stained with ethidium bromide.

Each PCR product was amplified in duplicate and sequenced. Contigs for wild-type CHPV, CH112, CH157 and CH256 were constructed and the entire length of each contig was covered by at least three sequences generated using different primers. The mutant nucleotide sequences were then aligned with the wild-type virus sequence using ClustalW software and the point mutations identified. Each mutant contained only a very small number of mutations, detailed in Table 3.3. The GenBank accession numbers for wtCHPV, CH112, CH157 and CH256 are KF468775, KF468772, KF468773, KF468774, respectively. All of the *td*CE mutants contained coding changes in the RNA polymerase (L) gene and mutants CH112 and CH256 contained additional mutations in the attachment (G) protein gene. Additionally, two of the *td*CE mutants contained a further silent point mutation(s). Mutant CH112 contained the point mutation U_{1980}→C in the P gene and U_{9958}→C in the L gene which altered the codon sequences for amino acid residues 206 and 1732 from AAU (asn) to AAC (asn) and GAU (asp) to GAC (asp), respectively. Mutant CH157 contained a U_{9022}→C mutation in the L gene causing an AAU (asn) to AAC (asn) codon change.

The presence of the mutations resulting in coding changes in the polymerase gene is consistent with the observation of reduced RNA transcriptase activity *in vitro* at 39°C in 10 of 12 CHPV *td*CE mutants relative to wtCHPV, with CH112, CH157 and CH256 exhibiting efficiencies of transcription at 39°C of 14%, 56% and 37% of the wild-type virus (Rasool & Pringle, 1986).

***td*CE mutant**	**E.O.P. In CE cells**	**Point mutation**	**Gene**	**Codon change**	**Amino acid change**
CH112	4.30	$U_{3941} \rightarrow C$	G	UCA to CCA	Ser_{297} to Pro
		$C_{5691} \rightarrow U$	L	UCG to UUG	Ser_{310} to Leu
		$C_{5760} \rightarrow U$	L	CCU to CUU	Pro_{333} to Leu
		$C_{7217} \rightarrow U$	L	CCA to UCA	Pro_{819} to Ser
		$U_{9958} \rightarrow C$	L	GAU to GAC	Non coding
		$U_{1980} \rightarrow C$	P	AAU to AAC	Non coding
CH157	2.61	$G_{9735} \rightarrow U$	L	GGG to GUG	Gly_{1658} to Val
		$U_{9022} \rightarrow C$	L	AAU to AAC	Non coding
CH256	3.84	$U_{4034} \rightarrow C$	G	UAU to CAU	Tyr_{328} to His
		$G_{7694} \rightarrow A$	L	GCC to ACC	Ala_{978} to Thr

Table 3.3| **Nucleotide positions and coding changes identified in recombinant CHPV *td*CE mutants.**

3.2.3 **Generation of recombinant viruses containing the identified point mutations**

To confirm which of the point mutations identified in the mutants were responsible for the *td*CE phenotype recombinant viruses containing each point mutation, and combinations of the L mutations in the case of mutant CH112, were generated. Quickchange site directed mutagenesis using mutagenic oligonucleotide primers (refer to Appendix 1 for sequences) was used to individually produce the $C_{5691}\rightarrow U$, $C_{5760}\rightarrow U$, $C_{7217}\rightarrow U$, $G_{9735}\rightarrow U$, $G_{7694}\rightarrow A$, $U_{3941}\rightarrow C$, $U_{4034}\rightarrow C$ point mutations in the full length anti-genomic clone of CHPV (pT7CV: See Appendix 2 for the plasmid map of pT7CV). An example of this strategy is shown in Figure 3.2a for the generation of $C_{5691}\rightarrow U$. The methylated, non-mutated parental DNA templates were digested with *DpnI* restriction endonuclease and remaining mutated, nascent DNA transformed into competent *E.coli* DH5α cells. Several colonies were grown in overnight cultures and plasmid DNA was purified. Combinations of mutations were made by sequential Quickchange reactions with the appropriate mutagenic primers.

DNA fragments containing the point mutations were re-cloned into pT7CV. To achieve this, fragments containing the point mutations were subsequently digested out of the plasmid using two restriction endonucleases that had unique sites in the plasmid, the correct size fragment extracted from agarose gels and ligated into wild type pT7CV that had been previously digested with the same restriction enzymes. This was done to reduce the length of DNA needed to be sequenced and problems due to other point mutations being inadvertently generated during the Quickchange reaction.

Figure 3.2b shows agarose gel images of the digested fragments. pT7CV containing either $C_{5691}\rightarrow U$, $C_{5760}\rightarrow U$ and $C_{5691\text{ and }5760}\rightarrow U$ were digested with the restriction endonucleases *PmlI* and *KpnI* to give 3086 and 11035 base pair products, the smaller of which contained the point mutation and was therefore extracted from the agarose gel. The pT7CV $C_{7217}\rightarrow U$ and $G_{7694}\rightarrow A$ plasmids were cut with *KpnI* and *SphI,* $C_{5691,\ 5760\text{ and }7217}\rightarrow U$, $C_{5760\text{ and }7217}\rightarrow U$ and $C_{5691\text{ and }7217}\rightarrow U$ with *PmlI* and *SphI* and $G_{9735}\rightarrow U$ with *SphI* and *RsrII.* These restriction digestion reactions generated fragments of 2409 and 11712, 5495 and 8626, and 1670 and 12451 base pairs respectively. In each case the smaller of the two products was then purified from an agarose gel (the fragment containing the point mutation) and ligated into identically digested pT7CV vector DNA. The ligation reactions were then transformed into bacteria, resultant clones cultured and plasmid DNA extracted.

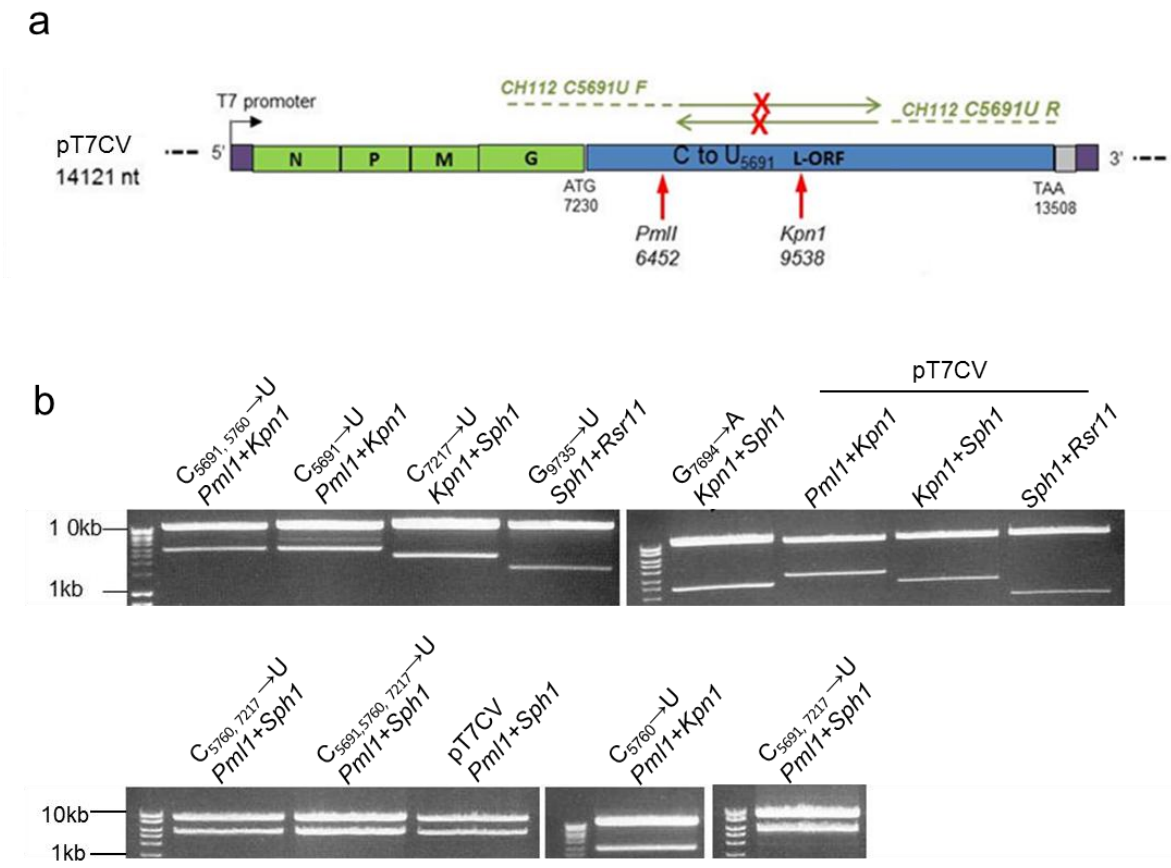

Figure 3.2| **Quickchange site directed mutagenesis to generate the host range mutations within the L gene**
A. Diagrammatic representation of the strategy used to generate the point mutations, using pT7CV C_{5691}→U as an example.
B. 1% (w/v) agarose gels of pT7CV (containing one or more specific point mutations) after digestion with two restriction enzymes.

A similar strategy was used to generate the two point mutations which were identified within the G gene of two of the *td*CE mutants. Mutagenic oligonucleotide primers (Appendix 1) were used in Quickchange site directed mutagenesis to produce the U_{3941}→C and U_{4034}→C mutations in pT7CV. Any non-mutated DNA was removed by *DpnI* digestion and remaining mutated, nascent DNA was transformed into competent *E.coli* DH5α cells. Several colonies were grown in overnight cultures and plasmid DNA was purified. pT7CV containing the U_{3941}→C and U_{4034}→C mutations were digested with *BsiwI* and *PmlI* or *PmlI* and *KpnI*

respectively and the 2124 and 3086 bp fragments (Figure 3.3) were ligated into wild-type pT7CV (previously digested with the same restriction enzymes). As before, the ligation reactions were transformed into bacteria, resultant clones cultured and plasmid DNA extracted.

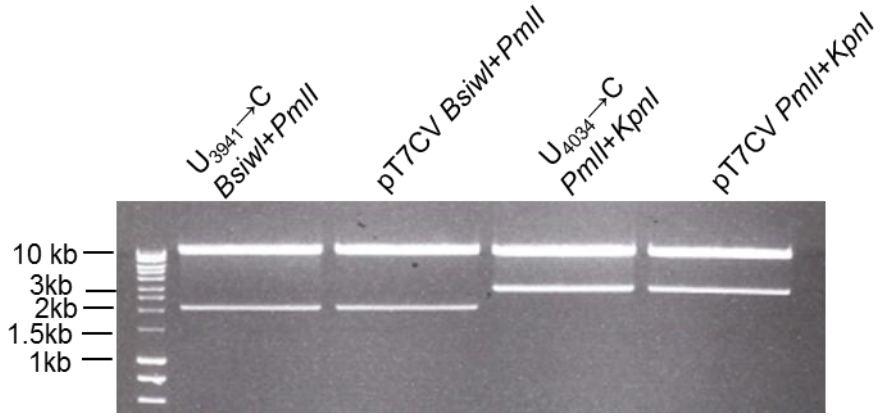

Figure 3.3| **Re-cloning DNA fragments containing the point mutations within the G gene into pT7CV**
1% (w/v) agarose gel of pT7CV (containing a specific point mutation) after digestion with two restriction enzymes

The plasmid DNA was analysed by restriction digestions with *BamHI*, yielding fragments of 349, 915, 2557, 5806 base pairs in length as expected (Figure 3.4a). To confirm that the correct point mutations were produced and other point mutations, additions or deletions had not been inadvertently made during the Quickchange reaction all of the insert sequences were verified by DNA sequencing. A partial chromatogram from the DNA sequencing results of the insert containing the C_{5691}→U change, as an example, is shown in Figure 3.4b.

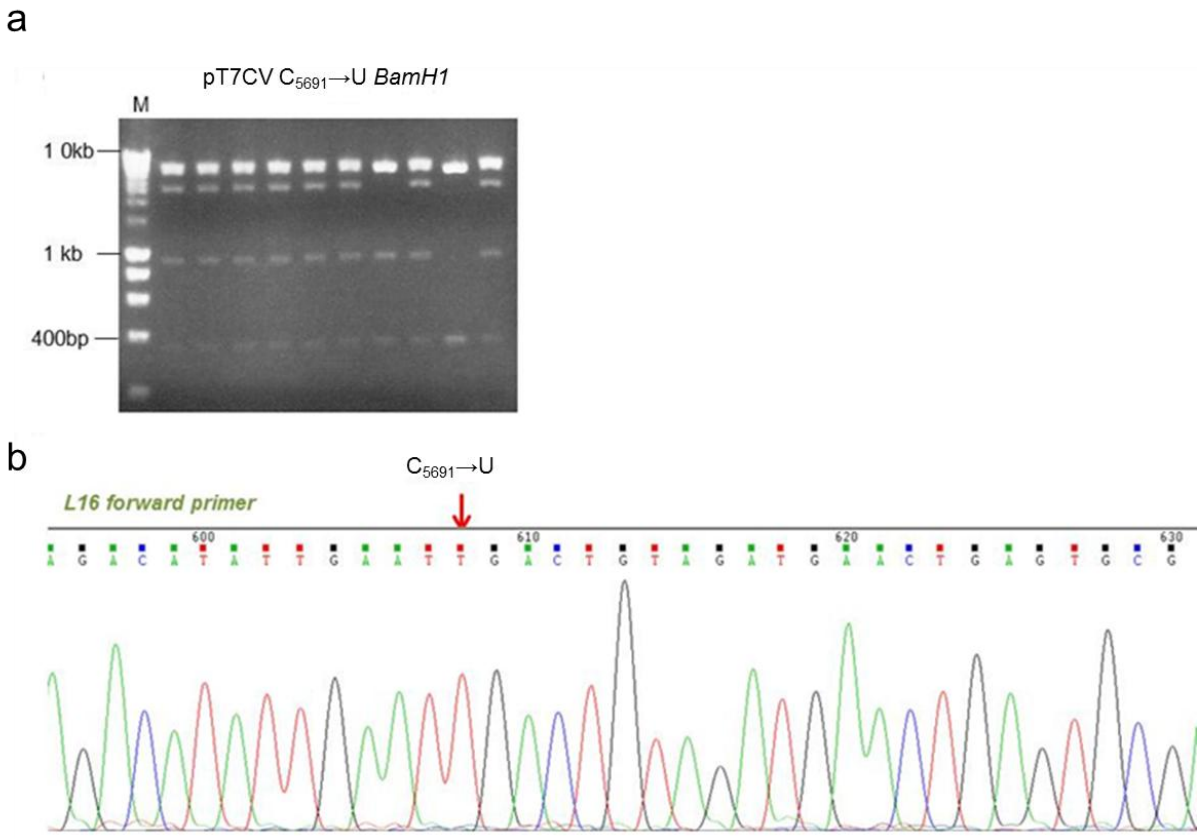

Figure 3.4| **Confirmation of the presence of the specific mutations**
A. An example of an analytical restriction digest (*BamHI* digestion) to check for other alterations to the full length CHPV vector following the ligation of the insert (containing point mutation(s) into pT7CV
B. Partial chromatogram of the DNA sequencing results of pT7CV C_{5691}→U using the *CV-L16* primer. The point mutation is shown by an arrow.

3.2.4 Recovery of recombinant viruses containing the point mutations associated with host range

Rescue of recombinant infectious virus was carried out for the wild type virus as control and for each of the nine combinations of point mutations generating coding changes in the virus RNA dependent RNA polymerase (L) gene or one of the two mutations in the attachment (G) protein gene using the CHPV reverse genetics system previously described (Marriott & Hornsey, 2011). The genomic plasmid (containing the point mutation(s)) and support plasmids pT7N, pT7P and pT7L were

transfected into BSRT-7/5 cells (refer to Appendix 2 for plasmid maps). After 48 hours, the supernatant was inoculated onto confluent monolayers of BSC-1 cells and virus was harvested when the cytopathic effect was extensive (approximately 24 hours post infection). The CHPV reverse genetics system is illustrated in Figure 3.5.

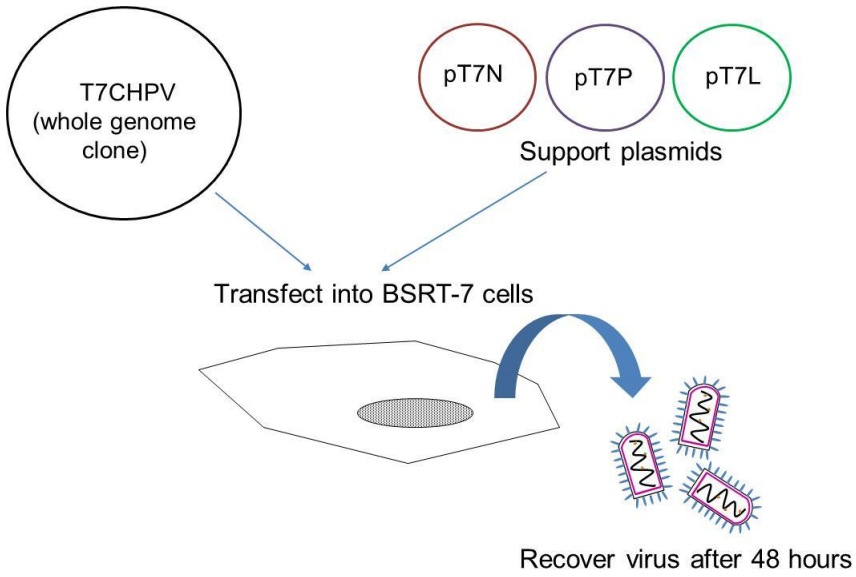

Figure 3.5| **A diagram summarising the plasmid requirements for rescue of infectious CHPV from plasmid DNA**

All recovered viruses were titrated in BSC-1 and CE cells at both 31°C and 39°C and E.O.P. scores calculated for each condition to confirm the *td*CE phenotype (Table 3.4). The data show that a single amino acid change in the virus RNA polymerase (L protein) of each mutant was solely responsible for the *td*CE host range dependent phenotype. All recombinant viruses containing the C_{7127}→U mutation in the L gene of mutant CH112 conferred the *td*CE phenotype while any combination of the C_{5691}→U and C_{5760}→U point mutations in the L gene alone or together did not (Table 3.4). The latter was demonstrated by E.O.P. scores for the respective recombinant viruses of less than two in CE cells. Furthermore, the results showed that the

mutations identified in the G gene of CH112 and CH256 were not involved in the *td*CE mutant phenotype. Similarly, only the presence of the G_{7694}→A mutation in the L gene of mutant CH256 and G_{9735}→U in the L gene of mutant CH157 conferred the *td*CE phenotype.

Gene with mutation(s)	Recombinant virus	Titre in BSC-1 cells (pfu/ml)		Titre in CE cells (pfu/ml)		Efficiency of plating	
		31°C	39°C	31°C	39°C	BSC-1	CE
n/a	rCV (wt)	9.9×10^8	3.1×10^8	3.0×10^7	1.3×10^7	0.50	0.36
L gene	rCV 112 ($C_{5691} \rightarrow U$)	9.3×10^8	1.5×10^8	4.9×10^7	1.5×10^7	0.79	0.51
	rCV 112 ($C_{5760} \rightarrow U$)	3.1×10^8	2.8×10^8	2.5×10^7	1.3×10^7	0.04	0.28
	rCV 112 ($C_{7217} \rightarrow U$)	3.8×10^8	8.9×10^7	2.3×10^7	7.5×10^2	0.63	**4.49**
	rCV 112 ($C_{5691,5760} \rightarrow U$)	4.2×10^8	7.6×10^7	3.9×10^7	9.8×10^6	0.74	0.60
	rCV 112 ($C_{5691,7217} \rightarrow U$)	1.8×10^8	7.6×10^7	1.7×10^7	1.3×10^2	0.37	**5.12**
	rCV 112 ($C_{5760,7217} \rightarrow U$)	1.1×10^8	2.4×10^7	9.8×10^6	2.8×10^2	0.66	**4.54**
	rCV 112 ($C_{5691,5760,7217} \rightarrow U$)	1.7×10^8	6.3×10^7	1.2×10^7	3.1×10^2	0.43	**4.59**
	rCV 157 ($G_{9735} \rightarrow U$)	9.3×10^7	1.4×10^7	2.3×10^7	1.0×10^4	0.82	**3.36**
	rCV 256 ($G_{7694} \rightarrow A$)	1.1×10^9	2.5×10^8	3.8×10^7	1.8×10^5	0.64	**2.32**
G gene	rCV 112 ($U_{3941} \rightarrow C$)	7.8×10^8	1.7×10^8	7.8×10^7	1.8×10^7	0.66	0.64
	rCV 256 ($U_{4034} \rightarrow C$)	3.5×10^8	1.2×10^8	3.1×10^7	1.8×10^7	0.46	0.24

Table 3.4| **Efficiencies of plating of mutated rCHPV viruses in BSC-1 and CE cells**
Viruses with E.O.P. values >2 in CE cells and therefore display the *td*CE phenotype are highlighted in red. Virus titres and E.O.P. values are the averages from triplicate repeats

3.3 Discussion

Host restricted and conditional host range mutants have been powerful tools for dissecting vesiculovirus replication, with the characterisation of several dual conditionally temperature sensitive/host restricted (ts/hr) mutants of VSV Indiana leading to the elucidation of amino acid residues that are essential for the methyltransferase (MTase) activities of the L protein (Grdzelishvili *et al.*, 2005; 2006; Simpson & Obijeski, 1974). A series of *td*CE mutants have been described for VSV (Pringle, 1978) and CHPV (Gadkari & Pringle, 1980; Rasool & Pringle, 1986) in which the viruses are capable of growth in mammalian cells at 31°C and 39°C but cannot grow at 39°C in primary avian cells. These mutants exhibit a greater than 100-fold reduction in viral titre at 39°C when grown in CE cells, emphasising the essential role of host cell factors in vesiculovirus replication.

The initial study reported reduced RNA transcriptase activity during *in vitro* transcription assays resulting in significantly lower amounts of viral RNA synthesised in the *td*CE mutants grown in avian cells at the restrictive temperature and viral protein synthesis was also found to be either considerably depressed or non-existent in all *td*CE mutants grown in avian cells at the restrictive temperature (Rasool & Pringle, 1986). This indicated that the growth restriction is caused by diminished RNA synthesis which in turn results in decreased production of viral polypeptides. *In vitro* RNA methylation activity of the virus RNA dependent RNA polymerase and heat shock protein induction were found to occur at similar levels as the wild type virus in all *td*CE mutants (Rasool & Pringle, 1986). Thus, these mutants contain lesion(s) affecting a different aspect of L protein function than the *hr1* VSV Indiana dual ts/hr mutant (Simpson & Obijeski, 1974) which was shown to

contain an amino acid substitution within the MTase domain of its L protein giving rise to deficiencies in mRNA cap methylation (Grdzelishvili *et al.*, 2005; 2006).

This research aimed to determine the molecular basis of CHPV host range. The data presented here demonstrate that for each of three *td*CE mutants, CH112, CH157 and CH256 the lesions responsible for the severe growth defect resides in the gene encoding the catalytic component of the virus RNA dependent RNA polymerase (L protein). The point mutations identified result in the following amino acid changes in the L protein: Pro_{819} to Ser, Gly_{1658} to Val and Ala_{978} to Thr in *td*CE mutants CH112, CH157 and CH256 respectively. The presence of the mutations resulting in coding changes in the polymerase gene is consistent with the observation of reduced RNA transcriptase activity *in vitro* at 39°C in 10 of 12 CHPV *td*CE mutants relative to wtCHPV, with CH112, CH157 and CH256 exhibiting efficiencies of transcription at 39°C of 14%, 56% and 37% of the wild-type virus (Rasool & Pringle, 1986).

The large protein of Rhabdoviruses is multifunctional and is comprised of 6 functional domains containing regions of greater amino acid conservation and highly variable intra domains (Poch *et al.*, 1990). The molecular interrelationship between the domains in the VSV L protein have also been established with conserved blocks I-IV arranged into a ring structure containing the RNA polymerase activity and an appendage of domains V and VI responsible for capping (polyribonucleotidyltransferase, PRNTase) and methylation (MTase) respectively (Rahmeh *et al.*, 2010). Specifically, domain III was found to confer the RNA-dependent RNA polymerase activity of the L protein. The pre-A and GDN motifs, which are highly conserved in the domain III of non-segmented negative sense (NNS) RNA viruses and related to other viral RNA-dependent RNA polymerases,

have been shown to be essential for RNA synthesis (Muller *et al.*, 1994; Sleat & Banerjee, 1993).

The locations of the point mutations responsible for the *td*CE phenotype within the CHPV L protein are shown in Figure 3.6. The point mutations conferring the host range phenotype of the *td*CE mutants are located between domains III and IV (CH112 $C_{7217} \rightarrow U$) or within domain IV (CH256 $G_{7694} \rightarrow A$) or VI (CH157 $G_{9735} \rightarrow U$) of the L gene. The $G_{9735} \rightarrow U$ change within domain VI lies in a stretch of highly conserved amino acids and immediately precedes a GXGXG motif (GDGSG sequence) which is 19 amino acids upstream of a lysine residue, which jointly have been implicated in polyadenylation or protein kinase functions (Cherian *et al.*, 2012). The GXGXG motif has a predicted S-adenosyl-L-methionine-binding site required by the virus encoded methyltransferase (Rahmeh *et al.*, 2009). While the methyltransferase activity of the L protein has been proposed to also lie within domain VI the CH157 mutant polymerase displays a normal mRNA capping function (Rasool & Pringle, 1986). The functions of protein sequence within close proximity to the locations of the CH112 and CH256 coding changes are unknown.

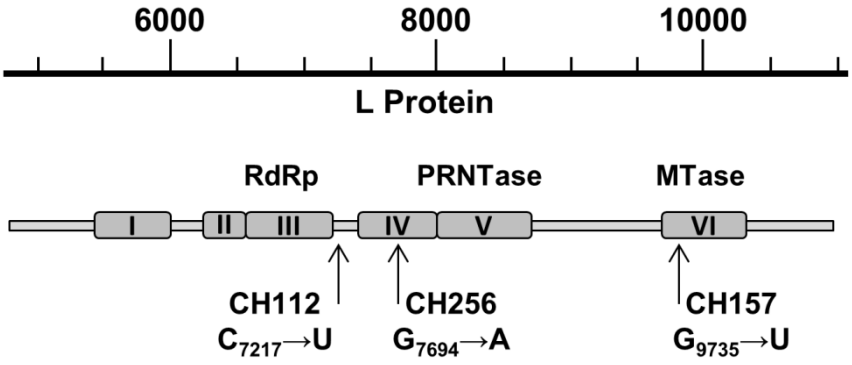

Figure 3.6| **Diagram of the CHPV L gene and location of the L protein coding sequences** The nucleotide positions within the 11,119 nt genome are indicated. The location of the 6 domains of the vesiculovirus L protein are indicated (I to VI) and the locations and nature of the *td*CE mutants in the L gene and protein are shown. The locations of the RNA dependent RNA polymerase (RdRp), polyribonucleotidyltransferase, (PRNTase) and methyltransferase (MTase) activities are also indicated.

In conclusion, the data presented in this chapter demonstrate that the conditional growth defect for each of three CHPV *td*CE mutants, CH112, CH157 and CH256 is caused by single amino acid changes in the virus RNA polymerase protein.

CHAPTER 4

Chapter 4: The construction and characterisation of tagged wild type CHPV and *td*CE mutant replication complex proteins

4.1 Introduction

The location of the *td*CE lesions within the polymerase protein gene described in chapter 3 coupled with the defect in virus RNA synthesis in the mutants (Rasool & Pringle, 1986) suggest that in CE cells the formation of functional replication complexes may be affected. Replication complexes are located throughout the cytoplasm of infected cells and are the sites of viral RNA synthesis, containing the viral RNA, viral replicative machinery: the catalytic component of the virus RNA dependent RNA polymerase (L protein), cofactor of the polymerase (P protein), nucleocapsid (N) protein and an intimately associated array of host cell proteins, required by the virus for replication. Studies in VSV have shown that infection leads to the induction of stress granule-like complexes, comprised of viral RNA, replicative proteins and several cellular antiviral proteins in the cytoplasm of infected cells. This has led to the hypothesis that the formation of inclusions is host-cell mediated and that they are in fact the replication complexes described previously (Dinh *et al.*, 2013a).

The nature of the host range phenotype indicates that the mutations in the viral polymerase affect an essential interaction with certain cellular factor(s) which are different in CE compared to BSC-1 cells. Thus, in order to further investigate the effects of the *td*CE mutations on CHPV replication, the intracellular localisation of components of the RNP complex (especially the two constituents of the viral polymerase: L protein and the P protein cofactor) was determined for wild-type

versus mutant L viruses in mammalian and chick cells at 31°C and 39°C. The differences in the host proteins bound by wild-type L viruses during an infection in BSC-1 and CE cells were also investigated.

Currently, there are no antibodies to specific CHPV proteins and thus in order to study the intracellular localisation and cellular binding partners of individual virus proteins, tagged proteins were used. Using the CHPV reverse genetics system (Marriott & Hornsey, 2011) (Figure 3.5) recombinant viruses containing tagged L and/or P proteins (constituents of virus replication complexes) were generated and used in this investigation. The L protein was tagged because the coding changes responsible for the host range defect in the *td*CE mutants resides within their L proteins. Tagged P proteins were also generated because as a component of the viral polymerase the phosphoprotein closely associates to the L protein and it has previously been used as a surrogate to study replication complex localisation in VSV-infected cells (Das *et al.*, 2006). A recombinant CHPV in which red fluorescent protein (RFP) was fused in-frame within a putative hinge region of the CHPV phosphoprotein, between residues 213 and 214 of P (rCV-P/RFP) had been previously made by Dr A.C. Marriott. Single-step growth curve analysis of this virus in BSC-1 cells showed a very similar virus yield (8.09 ± 0.07 $\log_{10}$ pfu/ml) to the recombinant wild-type virus (8.22 ± 0.02 $\log_{10}$ pfu/ml) indicating that the RFP insertion had minimal effect on virus growth in cell culture (Dr A.C. Marriott personal communication). The P-RFP fusion protein is stable and the resulting recombinant virus grows well in both mammalian and avian cells. Therefore rCV-P/RFP was utilised in this study to examine P protein localisation and binding partners.

4.2. Generation of recombinant viruses containing tagged proteins

4.2.1. Recombinant CHPV encoding eGFP in the variable region upstream of domain VI of L protein could not be recovered

The literature contains several examples where a large reporter gene has been inserted within the polymerase gene of a morbillivirus. The more distantly related L proteins of the *Morbillivirus* genus have 3 conserved domains separated by 2 highly variable hinge regions. A functional virus with the eGFP gene inserted within hinge region 2 of the measles virus L protein (corresponding to a region between blocks V and VI in rhabdoviruses) was successfully generated, which exhibited only slightly reduced polymerase activity (Duprex *et al.*, 2002). Similar insertions in rinderpest virus and canine distemper virus L proteins resulted in severely attenuated growth *in vivo* (Brown *et al.*, 2005). Rhabdoviruses do not contain hinge region 2, however, insertion of the eGFP ORF into a comparable position in the genome of VSV (55 residues upstream of the catalytic tetrad K-D-K-E of the MTase in L) was also tolerated, although produced a temperature sensitive phenotype (Ruedas & Perrault, 2009). The positions of the 6 domains within the CHPV L protein amino acid sequence including the location of the K-D-K-E motif is shown in Figure 1.7.

The demonstration that the polymerases of these NNS RNA viruses are able to accommodate such large insertions of sequence in this region highlights the functional independence of domain VI to the rest of the L protein in Rhabdoviruses (domain 2 and 3 of morbillivirus L). Attempts were made to engineer a recombinant CHPV encoding eGFP in this region of the polymerase protein. The insertion site chosen was 4 amino acids upstream of that used to generate the VSV recombinant

(Ruedas & Perrault, 2009) (i.e. 59 residues upstream of the MTase) because the VSV produced was temperature sensitive.

The open reading frame (ORF) of eGFP (without the stop codon) was amplified from pCVeGFP, a full length anti-genomic clone of CHPV with eGFP inserted between the M and G genes (constructed by Dr A.C. Marriott) using primers containing sites for the restriction endonuclease *Sal*I. A *Sal*I site, 5'*GTCGAC3',* was then introduced into pT7CV at nucleotide 9502 by Quickchange site directed mutagenesis using mutagenic oligonucleotides to generate $pT7CV_{salI}$ (refer to Appendix 1 for primer sequences). The PCR product containing the eGFP sequence flanked with *Sal*I sites was ligated into $pTCV_{salI}$ following digestion of both vector and insert with *Sal*I restriction enzyme. The resultant plasmid: $pT7CV_{LeGFP}$ was subsequently transfected into BSR-T7 cells alongside the support plasmids pT7N, pT7P and pT7L. However, virus could not be recovered suggesting that the resulting polymerase protein was non-functional.

4.2.2. Construction of Flag tagged virus proteins

Due to the unsuccessful attempts to insert large marker sequences within the CHPV L gene in a recombinant virus and because others have reported the generation of a temperature sensitive VSV encoding eGFP within the polymerase protein (Ruedas & Perrault, 2009) other tagging options were considered. Having such a large protein fused to the amino or carboxy terminus of the protein of interest frequently alters the properties of that protein including its folding, localisation and function and there are no examples in the literature of C- or N-terminally tagged L polymerase proteins. Therefore, the introduction of a fluorescent marker protein at these positions was also ruled out. Proteins often have higher tolerance to shorter epitope insertions and for

this reason the eight amino acid flag tag (amino acid sequence DYKDDDDK) was selected to be added to the carboxy terminus of CHPV L in the support plasmid (pT7L) and L in the full length virus clone (pT7CV) (for recovery of recombinant viruses containing L/Flag).

4.2.2.1. Construction of pT7L Flag plasmid

There are a limited number of suitable unique restriction enzyme sites within the 11,684 bp CHPV L gene and no restriction enzyme site directly after the L-ORF stop codon for use in insertion of additional sequences so an overlapping PCR strategy was used to insert the 24 nucleotide Flag sequence in pT7L (Figure 4.1 a). Overlapping portions of the L-ORF were amplified by PCR from pT7L using the *L F* and *L Flag R* primers in one reaction and the *L Flag F* and *L R* oligonucleotides in a second reaction to produce 268 and 175 bp PCR products (Figure 4.1 b). The outer primers (*LF* and *L R*) were subsequently used in a PCR reaction to join the two PCR products obtained in the previous step together, yielding a 405 bp product (Figure 4.1 c). This product was digested by *SalI* and *NsiI* releasing a 340 bp fragment (Figure 4.1 c) which was then ligated into a pT7L vector also digested with *SalI* and *NsiI*. The ligation reaction was transformed into competent *E.coli* DH5α cells and plated out. Colonies were grown overnight and plasmid DNA was extracted. As expected, fragments of 1253, 3394 and 7037 bp were produced when pT7L Flag was digested with *HincII* (Figure 4.1 d), thus identifying the plasmid and DNA sequencing with the *L30* primer showed the Flag sequence had been inserted in the correct location (Figure 4.1 e).

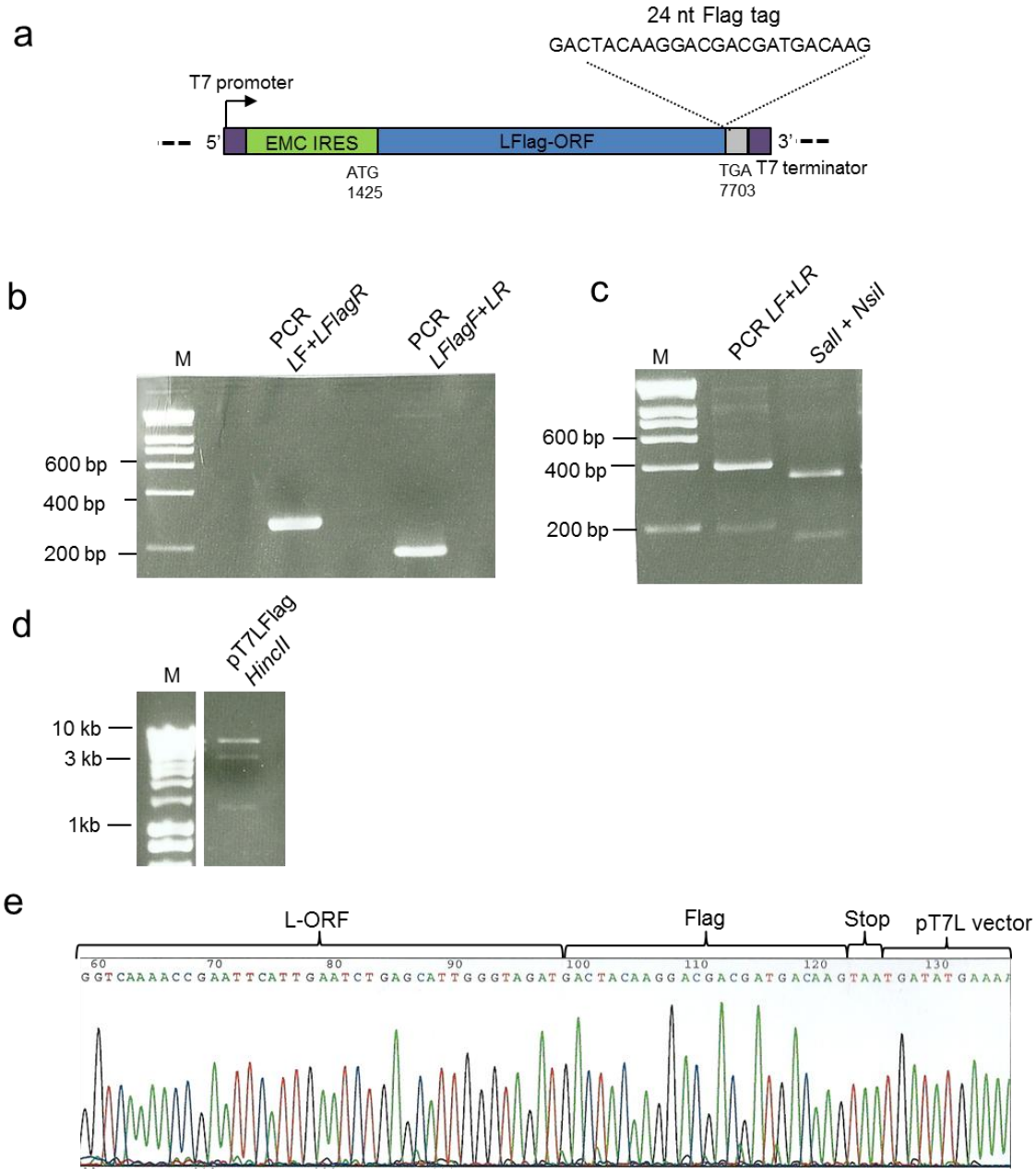

Figure 4.1| **Construction of carboxy-terminus Flag tagged pT7L (pT7LFlag)**
A. Map of pT7LFlag plasmid (vector backbone not shown)
B. 2% (w/v) agarose gel stained with ethidium bromide of the *LF* and *LFlagR* PCR product (268 bp) and *LFlagF* and *LF* PCR product (175 bp)
C. 2% (w/v) agarose gel electrophoresis of the *LF* and *LR* PCR product (405 bp) and the same PCR product after digestion with *SalI* and *NsiI* (340 bp)
D. Analytical 1% agarose gel to confirm the identity of pT7L Flag (*HincII* digest)
E. Partial chromatogram of the DNA sequencing results of pT7L Flag using the *L30* primer

4.2.2.2. The L/Flag protein is functional in minigenome assays

To establish whether the Flag protein remains stably associated with the L protein, a minigenome assay using an eGFP reporter minigenome was performed (see Appendix 2 for plasmid maps). In the minigenome reverse genetics system of CHPV (Marriott & Hornsey, 2011) the minimum requirements for viral transcription and replication: L, P and N proteins are each expressed from a separate plasmid which are under the control of T7 promoter and an encephalomyocarditis virus (EMCV) internal ribosome entry site (IRES) sequences. Upon transfection of the three plasmids into BSR-T7 cells, which constitutively express the bacteriophage T7 RNA polymerase, the L, P and N proteins are expressed and are able to transcribe and replicate a GFP minireplicon (an analogue for genomic RNA). GFP expression was analysed 24 hours after transfection. Slightly reduced but comparable amounts of GFP expression were present in pT7LFlag transfected cells in comparison with cells transfected with the wild type L vector (pT7L) (Figure 4.2). While this indicates that the L/Flag can substitute for L in the minigenome rescue, GFP expression was low in both conditions.

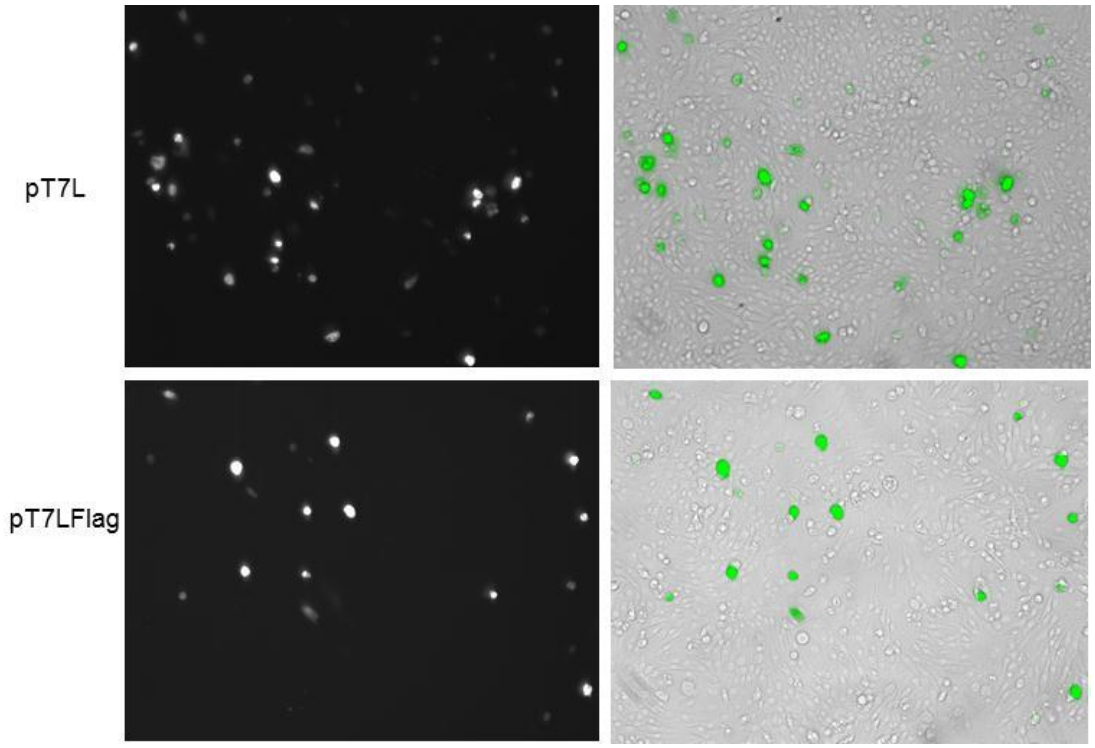

Figure 4.2| **Minigenome rescue with pT7L/Flag**
Confluent monolayers of BSR-T7 cells were transfected with 0.6 µg pT7N, 0.1 µg pT7P, 0.1 µg pT7L or pT7L/Flag and 0.2 µg mgT7GFP. 24 hours post transfection, GFP expression was analysed by fluorescence microscopy. The panels on the left hand side show GFP fluorescence and those on the right hand side are transmission images of the cells overlaid with GFP fluorescence.

4.2.2.3. Insertion of C-terminal Flag tag to L in wild type and tdCE mutant pT7CV using overlapping PCR

Since the L/Flag protein was shown to be functional in minigenome assays, the reverse genetics system was utilised to generate a recombinant virus encoding the L/Flag protein. In order to rescue virus containing L/Flag the flag epitope tag was inserted at the 3' of mutant and wild-type L genes in the full length clone of the virus (pT7CV) (Figure 4.3 a). This was achieved by overlapping PCR. It was not possible to use primers *L F* and *L R* primers that were used to generate pT7LFlag because NsI1 and Sal1 are not unique in the pT7CV plasmid.

Overlapping portions of the L-ORF were amplified by PCR from pT7CV and pT7CV G_{9735}→U using the *L F2* and *L Flag R* primers in one reaction and the *L Flag F* and *L R2* oligonucleotides in a second reaction to produce 1605 and 198 bp PCR products (Figure 4.3 b). The PCR was also carried out with pT7CV G_{9735}→U as the template because the PCR product contains the nucleotide which is mutated in the *td*CE mutant CH157. The outer primers (*LF2* and *L R2*) were subsequently used in a PCR reaction to join the two PCR products obtained in the previous step together, yielding a 1783 bp product (Figure 4.3 c). This product was digested by *SphI* and *Rsr11* resulting in a 1679 bp fragment (Figure 4.3 c) which was then ligated into a pT7CV or pT7CV G_{9735}→U vector also digested with *SphI* and *RsrII*. The ligation reaction was transformed into competent *E.coli* DH5α cells and plated out. Colonies were grown overnight and plasmid DNA was extracted. As expected, fragments of 373, 915, 2557, 5806 bp were produced when pT7CVLFlag was digested with *BamHI* (Figure 4.3 d), thus identifying the plasmid and DNA sequencing with the *L30* primer showed the Flag sequence had been inserted in the correct location.

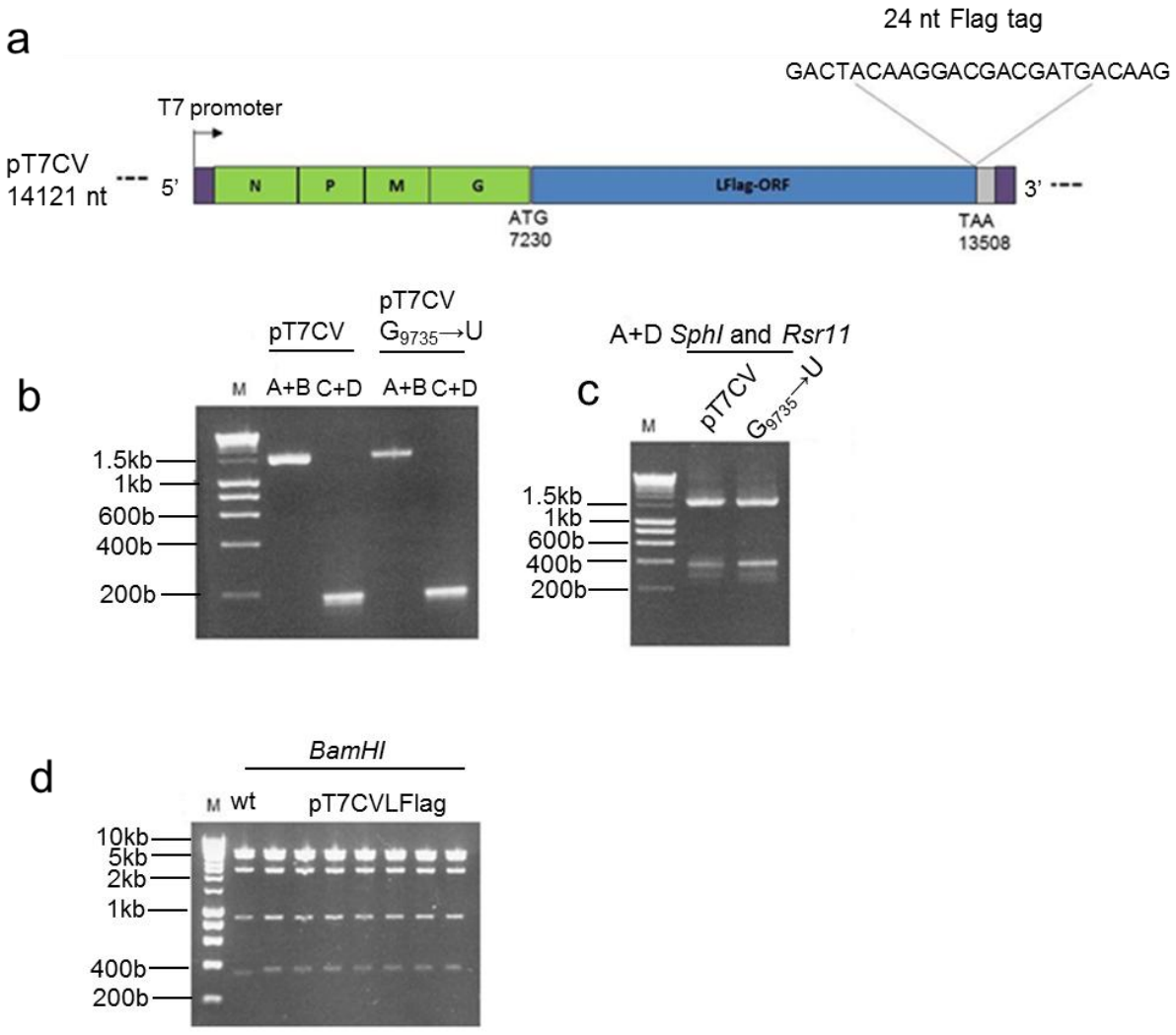

Figure 4.3| **Introduction of a 3' Flag tag in L in wild type and mutant genome clones**
A. Strategy for adding a flag tag to the L gene in the full length vector
B. 2% (w/v) agarose gel stained with ethidium bromide of the *L F2* (A) and *L Flag R* (B) PCR product (1605 bp) and *L Flag F* (C) and *L R2* (D) PCR product (198 bp)
C. 2% (w/v) agarose gel electrophoresis of the *LF2* (A) and *L R2* (D) PCR product after digestion with *SphI* and *Rsr11* (1679 bp).
D. Analytical 1% agarose gel to confirm the identity of pT7CV LFlag (*BamHI* digest). The expected fragments of 373, 915, 2557, 5806 base pairs in length were detected.

4.2.3. Construction of pT7CV-PRFP containing the *td*CE mutations with and without L/Flag

In order to investigate any effects of the *td*CE point mutations on the intracellular localisation and activity of the phosphoprotein (P protein), the L gene of the P/RFP virus was mutated to produce three *td*CE mutants, r7217P/RFP (C_{7217}→U),

r157P/RFP (G_{9735}→U) and r256P/RFP (G_{7694}→A) corresponding to *td*CE mutants CH112, CH157 and CH256, respectively. This was achieved by cloning DNA fragments containing one of the three critical *td*CE point mutations into pT7CV-PRFP (see Appendix 2 and Figure 4.4 a for plasmid map). Four dual tagged recombinant viruses: containing wild-type L or one of the three *td*CE mutations as well as both the L/Flag and P/RFP proteins were also generated. These were designated $rCV_{L/FlagP/RFP}$, $r7217_{L/FlagP/RFP}$ (C_{7217}→U), $r157_{L/FlagP/RFP}$ (G_{9735}→U) and $r256_{L/FlagP/RFP}$ (G_{7694}→A) for *td*CE mutants CH112, CH157 and CH256, respectively. Details of the cloning strategies are given below.

Mutant and wild-type L genes with and without a Flag tag were inserted into the pT7CV-PRFP backbone (Figure 4.4 a). To generate pT7CV-PRFP containing the 112 C_{7217}→U, 157 G_{9735}→U and 256 G_{7694}→A point mutations, the full length vectors with these mutations were digested with *PmlI* and *SphI* (112) or *SphI* and *RsrII* (157 and 256) and ligated into identically digested pT7CV-PRFP.

pT7CV-Flag/PRFP and Flag/PRFP plasmids with the 157 G_{9735}→U point mutation were made by ligating the wild type or mutation-containing 1679 bp *SphI* and *RsrII* digested PCR products with a 3' Flag tag (from the second stage of the overlapping PCR using *LF2* and *L R2* primers, see 4.2.2.3) into the pT7CV-PRFP backbone, also digested with *SphI* and *RsrII* restriction endonucleases. T7CV/Flag 112 C_{7217}→U and 256 G_{7694}→A (construction explained in 4.2.2.3) were digested with *PmlI* and *RsrII* or *KpnI* and *RsrII* respectively and the resultant 1670 and 4103 bp fragments ligated into T7CV-PRFP. This produced the T7CV-Flag/PRFP plasmid containing the specific point mutations.

As before, all the plasmids that were generated were transformed into competent *E.coli* DH5α cells. Colonies were grown and plasmid DNA was isolated. Analytical *BamHI* digestions of the plasmids producing fragments of 349 (373 for vectors containing flag), 1599, 2557, 4497, 5806 bp (Figure 4.4 b) confirmed the plasmid contained the RFP gene and had not undergone any large rearrangements. DNA sequencing confirmed the correct alterations had been made.

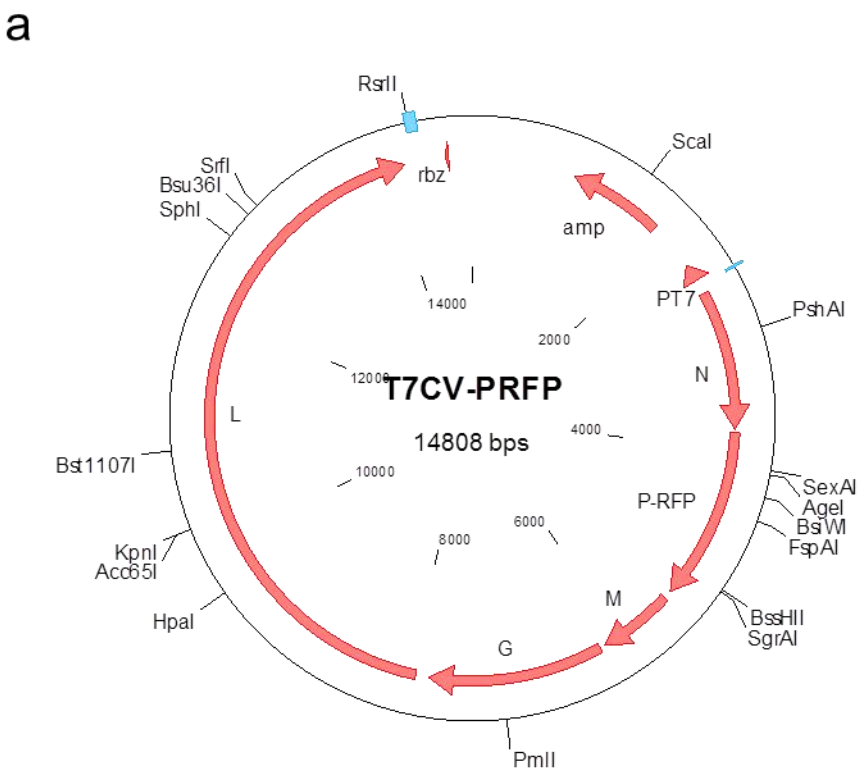

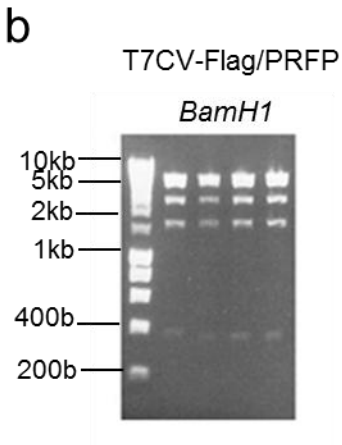

Figure 4.4| **Inserting mutant L and L/flag into PRFP backbone**

A) Plasmid map of pT7CV-PRFP

B) Analytical restriction digest of T7Flag/PRFP digested with *BamHI* on a 1% (w/v) agarose gel

4.2.4. Recovery and growth of P/RFP, L/Flag and dual recombinant viruses

4.2.4.1. Titres of the recovered recombinant viruses

The purified mutant PRFP, Flag and Flag/PRFP plasmids (described in sections 4.2.2.3 and 4.2.3) were subsequently used in full-length transfection experiments to recover infectious viruses containing the Flag, PRFP or Flag/PRFP linked with the *td*CE mutations. The recombinant viruses were then inoculated onto BSC-1 cells and incubated at 33°C until cytopathic effects were extensive. The virus stocks were harvested and the titres determined by plaque assay (Table 4.1). The recombinant viruses containing L/Flag epitope tags had extremely low titres compared with wild type CHPV and therefore could not be used at the M.O.I. required for the intended experiments. Therefore the viruses were grown at 33°C (which increased the viral titres by approximately 2 logs) and then at 31°C which resulted in a further log increase in titres, sufficient for the investigation. It was not possible to rescue the 157Flag/PRFP virus.

Recombinant virus	Titre at 37°C (pfu/ml)	Titre at 33°C (pfu/ml)	Titre at 31°C (pfu/ml)
rCV-L/Flag	2.48×10^4	9.25×10^6	7.15×10^7
r7217L/Flag (C_{7217}→U)	6.25×10^2	3.92×10^6	6.58×10^7
r112L/Flag ($C_{5691, 5760, 7217}$→U)	7.50×10^1	7.42×10^6	4.81×10^7
r157L/Flag (G_{9735}→U)	9.50×10^2	9.25×10^4	7.39×10^5
r256L/Flag (G_{7694}→A)	1.27×10^4	1.47×10^7	6.85×10^7
rCVeGFP	1.40×10^9		
rCV-P/RFP	3.80×10^7		
r7217P/RFP (C_{7217}→U)	2.28×10^7		
r112P/RFP ($C_{5691, 5760, 7217}$→U)	2.58×10^7		
r157P/RFP (G_{9735}→U)	2.35×10^5	5.99×10^6	6.53×10^6
r256P/RFP (G_{7694}→A)	6.45×10^7		
rCV-L/FlagP/RFP	7.68×10^4	8.77×10^5	2.05×10^6
$r7217_{L/FlagP/RFP}$ (C_{7217}→U)	2.50×10^2	5.34×10^5	7.83×10^7
$r112_{L/FlagP/RFP}$ ($C_{5691, 5760, 7217}$→U)	7.5×10^1	6.92×10^4	1.01×10^5
$r157_{L/FlagP/RFP}$ (G_{9735}→U)	X	X	X
$r256_{L/FlagP/RFP}$ (G_{7694}→A)	1.78×10^3	5.50×10^5	1.25×10^6

Table 4.1| **Titres of recombinant CHPV in BSC-1 cells at different temperatures** Recombinant viruses were grown in BSC-1 cells at 31°C, 33°C and 37°C and harvested when CPE was extensive. The resultant viruses were titrated on BSC-1 cells. X denotes virus not able to be rescued.

4.2.4.2. Single-cycle growth analysis of P/RFP and L/Flag recombinant viruses

The growth characteristics of recombinant CHPV (rCHPV), rCV-R/RFP and rCV-L/Flag were examined by single step growth analysis and the titre of virus present in the supernatant from 0 to 8 hours post-infection is shown in Figure 4.5. The growth curves show that both of the recombinant viruses containing tagged proteins are impaired in their growth in comparison with the wild-type virus, with rCV-L/Flag the most severely impaired. rCV-P/RFP reached the maximum titre of 7.3 $\log_{10}$ pfu/ml^{-1} 7 hours post-infection whereas rCHPV grew to a maximum titre of 9.3 $\log_{10}$ pfu/ml^{-1} by the same time point, i.e. approximately a 100-fold difference in growth. The

rCV-L/Flag virus lagged behind the other two viruses, with virus first detectable in the supernatant at 5 hours post-infection compared with 3 hours post-infection for CHPV and rCV-P/RFP. rCV-L/Flag reached a titre of 4.7 $\log_{10}$ pfu/ml^{-1}, which was approximately 500 and 50,000-fold lower than rCV-P/RFP and rCHPV, respectively. However, the stock of rCV-L/Flag virus which was grown at 31°C was 7.15 x 10^7 pfu/ml (Table 4.1).

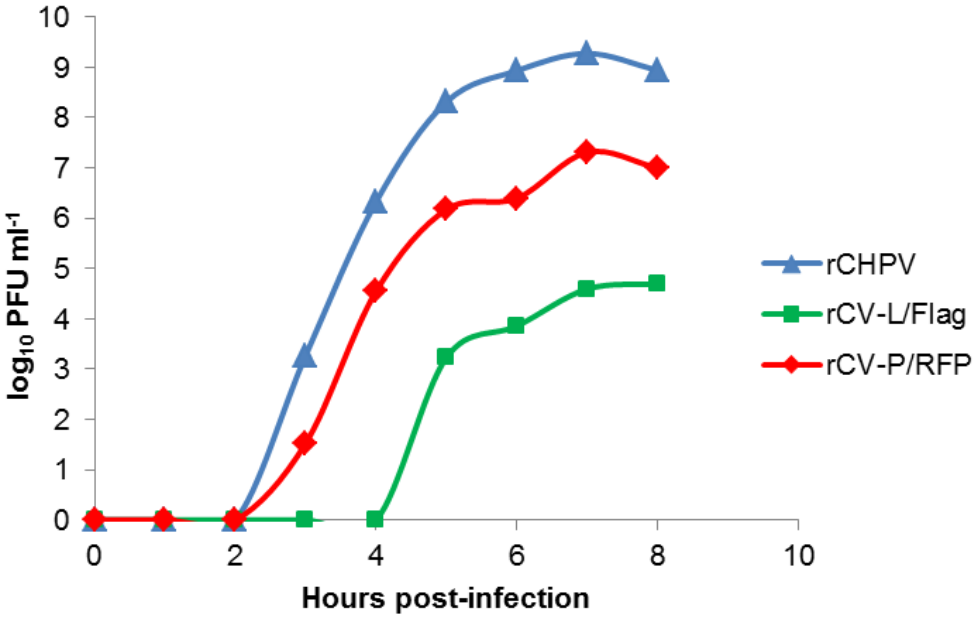

Figure 4.5| **Growth curve of wild-type and recombinant CHPV in BSC-1 cells at 37°C** BSC-1 cells were inoculated with rCHPV (blue), rCV-P/RFP (red) or rCV-L/Flag (green) at an M.O.I. of 10. Virus supernatant was collected at 0, 1, 2, 3, 4, 5, 6, 7 and 8 hours post-infection and titrated. Infections were carried out in duplicate.

4.2.4.3. Fluorescence of P/RFP recombinant viruses

To confirm the presence of the fluorescent RFP reporter construct BSC-1 cells were infected with the wild-type and *td*CE mutant P/RFP viruses at an M.O.I. of 3 pfu/cell and RFP visualised using epifluorescence microscopy. Discrete loci of RFP expression within the cytoplasm of infected cells were first observed 4 hours post-

infection (Figure 4.6). The initial signs of CPE were also seen at this time point, as shown in Figure 4.6 by several rounded infected cells. 24 hours after infection of the P/RFP viruses, the CPE was extensive and most of the remaining cells were fluorescing.

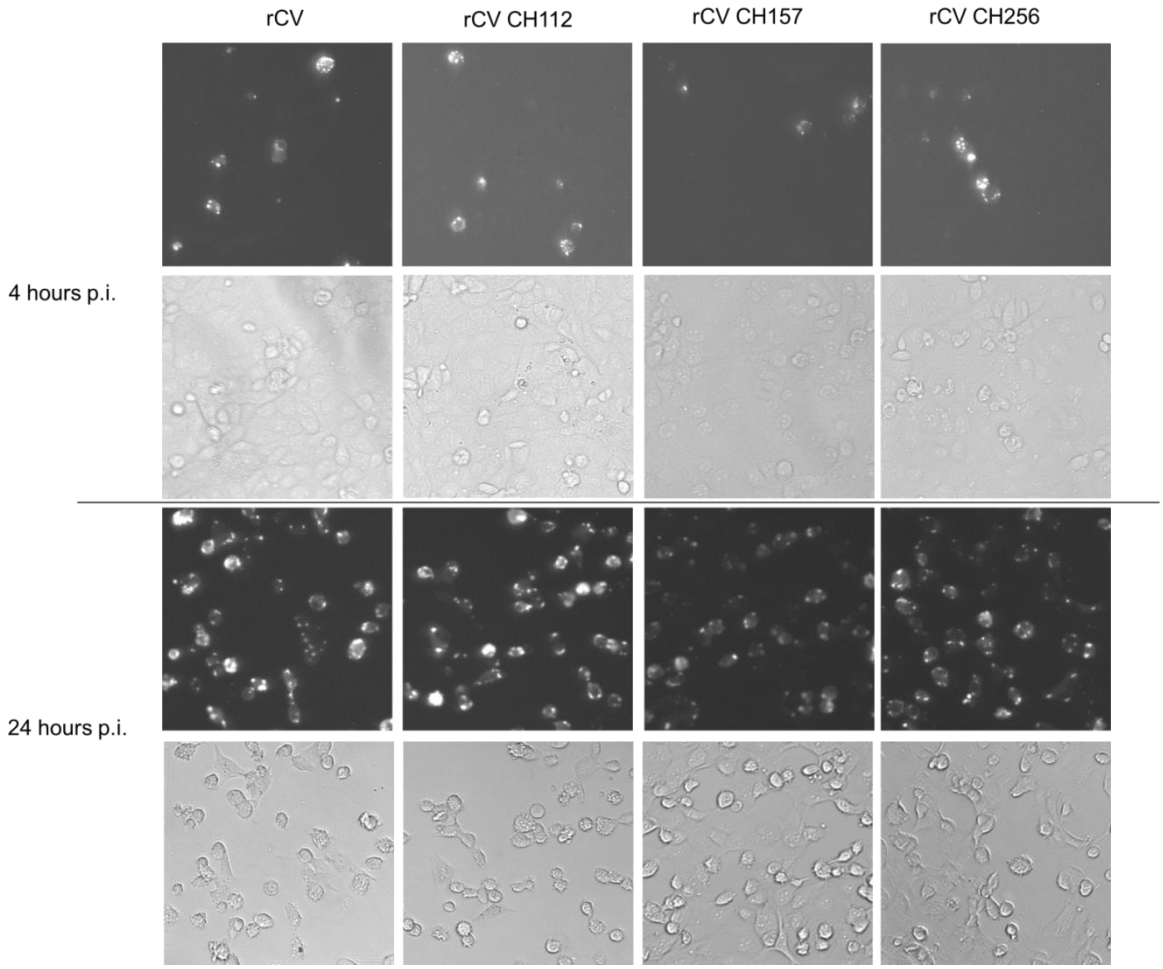

Figure 4.6| **RFP fluorescence in BSC-1 cells infected with wild-type and *td*CE mutant rCV-P/RFP**
BSC-1 cells were inoculated with rCV; rCV CH112(C_{7217} to U); rCV CH157; rCV CH256 P/RFP viruses at an M.O.I. of 3. Cells were incubated at 37°C and fluorescence was visualised using a fluorescence microscope at 4 and 24 hours post-infection. The top panel for each time point shows RFP fluorescence and the lower panel shows a transmission image of the cells for each condition.

4.2.4.4. L/Flag could not be detected in infected cells by immunofluorescence

To confirm the presence of functional L/Flag protein BSC-1 cells were infected with wild-type (rCV-L/Flag) and *td*CE mutation-containing L/Flag viruses (r7217L/Flag (C_{7217}→U), r157L/Flag (G_{9735}→U), r256L/Flag (G_{7694}→A)) at an M.O.I. of 3 pfu/cell. Cells were fixed at 4, 8 and 24 hours post-infection, permeabilised and stained with anti-Flag M2 antibody (Sigma). Following incubation with a secondary antibody conjugated to a fluorophore emitting green light, the cells were examined using confocal fluorescence microscopy. No fluorescence was detected in cells infected with any of the four recombinant viruses. A positive control for the anti-Flag antibody was used.

4.2.5. The P/RFP protein can be detected in infected cells by Western blot

To confirm the presence of the P/RFP protein in P/RFP virus-infected cells BSC-1 cells were infected with the P/RFP recombinant virus at a M.O.I of 5 pfu/cell. 5 hours post-infection, cell lysates were harvested and the P/RFP protein was detected by western blot (Figure 4.7). P/RFP is approximately 62.6 kDa in size (CHPV P protein is 32.6 and RFP is 30 kDa).

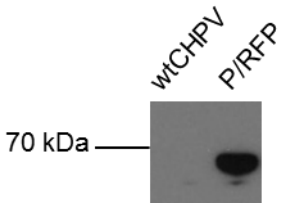

Figure 4.7| **Western blot of P/RFP protein expression in BSC-1 cells**
Whole cell lysates of wild type CHPV or P/RFP virus infected BSC-1 cells were electrophoresed on a 10% SDS-PAGE gel, transferred onto a Hybond ECL membrane and blotted with rabbit polyclonal anti-RFP antibody. A molecular mass marker protein was used to determine the approximate sizes of the protein.

4.2.6. The Flag-tagged CHPV L protein is stable

In order to demonstrate that the L proteins of the wild-type L protein Flag virus contain a C-terminal Flag tag BSC-1 cells were infected with rCV-L/Flag at a M.O.I of 5 and whole cell lysates harvested 12 hours post-infection. The expression of L/Flag in rCV-L/Flag infected BSC-1 cells was then analysed by western blot, using the anti-Flag M2 primary antibody (Figure 4.8). A 238.5 kDa band (the molecular weight of CHPV L protein) is present in cell lysates that had been inoculated with rCV-L/Flag but not in wild type CHPV infected lysates. This indicates that the L/Flag protein is functional during virus infection. The L/Flag protein was also detected in pelleted L Flag viruses (wild type L and *td*CE L mutant viruses), providing further confirmation that the Flag tags are stably attached to the L proteins of these viruses (Figure 4.8).

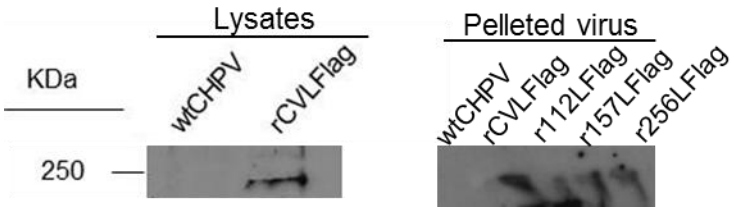

Figure 4.8| **Western blot of L/Flag protein expression in BSC-1 cells and pelleted virus** Whole cell lysates of wild type CHPV or rCV-L/Flag infected BSC-1 cells and pelleted wtCHPV and L Flag viruses (wild type control and *td*CE mutant viruses) were electrophoresed on a 7% SDS-PAGE gel, transferred onto a Hybond ECL membrane and blotted with mouse anti-Flag M2 antibody.

4.3. The location of CHPV *td*CE mutant replication complexes in permissive and non-permissive conditions

The presence of the amino acid substitutions conferring the *td*CE phenotype within the polymerase protein and the diminished RNA synthesis in the mutants suggest that the generation of functional replication complexes in CE cells may be disrupted. To determine whether the *td*CE point mutations disrupt the intracellular localisation of the P protein in the replication complexes the P/RFP recombinant viruses: r7217P/RFP (C_{7217}→U), r157P/RFP (G_{9735}→U), r256P/RFP (G_{7694}→A) and the control (wild-type L protein) CVP/RFP virus were used to infect cells at an M.O.I of 1 pfu per cell. Cells were fixed with 10% formaldehyde in PBS when fluorescence was clearly visible. There was no visible RFP expression in CE cells infected with P/RFP mutant L viruses at 39°C until 24 hours post-infection, whereas RFP was clearly visible after just 8 hours when the cells were incubated at 31°C (the latter was also true for CE cells inoculated with the wild type L virus at either temperature and BSC-1 cells under any condition).

The distribution of P/RFP in wild type and mutant L viruses in BSC-1 and CE cells at 31°C and 39°C determined by confocal fluorescence microscopy is shown in Figure 4.9. In infected BSC-1 cells at either temperature P/RFP was present in large bright cytoplasmic foci located primarily near the cell periphery (Figure 4.9 a-h). Several smaller punctate regions of fluorescence were also visible as well as very faint diffuse staining throughout the cell cytoplasm (Figure 4.9 a-h). A similar pattern of fluorescence was also observed with the P/RFP mutant L viruses in CE cells grown at 31°C and in wild type virus-infected CE cells grown at both temperatures (Figure 4.9 i-m). However, CE cells incubated at 31°C showed a slightly brighter diffuse cytoplasmic staining of P/RFP than BSC-1 cells. All three mutant L gene viruses showed a significantly different pattern in CE cells infected at 39°C, generating only a very diffuse pattern of RFP/P fluorescence (Figure 4.9 n-p) suggesting that the formation of replication complexes was significantly impaired in non-permissive conditions.

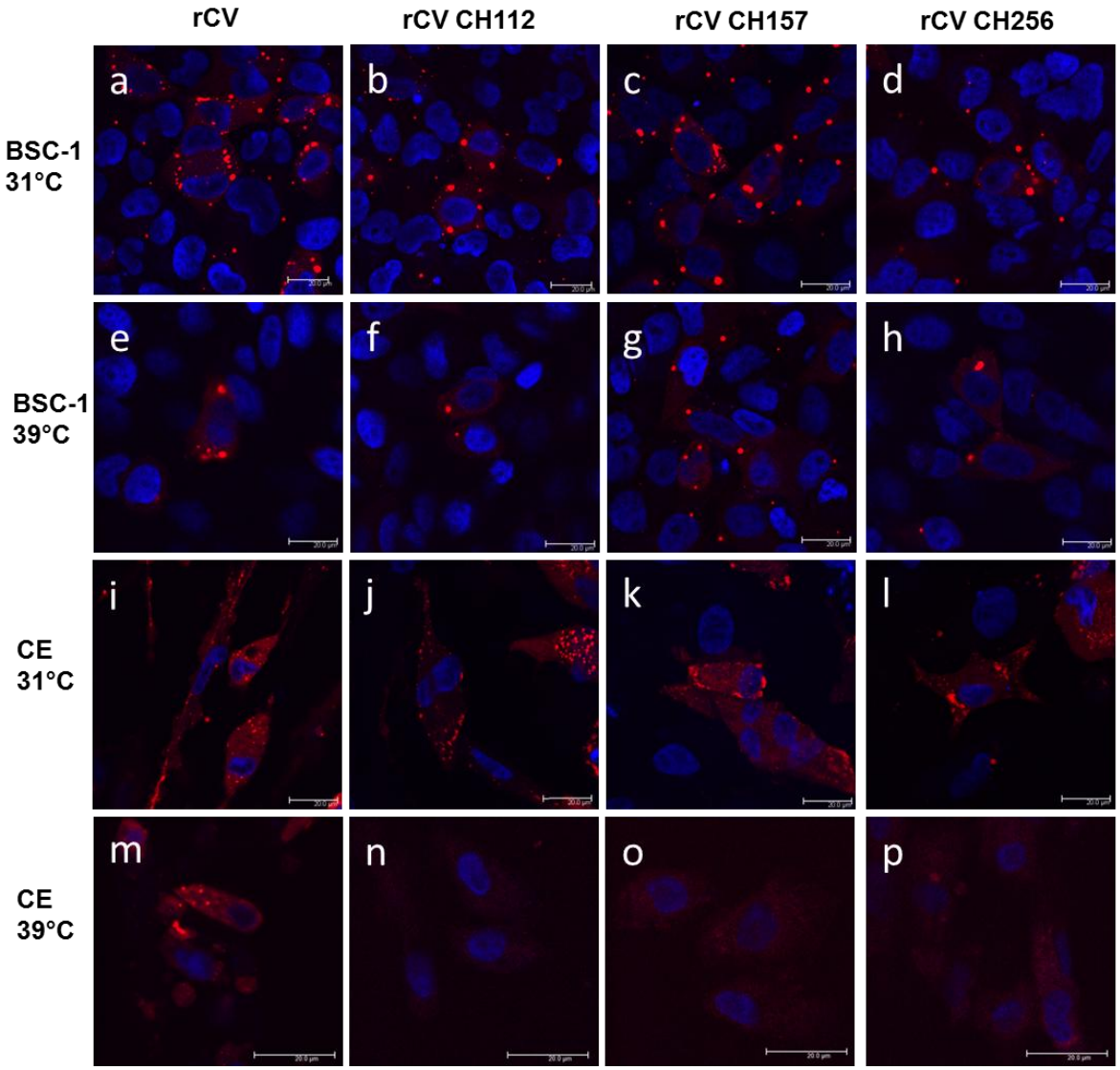

Figure 4.9| **Intracellular localisation of mutated rCV-P/RFP viruses in BSC-1 and CE cells.**
BSC-1 (a-h) and CE (i-p) cells infected with rCV (a, e, i, m); rCV CH112(C_{7217} to U) (b, f, j, n); rCV CH157 (c, g, k, o); rCV CH256 (d, h, l, p) P/RFP viruses at an M.O.I. of 1. Cells were incubated at 31°C (a-d, i-l) or 39°C (e-h, m-p) and fixed in 4% formaldehyde when RFP fluorescence was clearly visible. This was 8 hours post-infection for BSC-1 cells, CE cells incubated at 31°C and CE cells infected with rCV and incubated at 39°C. CE cells incubated with the mutant viruses at 39°C were fixed 48 hours post-infection. Nuclei were stained with DAPI.

4.4. Identification of cellular factors associated with CHPV L protein in mammalian and avian cells

4.4.1. Introduction and strategy

Host cell factors are essential to the life cycles of all viruses and the isolation of *td*CE mutants of CHPV emphasised their importance in the replication of vesiculoviruses. The critical host factors for CHPV are largely unknown, however, a recent RNAi screen identified 72 mammalian genes as essential for VSV infection (Panda *et al.*, 2011). Table 1.3 gives details of the cellular proteins shown to be involved in VSV replication. The objective of this research was to identify cellular proteins that associate with the catalytic component of the CHPV polymerase, the L protein. The strategy used to identify crucial cellular binding partner(s) was co-immunoprecipitation and the L protein binding partners were then characterised by mass spectrometry (University of Liverpool).

4.4.2. Determination of cellular binding partners of the CHPV L protein

BSC-1 and CE cells were infected with rCV-L/Flag at an M.O.I. of 5 pfu/cell and incubated at 31°C. Whole cell lysates were prepared at 8 hours post-infection. This time point was guided by the presence of RFP fluorescence from wild-type P/RFP virus infection of BSC-1 and CE cells (as L/Flag could not be detected in immunofluorescence). L/Flag fusion proteins were immunoprecipitated using anti-Flag M2 magnetic beads (Sigma) and eluted in 0.1M glycine HCl pH3. Lysates of rCHPV infected BSC-1 and CE cells were also prepared and immunoprecipitated. These were used as controls for the non-specific binding of proteins to the anti-flag M2 magnetic beads. Following neutralisation in Tris base, samples containing the

L/Flag fusion proteins were analysed by mass spectrometry at the University of Liverpool using the methodology outlined below. The immunoprecipitated samples were concentrated, digested with trypsin and peptide mixtures were analysed by online nanoflow liquid chromatography using the nanoACQUITY-nLC system (Waters MS technologies, Manchester, UK) coupled to an LTQ-Orbitrap Velos (ThermoFisher Scientific, Bremen, Germany) mass spectrometer. Progenesis LC-MS (version 4.1. nonlinear dynamics) software was used for the analysis and tandem mass spectrometry data were searched against the monkey, chicken and CHPV predicted proteomes.

Tables 4.2 and 4.3 show the proteins which were identified in the mass spectrometry analysis of immunoprecipitated L/Flag samples during mammalian and avian cell infection, respectively, and therefore are possible cellular binding partners of CHPV L protein. The cellular proteins are ranked highest to lowest according to maximum fold change, which takes into account the number of peptides used to identify the protein and the number used to quantify the protein. The greater the maximum fold change value the more peptides used to identify and quantify the protein and therefore the higher the probability that the interaction is correct. Only proteins with a maximum fold change value of 3 or greater were considered potential cellular interacting partners of L/Flag (126 proteins in mammalian cell samples and 25 proteins in avian cell samples) and thus were included in the tables, whereas those with values of less than 3 were considered to be non-specifically bound to L/Flag. The value of 3 was chosen as the cut-off point as it corresponds to the value seen with the CHPV G protein which has not been shown to specifically associate with the CHPV L protein, was identified with a maximum fold value of 2.9.

Mass spectrometry analysis of the cellular binding partners of the L/Flag fusion protein in mammalian cells identified all three members of the viral ribonucleoprotein (RNP) complex: L, P and N proteins (highlighted in yellow in Table 4.2) with high maximum fold change values. As the P and N proteins are known to interact with the L protein their detection provided confidence that the pull down was successful. The other two virus proteins, G and M were also identified but at significantly lower frequencies which can be attributed to background, non-specific interaction. The M protein was identified at a very high frequency in the mass spectrometry analysis of the L/Flag protein pull down in avian cells (highlighted in yellow in Table 4.3). This finding might be incorrect as the L and M proteins of vesiculoviruses have not been previously shown to interact.

Max fold change	Protein identified	Cellular functions
200.42	V-type proton ATPase subunit d 1	A constituent of the vacuolar ATPase (V-ATPase), an enzyme required for the acidification of eukaryotic intracellular organelles. Essential for receptor mediated endocytosis
55.75	Keratin, type I cytoskeletal 16	Intermediate filament protein
39.63	Vimentin	Intermediate filament protein
36.76	Actin, alpha cardiac muscle 1	Cell motility
27.75	Keratin, type I cytoskeletal 17	Intermediate filament protein
27.28	Keratin, type II cytoskeletal 7	Interacts with eukaryotic translation initiation factor 3 (eIF3), induces DNA synthesis
23.17	Coronin-1C, Actin Binding Protein	Cytokinesis, cell motility
21.95	Drebrin	Actin-binding protein
20.35	40S ribosomal protein S12	Component of the 40S ribosomal subunit
18.67	Phosphoprotein	
18.17	60S ribosomal protein L37	Component of the 60S ribosomal subunit
17.97	Keratin, type I cytoskeletal 18	Intermediate filament protein
17.41	Cystatin-A	Cysteine protease inhibitor with roles in cell-cell adhesion
17.36	Corneodesmosin	Cell-cell adhesion
15.41	Keratinocyte proline-rich protein	ND
14.96	Fatty acid-binding protein, epidermal	Fatty acid metabolism
14.03	Plectin	Connects immediate filaments with microtubules and microfilaments
13.42	Peptidyl-prolyl cis-trans isomerase A	Protein folding. Also binds cyclosporin and may be involved in cyclosporin-dependent immunosuppression.
12.76	Keratin, type II cytoskeletal 8	Intermediate filament protein
12.12	Transgelin-2	May function as a tumour suppressor

12.06	RNA-directed RNA polymerase L	
12.05	Actin, cytoplasmic 1	Cell structure and motility
9.89	Keratin, type I cytoskeletal 14	Intermediate filament protein
9.25	Small nuclear ribonucleoprotein Sm D1	Member of the small nuclear ribonucleoprotein (snRNP) family, RNA-binding protein
9.21	Protein arginine N-methyltransferase 1	Belongs to the protein arginine N-methyltransferase family, roles in post translational modifications
9.14	Histone H1.2	Required for the condensation of chromatin, roles in chromatin remodelling
9.05	Keratin, type II cytoskeletal 5	Structural constituent of the cytoskeleton
8.73	T-complex protein 1 subunit epsilon	Chaperone protein that facilitates the folding of proteins (including actin and tubulin) in an ATP-dependent manner
8.64	Mitochondrial inner membrane protein	Regulates mitochondrial cristae architecture
8.11	40S ribosomal protein S7	Component of the 40S ribosomal subunit
7.60	Putative RNA-binding protein 3	Stimulates protein synthesis, cold-inducible
7.59	Glial fibrillary acidic protein	Intermediate filament protein
7.43	Ubiquitin-40S ribosomal protein S27a	S27a is a component of the 40S ribosomal subunit. Ubiquitin is required for targeting proteins for degradation by the proteasome
7.37	60S ribosomal protein L29	Component of the 60S ribosomal subunit
7.14	DBIRD complex subunit ZNF326	Major constituent of the DBIRD complex required for integrating elongation with alternative splicing
7.07	Hornerin	Intermediate-filament associated protein, binds calcium ions
7.02	Tropomyosin alpha-3 chain	Actin-binding protein, roles in stability of the cytoskeleton
6.81	60S ribosomal protein L27a	Component of the 60S ribosomal subunit
6.76	Nucleoprotein	
6.62	Small nuclear ribonucleoprotein-	Member of the snRNP family, involved in pre-mRNA

	associated protein N	processing
6.44	Protein FAM98A	Roles in cell division
6.34	Transitional endoplasmic reticulum ATPase	Interacts with clathrin and heat shock protein 70 (Hsc70), roles in vesicle transport
6.26	Dermcidin	Peptidase activity
6.25	60S ribosomal protein L21	Component of the 60S ribosomal subunit
6.21	Ras-related protein Rab-1B	GTPase required for the transport of vesicles between the endoplasmic reticulum and Golgi
6.12	Eukaryotic translation initiation factor 3 subunit C	Constituent of the eukaryotic translation initiation factor 3 (eIF-3) complex, essential for the initiation of protein synthesis
6.10	Myosin regulatory light chain 12B	Cell migration and cytokinesis
6.05	60S ribosomal protein L13	Component of the 60S ribosomal subunit
5.91	Glyceraldehyde-3-phosphate dehydrogenase (GAPDH)	Carbohydrate metabolism
5.90	Heterogeneous nuclear ribonucleoprotein D-like	Member of the heterogeneous nuclear ribonucleoprotein (hnRNP) family of RNA-binding proteins. Stimulates transcriptional repression
5.75	KRR1 small subunit processome component homolog	Roles in the biogenesis of the 40S ribosomal subunit and ribosome assembly
5.72	Junction plakoglobin	Roles in cytoskeletal arrangement and transcriptional activation
5.65	Ubiquitin-60S ribosomal protein L40	L40 is a component of the 60S ribosomal subunit. Ubiquitin is required for targeting proteins for degradation by the proteasome
5.47	Keratin, type II cytoskeletal 1	Structural component of the cytoskeleton
5.41	Nucleolar protein 14	Roles in pre-18S RNA processing and export of the 40S subunit to the cytoplasm
5.26	Caveolin-1	Scaffolding protein in caveolae plasma membranes, stimulates cell cycle progression

5.21	Desmoplakin	Formation of desmosomes, associates with intermediate filaments
5.17	Alpha-enolase	Glycolysis, represses transcription, stimulates the generation of immunoglobulins
5.14	60S ribosomal protein L35	Component of the 60S ribosomal subunit
5.12	40S ribosomal protein S18	Component of the 40S ribosomal subunit
5.09	Protein PRRC2A	Involved in pre-mRNA splicing
4.88	Keratin, type I cytoskeletal 9	Structural constituent of the cytoskeleton
4.81	Heat shock protein HSP 90-beta	Chaperone that facilitates protein folding, constitutively expressed
4.80	T-complex protein 1 subunit alpha	Chaperone protein that facilitates the folding of proteins (including actin and tubulin) in an ATP-dependent manner
4.65	60S ribosomal protein L34	Component of the 60S ribosomal subunit
4.62	40S ribosomal protein S25	Component of the 40S ribosomal subunit
4.61	Protein LTV1 homolog	RNAi screening identified an involvement in cell cycle arrest at the G2 checkpoint
4.60	40S ribosomal protein S24	Component of the 40S ribosomal subunit
4.59	Splicing factor U2AF 65 kDa subunit	Splicing
4.58	Arf-GAP with coiled-coil, ANK repeat and PH domain-containing protein 2	A GTPase-activating protein (GAP) for ADP ribosylation factor 6 (ARF6), regulates vesicular trafficking
4.57	Peptidyl-prolyl cis-trans isomerase B	Stimulates protein folding
4.57	Tropomyosin alpha-1 chain	Binds to actin filaments, structural component of the cytoskeleton
4.50	60S ribosomal protein L39	Component of the 60S ribosomal subunit
4.47	Malate dehydrogenase, mitochondrial	Catalyses the oxidation of malate to oxaloacetate in the citric acid cycle
4.43	Thyroid hormone receptor-associated protein 3	Roles in pre-mRNA splicing, implicated in the coactivation of transcription

4.39	6-phosphofructo-2-kinase/fructose-2,6-bisphosphatase 3	Generation and degradation of fructose 2,6-bisphosphate
4.31	Heterogeneous nuclear ribonucleoprotein A1	Member of the heterogeneous nuclear ribonucleoprotein (hnRNP) family of RNA-binding proteins. Involved in exporting mRNA from the nucleus to the cytoplasm and packaging of pre-mRNA into hnRNP complexes
4.28	Chromatin target of PRMT1 protein	Implicated role in cell cycle progression
4.26	60S ribosomal protein L24	Component of the 60S ribosomal subunit
4.25	Cytosolic purine 5'-nucleotidase	Hydrolyses purine nucleotides (nucleic acid metabolism)
4.25	Calmodulin	Regulates a large number of kinases, phosphatases and ion channels
4.24	60S ribosomal protein L7a	Component of the 60S ribosomal subunit
4.17	Zinc finger protein 706	ND
4.14	Heterogeneous nuclear ribonucleoprotein H	Member of the heterogeneous nuclear ribonucleoprotein (hnRNP) family of RNA-binding proteins. Involved in the modulation of alternative splicing
4.10	TATA-binding protein-associated factor 2N	Involved in transcription initiation
4.06	Interleukin enhancer-binding factor 3	Post-transcriptional regulator of gene expression, inhibits the initiation of translation
4.03	Myosin light polypeptide 6	Constituent of the ATPase myosin motor protein
4.02	60S ribosomal protein L23a	Component of the 60S ribosomal subunit
4.01	Desmoglein-1	Component of desmosomes, facilitates cell to cell adhesion
4.00	Keratin, type II cytoskeletal 2 epidermal	Structural constituent of the cytoskeleton
4.00	Annexin A1	Calcium-dependent phospholipid binding protein which has roles in exocytosis and inhibiting inflammation
3.99	T-complex protein 1 subunit beta	Chaperone protein that facilitates the folding of proteins (including actin and tubulin) in an ATP-dependent manner

3.95	60S ribosomal protein L36a	Component of the 60S ribosomal subunit
3.95	14-3-3 protein zeta/delta	Adaptor protein which is responsible for regulating a large number of signalling pathways
3.78	Unconventional myosin-Ic	Involved in the transport of vesicles and transcription initiation
3.73	Annexin A4	Calcium-dependent phospholipid binding protein which has roles in endocytosis and exocytosis
3.70	40S ribosomal protein S10	Component of the 40S ribosomal subunit
3.67	Eukaryotic translation initiation factor 3 subunit I	Constituent of the eukaryotic translation initiation factor 3 (eIF-3) complex, essential for the initiation of protein synthesis
3.54	40S ribosomal protein S28	Component of the 40S ribosomal subunit
3.52	Serine/arginine repetitive matrix protein 1	Constituent of splicing mRNA complexes, regulates pre-mRNA processing
3.47	Small nuclear ribonucleoprotein Sm D3	Major component of the spliceosome which is essential for pre-mRNA processing
3.47	RNA-binding protein 28	Member of the snRNP family, involved in pre-mRNA processing
3.46	PHD finger-like domain-containing protein 5A	Member of the snRNP family, involved in pre-mRNA splicing and transcriptional upregulation of connexin 43
3.44	Eukaryotic translation initiation factor 3 subunit B	Constituent of the eukaryotic translation initiation factor 3 (eIF-3) complex, essential for the initiation of protein synthesis
3.44	Cellular nucleic acid-binding protein	Binds single stranded DNA and RNA and is involved in the cap-independent translation of ornithine decarboxylase mRNA
3.43	40S ribosomal protein S6	Component of the 40S ribosomal subunit. Promotes cell proliferation by preferentially translating specific mRNAs
3.42	RRP12-like protein	ND
3.39	Serine/threonine-protein kinase 38-like	Associated with the cytoskeleton
3.34	Eukaryotic translation initiation factor 4 gamma 1	Component of the EIF4F complex which is responsible for recruiting mRNA to ribosomes, 5’ cap recognition and removal

		of secondary structure from templates during translation initiation
3.33	Serum albumin	Major component of plasma
3.24	Alpha-centractin	Constituent of dynactin which is a multisubunit complex that binds to microtubules and dynein to mediate vesicular transport
3.21	40S ribosomal protein S29	Component of the 40S ribosomal subunit.
3.20	General transcription factor II-I	Regulates transcription
3.18	Serine/threonine-protein kinase 38-like	Inhibits apoptosis upon association with microtubule associated monooxygenase 1 (MICAL1)
3.18	40S ribosomal protein S23	Component of the 40S ribosomal subunit.
3.17	THO complex subunit 4	A chaperone protein which modulates dimerisation and activation of basic leucine zipper-containing transcription factors. Also involved in mRNA splicing and nuclear export
3.16	Nucleophosmin	Roles include modulating the tumour suppressor proteins ARF and p53, cell proliferation, generation of ribosomes, duplicating centrosomes and histone remodelling
3.15	40S ribosomal protein S30	S30 is a component of the 40S ribosomal subunit.
3.14	Coiled-coil-helix-coiled-coil-helix domain-containing protein 3, mitochondrial	Inhibits the transcription of the anti-apoptotic Bcl-2-binding protein BAG1 and is required to preserve the mitochondrial structure
3.13	60S ribosomal protein L28	Component of the 60S ribosomal subunit
3.08	Transcription factor BTF3	Binds to RNA polymerase 11, required for the initiation of transcription
3.07	Protein arginine N-methyltransferase 5	Inhibits cell proliferation, blocks EGF signalling and has roles in snRNP complex assembly
3.07	Eukaryotic translation initiation factor 4H	Constituent of the translation initiation complex, promotes EIF4A helicase activity
3.06	Heterogeneous nuclear	Member of the heterogeneous nuclear ribonucleoprotein

	ribonucleoprotein K	(hnRNP) family of RNA-binding proteins. Involved in the modulation of alternative splicing and the DNA damage response
3.04	60S ribosomal protein L27	Component of the 60S ribosomal subunit
3.03	Src substrate cortactin	Involved in the organisation of the actin cytoskeleton, cell migration
3.01	Peptidyl-prolyl cis-trans isomerase-like 3	Enhances protein folding
3.01	Galectin-1	Modulates cell proliferation and apoptosis
3.00	Bcl-2-associated transcription factor 1	Represses transcription, stimulates apoptosis

Table 4.2| **Proteins identified in immunoprecipitated L/Flag samples during mammalian cell infection**
BSC-1 cells were infected with rCV-L/Flag at an M.O.I. of 5 pfu/cell, incubated at 31°C and whole cell lysates prepared at 8 hours post-infection. Proteins bound to L/Flag were immunoprecipitated using anti-flag M2 magnetic beads (Sigma) and eluted in 0.1M glycine HCl pH3. Samples were analysed by LC-MS. The identified proteins are listed in order of maximum fold change highest to lowest, which takes into account the number of peptides used to identify the protein and the number used to quantify the protein. Cellular interacting proteins with maximum fold values of 3 or greater (126 proteins) were considered potential specific cellular binding partners of L/Flag and therefore were included in this table whereas those with values of less than 3 were considered to be background or non-specifically bound proteins. The cut-off value of 3 was selected because the CHPV G protein, which has not been shown to bind the CHPV L protein specifically, was identified with a maximum fold value of 2.9. Viral proteins are highlighted in yellow.

Max fold change	Protein identified	Cellular functions
5964.39	Matrix protein	
153.96	Annexin A1	Calcium-dependent phospholipid binding protein which has roles in exocytosis and inhibiting inflammation
153.13	Tropomyosin alpha-1 chain	Binds to actin filaments, structural component of the cytoskeleton
21.07	Collagen alpha-2(I) chain	Structural constituent of the extracellular matrix
10.48	40S ribosomal protein S13	Component of 40S ribosomal subunit
9.36	Non-histone chromosomal protein HMG-17	Modulates DNA-histone interaction
9.03	Nucleolin	Promotes chromatin condensation, formation of ribosomes
8.84	Histone H2A.Z	Constituent of nucleosomes
6.94	Keratin, type I cytoskeletal 19	Intermediate filament protein
5.02	Nucleophosmin	Chaperone for the core histones, ribosome assembly
4.88	Myosin light polypeptide 6	Constituent of the ATPase myosin motor protein
4.82	Cathepsin L1	Degrades proteins in lysosomes
4.62	Collagen alpha-1(I) chain	Major component of the extracellular matrix
4.44	Heat shock 70 kDa protein	Involved in protein folding in response to stress
4.38	Myosin-9	Cytokinesis, cytoskeleton remodelling
4.10	Ubiquitin-40S ribosomal protein S27a	S27a is a component of the 40S ribosomal subunit. Ubiquitin is required for targeting proteins for degradation by the proteasome
4.06	60S ribosomal protein L15	Component of 60S ribosomal subunit
3.94	Actin, cytoplasmic 2	Structural constituent of the cytoskeleton
3.94	40S ribosomal protein S4	Component of 40S ribosomal subunit

3.94	Fibronectin	Cell-cell adhesion, cell motility
3.76	78 kDa glucose-regulated protein	Member of the heat shock protein 70 family, assists in the formation of multimeric protein complexes in the endoplasmic reticulum
3.72	Elongation factor 1-alpha 1	Required in protein synthesis to stimulate the attachment of aminoacyl-tRNA to the A site of ribosomes
3.22	Annexin A2	Involved in exocytosis and cytoskeleton architecture
3.11	Ubiquitin-60S ribosomal protein L40	L40 is a component of the 60S ribosomal subunit. Ubiquitin is required for targeting proteins for degradation by the proteasome
3.08	Keratin, type I cytoskeletal 14	Intermediate filament protein
3.01	Vimentin	Intermediate filament protein

Table 4.3| **Proteins identified in immunoprecipitated L/Flag samples during avian cell infection**
CE cells were infected with rCV-L/Flag at an M.O.I. of 5 pfu/cell, incubated at 31°C and whole cell lysates prepared at 8 hours post-infection. Proteins bound to L/Flag were immunoprecipitated using anti-flag M2 magnetic beads (Sigma) and eluted in 0.1M glycine HCl pH3. Samples were analysed by LC-MS. The identified proteins are listed in order of maximum fold change highest to lowest. Cellular proteins with maximum fold values of 3 or greater (25 proteins) were included in this table and considered potential specific cellular binding partners of L/Flag. Proteins with values of less than 3 were considered to be non-specific, background proteins. The cut-off maximum fold value of 3 was chosen because the CHPV G protein, which has not been shown to specifically bind the CHPV L protein, was identified with a value of 2.9. Viral proteins are highlighted in yellow. Cellular proteins which were also identified in the mammalian cell samples to be associated with L/Flag are highlighted in purple.

The potential protein binding partners of L/Flag during mammalian and avian cell infection were classified based on their cellular functions and the proportions of each of the functional groups which are represented are illustrated in Figure 4.10. The functional diversity of proteins identified in the mammalian cell samples was greater than in the avian cell samples, which is reflected in the number of functional groups, 14 for mammalian cell and 6 for avian cell samples. 39% and 42% of the potential L/Flag interacting proteins in mammalian and avian cells respectively which were identified during this analysis are involved in cellular gene expression and comprised the largest functional group in both datasets. Many proteins with roles in the cytoskeleton, protein folding, vesicular transport and the cell cycle were also identified as L/Flag binding partners in both mammalian and avian cells. Proteins that function in RNA post-transcriptional modification were isolated as potential L/Flag interacting proteins during infection in mammalian cells, accounting for 11% of the co-immunoprecipitated proteins. The remaining 13% of L/Flag fusion proteins detected in the mammalian cell samples was comprised of proteins involved in carbohydrate metabolism, cell to cell interaction, lipid metabolism, post-translational modification, amino acid metabolism, nucleic acid metabolism, cell signalling and apoptosis.

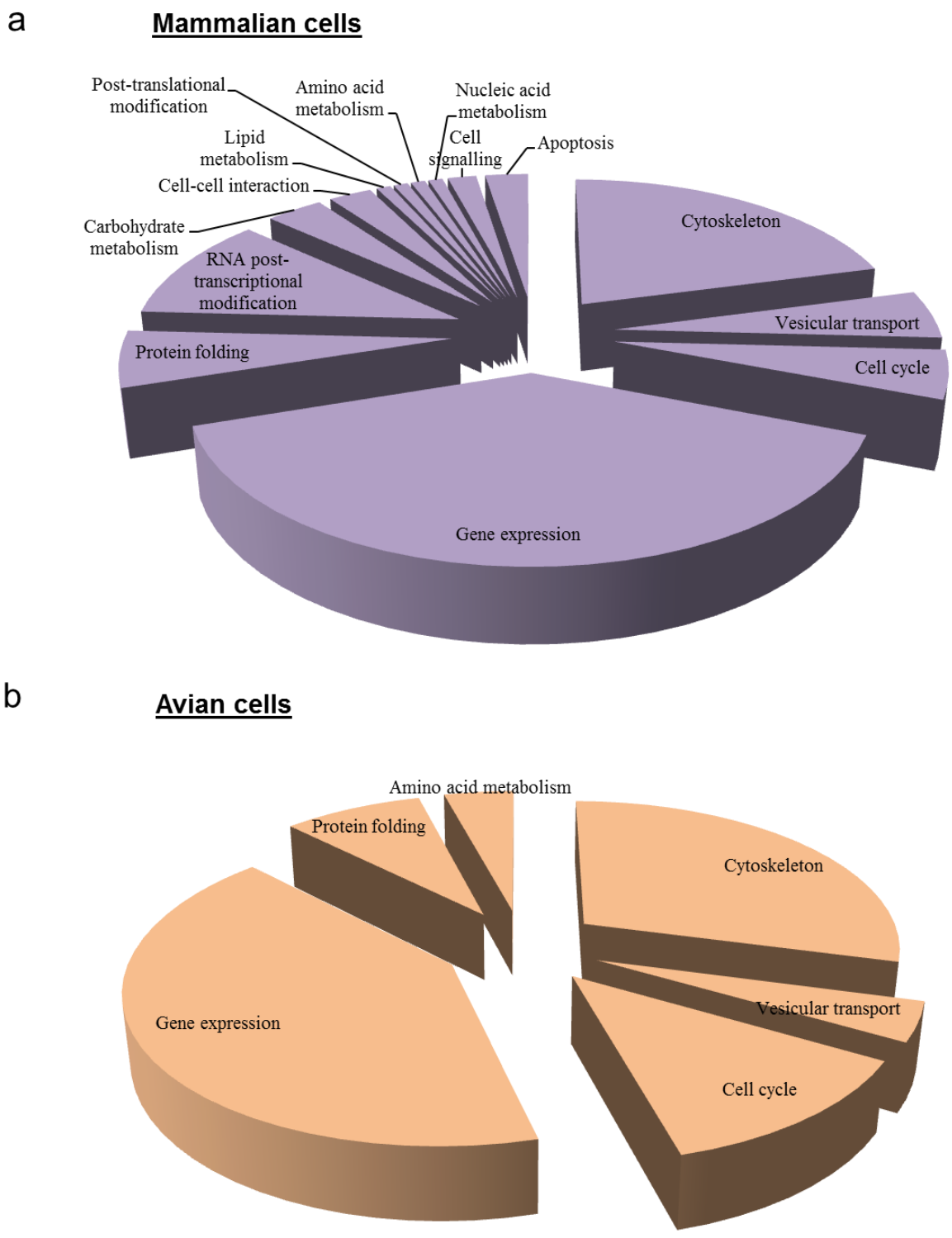

Figure 4.10| **Cellular functions of potential L/Flag interacting proteins**
The 126 mammalian and 25 avian proteins which were identified as potential L/Flag binding partners were categorised into groups based on their cellular functions. The proportions of each category of protein are depicted in pie charts for mammalian (a) and avian (b) cells.

4.5 Discussion

Studies have shown that the L proteins of the morbilliviruses are able to withstand the insertion of large reporter genes within hinge regions, intra domain regions of relatively low amino acid sequence conservation, with negligible effects on virus growth *in vitro* (Duprex *et al.*, 2002). This has sought to highlight both the conformational and functional independence of the conserved blocks. However, insertion of the eGFP ORF into a comparable position in the genome of VSV (55 residues upstream of the catalytic tetrad K-D-K-E of the MTase in L) produced a temperature sensitive phenotype (Ruedas & Perrault, 2009). In this study, the rescue of a recombinant CHPV containing GFP at a similar position between domains V and VI of CHPV L (4 amino acids upstream of the insertion site in the VSV recombinant) was unsuccessful, indicating that the engineered polymerase was non-functional. Addition of the 8 amino acid Flag epitope tag to the carboxyl terminus of the CHPV L protein was tolerated in the recovered virus, although viruses containing this insertion had reduced growth kinetics, growing to titres which were approximately 2 logs lower than the parental recombinant wild-type virus (Figure 4.5).

The replication cycle of CHPV occurs at RNP complexes within the cytoplasm of infected cells. Studies in VSV have shown RNP complexes are distributed throughout the cytoplasm but at early stages of infection these are located predominantly adjacent to the nucleus during nucleocapsid synthesis. Subsequently newly synthesised complexes are seen to traffic in a microtubule-dependent manner towards the cell membrane for virion assembly prior to progeny release (Das *et al.*, 2006). Thus, it is likely that the images in Figure 4.9 demonstrate the late stages of CHPV infection, as the P/RFP protein is primarily localised to the cell membrane.

Aggregations of VSV RNP complexes have been observed within infected cells (Das *et al.*, 2006). The data presented here supports this finding, large dots of fluorescence representing groups of RNP complexes were visualised upon infection of cells with rCV-P/RFP (Figure 4.6, 4.9). While replication complexes were initially thought to be virus induced, recently the presence of stress granule-like complexes comprised of viral RNA, replicative proteins and several cellular antiviral proteins were detected in VSV-infected cells leading to the suggestion that these are in fact the replication complexes and that their formation is host-cell mediated (Dinh *et al.*, 2013a).

The location of the *td*CE point mutations within the polymerase protein gene together with the significantly lower amounts of viral RNA synthesised by the mutants indicate that in CE cells at 39°C the generation of functional replication complexes may be disrupted. The P/RFP fusion protein mutants showed a striking difference in P protein distribution in CE cells infected with L mutant viruses compared with the wild type L virus at 39°C but not 31°C (Figure 4.9 panels m-p). At 31°C most P protein was organised into discrete localised clusters in replication complexes within the infected cell and especially near to the cell membrane. This organisation was lost at 39°C with the L gene mutant viruses in CE cells. Under these conditions the P protein showed a diffuse distribution throughout the cytoplasm with only very few and extremely indistinct foci present. The lack of P/RFP-containing foci in CE cells at the restrictive temperature, taken together with previous data showing defects in *in vitro* RNA transcriptase activity and polypeptide synthesis, supports the hypothesis that the defects in the mutant L proteins lead to disruption of replication complexes, reduced viral RNA synthesis and hence reduced viral protein synthesis in non-permissive conditions. The three point mutations

examined produce similar phenotypes, despite the amino acid changes being located in separate domains of the CHPV L protein (Figure 3.6).

The existence of host range (*hr*) and *td*CE mutants highlight the essential role of cellular proteins in the replication of CHPV. The nature of the *td*CE phenotype is suggestive that the coding changes within the L protein alter its relationship with specific cellular factor(s) that are not present in CE cells and are required to hold the polymerase in an active conformation at 39°C. By immunoprecipitating wild-type and *td*CE mutant P and L fusion proteins from mammalian and avian cells at 31°C and 39°C and analysing their binding partners by mass spectrometry it would be possible to decipher the effect(s) of the *td*CE lesions on the ability of the L protein to interact with host cell factors. This approach would facilitate the isolation of cellular protein(s) that interact with the virus replication complex in a manner that is absolutely essential for successful virus propagation. The first step was to establish whether this methodology works by identifying potential wild type L/Flag interacting proteins.

Vesiculoviruses are intimately associated with host cell factors. There is limited information about these cellular factors for CHPV, however, the known cellular interactions with VSV RNA or proteins are listed in Table 1.3. 72 mammalian genes were shown to be integral for VSV infection in a recent RNAi screen (Panda *et al.*, 2011). Using co-immunoprecipitation in conjunction with mass spectrometry 126 mammalian and 25 avian potential binding partners of the CHPV L protein, the catalytic component of the CHPV polymerase were identified (Tables 4.2, 4.3). However, the experimental approach used does not allow discrimination between direct and indirectly bound proteins and therefore many of these host cell proteins

may only associate with the CHPV L protein indirectly via interactions with one or several specifically bound cellular proteins. In addition, cellular proteins interacting with CHPV L protein at low concentrations may not be detected by this approach. The majority of the potential cellular binding partners of the L protein have cellular functions in gene expression or cytoskeleton structure (39% and 21% of the total identified proteins in mammalian cells and 42% and 29% of the total in avian cells). Several L interacting proteins were identified from both mammalian and avian cells including actin, which has also been shown to be required for clathrin-mediated endocytosis of VSV (Cureton *et al.*, 2009). Cytoskeletal proteins are used by a range of viruses predominantly at the stage of virus entry and egress, although a number of non-segmented negative sense (NNS) RNA viruses utilise these proteins for viral RNA synthesis. Examples of NNS RNA viruses that require actin for the efficient transcription of their mRNA include RSV (Burke *et al.*, 1998) and human parainfluenza virus 3 (Gupta *et al.*, 1998b), while VSV (Heinrich *et al.*, 2010), measles and Sendai (Moyer *et al.*, 1986) viruses have been demonstrated to use tubulin for viral mRNA synthesis. Therefore, the identification of actin as a possible cellular interacting partner of the CHPV L protein in this study is the first example of actin associating with a vesiculovirus protein. To provide further evidence for this interaction the immunoprecipitated L/Flag sample should be immunoblotted using an anti-actin antibody.

Tubulin has been shown to have several functions during VSV infection, for transcription (Moyer *et al.*, 1986) and microtubules are required to transport the viral mRNA from replication complexes to the cell membrane and this is essential for efficient translation (Heinrich *et al.*, 2010). Despite the important roles tubulin plays

in VSV replication direct interaction of the VSV RNP complex proteins with the cytoskeleton has not been demonstrated and tubulin was not identified as a possible CHPV L binding partner in this investigation. However, tubulin has been shown to interact with the VSV M protein to stimulate cell rounding, suggestive of a role in the cytopathic effect of the virus (Melki *et al.*, 1994).

CHPV L protein was found to interact with the intermediate filament proteins vimentin and keratin during infection of mammalian and avian cells. Previous studies have shown that other virus proteins also interact and modulate vimentin including the HIV-1 protease, which has been shown to digest vimentin resulting in its substantial reorganisation within host cells (Honer *et al.*, 1991). In addition, African swine fever virus stimulates the aggregation of vimentin and then localises to those sites for replication and assembly of virus particles (Stefanovic *et al.*, 2005). Conversely, disruption of the vimentin network prevents human cytomegalovirus infection (Miller & Hertel, 2009). VSV M protein-mediated changes in vimentin distribution have also been reported in VSV-infected cells (Lyles & McKenzie, 1997). Keratin 8, implicated as a CHPV L interacting protein in this investigation, has been shown to enhance hepatitis B virus (HBV) replication (Zhong *et al.*, 2013).

This research identified two members of the heat shock protein (Hsp) family of stress-inducible cellular chaperones, Hsp90 and Hsp70 as potential interacting partners of the L protein during infection in mammalian and avian cells, respectively. Hsp90, which has a specific set of protein substrates including some transcription factors and kinases, is postulated to be essential for the replication of a diverse range of viruses including rhabdoviruses, orthomyxoviruses (Momose *et al.*, 2002),

paramyxoviruses and bunyaviruses due to its crucial role in the correct folding of viral polymerases (Connor *et al.*, 2007). Specifically, Hsp90 has been shown to be involved in VSV replication and maintaining L protein stability via an interaction with the N protein (Connor *et al.*, 2007). Therefore, Hsp90 may also indirectly associate with the CHPV L protein by binding to the N protein. The involvement of Hsp70 in the replication of a number of viruses has also been demonstrated with the protein enhancing the replication of some viruses and inhibiting others. Expression of Hsp70 is crucial in suppressing VSV (Kim *et al.*, 2013) and measles virus (Carsillo *et al.*, 2006) neurovirulence *in vivo* due to Hsp70-dependent induction of the type I IFN response despite its role in slightly enhancing virus gene expression (Kim *et al.*, 2013). Furthermore, Hsp70 directly binds to the RNP proteins of influenza A virus PB1 and PB2, inhibiting the replication of the virus (Li *et al.*, 2011). In contrast, Hsp70 was shown to upregulate flavivirus replication through direct interactions with HCV replicative proteins NS5A, NS3 and NS5B (Chen *et al.*, 2010) and JEV NS5 (Ye *et al.*, 2013).

The other major functional group of host cell proteins implicated as possible CHPV L protein partners in this study have cellular roles in gene expression and include ribosomal proteins, eukaryotic translation initiation factors (eIF4G, H and eIF3B, C, I), members of the heterogeneous nuclear ribonucleoprotein (hnRNP) family of RNA-binding proteins (hnRNP D, K, A1, H) and transcription factors. These findings are consistent with the dependency of vesiculoviruses on the host cell replicative machinery for viral polypeptide synthesis. The scaffolding protein eIF4G is a constituent of the eIF4F complex, which is required for the initiation of cellular protein synthesis. VSV infection alters the phosphorylation state of the eIF4F

complexes, impairing host cell translation (Connor & Lyles, 2002). eIF4H stimulates eIF4A, a component of the eIF4F complex with ATP-dependent helicase activity responsible for unwinding secondary RNA structures to facilitate ribosome binding. The eIF3 complex regulates the assembly of the pre-initiation complex and scanning for the AUG start codon for the initiation of protein synthesis and the eIF3 subunits A, G, I have been shown to be essential for VSV infection during RNAi screening experiments (Panda *et al.*, 2011).

The hnRNP RNA-binding proteins have a range of cellular functions in gene expression, mRNA metabolism, chromatin re-modelling, nuclear export of mRNA, mRNA processing and the cell cycle. These proteins are principally localised to the nucleus, however, in cells infected with VSV an increase in cytoplasmic hnRNPs has been documented (Pettit Kneller *et al.*, 2009). One of the hnRNP proteins identified as a possible CHPV L interacting protein in this study, hnRNP K, has been suggested to be essential for VSV infection by inhibiting apoptosis, enhancing virus replication and release by modulating the expression of several host cell proteins including the upregulation of alanine deaminase like (ADAL), ARF1, Bcl-Xl, Bcl-2 and BagI and downregulation of Bcl-Xs and Bik (pro-apoptotic factors) (Dinh *et al.*, 2013b). hnRNP K has been shown to support the replication of a number of other viruses such as Sindbis virus through an interaction with nonstructural protein 2 (Burnham *et al.*, 2007), HCV by directly binding to the core protein of the virus (Hsieh *et al.*, 1998) and Epstein Barr virus through an interaction with EBNA2 (Gross *et al.*, 2012). The involvement of hnRNP A1 protein (identified as a potential CHPV L interacting partner in this analysis) in supporting norovirus replication by facilitating the circularisation of the viral genome has also been demonstrated (Lopez-Manriquez

et al., 2013). hnRNP D has also been shown to play several roles in viral infections, supporting the translation of HCV mRNA (Paek *et al.*, 2008) and inhibiting Nipah virus transcription (Hino *et al.*, 2013). In addition, hnRNP U was postulated to inhibit cellular mRNA synthesis through an interaction with leader RNA in VSV-infected cells (Gupta *et al.*, 1998a).

In this chapter, the lesions responsible for the severe growth defect of three CHPV *td*CE mutants, CH112, CH157 and CH256 were shown to severely affect the ability of the viruses to assemble large replication complexes in the cytoplasm of cells in the non-permissive conditions. The identification of 126 mammalian and 25 avian proteins with cellular roles predominantly in gene expression and cytoskeleton structure which may associate with the CHPV L protein was also described, providing the first analysis of potential CHPV L binding partners. Further investigation will be required to validate the potential interactions identified.

CHAPTER 5

Chapter 5: The pathogenesis of Chandipura virus-induced encephalitis

5.1 Introduction

CHPV causes a neurological disease in humans and there have been several epidemics of CHPV-induced encephalitis in children (Chadha *et al.*, 2005; Gurav *et al.*, 2010; Tandale *et al.*, 2008). The virus also causes a neurological disease in experimentally infected young mice by any route of administration, while infection leading to encephalitis of adult mice is only achieved by intracranial injection of CHPV (Jortner *et al.*, 1973). In young mice the disease is exhibited as a progressive paralysis prior to death. Further information about the mouse model of CHPV pathogenesis including details about the range of symptoms observed is given in section 1.6.2. One report into CHPV pathology described extensive regions of necrosis in the internal and external granular layers of mouse cerebellum 96 hours after intraperitoneal inoculation of CHPV (Jortner *et al.*, 1973), implicating the cerebellum as an important site of CHPV replication in the brain.

While there has been some increase in our understanding of the immunological response to CHPV very little is currently known about the underlying aspects of pathogenesis of any vesiculovirus. Specifically in the case of CHPV, there is limited information about the progress of CHPV disease in the mouse model. Moreover, the site(s) of infection within the brain, the pattern of spread with time after infection and any host range specificities in terms of the cell tropism of CHPV are all unknown. Mice are recognised as the standard model for studying virus pathogenesis and are

the only species used to date to study CHPV and IFHV-induced encephalitis. There is a small but growing literature on the immunology of CHPV infection and all of the work to date has been performed in mice. Therefore mice were chosen to investigate the process of neurological disease caused by CHPV in this study in order to generate data that is comparable with other information in the literature. Suckling mice between the ages of 7-11 days old were used as animals at this age present with neurological symptoms following infection through any route of virus administration.

Additionally, there is limited information about the brain cell types susceptible to CHPV infection. Currently, neurones are the only brain cell type that have been shown to be permissive to CHPV infection and apoptotic and necrotic CHPV-infected neuronal cells have been observed following infection of several neuronal cell lines and *in vivo* infection of mice (Ghosh *et al.*, 2013; Jortner *et al.*, 1973). Viruses often have a tropism for certain cell types and this is fundamental to the disease they induce. For example, the neuropathogenic *Alphavirus* Semliki Forest virus (SFV) (family *Togaviridae*), a positive sense single stranded RNA virus, exhibits a strong tropism for neurones and oligodendrocytes, while SFV infection of astrocytes has not been demonstrated (Fazakerley, 2004).

Ex vivo cultures of brain tissue including cerebellum, hippocampus, cerebral cortex and retina have been utilised in the neuroscience community for studies of brain cell function and development, as well as in research into a wide range of neurological diseases such as Parkinson's disease, Alzheimer's disease, stroke and epilepsy. These cultures are able to retain the physiological proportions of brain cell types and normal tissue architecture for several weeks after preparation and therefore have the advantage that they can be used in experiments that take longer than 6 hours, the

maximum survival time of acute brain slices. Cultures of brain tissue have been used to investigate viral tropism for several systems. Cerebella and hippocampal slice cultures were employed in a study of Borna disease virus (BDV) (Friedl *et al.*, 2004), coronal brain slice cultures were used in a model of reovirus pathogenicity (Dionne *et al.*, 2011) and the brain site involved in cytomegalovirus latency (Tsutsui *et al.*, 2002) and herpes simplex virus type 1 (HSV-1) neurotropism (Braun *et al.*, 2006) were investigated using cultures of brain tissue. Organotypic cultures of mouse cerebellar were employed to investigate the cell tropism of CHPV in this study. This chapter reports on the investigation of CHPV-induced neurological disease using *ex vivo* and *in vivo* approaches.

For guidance labelled diagrams of superior and sagittal views of the mouse brain are shown in Figure 5.1.

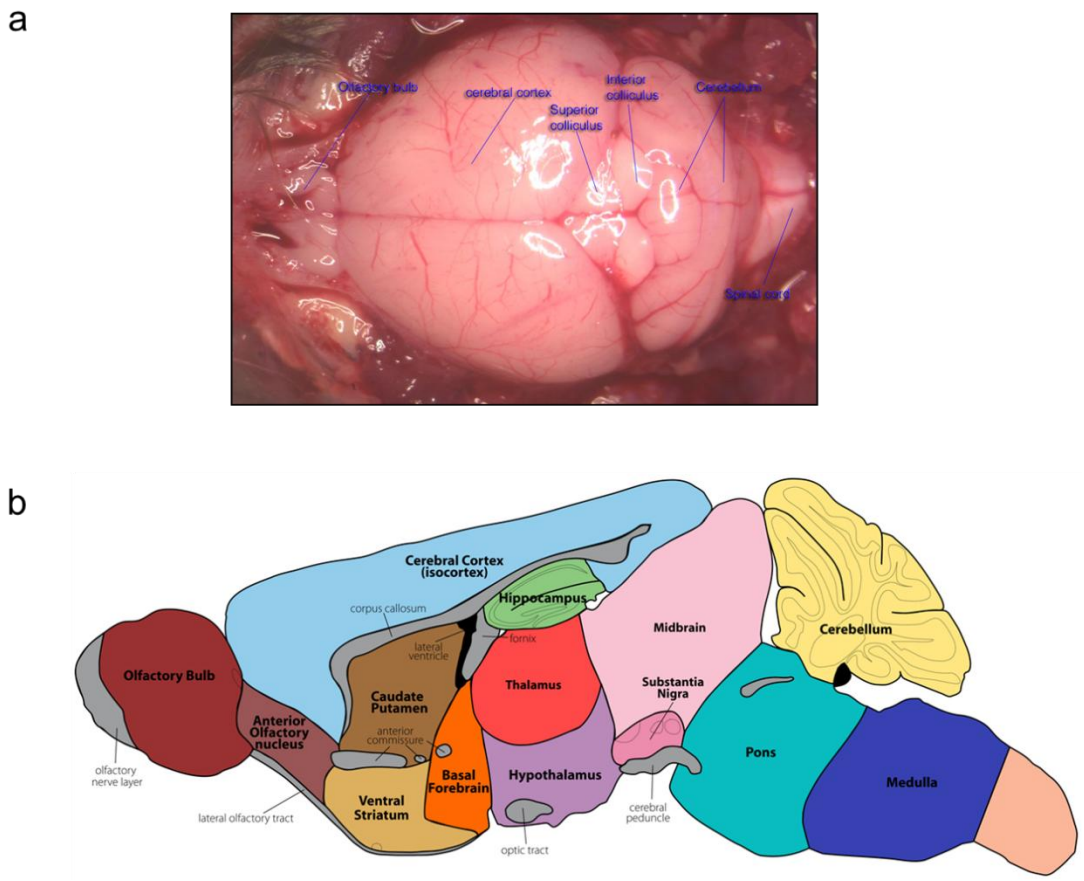

Figure 5.1| **The mouse brain**
A. Superior view of a mouse brain
B. Diagram of a sagittal section through the mouse brain (obtained from the GENSAT mouse brain atlas, sagittal section 07, http://www.gensat.org/imagenavigator.jsp?imageID=13507)

5.2 *Ex vivo* investigation of the cell tropism of CHPV

5.2.1 rCVeGFP-infection of cerebellar slice cultures

To determine whether CHPV was able to proliferate in mouse cerebellar slice cultures the recombinant virus rCVeGFP, which contains a GFP gene inserted between the M and G genes of CHPV (Marriott & Hornsey, 2011) (Figure 5.2) was used as it allowed the progress of CHPV infection to be followed in real time with samples fixed at appropriate times post-infection.

Figure 5.2| **Diagram of rCVeGFP genome**

In a preliminary experiment cerebellum slice cultures from seven day old mice were prepared by Dr Daniel Fulton and cultured for seven days to allow time for the loss of any dead cells. The slices were inoculated with $1x10^6$ pfu per slice of rCVeGFP and observed using an epifluorescence microscope. GFP fluorescence was first observed at approximately 6 hours post-infection and at this time the appearance of GFP was restricted to several small regions at the periphery of the slices (not shown). This restriction may be due to variation in the thickness of the cultured brain slices with the edges tending to be thinner and thus more accessible to virus. At 12 hours post-infection GFP expression remained confined to the edges of the slices (although the infection had spread further inwards compared to at 6 hours post-infection). 24 hours after the tissue was infected with virus, rCVeGFP-infected cells were detected in the cerebellar slices, with the fluorescence found in specific regions only.

Having demonstrated that cerebellar slice cultures support CHPV replication and that infection was restricted within the slices, the location of virus-infected cells within the histology of the cerebellum was examined. A labelled photomicrograph illustrating the structure of the cerebellum is shown in Figure 5.3 a. Slices of mouse cerebella were infected with rCVeGFP, as above. 24 hours post infection the slices were fixed and stained with anti-MBP (myelin basic protein), an antibody specific for oligodendrocytes that stains the white matter or myelin component of the cerebellum, thus facilitating the identification of specific regions of the tissue

containing virus. Further details about the specificity of this and other brain cell markers used in this research is shown in Table 5.1. The sections were counterstained with a secondary antibody coupled to a fluorophore emitting red light and examined using a 10 x microscope objective (Figure 5.3 b). Using a low magnification it was possible to visualise the majority of each slice in one field of view and the anti-MBP stain allowed the cerebellum histology to be clearly observed. A striking restricted localisation of the virus was observed and virus-infected cells were found in large numbers in the internal and external granule layers, consistent with other research which reported extensive localised necrosis in these regions (Jortner *et al.*, 1973). Limited co-localisation of rCVeGFP-infected cells and white matter and little penetration of virus into the molecular layer was observed.

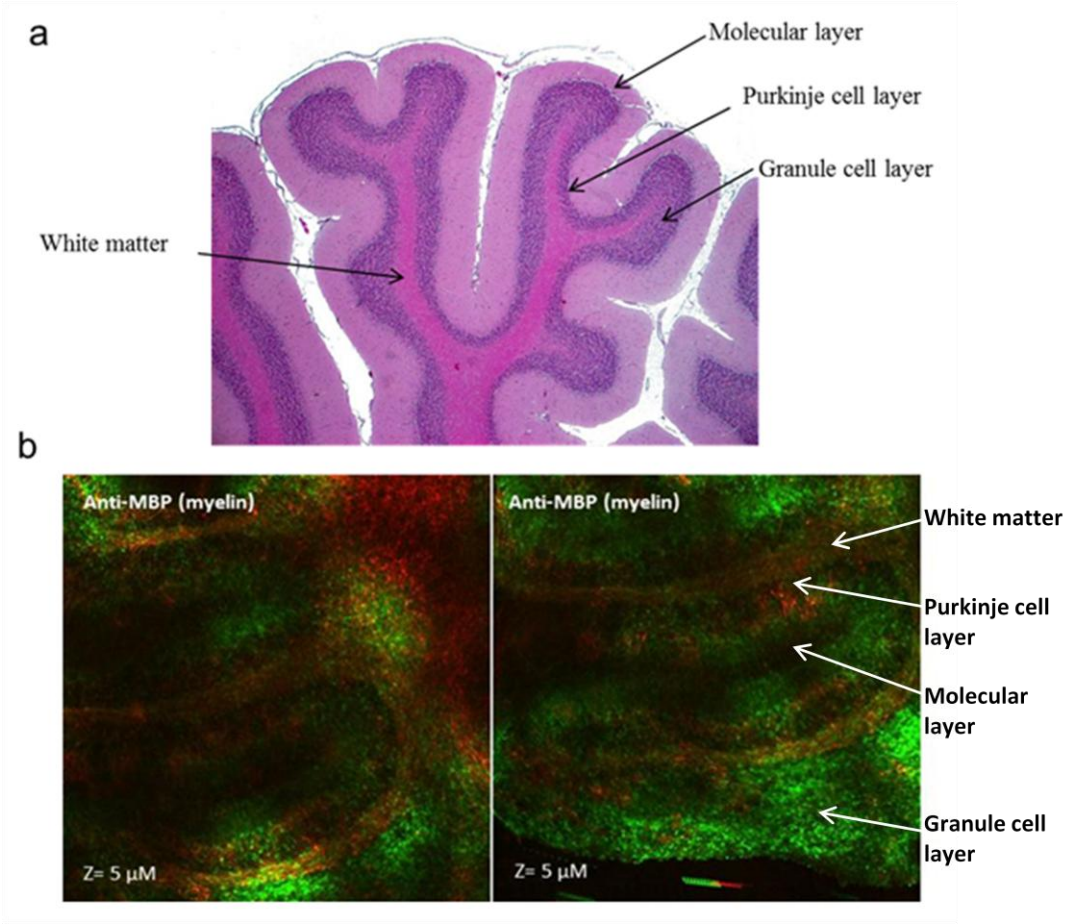

Figure 5.3 | r**CV-eGFP-infected mouse cerebellum stained for myelin**
A. Labelled photomicrograph of mouse cerebellum stained with haematoxylin and eosin. Obtained from http://pictures.doccheck.com/en/photos/54843/12440/cerebellum/.
B. Cultures of mouse cerebellar were infected with rCVeGFP and incubated for 24 hours at 37°C. The slices were then fixed, blocked and stained using anti-MBP antibody in order to visualise the architecture of the cerebellum (red). The virus-infected cells are shown in green. Fluorescence was observed using a Leica SP5 confocal fluorescence microscope. The images are 5µM thick Z stacks.

Antibody	**Specificity**
Anti-MBP (myelin basic protein)	Developing and adult myelin, developing oligodendrocytes
Anti-NG2	NG2 Chondroitin Sulfate Proteoglycan on oligodendrocyte precursor cells (O-2A progenitor cells). The stain appears as clusters on the cell surface. The antibody does not stain differentiated oligodendrocytes well
Anti-ccI	Adenomatous polyposis coli (APC) protein found on oligodendrocyte cell bodies. The antibody also labels some astrocytes and purkinje cells.
Anti-Olig2	Oligodendrocyte marker, transcription factor
Anti-CD11b	Integrin alpha-M/beta-2 is predominantly expressed in monocytes and granulocytes
Anti-MAP2	Microtubule associated protein 2 is expressed only in the cytoplasm of neuronal cells (predominantly in perikarya and dendrites). It is also found in neurone-restricted progenitors
Anti-NeuN (NEUronal Nuclei)	An RNA-binding protein expressed in differentiated post-mitotic neuronal nuclei, perikarya and some proximal neurone processes in fetal and adult brain (although some neurones including Purkinje cells, dentate nucleus neurones and inferior olivary cells are not recognised at all development stages).
Anti-β-III tubulin	Class II β tubulin (intracellular microtubules) is expressed specifically in mature neurones
Anti-calbindin	Purkinje cell bodies and fibers
Anti-GABA-A receptor α 6	Mature cerebellar granule cells from ~post-natal day 14
Anti-GFAP	Glial fibrillary acidic protein is a class III intermediate filament which is the main constituent of intermediate filaments in astrocytes. It is a cell specific marker for differentiated astrocytes

Table 5.1| **Specificities of brain cell markers**

5.2.2 Elucidating the identity of rCVeGFP-positive cells using brain cell marker proteins

The CHPV-infected brain cell types were investigated using a range of brain cell marker proteins which are listed in Table 5.1. Each cell type specific stain was used on at least three different cerebellum slices and the percentage of cells with co-localising signals calculated from five fields of view for each slice. rCVeGFP-infected cerebellum slice cultures were fixed at 12 and 24 hours post infection and subjected to immunohistochemistry to detect brain cell-specific markers and immunofluorescence to detect the GFP reporter present in the recombinant CHPV. Morphologically, the virus-infected cells detected by GFP fluorescence were similar to interneurons or granule cells, a type of small neuron. Granule cells account for approximately half the neurones in the CNS and are densely packed within the cerebellar granule layer, as were the CHPV-infected cells (Figure 5.3 b). The rCVeGFP-infected cells are also similar to granule cells in size (approximately 10 μm) and abundance in mouse cerebellum. An anti-GABA-A receptor α6 antibody, specific for granule cells was used in immunofluorescent analysis of the infected cerebellar slices. The results showed that approximately only 1% of virus-infected cells co-localised with those stained with the granule cell specific antibody: anti-GABA-A receptor α6 though the remainder did not (Figure 5.4).

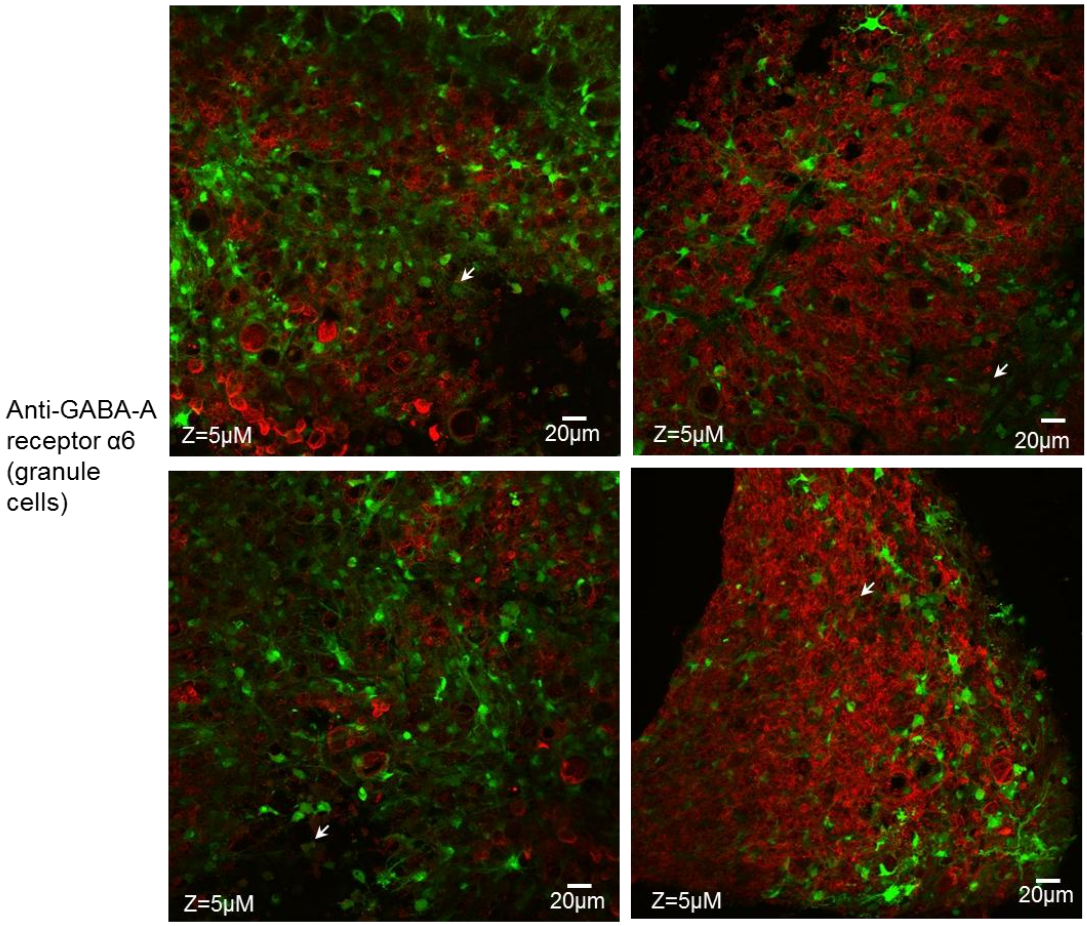

Figure 5.4| **Confocal micrographs of mouse cerebellar slices inoculated with rCVeGFP and stained for granule cells**

rCVeGFP-infected cells fluoresce green and cell marker proteins were stained with anti-GABA-A receptor α6 primary antibody followed by a red alexa secondary antibody. Fluorescence was visualised using a Leica SP5 confocal fluorescence microscope. The images are 5μM thick Z stacks. Scale bar of 20 μm is shown on each image. Several GABA-A receptor α6-positive cells infected with rCVeGFP are highlighted with arrows.

As previous studies have reported CHPV infection of neurones (Ghosh *et al.*, 2013; Jortner *et al.*, 1973) and the morphological similarity between the virus-infected cells and small neurones, granule cells, and also the restricted localisation of CHPV-infected cells within regions of the cerebellum where granule cells are abundant (i.e. the internal and external granule layers) has been observed in this investigation, two other neurone-specific antibodies were used in the analysis of the rCVeGFP-infected

cerebellar sections. Immunohistochemistry was performed using anti-MAP2 and anti-NeuN antibodies, which recognise neurone-restricted progenitors and differentiated post-mitotic neuronal cells, respectively. Approximately 80% of virus-infected and MAP-2-positive cells were shown to co-localise (Figure 5.5 a, b), while there was no co-labelling of virus-infected and NeuN-stained cells (Figure 5.5 c, d). These results indicate that CHPV preferentially infects neurone-restricted progenitor cells which have not yet fully differentiated.

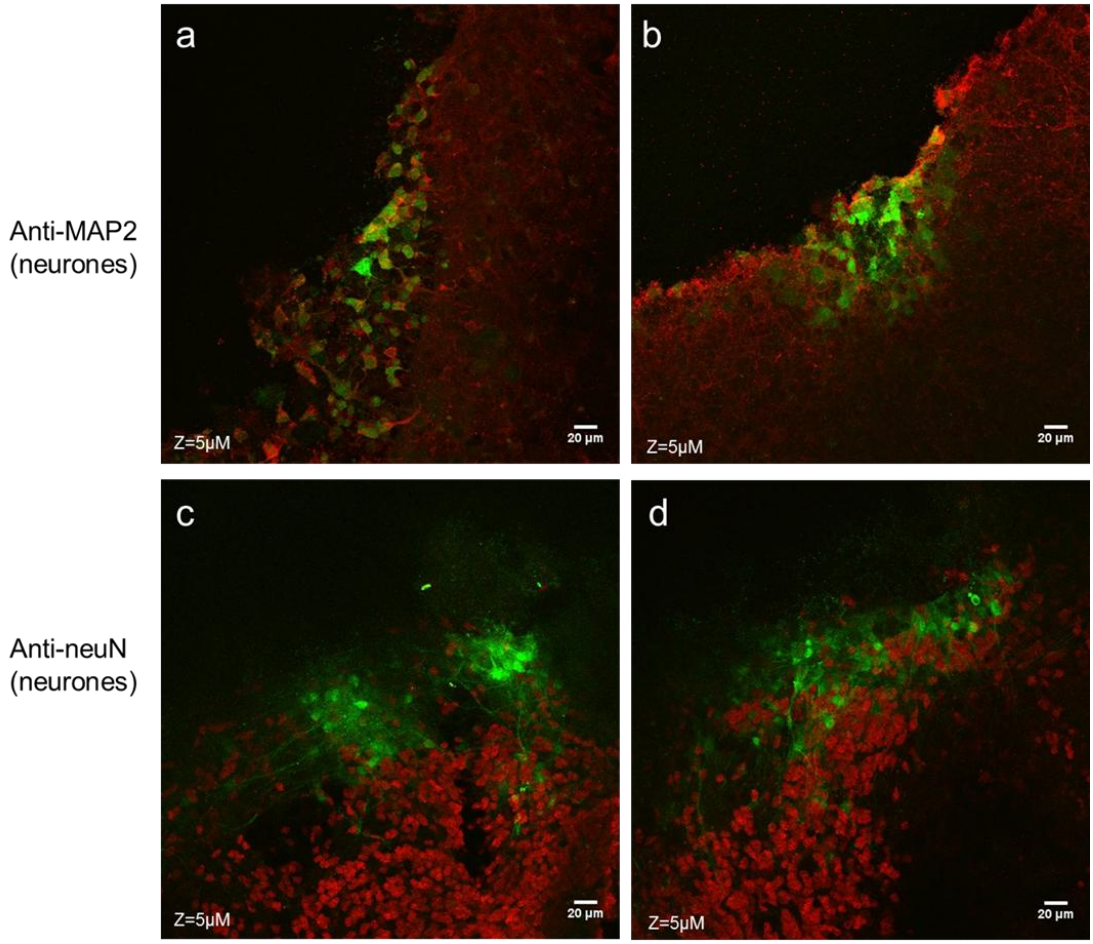

Figure 5.5| **Confocal micrographs of mouse cerebellar slices inoculated with rCVeGFP, fixed at 12 hours post-infection and stained for neurones**
rCVeGFP-infected cells fluoresce green and cell marker proteins were stained with either anti-MAP2 (a, b) or anti-neuN (c, d) primary antibodies followed by a red alexa secondary antibody. Fluorescence was visualised using a Leica SP5 confocal fluorescence microscope. The images are 5µM thick Z stacks. Scale bar shown.

The spread of CHPV infection in the cultures of cerebellar slices was also investigated by fixing the cerebellar sections 24 hours post-infection. The neuronal cell markers MAP2, neuN and βIII-tubulin (which is expressed in mature neurones) in rCVeGFP-infected tissue were stained and the slices examined by confocal fluorescence microscopy (Figure 5.6). As seen at 12 hours post-infection there was co-localisation of virus-infected and MAP2-expressing cells, but at a slightly lower level (approximately 55%) at this later time point (Figure 5.6 a, b, c). However, in contrast to the situation at 12 hours post-infection, a few NeuN-positive cells were infected, as shown by several yellow regions in Figure 5.6 d, e, f. A very small number of cells stained for βIII-tubulin were also infected with rCVeGFP (Figure 5.6 h). Thus, by 24 hours post-infection mature neurones (as well as immature neurones) were infected with CHPV, although the levels of co-localisation were consistently low (approximately 2%).

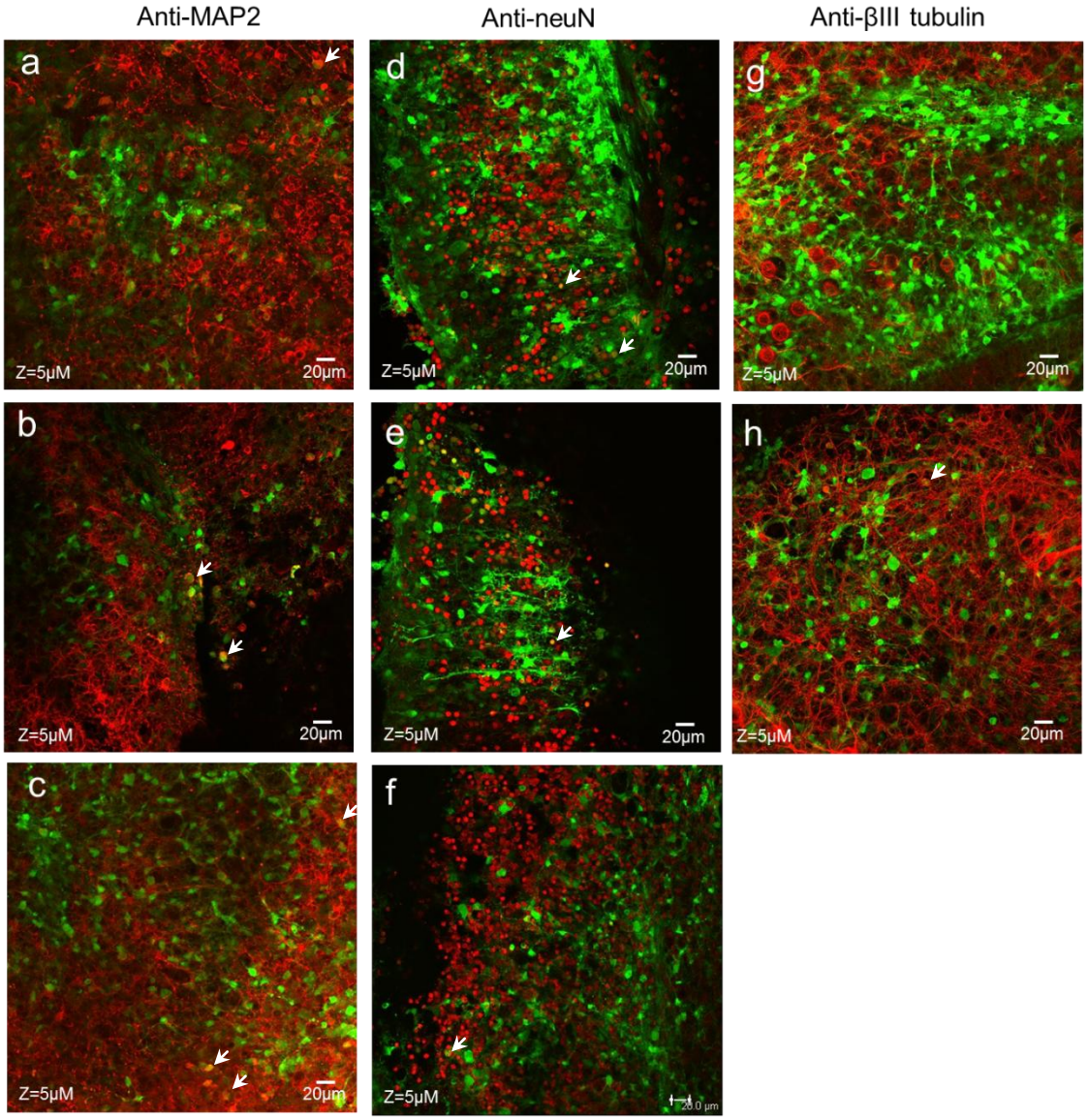

Figure 5.6| **Confocal micrographs of mouse cerebellar slices inoculated with rCVeGFP, fixed at 24 hours post-infection and stained for neurones**
rCVeGFP-infected cells fluoresce green and cell marker proteins were stained with anti-MAP2 (a, b, c), anti-neuN (d, e, f) or anti-βIII tubulin (g, h) primary antibodies followed by a red alexa secondary antibody. Fluorescence was visualised using a Leica SP5 confocal fluorescence microscope. The images are 5μM thick Z stacks. Scale bar of 20 μm shown on each image. Several infected cell marker-positive cells are highlighted with arrows.

To further define the types of neurone infected with CHPV an antibody specific for calbindin, a marker for Purkinje neurones, was used to stain the cultures fixed at 24 hours post-infection. Purkinje neurones have a large cell body (approximately 20 μm) and an elaborate array of branching dendrites which extend into the cortex of the

cerebellum. They are fundamental to the function of the cerebellum as they serve as the only route for signals from the cerebellum to the rest of the brain. No co-localisation between CHPV-infected and calbindin-positive cells was observed (Figure 5.7).

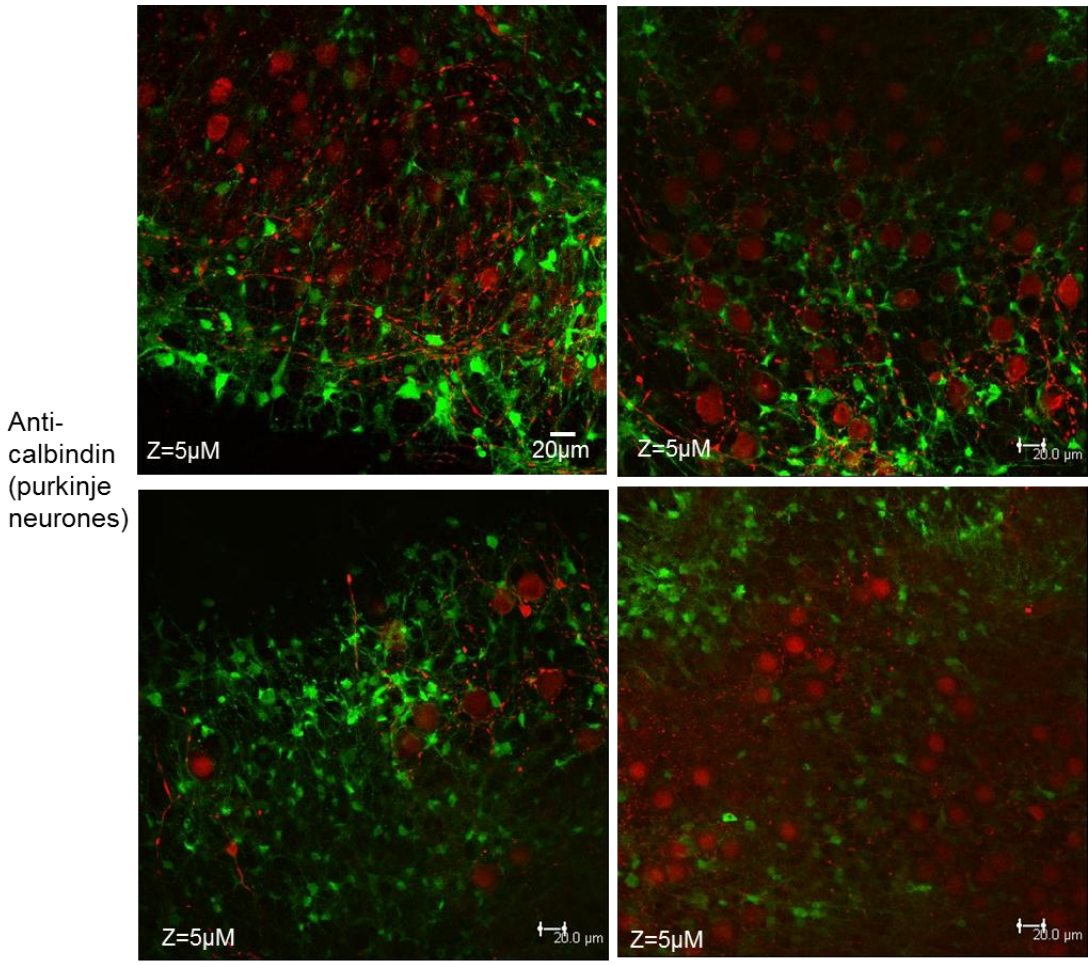

Figure 5.7| **Confocal micrographs of mouse cerebellar slices inoculated with rCVeGFP, fixed at 24 hours post-infection and stained for purkinje neurones**
rCVeGFP-infected cells fluoresce green and cell marker proteins were stained with anti-calbindin primary antibody followed by a red alexa secondary antibody. Fluorescence was visualised using a Leica SP5 confocal fluorescence microscope. The images are 5µM thick Z stacks. Scale bar of 20 µm is shown on each image.

Microglia are the immunocompetent cells of the CNS, transforming into active phagocytic macrophages in response to pathogen invasion. Thus, it was important to investigate their potential role in CHPV-induced pathology. Cerebellar slice cultures infected with rCVeGFP and fixed 12 and 24 hours post-infection were also immunostained for the microglia marker CD11b. Co-localisation of virus-infected and anti-CD11b immunostained cells was not observed at 12 hours post-infection, as shown by the absence of overlapping signals in Figure 5.8 a, b. However, at 24 hours post-infection approximately 15% of cells infected with rCVeGFP were microgila (determined by a positive signal with anti-CD111b; Figure 5.8 c, d).

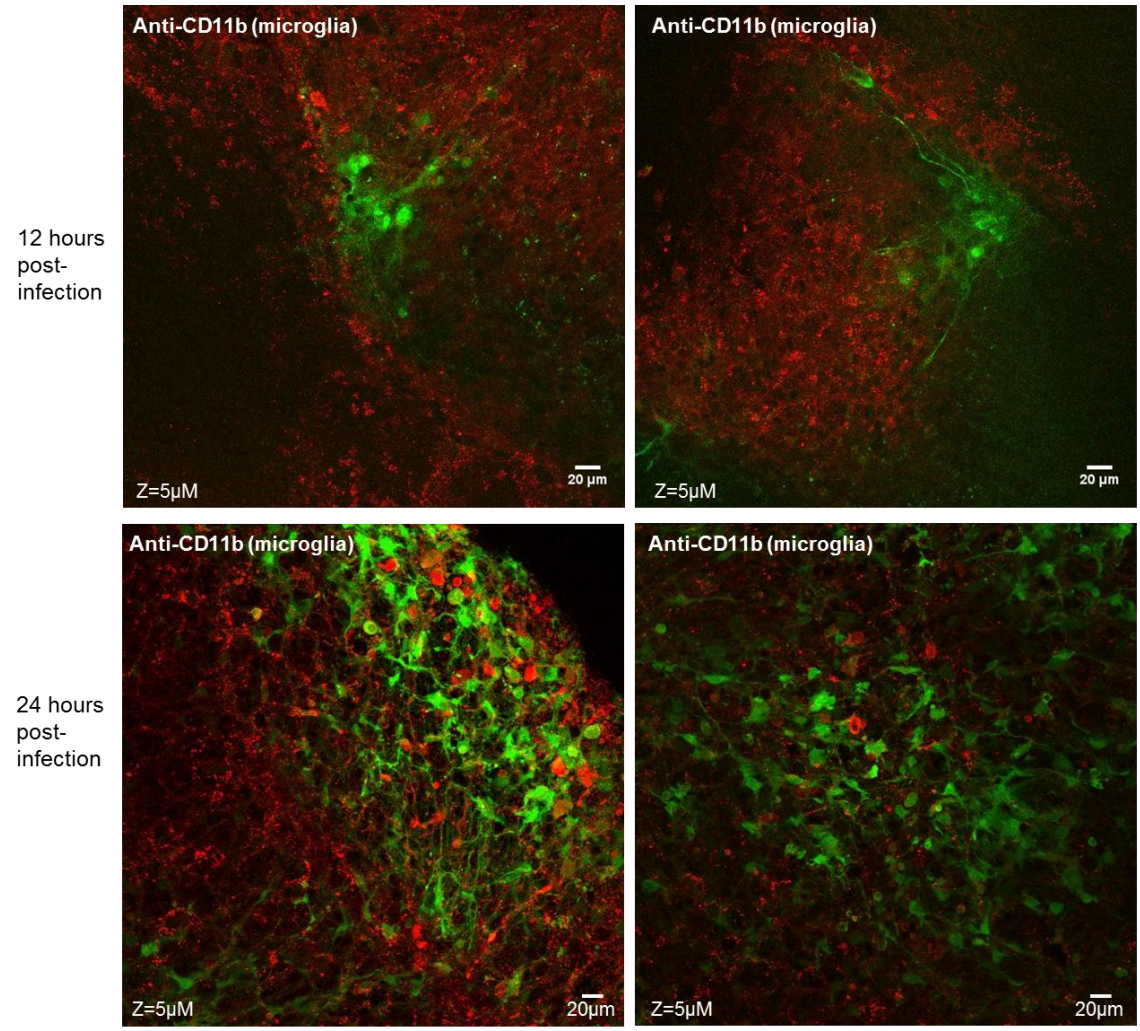

Figure 5.8| **Confocal micrographs of mouse cerebellar slices inoculated with rCVeGFP and stained for microglia**
Cerebellar slice cultures were infected with rCVeGFP and fixed at 12 and 24 hours post-infection. rCVeGFP-infected cells fluoresce green and cell marker proteins were stained with anti-CD11b primary antibody followed by a red alexa secondary antibody. Fluorescence was visualised using a Leica SP5 confocal fluorescence microscope. The images are 5μM thick Z stacks. Scale bar shown.

The infection of oligodendrocytes, a further type of glial cell, by CHPV has not been investigated, although a tropism for the cells has been demonstrated by the neuropathogenic virus SFV, a widely used model to study viral encephalitis (Fazakerley, 2004). The major function of oligodendrocytes is to generate myelin which is essential for the efficient conduction of nerve impulses. The rCVeGFP-

infected tissue sections were stained with primary antibodies against NG2 chondroitin sulfate proteoglycan, Adenomatous polyposis coli protein (CCI) and the transcription factor Olig2. NG2 serves as a marker for oligodendrocyte precursor cells, CCI is predominantly expressed on the cell bodies of differentiated oligodendrocytes and Olig2 is a transcription factor expressed in oligodendrocytes at all stages of development. The slices were then incubated with a secondary antibody conjugated to a red Alexa Fluor® (either 568 or 594). Analysis of the slices by confocal fluorescence microscopy showed only a few of the virus infected cells were stained for oligodendrocyte marker proteins at 12 hours post-infection (Figure 5.9). Two Olig2-positive cells which had been infected with rCVeGFP are highlighted with arrows in Figure 5.9 i.

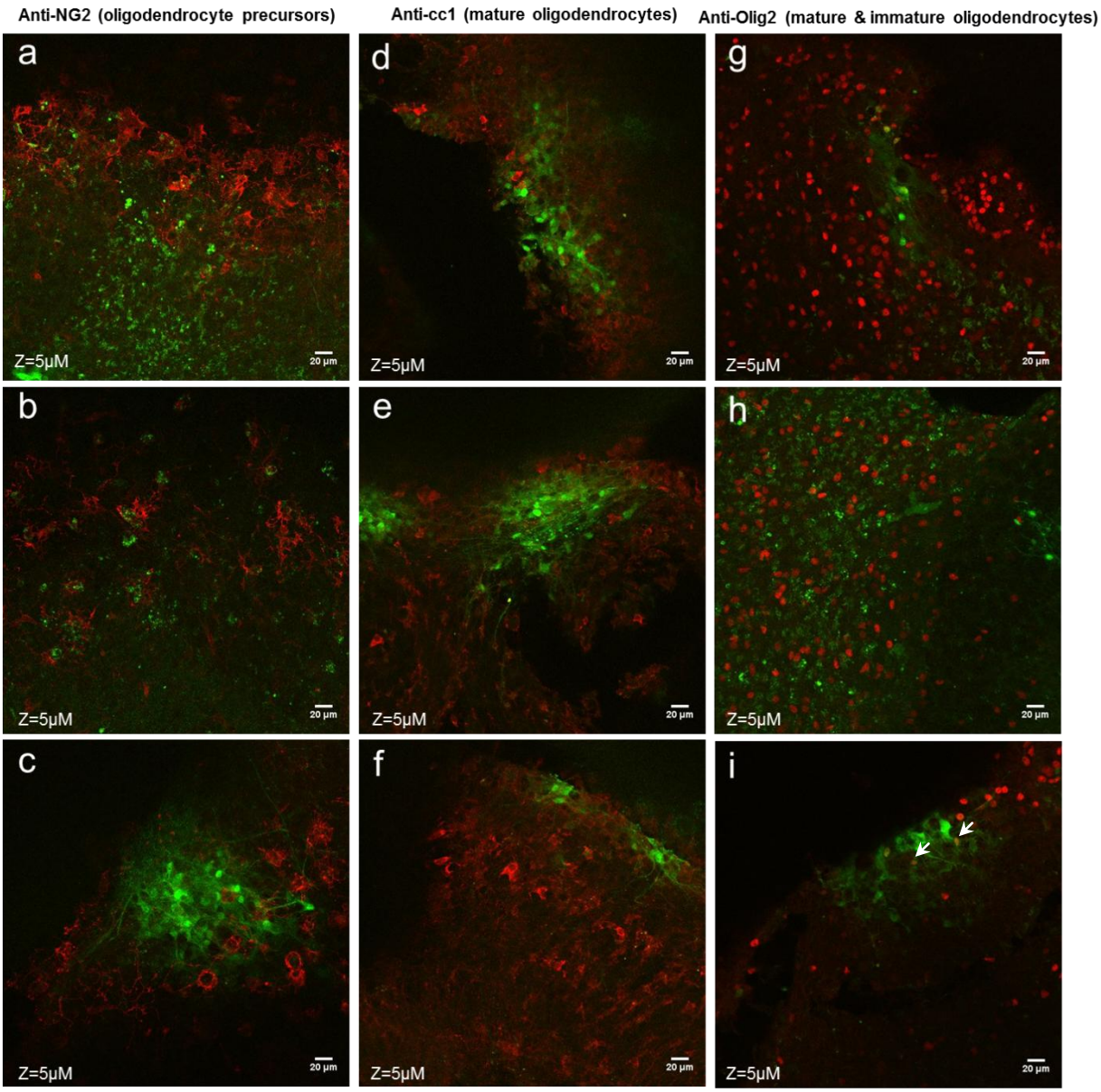

Figure 5.9| **Confocal micrographs of mouse cerebellar slices inoculated with rCVeGFP, fixed at 12 hours post-infection and stained for oligodendrocytes**
Slices were fixed 12 hours post-infection. rCVeGFP-infected cells fluoresce green and cell marker proteins were stained with anti-NG2 (a, b, c), anti-cc1 (d, e, f) or anti-Olig2 (g, h, i) primary antibodies followed by a red alexa secondary antibody. Fluorescence was visualised using a Leica SP5 confocal fluorescence microscope. The images are 5μM thick Z stacks. Scale bar shown. Co-localisation of virus-infected and oligodendrocyte cell marker-positive cells is illustrated by arrows.

There was an increase in the number of rCVeGFP-infected oligodendrocytes at 24 hours post-infection compared with 12 hours post-infection, as shown by a rise in virus-infected NG2-, ccI and olig2-positive cells (Figure 5.10).

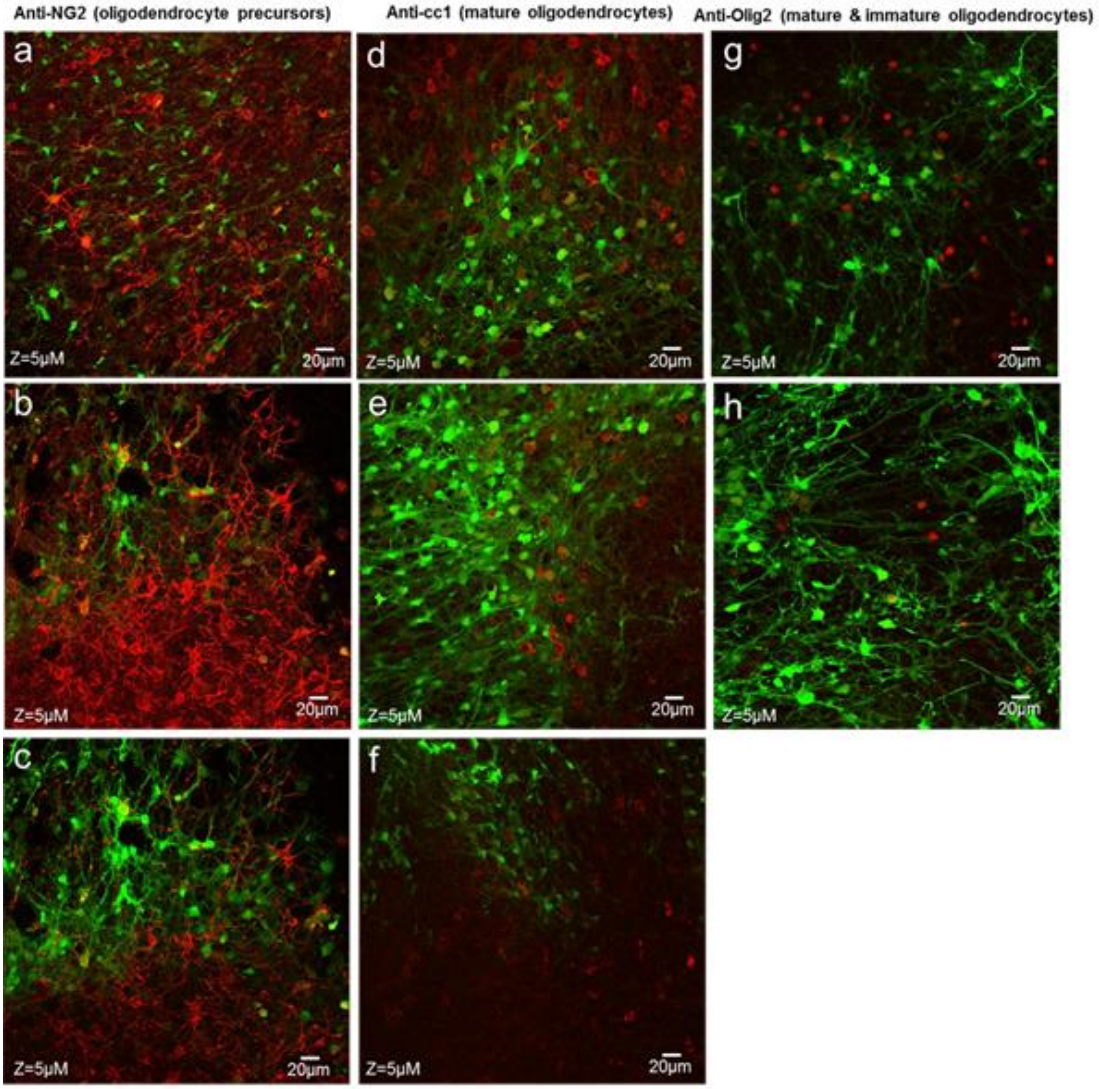

Figure 5.10| **Confocal micrographs of mouse cerebellar slices inoculated with CVeGFP, fixed at 24 hours post-infection and stained for oligodendrocytes**
CVeGFP-infected cells fluoresce green and cell marker proteins were stained with anti-NG2 (a, b, c), anti-cc1 (d, e, f) or anti-Olig2 (g, h) primary antibodies followed by a red alexa secondary antibody. Fluorescence was visualised using a Leica SP5 confocal fluorescence microscope. The images are 5μM thick Z stacks. Scale bar shown.

Astrocytes, another class of glial cell, perform a variety of important functions in the brain including supporting neurones, maintaining brain homeostasis by removing glutamate and regulating the levels of potassium, connecting neurones with the vascular system and controlling synapse formation and maintenance (Nedergaard *et al.*, 2003). The presence of rCVeGFP-infected astrocytes was investigated using immunohistochemistry with an anti-glial fibrillary acidic protein (GFAP) antibody, which is specific for differentiated astrocytes. A small number of GFAP-immunoreactive astrocytes were infected with virus, demonstrating that these cells are also permissive to CHPV infection (Figure 5.11).

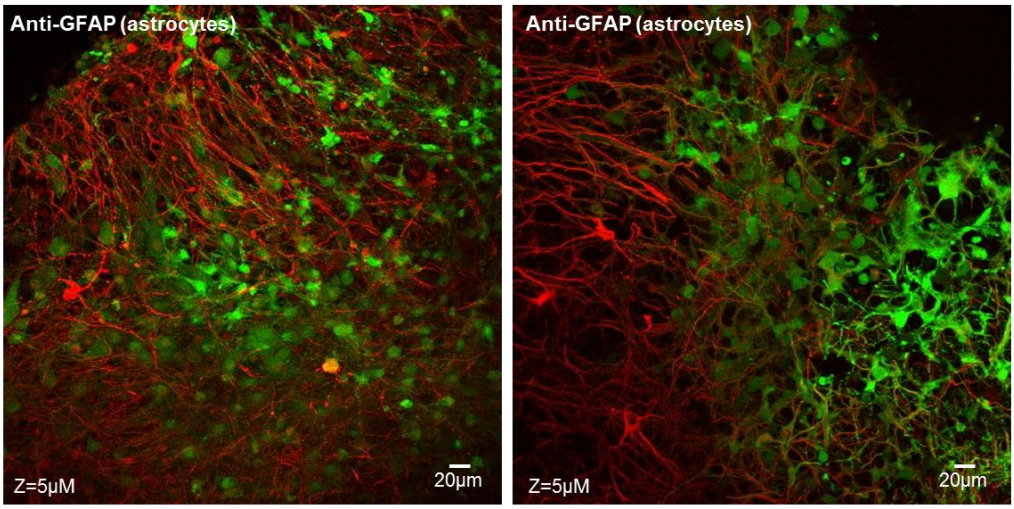

Figure 5.11| **Confocal micrographs of mouse cerebellar slices inoculated with rCVeGFP, fixed at 24 hours post-infection and stained for astrocytes**
rCVeGFP-infected cells fluoresce green and cell marker proteins were stained with anti-GFAP primary antibody followed by a red alexa secondary antibody. Fluorescence was visualised using a Leica SP5 confocal fluorescence microscope. The images are 5µM thick Z stacks. Scale bar shown.

5.3 Establishing an *in vivo* model of CHPV-induced encephalitis

5.3.1. Dose-dependent induction of encephalitis in mice by CHPV

5.3.1.1. *Titration of CHPV in mice*

Wild type CHPV strain I653514 was used in the early studies in mice and therefore was selected for use in this investigation to allow comparison with previously published data. A recombinant wild-type virus, designated rCHPV derived from strain 1653514 was generated and also tested. The initial step in this investigation was to establish the appropriate dose of wild type CHPV and rCHPV to elicit clear signs of infection between 2-5 days post-infection. This was necessary as variation in the infectious dose required to initiate disease with different strains is well recognised. This virus strain and the initial infectious dose used in the titration study (refer to section 2.3.2 for the method) was guided by these. The ability to observe the clinical symptoms of CHPV infection between 2-5 days post-infection was considered ideal as it provided a sufficient window in which to study the progression of neurological disease in the mouse model. A staged approach was used in the titration experiments with three mice being tested with the initial dose and then observed. The dose was altered as appropriate (lowered if the initial dose tested resulted in rapid disease onset) and another group of three animals tested. This process was repeated until a dose of virus was identified that caused observable disease in all three animals with paralysis in two limbs seen on or near day three after infection. This staggered approach was taken to reduce the numbers of animals required for the experiments, in accordance with the Home Office licence. The study did not require that the animals progress to the most advanced stage of disease before

analysis and therefore any animals presenting with paralysis in two limbs were immediately culled.

Three ICR (CD1) mice (7-11 days old) were infected by the intraperitoneal route with the initial dose of 1.0×10^4 pfu of wild-type CHPV per mouse. The mice were observed twice daily from the time of infection for signs of disease and the total weight of the group was measured daily. The group weight of the mice was measured as an additional monitor of general health. The progress of disease was recorded using a quantitative scoring system which is explained in section 2.3.1. The results are shown in Figure 5.12. The 1.0×10^4 pfu dose of virus resulted in a very rapid onset of disease with the first observable symptoms at day 2 post-infection. By day 3 post infection the disease had progressed further with one of the mice exhibiting paralysis of two limbs (which is the end point of the experiment, a score of 4 in the clinical scoring system) and the other two mice showing paralysis in one of the hind limbs (the side adjacent to the site of inoculation). Following an initial increase at day 1 post infection the weight of the mice declined rapidly over the observation period, with the group weight at day 3 post-infection almost 10% lower than on the day of virus inoculation and lower than their initial group weight. A domed appearance to the head of the most severely affected mouse on day 3 post-infection with CHPV was also observed, suggestive of an accumulation of fluid surrounding the brain.

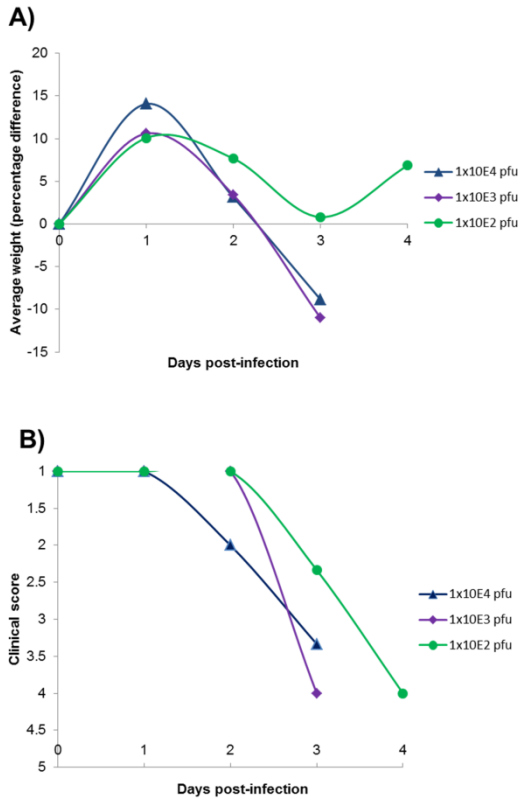

Figure 5.12| **Progress of wild-type CHPV infection at different doses**

Groups of three mice were inoculated intraperitoneally with either $1x10^4$, $1x10^3$ or $1x10^2$ pfu of wild type CHPV. For each dose the progress of disease is shown as the collective average weight (calculated as the percentage difference compared to day 0) (A) and the average clinical score (B).

The progress of disease produced by 1.0×10^4 pfu CHPV was considered too rapid for practical study and therefore a lower dose was required to study the progress of disease. A 10-fold lower dose (1.0×10^3 pfu per mouse) was used to inoculate a second group of three mice and disease monitored as before (Figure 5.12). The first symptoms of disease were observed at day 3 post-infection (a day later than seen at the higher dose), however, disease progression remained too rapid for use in the study. The average weight profiles of the infected animals were very similar at the two doses. The study was repeated using an inoculum containing 1×10^2 pfu of

CHPV per mouse, the results of which are shown in Figure 5.12. This dose elicited a more gradual disease progression. The initial clinical signs of infection were observed 3 days post-inoculation. However, unlike with the case at the higher doses, none of the three mice inoculated with 1.0×10^2 pfu of CHPV displayed the most severe symptoms (score of 4) until day 4 post-infection. Furthermore, the reduction in weight compared to the uninfected control mice was less marked, not falling below the starting average weight, and occurred more gradually. There was a slight increase (6%) in group weight at day 4 post-infection compared with the initial group weight, despite all of the mice displaying symptoms. Taken together, these results indicated that a dose of 1.0×10^2 pfu per mouse was appropriate for the next stage of the investigation as it was sufficient to elicit symptoms in each of the mice and provided a suitable window in which to study the progression of CHPV-induced encephalitis.

The clinical signs of disease progression of seven out of the nine mice used in the pilot study were consistent with descriptions in the literature: unilateral paralysis of the hind limb nearest the injection site followed by bilateral hind limb paralysis (after which would be forelimb paralysis and death if the mice were allowed to progress to this stage) (Jortner *et al.*, 1973). However, the other two mice displayed paralysis in one of the forelimbs (the same side of the body as the inoculation) following the initial unilateral hind limb paralysis. Thus, the disease progression of CHPV after intraperitoneal inoculation of the virus in young mice is variable and does not always follow the previously documented stages.

5.3.1.2. *Virus was detected in the brains (but not lungs or liver) of infected mice*

In order to investigate the site(s) of CHPV replication in the mouse model, the brains, lungs and livers were removed from six of the mice which were culled following infection with wild-type CHPV (two from each of the doses used in the pilot study above, section 5.3.1.1.). The tissues were homogenised in PBS and virus was titrated in BSC-1 cells. The titres obtained are shown in Table 5.2. Virus was detected at high titre (with an average of 4.78 $x10^9$ pfu/ml) in each of the six brain samples tested. No virus was found in any of the other organs, indicating that less than 200 pfu/ml of virus was present in these samples (i.e. 200 pfu/ml was the detection limit of the assay used).

Sample	Average titre (pfu/ml)
Mouse 1 brain	4.78×10^6
Mouse 1 lungs	<200
Mouse 1 liver	<200
Mouse 2 brain	3.50×10^9
Mouse 2 lungs	<200
Mouse 2 liver	<200
Mouse 3 brain	1.15×10^{10}
Mouse 3 lungs	<200
Mouse 3 liver	<200
Mouse 4 brain	7.10×10^9
Mouse 4 lungs	<200
Mouse 4 liver	<200
Mouse 5 brain	2.45×10^9
Mouse 5 lungs	<200
Mouse 5 liver	<200
Mouse 6 brain	4.10×10^9
Mouse 6 lungs	<200
Mouse 6 liver	<200

Table 5.2| **Titre of virus present in the brain, lungs and liver after infection with wild-type CHPV**
Brain, lungs and liver were extracted from six mice showing symptoms of infection with CHPV (scoring 4 on the clinical assessment scale). The homogenised samples were subsequently used in plaque assays in BSC-1 cells. The detection limit for the assay was 200 pfu/ml virus.

5.3.2. **Progression of wild-type CHPV infection *in vivo***

5.3.2.1. *Weight change and clinical assessment*

A dose of 50 pfu was used to elicit clear signs of infection between 2-5 days post-infection. Four groups of six 7-11 day old mice were inoculated intraperitoneally with 50 pfu of wild type CHPV and 5 mice (two from one group and one from each of the other groups) were sacrificed on 1, 2 and 3 days post-infection. The brains were removed and divided along the midsagittal plane. One half of each brain was homogenised for virus titration (section 5.3.2.2) and the other half was fixed for pathological examination (section 5.3.2.3). PBS was inoculated into the peritoneal cavity of a group of 6 uninfected control mice. All infected and uninfected mice were observed at daily intervals for signs of disease and the weight of the animals in each group and the clinical scores were recorded**.** The number of mice used in the experiment was the minimum number of animals necessary to provide statistically robust data. The collective weight of each group at each time point was expressed as percentage change compared to day 0 and the average of the 6 groups was then calculated. The clinical scores for each time point were summed and an average calculated.

The average weight changes and clinical scores (the mean of groups A-D) are shown in Figure 5.13 A and B respectively. The uninfected control group showed a steady increase in weight, gaining an average of 9% in weight each day over the 3 day observation period. Infection with wild-type CHPV severely inhibited weight gain in the suckling mice and the clinical scores obtained closely reflected the weight change data. The first **s**ymptoms of CHPV disease occurred at day 2 post-inoculation of 50 pfu of wild-type CHPV. Day 2 post-infection is also the time point where the infected mice separate from the trajectory of the uninfected control mice in terms of

weight, with a 2% average decrease in body weight in the experimental groups compared with a 9% increase in weight in the uninfected control group. There was a further 2% average reduction in weight by the following day in the infected mice, by which point the average score was 4 (i.e. paralysis in two limbs) in the clinical assessment system, the end point in this experiment. The differences between the mean group weights of the uninfected and infected animals were shown to be significantly different on day 2 and 3 post-infection (one tailed unpaired Student's t-test, $p \leq 0.05$).

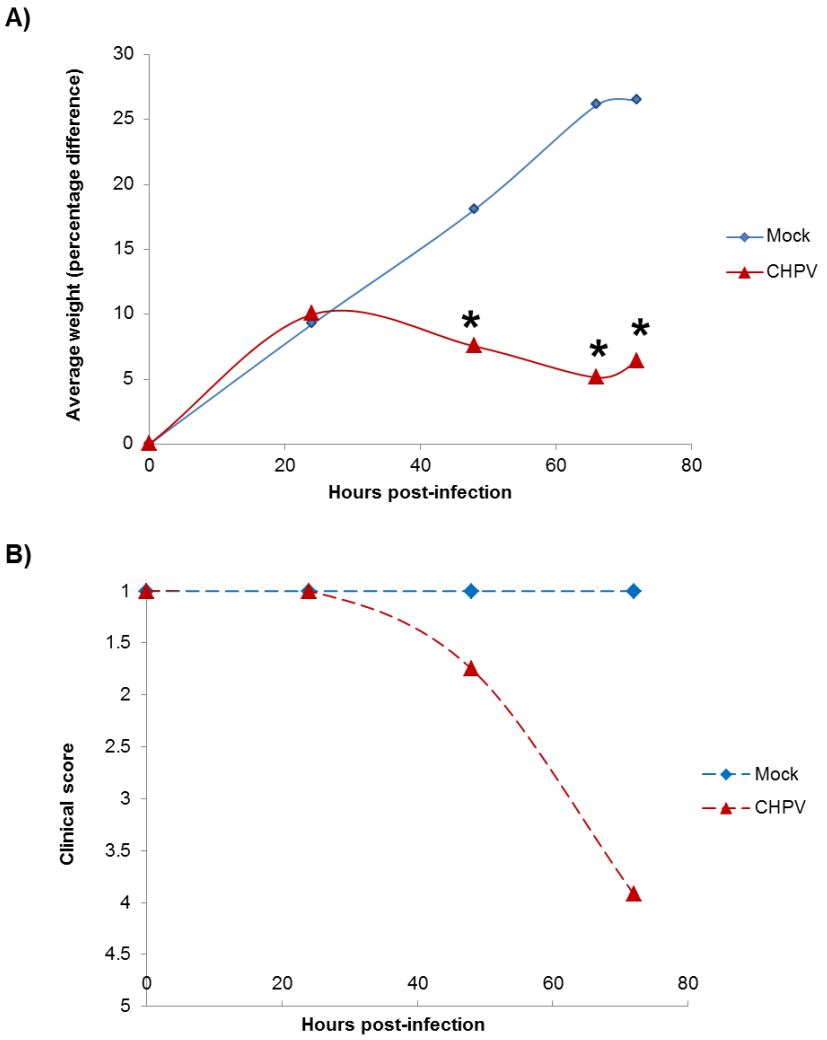

Figure 5.13| ***In vivo* timecourse of wild-type CHPV infection**
Suckling CDI mice (7-9 days old) were inoculated with 50 pfu of wild-type CHPV (red) or PBS (blue) by the intraperitoneal route. Weight data are expressed as a percentage change compared to the group weight at day 0. The change in mean weight (A) and average clinical scores (B) are given. The statistical significance of body weight changes on any one day was determined by a one tailed unpaired Student's t-test and is indicated by an asterisk ($p \leq 0.05$).

5.3.2.2. *Virus was detected in the mouse brain 24 hours post-infection with wild-type CHPV*

Five mice were sacrificed at 1, 2 and 3 days post infection with wild-type CHPV (above in section 5.3.2.1). Mice which showed paralysis of two limbs (i.e. the endpoint of the experiment) were culled and also sampled. Brains were removed from all of the sacrificed animals to be sampled and divided into two down the midsagittal plane. One half of each brain was homogenised in 500 µl of PBS and virus titrated in BSC-1 cells. The virus titres are shown in Table 5.3. Virus was present in the brain samples of each animal tested by 24 hours after intraperitoneal infection and the mean titre increased rapidly by 48 hours post-inoculation and decreased slightly by 72 hours post-inoculation. At 24 and 48 hours post-infection there was a 392-fold and 10 million-fold increase in viral titre in the brains of infected mice, respectively, compared to the 50 pfu starting inoculum.

Time post-infection (hours)	Average titre per sample (pfu/ml)	Average titre (pfu/ml)
24	$1.40x10^4$	$1.96x10^4$
	$7.15x10^3$	
	$1.38x10^4$	
	$8.75x10^3$	
	$2.40x10^5$	
48	$2.02x10^8$	$5.22x10^8$
	$1.50x10^9$	
	$4.75x10^8$	
	$9.13x10^7$	
	$4.55x10^9$	
	$8.68x10^9$	
	$1.43x10^8$	
	-	
	$1.09x10^7$	
	$3.60x10^9$	
72	$7.39x10^7$	$1.05x10^8$
	$8.47x10^8$	
	$1.00x10^{10}$	
	$2.72x10^4$	
	$6.13x10^3$	
	$2.83x10^8$	
	$1.74x10^9$	
	$4.93x10^9$	
	$6.00x10^9$	

Table 5.3| **Titre of virus present in the brain after infection with wild-type CHPV strain I653514**

At daily intervals 1 mouse from each experimental group was sacrificed using a schedule 1 method. Eight mice were culled because they displayed paralysis in two limbs and one had died (highlighted in pink and red respectively). The brains were removed from all of the sacrificed animals and divided into two down the midsagittal plane and one half was assayed for virus. Virus titres are the averages from duplicate repeats (column 2) and the overall average titre at each time point (i.e. the mean titre of the samples). The titre data from the fatal infection was not included in the average titre for the time point. The average titres given are the geometric mean across the groups.

Large variations were seen in the individual viral titres obtained per sample at the 72 hour time point, approximately a two million-fold difference between the lowest and highest titre. However, seven out of nine mice that were culled at the 72 hour time point had a titre greater than $7.0x10^7$ pfu/ml.

5.3.2.3. *Pathological examination of brains from mice infected with wild-type CHPV showed pronounced damage to the cerebellum*

The brains were removed from all of the sacrificed animals in the wild-type CHPV timecourse (section 5.3.2.1) and divided along the midsagittal plane. As detailed above in section 5.3.2.2 one half of each brain was used in titration experiments on BSC-1 cells, in order to determine the titre of virus present in the brain at each stage of infection. The other half was fixed in 4% paraformaldehyde in PBS. Sagittal sections were prepared and stained with haematoxylin and eosin (H&E) (University of Edinburgh).

Analysis of the brain sections infected with CHPV strain I653514 at post-infection day 1 appeared comparable to the uninfected samples (post-infection day 1 samples not shown). The first signs of virus infection in the brain were observed at day 2 post-infection (Figure 5.14). The histopathological lesions were restricted to the cerebellum and included neuronal damage including cell shrinkage and purkinje neurones with pyknotic nuclei (Figure 5.14 f) and substantial areas of cell death (Figure 5.14 d-f). There was also evidence of inflammation and infiltration of mononuclear infiltrates, indicative of an active immune response. At day 3 post-infection the histopathologic changes in the cerebellum were even more pronounced with severe neuronal vascular degeneration, large regions of cell death (Figure 5.14 g, h) and large numbers of mononuclear cells (Figure 5.14 i). On day 3 post-

infection cell death was also observed in the hippocampus (Figure 5.15 b, c) and there were several regions of vacuolation in the cortex (Figure 5.15 d).

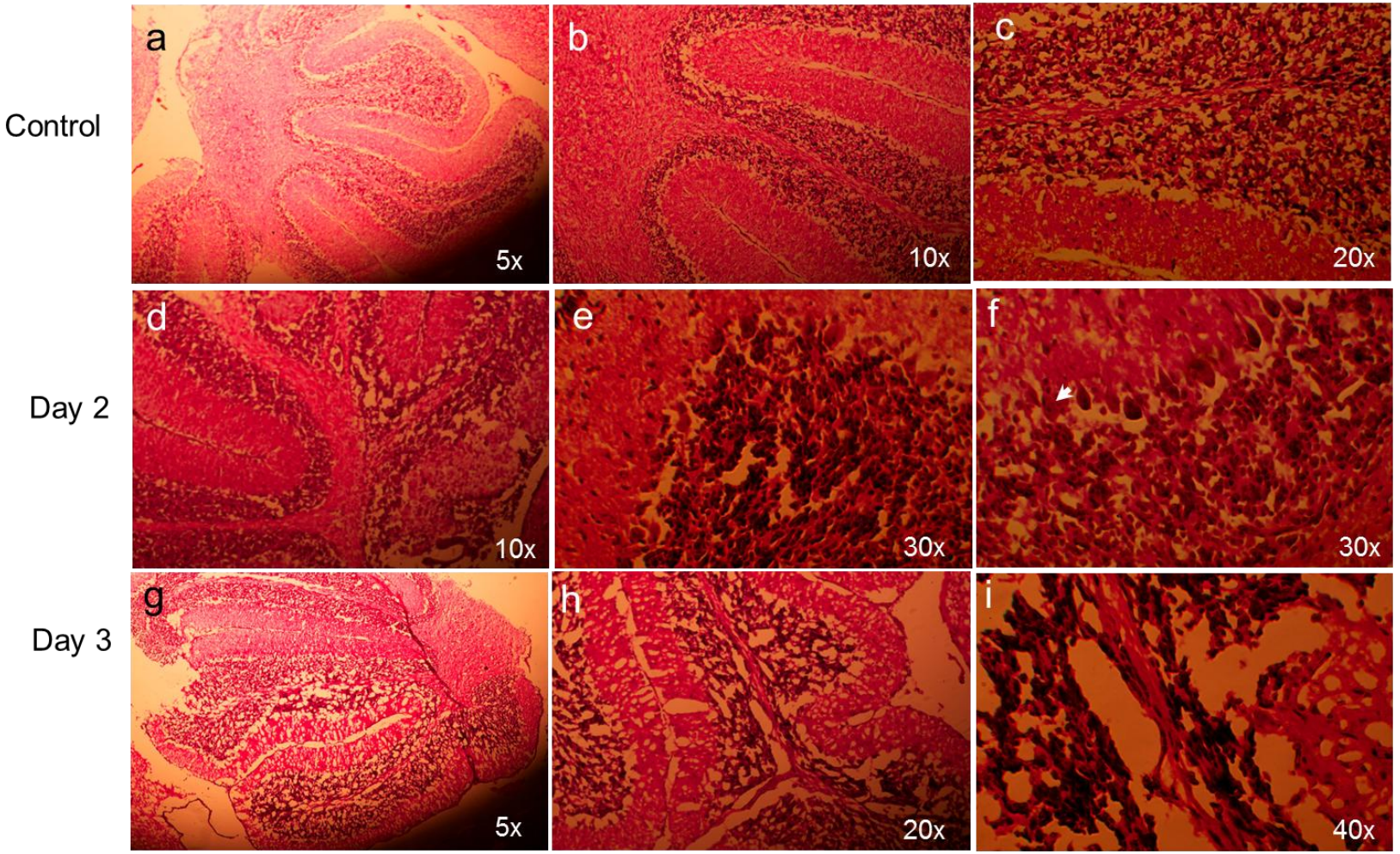

Figure 5.14| **Sagittal brain sections stained with haematoxylin and eosin from mice inoculated with CHPV strain I653514**

5µM paraffin processed sagittal sections from control samples (a-c) and mice infected with CHPV and sampled at post-infection day 2(d-f) or post-infection day 3 (g-i). A pyknotic nucleus is indicated by an arrow in panel f.

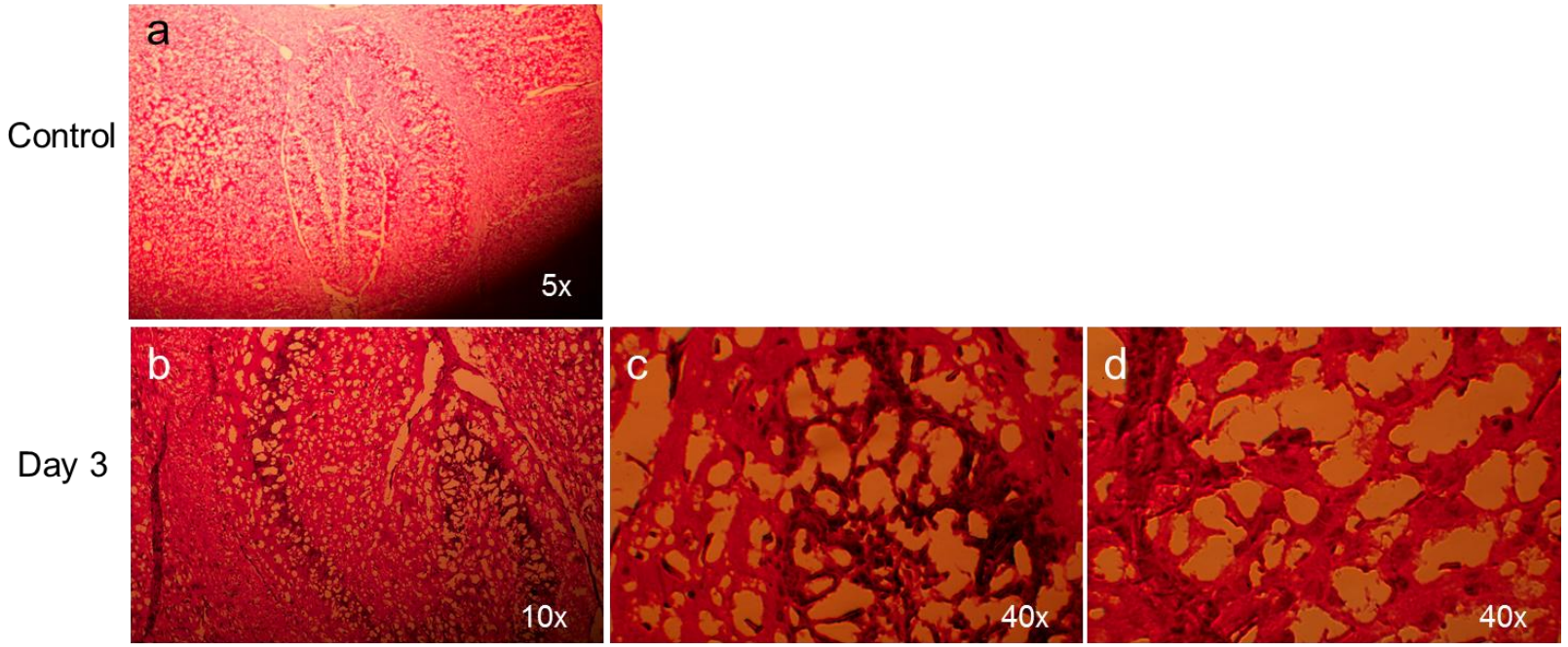

Figure 5.15| **Sagittal brain sections stain with haematoxylin and eosin from mice inoculated with CHPV strain I653514**
The 5µM sections were processed in paraffin. Representative photomicrographs of hippocampus in control (a) and in virus-infected mice at post-infection day 3 (b, c) and cortex from a CHPV-infected section at post-infection day 3 (d).

5.3.3. The dose of recombinant wild-type CHPV required to cause encephalitis

The availability of the CHPV reverse genetics system (Marriott & Hornsey, 2011) provided a unique opportunity to explore the site of CHPV infection in the mouse brain and the cell types permissive to infection, by enabling the generation of a number of recombinant viruses containing reporter genes. It was important, therefore, to firstly compare the pathogenesis of the genetically modified viruses with the wild type virus in mice to validate the biological significance of work using the recombinant viruses. Viruses grown extensively in tissue culture can have a different pathogenicity to the parental virus, either due to point mutations which have accumulated in the parental virus as a consequence of repeated passages in cell lines or non-coding, epigenetic alterations. rCHPV does not contain any mutations with respect to CHPV strain I653514 but there may be epigenetic changes including differences in glycosylation. For this reason a rCHPV was used as the comparison with the tagged recombinant viruses. Section 4.1.4 contains details of the recovery of rCHPV.

5.3.3.1. *A ten-fold higher dose of rCHPV (500 pfu) was required to induce encephalitis compared with wild-type CHPV* strain I653514

A group of six 8 day old ICR (CDI) mice were inoculated with 50 pfu of rCHPV by the intraperitoneal route. This was the dose of wild-type CHPV (strain I653514) capable of inducing fatal encephalitis. The group weight and clinical assessment scores for the mice over a 9 day observation period are shown in Figure 5.16 A and B respectively. The weight of the animals in the experimental group remained similar to the uninfected control mice, increasing steadily throughout the duration of

the experiment, despite 2 out of 6 mice becoming sick. The first symptoms were observed on day 6 post-infection, as shown by the increase in clinical score in Figure 5.16 B. These results indicated that the rCHPV was considerably less pathogenic than the wild-type virus where intraperitoneal inoculation of 50 pfu resulted in an average clinical score of 3.92 at day 3 post-infection and a highly significant reduction in mean weight at both day 2 and 3 post-infection with respect to the control group.

To establish the dose of rCHPV required to produce a disease progression equivalent to that of the wild-type virus another group of six 8 day old ICR (CDI) mice were inoculated with the 10-fold higher dose of 500 pfu of rCHPV. At this dose all six of the infected mice developed disease and reached the end point 5 days post-infection (Figure 5.16 B). Moreover, the relative percentage increase in group weight from day 0 to 5 was 20% lower in the rCHPV-infected group than the mock group (Figure 5.16 A). Despite being a lethal dose, there was a delay in the onset of clinical disease of 1-day and a 2-day delay in the progression of disease compared with the wild-type virus (Figure 5.13).

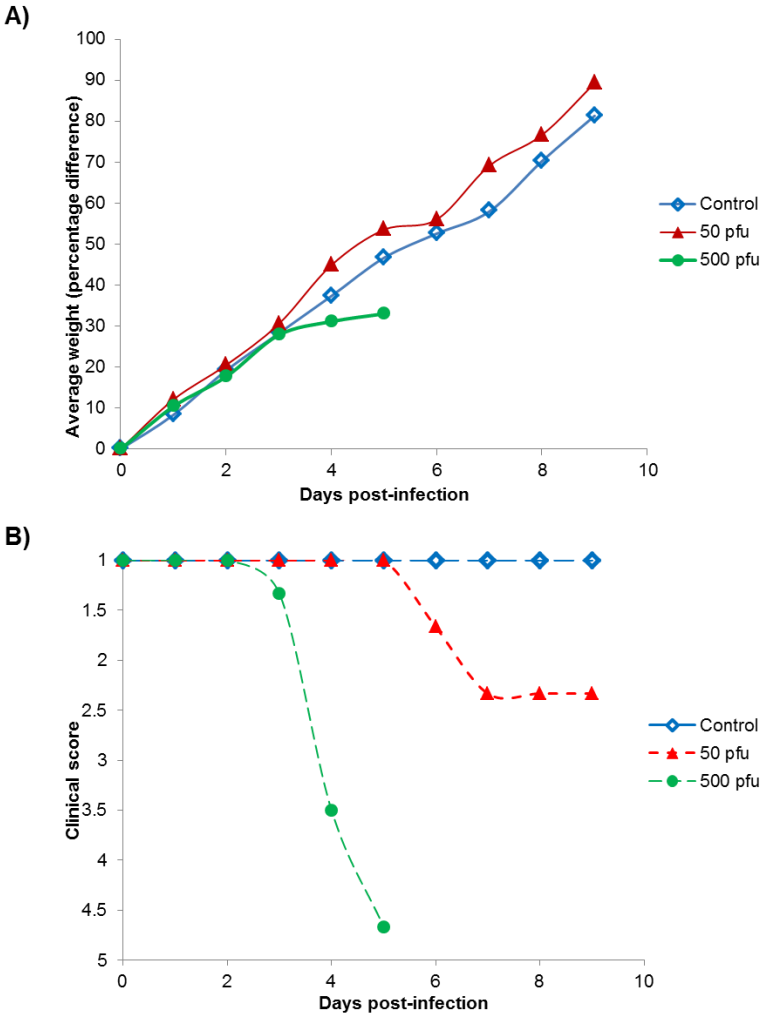

Figure 5.16| **Progress of recombinant wild-type CHPV infection at different doses** Groups of six mice were inoculated intraperitoneally with either 50 pfu or 500 pfu of recombinant wild type CHPV (rCHPV) or PBS. For each dose the progress of disease is shown as the collective average weight (calculated as the percentage difference compared to day 0) (A) and the average clinical score (B).

5.3.4. Progression of recombinant wild-type CHPV infection *in vivo*

5.3.4.1. *Weight change and clinical assessment*

rCHPV (500 pfu per mouse) was administered intraperitoneally to 6 groups of 8 day old ICR (CDI) mice (6 mice per group) and group weights and clinical scores were measured daily. PBS was inoculated into the peritoneal cavity of a group of 6 control mice. 6 mice were sacrificed at each of 1, 2, 3, 4 and 5 days post infection. The brains were removed and divided as described previously. One half of each brain was homogenised for virus titration (section 5.3.4.2) and the other half was fixed for pathological examination (section 5.3.4.3).

The average relative percentage weight change and clinical scores for the virus-infected and uninfected mice throughout the timecourse are shown in Figure 5.17. The onset of clinical symptoms in the virus-infected group occurred on day 3 post-infection and the mean clinical score of the virus group on the last day of the experiment was 1.7 (as the majority of the mice did not develop disease). This was reflected in the mean weight changes, which remained similar for the rCHPV-treated and uninfected animals throughout the experiment (Figure 5.17 A).

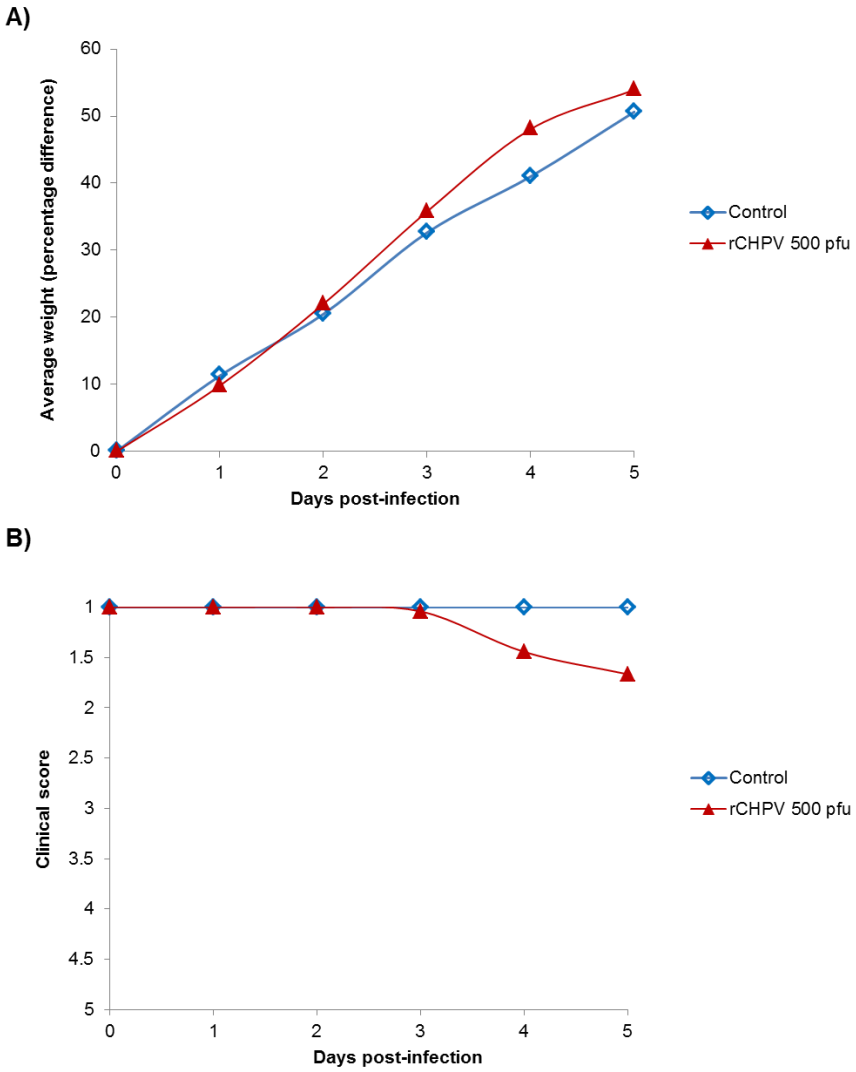

Figure 5.17| ***In vivo* timecourse of recombinant wild-type CHPV infection (500 pfu)** Suckling CDI mice (8 days old) were inoculated with 500 pfu of rCHPV or PBS by the intraperitoneal route. The average daily percentage change in weight for the virus-infected and the mock group is shown in A, whilst the average clinical disease assessment for is given in in B.

As very few of the mice developed encephalitis upon intraperitoneal injection of 500 pfu of rCHPV the experiment was repeated using a dose of 1000 pfu of virus per mouse (Figure 5.18). There was a reduction in percentage weight gain (relative to the mock) at day 4 post-infection, followed by a further decrease in weight at day 5 post-infection) in the rCHPV-infected group (Figure 5.18 A). The onset of symptoms began on day 3 post-infection of rCHPV and progressed rapidly thereafter (Figure 5.18 B). By post-inoculation day 5 severe disease was observed in the virus

group and the end point was reached. Thus this dose of rCHPV is lethal and therefore would provide tissue samples with which to study the pathology of CHPV-induced encephalitis. The average weight change of the rCHPV-infected group at day 2 post-infection was found to be significantly higher than the mean mock weight at this timepoint, a shown by an asterisk in Figure 5.18 A. The animals in both groups then resumed weight gain at similar levels until day 4 post-infection when the infected mice showed a highly significant loss of weight. The infected mice showed another significant weight loss on day 5.

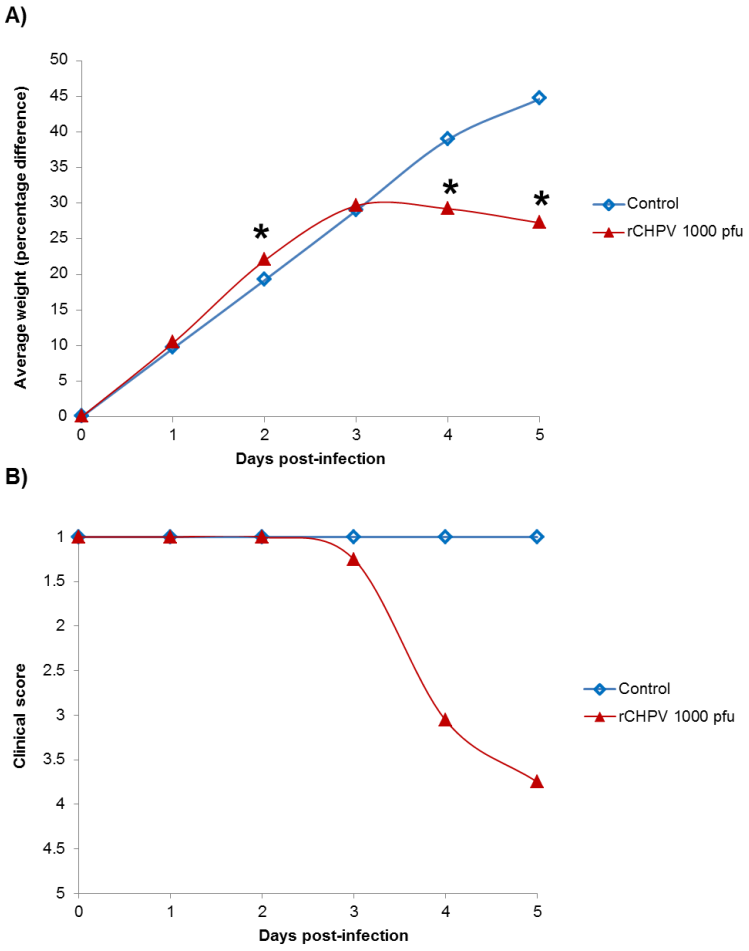

Figure 5.18| ***In vivo* timecourse of recombinant wild-type CHPV infection (1000 pfu)** Suckling CD1 mice (8 days old) were inoculated with 1000 pfu of wild-type CHPV (red) or PBS (blue) by the intraperitoneal route. The average daily percentage change in weight for the virus-infected and the uninfected groups are shown in A, whilst the clinical disease assessment for each is given in B. The statistical significance of body weight changes on any one day was determined by a one tailed unpaired Student's t-test and is indicated by an asterisk ($p \leq 0.05$).

5.3.4.2. *Virus was detected at high titre in the mouse brain 3 days post-infection with rCHPV*

6 mice per time point from the 1000 pfu rCHPV timecourse (above in section 5.3.4.1) were sacrificed at 1, 2, 3, 4 and 5 days post-infection. The brains were removed and divided into two as before with one half assayed for virus. The virus titres are shown in Table 5.4. Mice which showed paralysis in two limbs (i.e. the endpoint of the experiment) were culled but not sampled because including them would have skewed the data so that the mice which experienced a more gradual disease progression were sacrificed for sampling at the later time points (as they were the only ones left). These mice may have had a lower than average brain viral titre if the animals that were culled were allowed to progress to the most advance stage of disease had been included in the average.

Virus was detected in the brain at post-inoculation day 1 in 5 out of 6 mice tested with an average titre of $4.30x10^2$ pfu/ml. At day 2 post-infection the level of virus present in the majority of brain samples (5 out of 6) remained fairly low, although the average titre was high because of the $1.54x10^6$ pfu/ml of virus in one of the samples. All of the mice sampled had high levels of virus in the brain at day 3 post-infection, an approximately 80,000-fold increase in comparison with the 1000 pfu starting inoculum which was introduced into the peritoneal cavity. The average viral titre in the brain increased further by day 4 post-infection (200,000-fold higher than the virus administered). There was a slight reduction in virus titre on day 5 compared with the previous day. This was probably because the majority of mice displayed the most severe symptoms by day 4 post-infection and so were culled and therefore the mice sampled on day 5 were those that experienced a slower than average disease progression.

There was a 2-day delay in the appearance of virus at high titre in the mouse brain after intraperitoneal inoculation of 1000 pfu rCHPV compared with when 500 pfu of wild-type CHPV strain I653514 was administered. This is consistent with an identical delay in the onset of clinical symptoms.

Time post-infection (days)	Average titre per sample (pfu/ml)	Average titre (pfu/ml)
1	0	$4.30x10^2$
	$1.03x10^3$	
	$1.20x10^3$	
	$5.00x10^1$	
	$2.75x10^2$	
	$2.50x10^1$	
2	$2.50x10^1$	$2.57x10^5$
	$1.54x10^6$	
	$7.50x10^1$	
	$1.75x10^2$	
	0	
	$7.50x10^1$	
3	$8.25x10^7$	$8.02x10^7$
	$6.75x10^3$	
	$2.55x10^7$	
	$1.73x10^8$	
	$2.00x10^8$	
	$3.10x10^4$	
4	$2.53x10^8$	$2.14x10^8$
	$1.73x10^6$	
	$9.00x10^7$	
	$4.93x10^8$	
	$3.25x10^8$	
	$1.20x10^8$	
5	$1.38x10^6$	$8.11x10^7$
	$2.23x10^8$	
	$2.00x10^5$	
	$1.00x10^8$	

Table 5.4| **Titre of virus present in the brain after infection with recombinant wild-type CHPV**

At daily intervals 1 mouse from each virus group was sacrificed using a schedule 1 method. The brains were removed from all of the sacrificed animals and divided into two down the midsagittal plane. One half of each brain was homogenised in 500 µl of PBS and titrated on BSC-1 cells. Virus titres are the averages from duplicate repeats (column 2) and the overall average titre at each time point (i.e. the mean titre from the samples).

5.3.4.3 Pathological examination of brains from mice infected with rCHPV

The other half of the brains from the rCHPV-infected mice, which were sampled daily from 1 to 5 days post-infection and uninfected control mice (section 5.3.4.1) were fixed in 4% paraformaldehyde in PBS for pathological analysis. Sagittal sections from these samples were prepared and then stained with haematoxylin and eosin (H&E) (University of Edinburgh). Figure 5.19 contains representative photomicrographs from the analysis of the sections.

In line with the virus titre data and the clinical scores, the initial pathological changes were first observed on day 3 post-infection, a day later than following inoculation of CHPV strain I653514. These changes included some neuronal damage including cell shrinkage and pyknotic nuclei (Figure 5.19 c) and mononuclear infiltrates (Figure 5.19 d) in the cerebellum. At days 4 and 5 post-infection the pathology was more striking with large zones of complete cell death in the cerebellum (Figure 5.19 f-k). Some cell death was also observed in the hippocampus and cortex at days 4 and 5 post-infection (not shown).

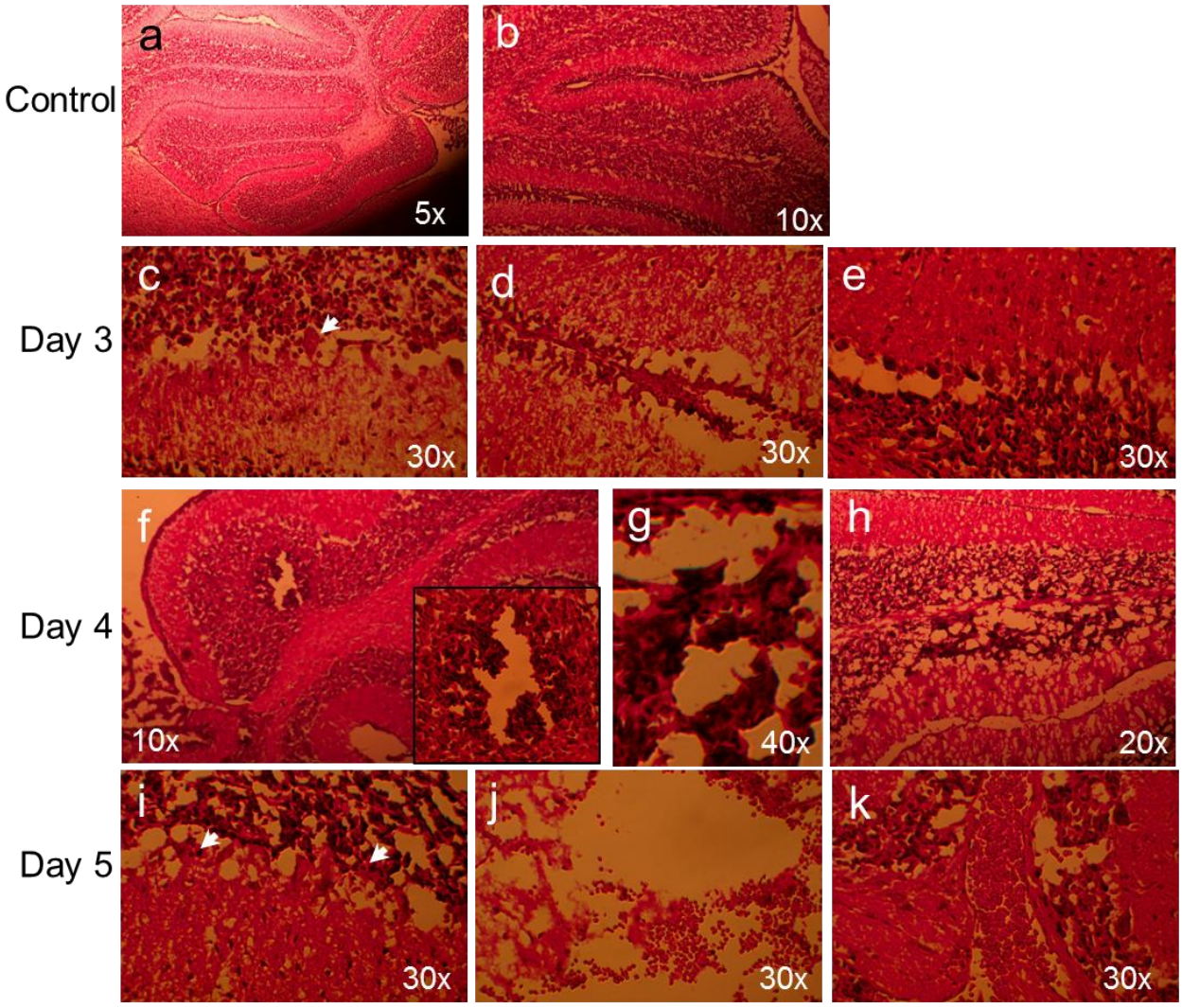

Figure 5.19| B**rain sections stained with haematoxylin and eosin from mice inoculated with 1000 pfu of rCHPV**

5µM sections were prepared and processed in paraffin. Representative photomicrographs showing regions of the cerebellum from control (a, b) and virus-infected mice at post-infection day 3 (c, d, e), 4 (f, g, h) and 5 (i, j, k). Pyknotic nuclei and neurones with central chromatolysis are shown by arrows.

5.3.5. The dose of a GFP-tagged CHPV (CVeGFP) required to cause encephalitis

To investigate the site(s) of infection and the cellular tropism of CHPV in the brain the recombinant CHPV, rCVeGFP (Marriott & Hornsey, 2011) was used. A diagram of the rCVeGFP genome is shown in Figure 5.2. The pathogenicity of this virus in mice was compared to that of rCHPV to confirm that the genetically modified virus

behaved in the same way as the wild-type tissue culture-derived virus. Introduction of the eGFP gene had little observable effect on the growth of the virus in tissue culture.

5.3.5.1. *A dose of 1000 pfu of CVeGFP was required to induce encephalitis*

6 8 day old mice were inoculated intraperitoneally with 50 pfu of CVeGFP. This dose had no effect on the observed weight relative to the uninfected animals but did induce disease, as illustrated in Figure 5.20. The initial symptoms were observed on day 5 post-infection. A 10-fold increase in the dose of CVeGFP administered (500 pfu per mouse) led to more severe disease; showing the first signs of infection on post-infection day 4 and progressing to the experimental endpoint on day 6 (Figure 5.20). Intraperitoneal injection of 1000 pfu resulted in severe disease in all of the mice with the initial signs evident on day 3 and the endpoint reached on day 6 post-infection. Thus, 1000 pfu was deemed a suitable dose to further investigate the progression of CHPV-induced encephalitis. *In vivo* infection with CVeGFP (at any of the three doses) did not lead to weight loss (as observed for CHPV strain I653514 and rCHPV) and levels remained comparable to the uninfected mice throughout the study.

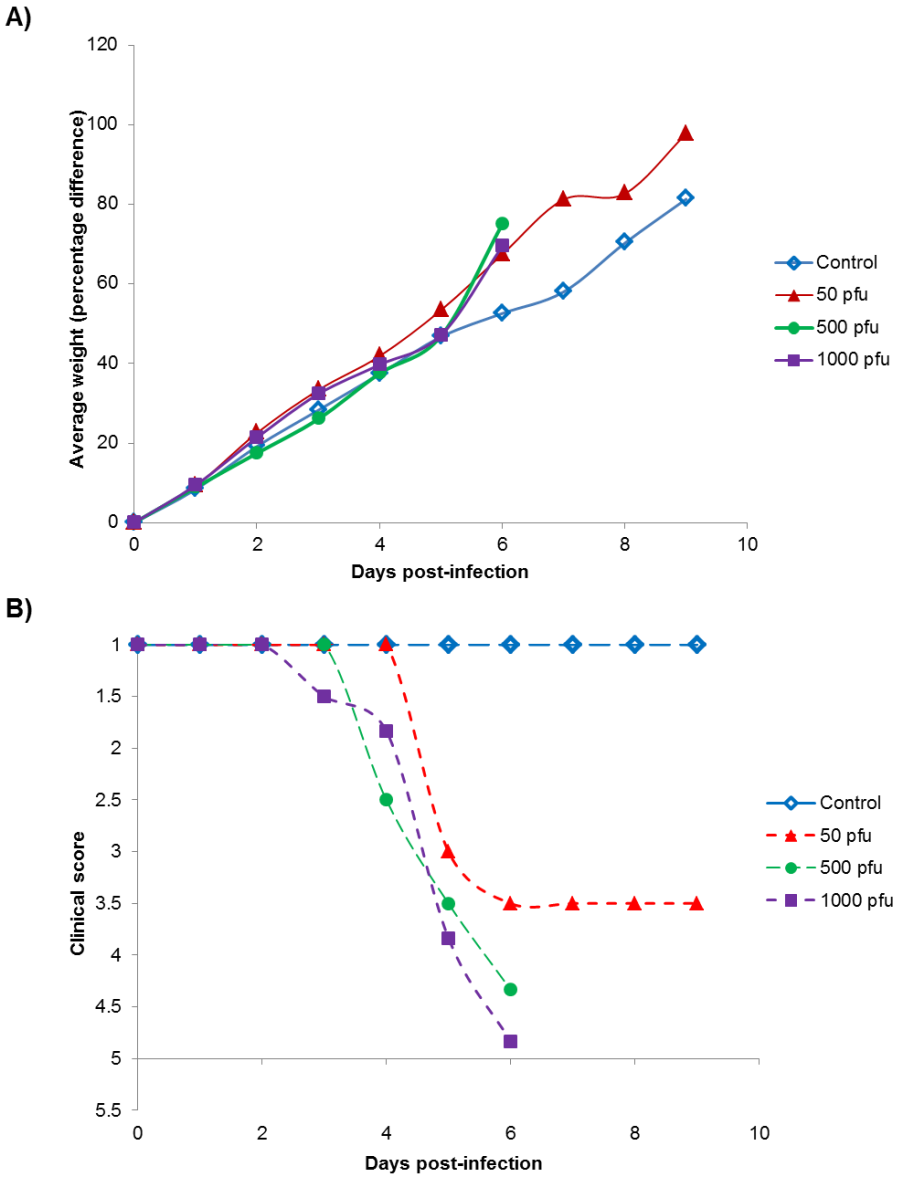

Figure 5.20| **Progress of CVeGFP infection at different doses**
Groups of six mice were inoculated intraperitoneally with either 50 pfu, 500 pfu or 1000 pfu of CVeGFP or PBS. For each dose the progress of disease is shown as the collective average weight (A) (calculated as the percentage difference compared to day 0) and the average clinical score (B).

5.3.6. Progression of CVeGFP infection *in vivo*

5.3.6.1. *Weight change and clinical assessment*

6 groups of 6 8 day old mice were infected with 1000 pfu CVeGFP via the intraperitoneal route and observed for signs of clinical disease. PBS was inoculated into the peritoneal cavity of a group of 6 control mice. Each day 5 mice were culled

and the brain removed. Brains were divided along the midsagittal plane. One half of each brain was homogenised for virus titration (section 5.3.6.2) and the other half was fixed for pathological examination (section 5.3.6.3). The group body weight changes (relative to day 0) for the virus-infected group was comparable to the uninfected group throughout the study, despite the mice exhibiting severe symptoms of disease (Figure 5.21). Symptoms were first observed on day 5 post-infection.

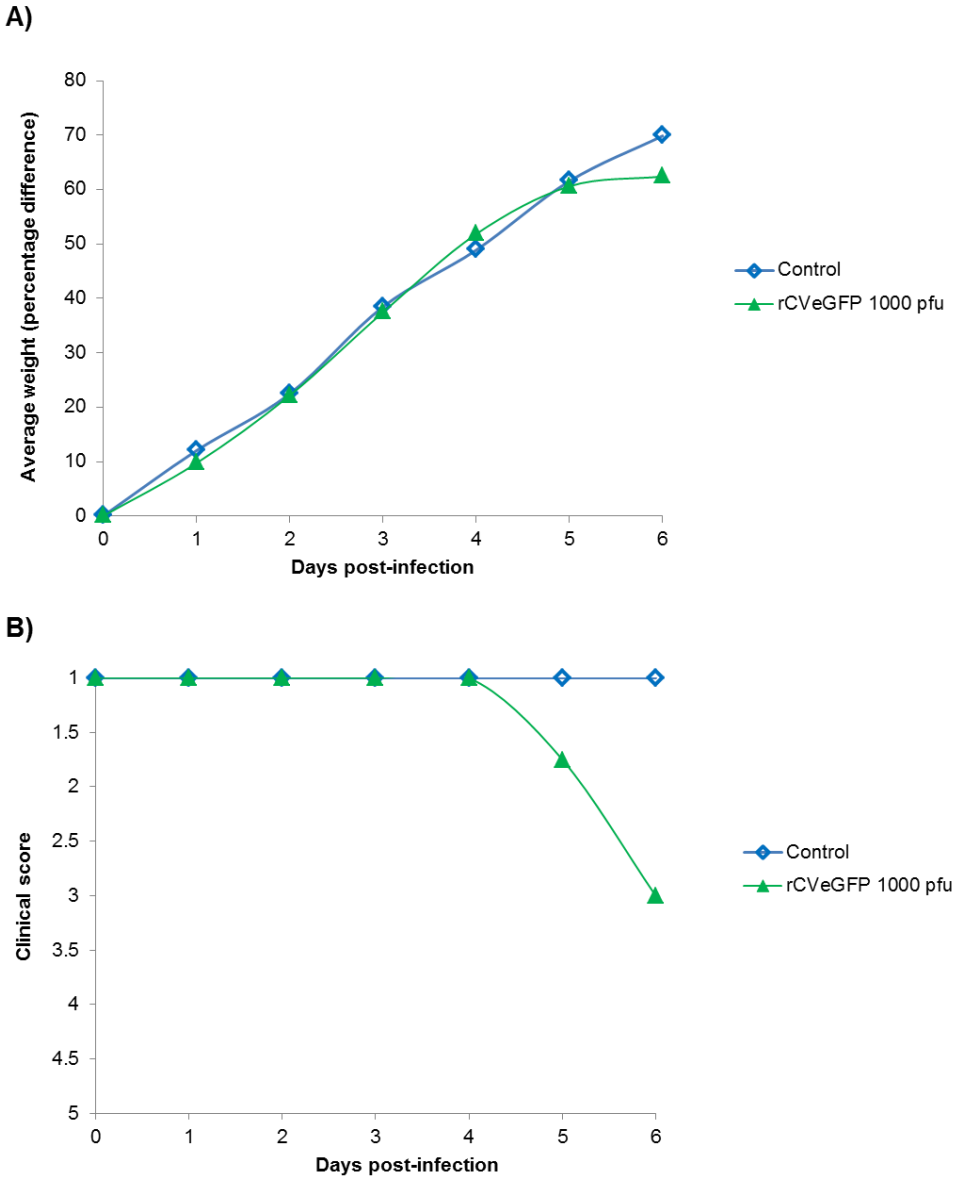

Figure 5.21| ***In vivo* timecourse of CVeGFP infection (1000 pfu)**
Suckling CD1 mice (8 days old) were inoculated with 1000 pfu of CVeGFP (green) or PBS (blue) by the intraperitoneal route. The change in mean weight for the virus-infected and the uninfected group is shown in A, whilst the average clinical scores are given in B.

5.3.6.2. There was a two day delay in the onset of CVeGFP-induced encephalitis compared with rCHPV

To allow comparison, the mean group weights and clinical scores of mice infected with 1000 pfu of rCHPV (Figure 5.18) and 1000 pfu of rCVeGFP (Figure 5.21) are given in Figure 5.22. The results indicate that the insertion of eGFP in the CHPV genome between the M and G genes produced a virus that had different characteristics *in vivo*. There was a 2-day delay in disease onset and progression compared to infection with rCHPV. The summed clinical scores for rCHPV-infected mice were significantly higher than rCVeGFP-infected mice from post-inoculation day 3, as determined by one tailed Mann-Whitney U tests (Figure 5.22 B). Intraperitoneal injection of 1000 pfu of rCHPV produced a fatal encephalitis in all mice by day 5 post-infection. Animals given this dose of rCHPV also showed significant weight loss compared to the non-infected control group on days 4 and 5. In contrast, relative weight change was unaffected by infection with rCVeGFP, as shown by values comparable to the controls in Figure 5.21. However, Figure 5.22 A shows the mean weights of mice infected with rCVeGFP being significantly higher than the mock from day 3. This is because the mock values in this figure were derived from the average weights of uninfected mice, which were substantially lower than the mock group in the rCVeGFP experiment (Figure 5.21).

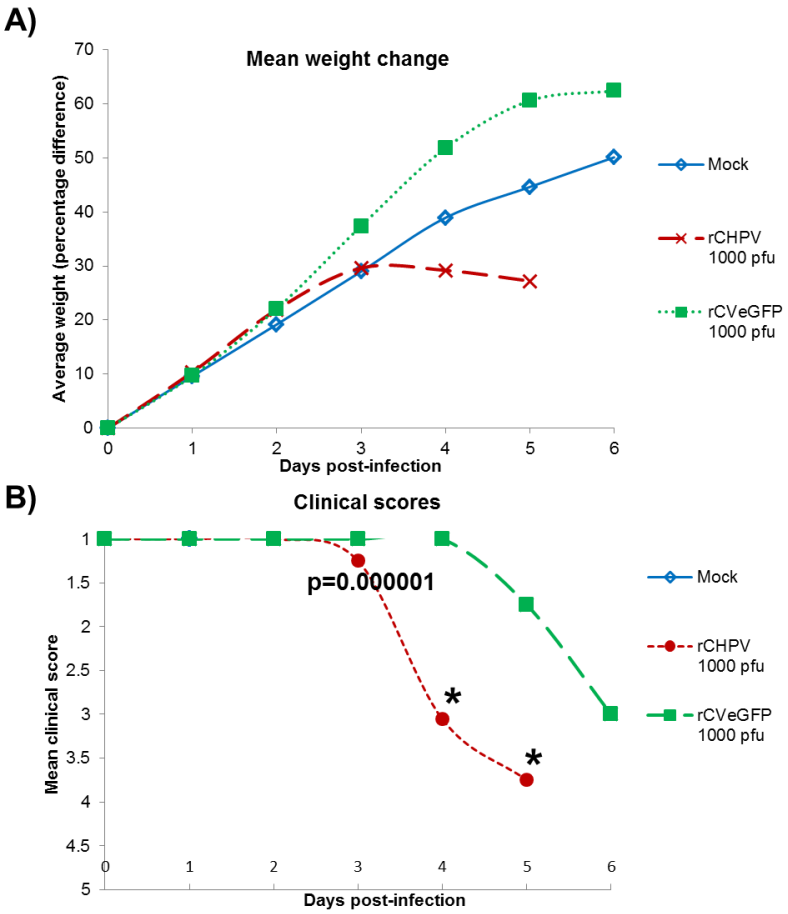

Figure 5.22| **Comparison of rCHPV and rCVeGFP pathogenesis (1000 pfu)**
Changes in mean weight (A) and average clinical score (B) after intraperitoneal inoculation of 1000 pfu of rCHPV (red) or 1000 pfu of rCVeGFP (green). Weight data are expressed as a percentage change compared to the group weight at day 0. Statistical significance of summed clinical scores for day 3 was determined by a one tailed Mann-Whitney U test, indicated by p value. The differences between the clinical scores for rCHPV and rCVeGFP for days 4 and 5 post-infection were highly significant, indicated by an asterisk.

5.3.6.3. Virus was detected at high titre in the mouse brain four days post-infection with CVeGFP

One mouse from each group in the 1000 pfu CVeGFP timecourse study (section 5.3.6.1) was sacrificed each day following virus inoculation. The brains were removed and one half of each brain was homogenised in 500 µl of PBS and virus was titrated in BSC-1 cells. The titres of virus obtained in the brain after intraperitoneal inoculation of 1000 pfu of CVeGFP are shown in Table 5.5.

The earliest time point virus was detected in the brain at this dose was day 1 post-infection although only in 2 out of the 6 samples. In these samples the titres were very low and may represent contamination by virus in the blood resulting from viraemia though this was not tested directly. The average titre increased on day 2 post-infection to 4.55 $x10^3$ pfu/ml, however, only 2 out of 6 samples tested positive for virus and one of those only had a titre of $2.50x10^1$ pfu/ml. By day 3 post-infection, the average titre had increased further to $1.51x10^4$ pfu/ml and virus was found in half of the samples. The average viral titre continued to rise at day 4 and 5 post-infection and virus was detected in the brains of each of the mice sampled at day 5 post-infection. The titre data after intraperitoneal inoculation of 1000 pfu of CVeGFP varied considerably between the samples at each of the time points.

Time post-infection (days)	Average titre per sample (pfu/ml)	Average titre (pfu/ml)
1	0	$3.33x10^1$
	0	
	0	
	$5.00x10^1$	
	$1.50x10^2$	
	0	
2	0	$4.55x10^3$
	$2.50x10^1$	
	0	
	0	
	0	
	$2.73x10^4$	
3	$2.50x10^1$	$1.51x10^4$
	$7.43x10^4$	
	0	
	0	
	0	
	$1.65x10^4$	
4	0	$8.88x10^5$
	0	
	0	
	$2.50x10^1$	
	$5.22x10^6$	
	$1.14x10^5$	
5	$2.25x10^6$	$2.13x10^6$
	$4.50x10^4$	
	$2.00x10^2$	
	$1.00x10^3$	
	$1.05x10^7$	
	$7.50x10^1$	
6	0	$4.86x10^5$
	$1.83x10^6$	
	$2.50x10^3$	
	$1.10x10^5$	

Table 5.5| **Titre of virus present in the brain after intraperitoneal inoculation of 1000 pfu of rCVeGFP**

At daily intervals 1 mouse from each experimental group was sacrificed using a schedule 1 method. The brains were removed from all of the sacrificed animals and divided into two down the midsagittal plane. One half of each brain was homogenised in 500 µl of PBS and titrated in BSC-1 cells. Virus titres are the averages from duplicate repeats (column 2) and the overall average titre at each time point (i.e. the mean titre of the samples).

5.3.6.4. Significantly lower levels of virus was present in the brains of CVeGFP-infected mice compared to rCHPV-infected mice at days 3 and 4 post-inoculation

The average viral titres detected in the brain after intraperitoneal inoculation of 1000 pfu of rCHPV or rCVeGFP are shown in Figure 5.23. Mice infected with rCVeGFP were found to have significantly lower levels of virus present in the brain than rCHPV-infected mice at 3 and 4 days post-infection. This was determined using a two tailed Mann-Whitney U test.

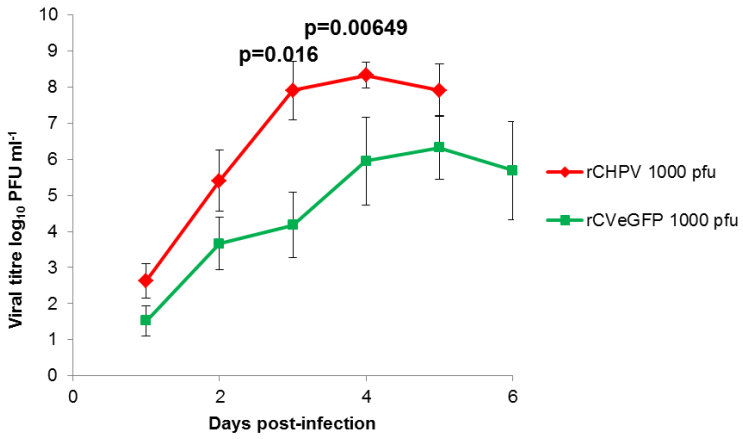

Figure 5.23| **Virus titre in rCHPV and rCVeGFP brain samples**
Average virus titre determined from brain samples from mice inoculated with 1000 pfu rCHPV (red) and rCVeGFP (green). Error bars show the standard error of the mean. Statistical significance of each day was determined by a two tailed Mann-Whitney U test. Statistically significant differences are indicated by p value for days 3 and 4.

5.3.6.5. r*CVeGFP passaged in the mouse brain contains functional GFP*

Plaques obtained from the titration of brain samples taken from mice inoculated with rCVeGFP (section 5.3.6.1) were visualised using epifluorescence microscopy, to confirm the expression of GFP (not shown).

In addition, RNA was extracted from 5 of the homogenised brain samples and reverse transcribed to generate cDNA using random hexanucleotide primers. The

GFP sequence was amplified from the cDNA by PCR using the *MGFPF* and *GGFPR* oligonucleotides which correspond to the end of the M gene and start of the G gene for the forward and reverse primer, respectively (Appendix 1). The PCR product was visualised on an agarose gel and the fragment was purified and sequenced using the *MGFPF* and *GGFPR* primers (in separate reactions). The GFP sequence was confirmed to be present in each of the samples tested.

5.3.6.6. *Pathological examination of brains from mice infected with rCVeGFP*

Half of each brain taken from the animals in the rCVeGFP timecourse (section 5.3.6.1) were fixed in 4% paraformaldehyde in PBS for pathological examination by collaborators at the Pirbright Institute. Sagittal sections were prepared and stained with haematoxylin and eosin (H&E). No evidence of pathology was observed in sections of brain from rCVeGFP-infected mice at day 1 post-infection and the sections were comparable to the uninfected control samples. Representative micrographs of the virus-infected brain samples at day 2 and 3 post-infection and uninfected samples at day 3 are shown in Figures 5.24 and 5.25.

Sections of brain from mice infected with rCVeGFP at day 1 (not shown) and 2 post-infection looked comparable to the mock non-infected counterparts (Figure 5.24). The first signs of virus infection in the brain were observed at day 3 post-infection (Figure 5.25). These changes included indications of inflammation including some perivascular cuffing and infiltrating mononuclear cells in the cerebellum (Figure 5.25 a) and also inflammation in the rostral migratory stream in the subventricular zone. In addition, there were regions of neuronal damage in the cerebellum including Purkinje neurones with pyknotic nuclei (Figure 5.25 g) and areas of complete cell

death. Some vacuolation in the cortex accompanied with eosinophilia was also observed (not shown) and limited inflammation in white matter tracts was observed. The hippocampus, and the dentate gyrus appeared normal in all mice.

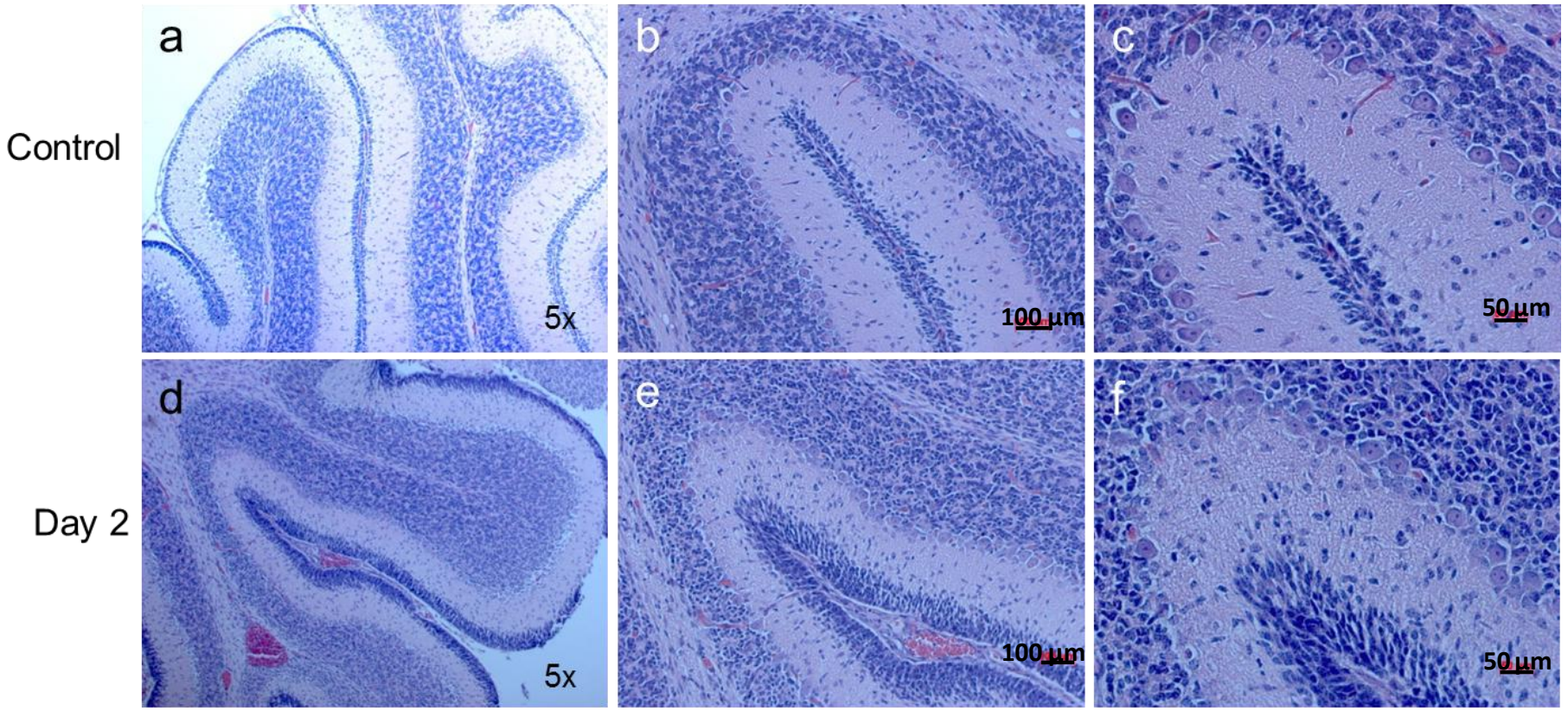

Figure 5.24| B**rain sections stained with haematoxylin and eosin from mice inoculated with 1000 pfu of rCVeGFP**
5µM sections were prepared and processed in paraffin. Representative photomicrographs showing regions of the cerebellum from control (a, b, c) and virus-infected mice at post-infection day 2 (d, e, f).

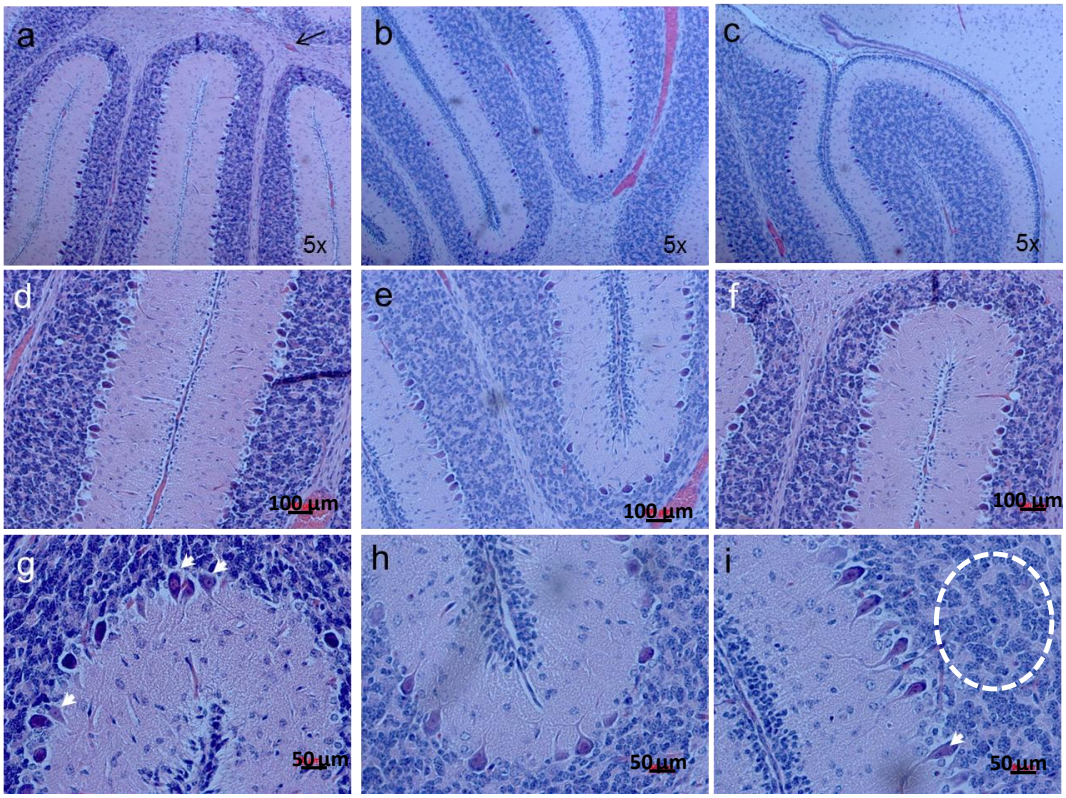

Figure 5.25| B**rain sections stained with haematoxylin and eosin from mice inoculated with 1000 pfu of rCVeGFP**
5µM sections were prepared and processed in paraffin. Representative photomicrographs showing regions of the cerebellum from virus-infected mice at post-infection day 3. Pyknotic nuclei and neurones with central chromatolysis are indicated with white arrowheads and a perivascular cuff by an arrow. An area containing large scale cell death is indicated by a dashed line.

5.3.7. Brain cell types infected with rCVeGFP following intraperitoneal inoculation of mice with the virus

Brains from suckling mice injected with 1000 pfu CVeGFP via the intraperitoneal route (section 5.3.6) and sacrificed at day 5 post-infection were removed and divided along the midsagittal plane. One half of each brain was used to determine the titre of virus present in the brain at each stage of infection (section 5.3.6.3). The other half was fixed in 4% paraformaldehyde in PBS, paraffin embedded and sagittal sections prepared by collaborators at the Pirbright Institute. The tissue sections were studied using immunohistochemistry to detect GFP present in recombinant CVeGFP and/or

brain cell-specific markers. This was carried out for comparison with the data from the *ex vivo* slice cultures (section 5.2), which if gave comparable results would indicate that cerebellar slice cultures provide a suitable model with which to study CHPV pathogenesis. In addition, this approach allowed the sites of CHPV infection throughout the mouse brain to be studied, rather than the analysis being limited to the cerebellum.

The saggital sections were stained with anti-GFP (counterstained with a secondary antibody coupled to green Alexa Fluor® 488) and an antibody against one of the following brain cell specific markers: GABA-A receptor α 6, MAP2, NeuN, calbindin, CD11b, cc1, GFAP (counterstained with a secondary antibody conjugated to a red Alexa Fluor® either 568 or 594). The results are shown in Figure 5.26. Consistent with the histopathological examination virus-infected cells were predominantly restricted to the cerebellum (Figure 5.26 a-g), though low levels of GFP expression were found in the hippocampus in some of the samples with high virus titres (Figure 5.26 h). In the cerebellum, approximately 65% of cells were positive for both GFP and the granule cell marker protein GABA-A receptor α 6 (Figure 5.26 a). This is in contrast with the results from the *ex vivo* analysis of cerebellar slice cultures infected with rCVeGFP which found that approximately only 1% of virus-infected cells co-localised with those stained with the granule cell specific antibody (Figure 5.4). However, it was noted during the analysis that morphologically rCVeGFP-infected cells were similar to granule cells and that they were localised to the granule cell layers (Figure 5.3).

Approximately 1% of virus-infected cells co-localised with the two other neurone-specific antibodies anti-MAP2 and anti-NeuN, which are specific for neurone-restricted progenitors and differentiated post-mitotic neuronal cells, respectively

(Figure 5.26 b, c). No evidence of rCVeGFP infection of purkinje neurones was observed, as demonstrated by the absence of co-localisation in Figure 5.26 d. A small number of GFAP-immunoreactive astrocytes (Figure 5.26 g) and cc1-positive mature oligodendrocytes (Figure 5.26 f) were infected with virus, demonstrating that these cells are also permissive to CHPV infection, although are infrequently infected. In addition, approximately 15% of virus-infected cells were microglia (as shown by dual GFP and CD11b positivity) (Figure 5.26 e).

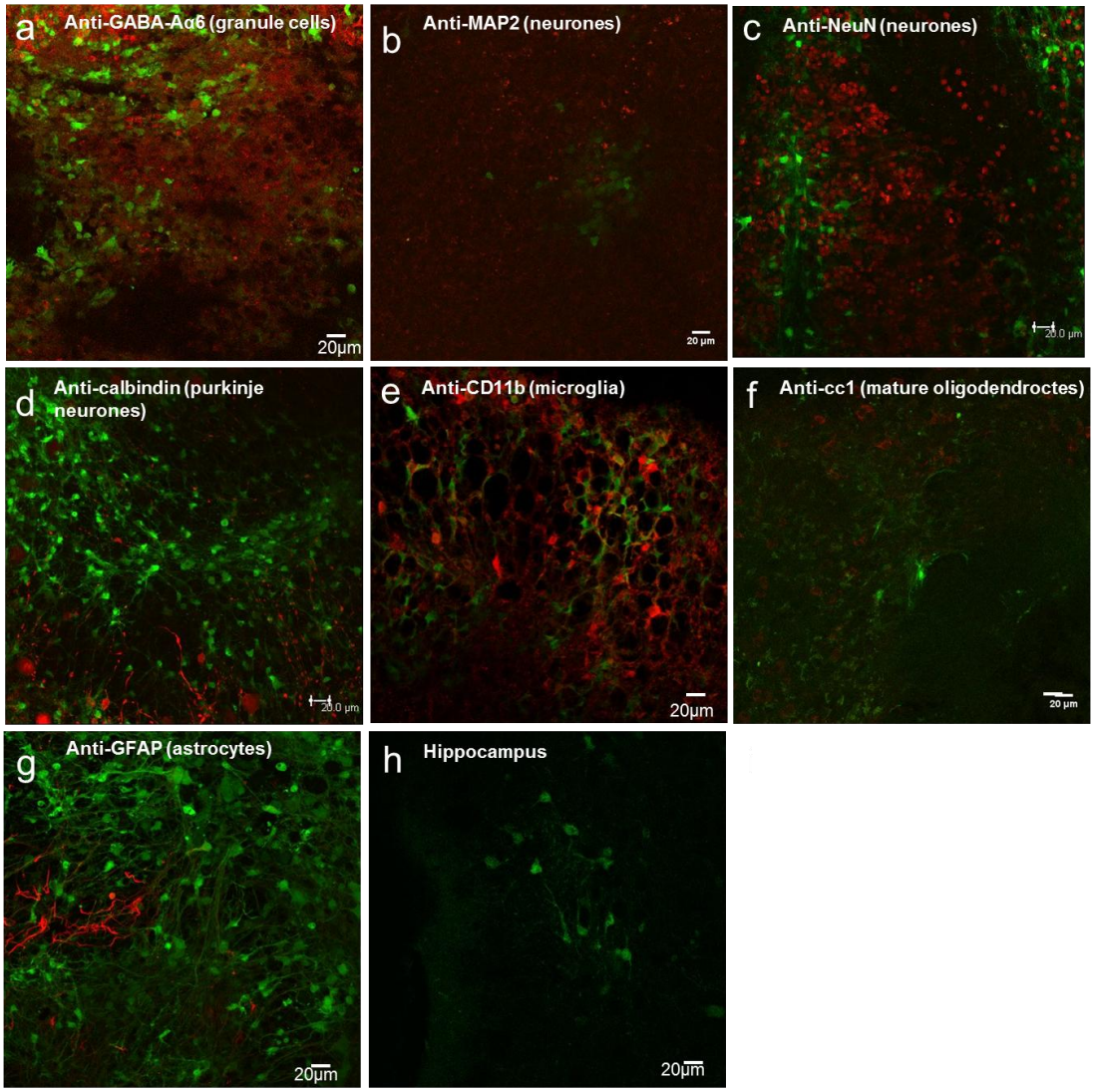

Figure 5.26| **Confocal micrographs of brain sections from mice infected with rCVeGFP and stained for brain cell-specific marker proteins**

Images are of the cerebellum (a-g) and the hippocampus (h). CVeGFP-infected cells stained with anti-GFP and a secondary green alexa antibody and cell marker proteins were stained with either anti-GABA-A receptor α6 (a), anti-MAP2 (b), anti-neuN (c), anti-calbindin (d), anti-CD11b (e), anti-cc1 (f), or anti-GFAP (g) primary antibodies followed by a red alexa secondary antibody. Panel H shows GFP-expressing cells in the hippocampus. Fluorescence was visualised using a Leica SP5 confocal fluorescence microscope. Scale bar shown.

5.4 The effect of *tdCE* point mutations on the pathogenesis of infection

The three temperature-dependent host range mutants (*td*CE) of CHPV characterised in this study contain a single point mutation in the gene encoding the L protein which severely inhibits their growth at 39°C in primary avian cells (but not at 31°C or at either temperature in mammalian cells). The objective was to determine whether these mutations have a direct effect on the pathogenesis of CHPV *in vivo*.

Groups of 6 ICR CD1 mice (8 days old) were intraperitoneally inoculated with *td*CE rCV 112 ($C_{7217} \rightarrow U$) and rCV 157 ($G_{9735} \rightarrow U$) at a dose of 50 and 1000 pfu per mouse. Only two of the three *td*CE mutant viruses were used to limit the number of animals required in experiments. None of the mice became unwell or showed symptoms of CHPV-induced encephalitis following infection with 50 or 1000 pfu of either virus (Figure 3.27 a, b, d, e). When the dose of rCV 112 ($C_{7217} \rightarrow U$) was increased to 5000 pfu 2 out of 6 mice developed disease with the first symptoms observed on day 5 post-infection and paralysis of two limbs on day 7 post-infection. Therefore, there was a 2-day delay in the onset of symptoms and a 2-day delay in the progression of disease to the experimental endpoint compared with the wild-type control virus (rCHPV). Furthermore, this dose was 5-fold higher than the dose of rCHPV which induced disease. In line with the clinical assessment, the group weight of the rCV 112 ($C_{7217} \rightarrow U$) -infected mice decreased at day 5 post-infection in comparison with the uninfected group. These results indicate that the host range mutations substantially attenuate (but do not prevent) the pathogenesis of CHPV in mice.

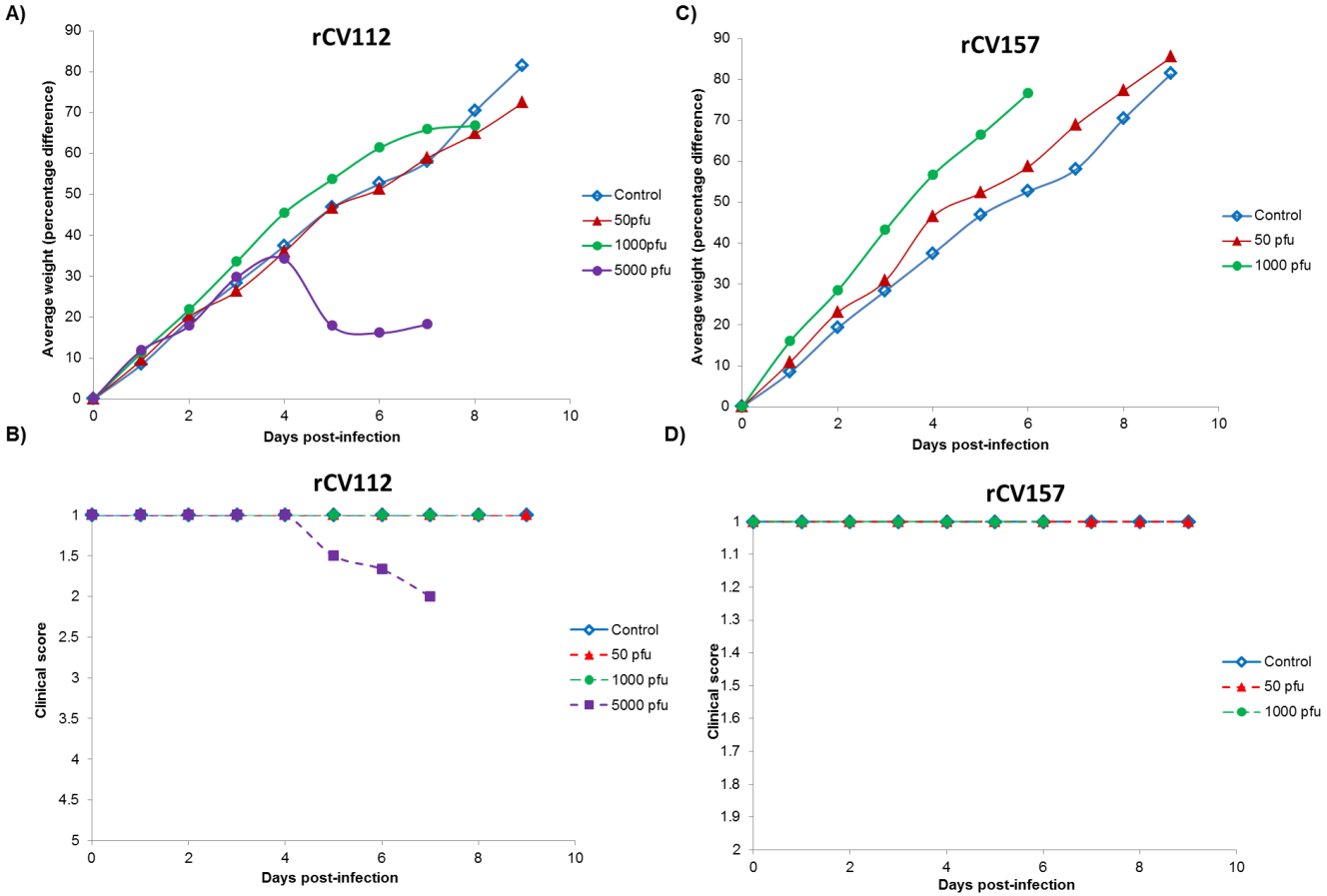

Figure 5.27 **Progress of *td*CE mutant virus infection at different doses**

Groups of six mice were inoculated intraperitoneally with either 50 pfu, 1000 pfu or 5000 pfu of rCV 112 ($C_{7217} \rightarrow U$) (A,B), rCV 157 ($G_{9735} \rightarrow U$) (C,D) or PBS (shown in blue). For each dose the progress of disease is shown as the collective average weight (calculated as the percentage difference compared to day 0) (A, C) and the average clinical score (B, D).

5.5 Discussion

Experimental infection of young mice with CHPV produces a fatal neurological disease (Jortner *et al.*, 1973) and there have been a number of outbreaks of CHPV-induced neurological disease, referred to as encephalitis, in humans between 9 months and 16 years old (Chadha *et al.*, 2005; Gurav *et al.*, 2010; Tandale *et al.*, 2008). Early studies in mice showed that the virus is able to cross the blood brain barrier to infect the CNS (after intraperitoneal or intravenous administration) resulting in a dose-dependent encephalitis by haematogenous spread in suckling mice but not in adults (Balakrishnan & Mishra, 2008; Jortner *et al.*, 1973). The data presented here support these findings. Intraperitoneal inoculation of 8 day old ICR (CD1) mice with 50 pfu of CHPV strain I653514, which was also used in the early studies in mice, was shown to induce neurological disease. The first symptoms of CHPV disease were typically uncoordinated movements and unilateral paralysis of the hind limb nearest the injection site and weight loss at day 2 post-infection. Paralysis progressed rapidly and paralysis of two limbs (usually bilateral hind limb paralysis) and a further reduction in weight occurred at day 3 post-infection. Initial studies found that forelimb paralysis occurred in the final stages of disease after which the mice succumbed to infection (Jortner *et al.*, 1973). Paralysis of two limbs was taken as the humane end point used in this study. The collective weight of the virus-infected group was shown to be significantly lower than the uninfected group on day 2 and 3 post-infection (one tailed unpaired Student's t-test, $p \leq 0.05$).

There was a 392-fold and 10 million-fold increase in viral titre in the brains of CHPV-infected mice at day 1 and 2 post-infection respectively, compared to the initial inoculum. Virus was not detected in the lungs or liver of infected animals

(Table 5.2). This contrasts with previous research which detected the presence of low levels of virus in the blood, skeletal muscle, liver, lung and spleen and subsequently at high titres in the brain (Jortner *et al.*, 1973) which was taken to indicate that peripheral infection of CHPV in suckling mice induces viraemia and haematogenous spread ensures the dissemination of virus throughout the body. One study demonstrated the rapid generation of anti-CHPV IgM antibodies upon experimental peripheral infection of young mice which may reduce viral titres present in the blood and other organs (Balakrishnan & Mishra, 2008). A recent study detected rising levels of CHPV RNA in nervous tissue progressively further away from the site of inoculation during the course of infection indicating that CHPV may also spread from the peripheral nerves to the brain via axonal transport (Anukumar *et al.*, 2013). Infection of mice with the Alphavirus Semliki Forest virus (SFV) (family *Togaviridae*), a positive sense single stranded RNA virus, is a well-established model to study the pathogenesis of viral encephalitis (Fazakerley, 2004). While SFV and CHPV have considerably different molecular organisations and replicative cycles they are similar in the disease they induce. When inoculated in the periphery SFV causes transient plasma viraemia and once in the circulation SFV is able to invade the CNS through cerebral endothelial cells and replicate, initially at perivascular foci (Fazakerley, 2004). A similar process has been proposed for CHPV infection.

CHPV-induced encephalitis in adult mice is only achieved by direct intracranial injection (Sokhei & Obukhova, 1984). The mechanism of age-dependent susceptibility of CHPV disease has not been clarified, however, important contributory factors are likely to include an immature host immune response and immature nervous system in young mice (Balakrishnan & Mishra, 2008). A range of

other neurotropic viruses have also been shown to produce age-related CNS disease including Japanese encephalitis (JE), Yellow fever, St Louis encephalitis, West Nile, Sindbis, measles, Semliki Forest and herpes viruses (Oliver & Fazakerley, 1998). Different strains of SFV exhibit different levels of virulence and the disease outcome is often strongly age related. Intraperitoneal inoculation of mice with the L10 strain of SFV results in panencephalitis, regardless of the age of the mice. On the other hand, although SFV strain A7(74) is able to initiate infection at perivascular foci in all mice, dissemination of virus infection throughout the brain and thus fatal encephalitis is only achieved in mice aged 11 days old or less on the day of inoculation (Oliver & Fazakerley, 1998). This is irrespective of the route of virus administration and therefore the same is true following intracerebral inoculation of the virus. Restriction of SFV strain A7(74) replication in the CNS of adult mice is not a result of a maturing immune system because virus infection in nude (athymic, without T lymphocytes) and SCID (severe combined immunodeficiency, impaired in their ability to produce B and T cells) mice remains localised (Fazakerley *et al.*, 1993). However, a subclinical, persistent SFV infection ensues in mice deficient in T-lymphocytes. The data suggest that the age-dependent nature of SFV strain A7(74) virulence is a product of neuron maturity with mature neurons unable to support productive infection and induce apoptosis to facilitate the dissemination of virus progeny to adjacent cells (Fazakerley *et al.*, 1993). The underlying molecular basis for the restriction of SFV strain A7(74) in mature neurones has not been characterised. The age-related pattern of disease associated with CHPV infection may involve one or more of these factors and remains to be explored.

A number of studies have used *ex vivo* cultures of brain tissue to investigate viral tropism (Braun *et al.*, 2006; Dionne *et al.*, 2011; Friedl *et al.*, 2004; Tsutsui *et al.*, 2002), balancing a need for normal tissue architecture and physiological proportions of brain cell types while minimising the number of *in vivo* experiments conducted. This study is the first example of *ex vivo* cultures of brain tissue used to investigate the cellular tropism of a vesiculovirus. Using a recombinant virus rCVeGFP which expressed the eGFP reporter protein cerebellar slice cultures were demonstrated to support CHPV replication with GFP expression first visible approximately 6 hours post-infection.

Analysis of the cerebellar slices by confocal fluorescence microscopy, fixed at 12 hours post-infection demonstrated that a large proportion (approximately 80%) of rCVeGFP-infected cells were neuron-restricted progenitor cells, as shown by the high level of co-localisation of virus-infected and MAP-2-positive cells in Figure 5.4 a, b. Strikingly, cells positive for both neuN, a marker protein specific for differentiated post-mitotic neurones, and virus were not observed at this time point (Figure 5.4 c, d). Analysis of rCVeGFP-infected cerebellar slices fixed at 24 hours post-infection showed a slight reduction in the number of virus-infected neurone-restricted progenitor (MAP-2-positive) cells (Figure 5.7). In contrast to at 12 hours post-infection, a small proportion of mature neurones, as determined by NeuN and βIII-tubulin positivity were infected with virus at 24 hours post-infection. However, only approximately 1% of CHPV-infected cells in the cerebellum were MAP2 or NeuN positive in brain samples following *in vivo* CHPV infection (Figure 5.26 b, c). No evidence for CHPV infection of purkinje neurones was demonstrated by immunohistochemistry in the *ex vivo* samples, though there was evidence of damage to these cells detected in the *in vivo* analysis described below.

Using an anti-MBP antibody to highlight the cerebellum structure, virus infected cells from *ex vivo* infection were shown to be present in large numbers in the granule layers of the cerebellum. Small neurones called granule cells are abundant in these regions of the tissue and the rCVeGFP-infected cells have similar morphologies to this type of neurone. During *in vivo* infection of rCVeCHPV, approximately 65% of virus infected cells in the cerebellum were shown to be granule cells (Figure 5.26 a). This is in contrast with the results from the *ex vivo* analysis of cerebellar slice cultures infected with rCVeGFP which found limited co-localisation of virus infected and GABA-A receptor α6 (granule cell specific marker protein)-positive cells (Figure 5.3), although there have been reports that the GABA-A receptor α6 subunit is only expressed on cerebellar granule cells at approximately post-natal day 14 (Dr D. Fulton personal communication). The brain samples from the *in vivo* infections were from slightly older mice (11 days old) than the slices used in the *ex vivo* analysis (7 days old), which may be an important factor regarding the detection of granule cells by this antibody and therefore may explain the differences in the numbers of granule cells shown to be infected with virus by the two methodologies. Thus, infection of granule cells cannot be discounted on the basis of the *ex vivo* results.

While CHPV infection of microglia was not demonstrated at 12 hours post-infection of cerebellar slice cultures, 15% of virus-infected cells expressed the microglia specific protein at 24 hours post-infection (Figure 5.10). Moreover, 15% of virus-infected cells were shown to be microglia in brain samples from CHPV-infected mice (Figure 5.26 e). Infection of microglia with a number of viruses including HIV-1 (Wang *et al.*, 2008) and herpes simplex virus 1 (Lokensgard *et al.*, 2002) have

been shown to be important contributing factors in the virus-mediated neuropathology.

In rCVeGFP-infected cerebellar slice cultures approximately 1-3% and 5-8% of virus-infected cells were shown to co-localise with immature and mature oligodendrocytes at 12 and 24 hours post-infection respectively (Figure 5.9, 5.10), indicating that while oligodendrocytes are permissive to CHPV replication, infection of these cells occurs infrequently. This is consistent with the analysis of brain slices from infected mice, which found 1-3% of virus-infected cells were oligodendrocytes (Figure 5.26). There was limited evidence for signal overlap between astrocytes and virus-infected cells following *ex vivo* infection of brain tissue, while 1% of virus-infected cells from virus-infected mice were shown to be positive for the astrocyte specific marker protein. Taken together, the results suggest CHPV predominantly infects neurone progenitor cells, granule cells and microglia with only a few fully differentiated neurones, oligodendrocytes and astrocytes infected by the virus.

Pathological analysis of brains from mice infected *in vivo* with CHPV showed pronounced damage to the cerebellum. Signs of virus infection including inflammation, neuronal lesions and regions of complete cell death were first observed at day 2 post-infection and were more pronounced at day 3 post-infection. Small areas of cell death were observed in the hippocampus and cortex at day 3 post-infection. However, samples from uninfected mice used as a control in the analysis were only prepared on post-infection day 3 when the mice were 11 days old. As the developing mouse brain changes very rapidly further control samples from post-infection day 1 and 2 will be necessary to properly assess any virus-induced changes on each day of the timecourse. The pathological process seen by analysis of samples taken from animals infected *in vivo* was consistent with those from the examination

of *ex vivo* tissue sections from rCVeGFP-infected mice which found that virus-infected cells were predominantly restricted to the cerebellum (Figure 5.26 a-g). In samples taken from *in vivo* infections low levels of GFP expression were found in the hippocampus in some of the samples with high virus titres (Figure 5.26 h). A prominent characteristic of SFV-induced disease is the CD8+ T lymphocyte-dependent generation of lesions of demyelination (Fazakerley & Walker, 2003). CHPV has also been shown to cause some demyelination, although lesions in grey matter occurred with increased frequency and severity (Jortner *et al.*, 1973). However no signs of demyelination following infection were observed in this study of CHPV disease. The analysis of the sections detected clear evidence of severe damage to the Purkinje cell layer including cell shrinkage and pyknotic nuclei. This is also the first report of significant damage occurring outside of the cerebellum in CHPV infected mice.

Despite the clear CNS involvement in CHPV disease, cell tropism which underpins many aspects of disease has not been extensively investigated for this virus and neurones are the only brain cell type currently known to be susceptible to infection (Ghosh *et al.*, 2013; Jortner *et al.*, 1973). Viruses can have strict tropisms for specific cell types, for example SFV almost exclusively infects neurones and oligodendrocytes in the CNS (Fazakerley, 2004). SFV infection of astrocytes has not been demonstrated. The CHPV reverse genetics system (Marriott & Hornsey, 2011) provided an opportunity to investigate the site of CHPV infection in the mouse brain and the cell tropism of the virus by permitting the generation of recombinant viruses containing reporter genes including rCVeGFP, which was used in this study. Introduction of large reporter genes can alter virus characteristics. Also, the

pathogenicity of viruses grown in tissue culture can differ substantially from the wild type counterpart, due to the accumulation of point mutations and epigenetic changes. A dose-response analysis showed that 1000 pfu of rCHPV and rCVeGFP induced neurological disease when administered intraperitoneally to 8 day old mice, 20-fold higher than the dose of CHPV strain I653514 shown to induce encephalitis. There was a 2 day delay in the onset of rCVeGFP-induced disease compared with rCHPV, with the first symptoms observed on day 3 and day 5 post-infection, respectively. Also, in contrast with mice infected with rCHPV, which displayed significant weight loss compared to the uninfected control group on days 4 and 5 post-infection, the weight change of mice infected with rCVeGFP remained comparable to the uninfected mice throughout the timecourse. Thus, the addition of the eGFP gene in the genome of CHPV generated a virus with different characteristics *in vivo*. However, the histopathological changes in the brains of rCHPV and rCVeGFP-infected mice were comparable with each other and to CHPV strain I653514, validating their use in the investigation. Importantly, all three viruses produced pathological changes (evidence of inflammation and neuronal damage) which were almost exclusively restricted to the cerebellum.

The temperature-dependent host range mutants (*td*CE) of CHPV are severely impaired in their growth *in vitro* under non-permissive conditions due to single amino acid changes residing in the RNA polymerase protein. These changes were also shown to have marked effects on the assembly of replication complexes. Intraperitoneal inoculation of two of these viruses, namely rCV 112 ($C_{7217} \rightarrow U$) and rCV 157 ($G_{9735} \rightarrow U$) into young mice showed that these viruses have reduced pathogenicity *in vivo* in comparison with the rCHPV. Interestingly, slower disease progression and increased propensity for immune-mediated demyelination was

exhibited by a temperature-sensitive mutant of CHPV (*ts*472) (Dal Canto *et al.*, 1979). This CHPV mutant was also shown to have a reduced capacity for neuronal replication (Dal Canto *et al.*, 1979).

The data presented in this chapter indicate that the site of CHPV-infection in the mouse brain is the cerebellum with immature neurones, granule cells and microglia preferentially infected. However, a broad range of brain cells (both neurones and glial cells including astrocytes and oligodendrocytes) were shown to be permissive to infection with CHPV. In addition, two *td*CE mutants of CHPV exhibited attenuated growth *in vivo*.

CHAPTER 6

Chapter 6: Conclusions and future questions

Viruses are obligate intracellular parasites and the small coding capacity of viruses ensures their dependence on an array of cellular machinery and factors at every stage of their replication cycles. Thus, host range underpins every stage of virus infection. Specific cellular proteins are utilised as receptors and co-receptors to initiate infection and viral entry often involves the hijacking of the endocytic pathway of the cell and the host cytoskeleton. Once inside the cell cellular proteins are required to transport the virus to its favoured site of replication. Virus gene expression and replication itself is dependent on numerous host factors such as helicases, transcription factors, eukaryotic translation initiation factors and proteases. Viruses also interact with a plethora of host factors and signalling pathways to modulate host protein synthesis, the host immune response, apoptosis and the cell cycle to produce a cellular environment conducive to virus replication, enabling the establishment of persistency in the case of some viruses or a timely exit from the cell in the case of others. Host cell proteins such as cellular chaperones and proteases are also frequently exploited by viruses for the assembly and maturation of their particles. Lastly, exit of progeny virions from the host cell ready for dissemination and infection of other hosts is intimately associated with cellular factors. This research explored aspects of the host range of the vesiculovirus Chandipura virus (CHPV).

Temperature-dependent host range (*td*CE) mutants of CHPV are characterised by a severe growth defect under non-permissive conditions; growth in chicken embryo at 39°C (Gadkari & Pringle, 1980; Rasool & Pringle, 1986). However, their growth at 31°C in chicken embryo and at 31°C or 39°C in mammalian cells is unaffected,

growing to titres comparable to the wild type virus. The characterisation of host restricted and conditional host range mutants have proved powerful mechanisms for uncovering aspects of vesiculovirus replication, with several key amino acid residues in the methlytransferase (MTase) domain of the L protein delineated through the study of mutants of VSV Indiana (Grdzelishvili *et al.*, 2005; 2006; Simpson & Obijeski, 1974). The genomes of three *td*CE mutants of CHPV; CH112, CH157 and CH256 were sequenced in this study and compared with the wild type virus. Generation of recombinant viruses containing the identified point mutations using the reverse genetics system of CHPV (Marriott & Hornsey, 2011) demonstrated that a single point mutation within the L gene of each mutant, which resulted in a single coding change in the amino acid sequence of the catalytic component of the virus RNA-dependent RNA polymerase confers the host range phenotype described. The lesions responsible for the host range specificity are located between domains III and IV (CH112 $C_{7217} \rightarrow U$) or within domain IV (CH256 $G_{7694} \rightarrow A$) or VI (CH157 $G_{9735} \rightarrow U$) of the CHPV L gene. Domain VI of the L gene encodes the virus MTase, though the mutant containing a lesion in this domain possesses normal MTase activity (Rasool & Pringle, 1986). This lesion is located in a region of highly invariant amino acids which contain an important binding site for the MTase, the GXGXG motif (Rahmeh *et al.*, 2010).

The role of the *td*CE mutations in giving rise to the conditional host range phenotype is unknown. As the cofactor of the polymerase, the direct binding of the P protein to the L protein is essential for virus replication. A series of recombinant viruses encoding wild type or mutant L proteins and the P/RFP fusion protein were generated to allow visualisation of the replication complexes in cells under

permissive and non-permissive conditions. Analysis of these viruses showed that for each of the three mutants analysed the host range lesions inhibit the formation of large replication complexes in the cytoplasm of host cells in non-permissive conditions. These complexes are postulated to bring together the viral RNA and viral replicative machinery with an array of essential cellular proteins for efficient replication, although their assembly may be host cell mediated (Dinh *et al.*, 2013a). This strongly suggests that the single point mutations lead to an altered L protein that is incapable of forming the replication complex in chick embryo cells at high temperature. The host-range nature of the phenotype suggests that this is due to an altered interaction with a host cell factor found in the chick embryo cells.

As a preliminary step in identifying host cell proteins that interact with the CHPV replication complex a recombinant virus containing a Flag tag at the carboxy terminus of the CHPV L protein was used to infect mammalian and avian cells. 126 mammalian and 25 avian potential CHPV L interacting proteins were identified by immunoprecipitating the L/Flag protein and analysing L/Flag fusion proteins by mass spectrometry. In assessing the roles of the interacting proteins it is important to appreciate that the approach used to identify potential interacting proteins in this study was unable to discriminate between proteins which bind directly to the L protein and those that indirectly interact with L protein via other host factors or viral proteins (N and P). The majority of the proteins identified have cellular functions principally in gene expression (including eukaryotic translation initiation factors, ribosome subunits, hnRNP proteins), cytoskeleton architecture and protein folding (Figure 4.10). Many viruses have been shown to be reliant on the cytoskeleton at various stages in their lifecycles including VSV and RSV which require tubulin and

actin, respectively for their mRNA synthesis (Burke *et al.*, 1998; Heinrich *et al.*, 2010). The data presented here identified actin as a cellular protein which may associate with CHPV L, the first report of actin interacting with a vesiculovirus protein. The intermediate filament protein vimentin was also identified as a possible CHPV L protein partner. Association with, and regulation of, vimentin by the HIV-1 protease (Honer *et al.*, 1991) and VSV M (Lyles & McKenzie, 1997) proteins have previously been demonstrated suggesting that this is a common factor associated with the replication of a range of viruses.

A particularly interesting potential cellular protein interacting with the CHPV L protein was Hsp-90. This protein chaperone is essential for the accurate folding of viral polymerases from diverse virus families including rhabdoviruses (Momose *et al.*, 2002). The VSV N protein has been shown to interact with Hsp90 to ensure L protein stability (Connor *et al.*, 2007) and therefore the identification of Hsp90 in this study may be due to an indirect interaction through the N protein. Hsp70, which triggers an antiviral response against VSV replication through its ability to induce the type 1 interferon response (Kim *et al.*, 2013), was also identified in this analysis.

Several members of the hnRNP family of proteins were identified as possible CHPV L protein partners. While these are nuclear proteins their increased presence in the cytoplasm of VSV-infected cells has been described and hnRNPK and hnRNPU in particular have been shown to play essential roles in VSV infection by regulating an array of cellular proteins with the effect of suppressing apoptosis (Dinh *et al.*, 2013b) and inhibiting host cell mRNA production via an association with leader RNA (Gupta *et al.*, 1998a). hnRNP family members have also been shown to support the

replication of a variety of other viruses including flaviviruses (Hsieh *et al.*, 1998), togaviruses (Burnham *et al.*, 2007), herpesviruses (Gross *et al.*, 2012), caliciviruses (Lopez-Manriquez *et al.*, 2013) and paramyxoviruses (Hino *et al.*, 2013).

To confirm the potential partners involved in CHPV L protein interactions further investigation will be required. Firstly, it will be necessary to perform Western blot analysis of selected cellular proteins in the L/Flag immunoprecipitated samples. An additional control for non-specific binding of proteins to the anti-flag M2 magnetic beads is also required and the experiments will need to be repeated at least three times for quantitative statistical analysis of the mass spectrometry results. Also, it would be of interest to explore whether any of the L interacting proteins are required for CHPV replication and RNAi could be performed to knockdown selected cellular proteins to investigate this. Drugs which affect cytoskeletal arrangement such as nocodazole, colcemid and cytochalasin D could also be utilised to explore the roles of cytoskeletal proteins in CHPV replication. The use of various drugs to inhibit actin assembly enabled a requirement for actin at the internalisation stage of VSV infection to be deduced (Cureton *et al.*, 2009).

The nature of the *td*CE mutant phenotype is suggestive of the involvement of an essential host cell factor(s) and the immunoprecipitation/mass spectrometry approach could be employed to look for differences in the cellular proteins bound to the polymerase proteins during permissive and non-permissive conditions. This would further characterise the *td*CE phenotype. The required immunoprecipitations for this have been carried out although time constraints did not permit the mass spectrometry analysis to be completed. Wild-type and *td*CE mutant P/RFP fusion proteins from

mammalian and avian cells at 31°C and 39°C have also been immunoprecipitated. Mass spectrometry analysis of these samples would further substantiate the findings from the L fusion protein work as the P and L proteins are binding partners.

An interesting facet of CHPV host range is the marked differences in replication of the virus in mammalian versus insect cells. This could also be investigated using the approach outlined above for the characterisation of the *td*CE mutants with pull down experiments in mammalian and insect cells to identify differences in cellular binding partners. It would also be interesting to study the M protein of the virus during infection of mammalian and insect cells, as expression of the M protein alone is cytotoxic to mammalian cells (Blondel *et al.*, 1990) and the CHPV M protein has been shown to inhibit cellular transcription (Taylor *et al.*, 1999). Alteration of the $_{37}$PSAP$_{40}$ motif in the M protein of VSV to four alanines was sufficient to induce cytopathogenicity in the insect cell line C6/36 and attenuate pathogenicity in mice, highlighting the key role of the motif in host range (Irie *et al.*, 2012).

CHPV has been associated with several outbreaks of neurological disease in children and also induces encephalitis in peripherally infected young but not adult mice. This reflects a different aspect of host range specificity in terms of replication in the CNS and neuropathogenesis in young rather than older hosts. An *in vivo* model of CHPV-induced encephalitis was established and used the recombinant virus rCVeGFP (Marriott & Hornsey, 2011) to follow the progress of disease. Peripheral infection of young mice with rCVeGFP induced encephalitis but the onset and progression of disease occurred two days later than infection with rCHPV. GFP expression was found to be predominantly localised to the cerebellum in brain samples from mice

infected with rCVeGFP, implicating the cerebellum as the principle site of CHPV replication in the mouse brain. This was supported by histopathological analysis of brain samples from recombinant wild type CHPV (rCHPV)-infected mice, showing large zones of cell death and neuronal damage which was almost completely restricted to the cerebellum.

To further the neuropathogenesis work, it would be interesting to ascertain whether the attachment protein (G protein) of the virus is responsible for the identified tropism of CHPV. The established HIV-1-based self-inactivating lentiviral vector system (Coleman *et al.*, 2003) was used to generate lentivirus pseudotyped with the CHPV G glycoprotein to investigate this, but due to time limitations the experiments were not carried out. CHPV strains obtained during outbreaks in India contain several point mutations in the G gene raising questions about the effects of these changes on the pathogenicity of the virus which could be tested in the mouse model to further identify virus factors associated with pathogenesis. An important associated question is whether specific genotypes of CHPV are found in different geographical areas which may explain the restriction of disease to specific areas.

Defining and characterising the age-related virulence of CHPV is an important aspect of pathogenesis that remains unexplored. It has been shown that the disease produced by several strains of SFV is strongly linked to the age of the host. The age-dependent virulence of SFV strain A7(74) was shown to be a consequence of neuron maturity with mature neurons unable to support a productive virus infection and induce apoptosis to enable virus spread (Fazakerley *et al.*, 1993). In addition, an intact interferon response is essential for the control and clearance of many viruses

and the role of interferon in CHPV pathogenesis has not yet been established. This could be investigated using IFNAR-1$^{-/-}$ mice which lack the α chain of the interferon receptor. The potential role of the immune system in the age-related pathogenicity of the virus could be explored using a range of adult genetically modified mice, for example severe combined immunodeficiency (SCID), athymic nu/nu, microMT mice to dissect the parts of the immune system involved in the host restriction.

The recombinant rCVeGFP virus was also used to uncover the cellular tropism of the virus following *in vivo* infection of suckling mice and *ex vivo* infection of cerebellar slice cultures. By examining rCVeGFP-infected brain slices following immunohistochemistry using a number of antibodies which are specific for a range of brain cell specific proteins CHPV was shown to predominantly infect immature neurons, granule cells and microglia. A low level of CHPV-infection of mature neurones, astrocytes and oligodendrocytes was also demonstrated. Thus, the data indicate that CHPV infection of immature neurones may be important for the establishment of disease in young animals. Staining rCVeGFP-infected brain samples with an antibody specific for nestin, which is an intermediate filament protein expressed in progenitor cells of the nervous system would help to further define the cellular tropism of CHPV. Interestingly, pathological analysis of brain samples from CHPV-infected mice found evidence of inflammation in the rostral migratory stream in the subventricular zone. Neurogenesis takes place in the subventricular zone and neurons then relocate to other regions of the brain via the rostral migratory stream. Taken together, this data indicates that infection of this region of the brain may be due to a propensity of the virus for infection of immature

neurons. The level of neuronal maturity as a key determinant for virus infection has been previously demonstrated for the A7(74) strain of SFV (Fazakerley *et al.*, 1993).

The CHPV system offers an opportunity to explore the interaction of a vesiculovirus within a host at the cellular and whole animal levels. The data presented here show that it is a tractable system in which the application of reverse genetics can be used to study the role of virus proteins in host range at both levels. The data has shown for the first time that CHPV directly targets specific cells within the developing brains of suckling mice and further work will provide insight into the specific key molecular interactions involved in CHPV neuropathogenesis.

REFERENCES

Ahmed, M. & Lyles, D. S. (1998). Effect of vesicular stomatitis virus matrix protein on transcription directed by host RNA polymerases I, II, and III. *J Virol* **72**, 8413-8419.

Ahmed, M., McKenzie, M. O., Puckett, S., Hojnacki, M., Poliquin, L. & Lyles, D. S. (2003). Ability of the matrix protein of vesicular stomatitis virus to suppress beta interferon gene expression is genetically correlated with the inhibition of host RNA and protein synthesis. *J Virol* **77**, 4646-4657.

Albertini, A. A., Merigoux, C., Libersou, S., Madiona, K., Bressanelli, S., Roche, S., Lepault, J., Melki, R., Vachette, P. & Gaudin, Y. (2012). Characterization of monomeric intermediates during VSV glycoprotein structural transition. *PLoS Pathog* **8**, e1002556.

Aljofan, M. (2013). Hendra and Nipah infection: emerging paramyxoviruses. *Virus Res* **177**, 119-126.

Anukumar, B., Amirthalingam, B. G., Shelke, V. N., Gunjikar, R. & Shewale, P. (2013). Neuro-invasion of Chandipura virus mediates pathogenesis in experimentally infected mice. *Int J Clin Exp Pathol* **6**, 1272-1281.

Anukumar, B. & Shahir, P. (2012). Chandipura Virus infection in mice: the role of toll like receptor 4 in pathogenesis. *BMC Infect Dis* **12**, 125.

Balakrishnan, A. & Mishra, A. C. (2008). Immune response during acute Chandipura viral infection in experimentally infected susceptible mice. *Virol J* **5**, 121.

Banerjee, A. K. (1987). The transcription complex of vesicular stomatitis virus. *Cell* **48**, 363-364.

Baquero, E., Buonocore, L., Rose, J. K., Bressanelli, S., Gaudin, Y. & Albertini, A. A. (2012). Crystallization and preliminary X-ray analysis of Chandipura virus glycoprotein G. *Acta Crystallogr Sect F Struct Biol Cryst Commun* **68**, 1094-1097.

Basak, S., Mondal, A., Polley, S., Mukhopadhyay, S. & Chattopadhyay, D. (2007). Reviewing Chandipura: a vesiculovirus in human epidemics. *Biosci Rep* **27**, 275-298.

Basak, S., Polley, S., Basu, M., Chattopadhyay, D. & Roy, S. (2004). Monomer and dimer of Chandipura virus unphosphorylated P-protein binds leader RNA differently: implications for viral RNA synthesis. *J Mol Biol* **339**, 1089-1101.

Bhatt, P. N. & Rodrigues, F. M. (1967). Chandipura: a new Arbovirus isolated in India from patients with febrile illness. *Indian J Med Res* **55**, 1295-1305.

Bhattacharya, R., Basak, S. & Chattopadhyay, D. J. (2006). Initiation of encapsidation as evidenced by deoxycholate-treated Nucleocapsid protein in the Chandipura virus life cycle. *Virology* **349**, 197-211.

Black, B. L. & Lyles, D. S. (1992). Vesicular stomatitis virus matrix protein inhibits host cell-directed transcription of target genes in vivo. *J Virol* **66**, 4058-4064.

Blondel, D., Harmison, G. G. & Schubert, M. (1990). Role of matrix protein in cytopathogenesis of vesicular stomatitis virus. *J Virol* **64**, 1716-1725.

Bose, S., Mathur, M., Bates, P., Joshi, N. & Banerjee, A. K. (2003). Requirement for cyclophilin A for the replication of vesicular stomatitis virus New Jersey serotype. *J Gen Virol* **84**, 1687-1699.

Braun, E., Zimmerman, T., Hur, T. B., Reinhartz, E., Fellig, Y., Panet, A. & Steiner, I. (2006). Neurotropism of herpes simplex virus type 1 in brain organ cultures. *J Gen Virol* **87**, 2827-2837.

Brown, D. D., Rima, B. K., Allen, I. V., Baron, M. D., Banyard, A. C., Barrett, T. & Duprex, W. P. (2005). Rational attenuation of a morbillivirus by modulating the activity of the RNA-dependent RNA polymerase. *J Virol* **79**, 14330-14338.

Brown, E. L. & Lyles, D. S. (2003). Organization of the vesicular stomatitis virus glycoprotein into membrane microdomains occurs independently of intracellular viral components. *J Virol* **77**, 3985-3992.

Buchholz, U. J., Finke, S. & Conzelmann, K. K. (1999). Generation of bovine respiratory syncytial virus (BRSV) from cDNA: BRSV NS2 is not essential for virus replication in tissue culture, and the human RSV leader region acts as a functional BRSV genome promoter. *J Virol* **73**, 251-259.

Burke, E., Dupuy, L., Wall, C. & Barik, S. (1998). Role of cellular actin in the gene expression and morphogenesis of human respiratory syncytial virus. *Virology* **252**, 137-148.

Burnham, A. J., Gong, L. & Hardy, R. W. (2007). Heterogeneous nuclear ribonuclear protein K interacts with Sindbis virus nonstructural proteins and viral subgenomic mRNA. *Virology* **367**, 212-221.

Burt, F. J., Rolph, M. S., Rulli, N. E., Mahalingam, S. & Heise, M. T. (2012). Chikungunya: a re-emerging virus. *Lancet* **379**, 662-671.

Campbell, R. E., Tour, O., Palmer, A. E., Steinbach, P. A., Baird, G. S., Zacharias, D. A. & Tsien, R. Y. (2002). A monomeric red fluorescent protein. *Proc Natl Acad Sci U S A* **99**, 7877-7882.

Carsillo, T., Traylor, Z., Choi, C., Niewiesk, S. & Oglesbee, M. (2006). hsp72, a host determinant of measles virus neurovirulence. *J Virol* **80**, 11031-11039.

Chadha, M. S., Arankalle, V. A., Jadi, R. S., Joshi, M. V., Thakare, J. P., Mahadev, P. V. & Mishra, A. C. (2005). An outbreak of Chandipura virus encephalitis in the eastern districts of Gujarat state, India. *Am J Trop Med Hyg* **73**, 566-570.

Chattopadhyay, D. & Banerjee, A. K. (1987). Phosphorylation within a specific domain of the phosphoprotein of vesicular stomatitis virus regulates transcription in vitro. *Cell* **49**, 407-414.

Chattopadhyay, D. & Raha, T. (1997). Single serine phosphorylation within the acidic domain of Chandipura virus P protein regulates the transcription in vitro. *Virology* **239**, 11-19.

Chen, Y. J., Chen, Y. H., Chow, L. P., Tsai, Y. H., Chen, P. H., Huang, C. Y., Chen, W. T. & Hwang, L. H. (2010). Heat shock protein 72 is associated with the hepatitis C virus replicase complex and enhances viral RNA replication. *J Biol Chem* **285**, 28183-28190.

Cherian, S. S., Gunjikar, R. S., Banerjee, A., Kumar, S. & Arankalle, V. A. (2012). Whole genomes of Chandipura virus isolates and comparative analysis with other rhabdoviruses. *PLoS One* **7**, e30315.

Clark, G. G., Calisher, C. H., Crabbs, C. L., Canestorp, K. M., Tesh, R. B., Bowen, R. A. & Taylor, D. E. (1988). Malpais spring virus: a new vesiculovirus from mosquitoes collected in New Mexico and evidence of infected indigenous and exotic ungulates. *Am J Trop Med Hyg* **39**, 586-592.

Coleman, J. E., Huentelman, M. J., Kasparov, S., Metcalfe, B. L., Paton, J. F., Katovich, M. J., Semple-Rowland, S. L. & Raizada, M. K. (2003). Efficient large-scale production and concentration of HIV-1-based lentiviral vectors for use in vivo. *Physiol Genomics* **12**, 221-228.

Connor, J. H. & Lyles, D. S. (2002). Vesicular stomatitis virus infection alters the eIF4F translation initiation complex and causes dephosphorylation of the eIF4E binding protein 4E-BP1. *J Virol* **76**, 10177-10187.

Connor, J. H., McKenzie, M. O., Parks, G. D. & Lyles, D. S. (2007). Antiviral activity and RNA polymerase degradation following Hsp90 inhibition in a range of negative strand viruses. *Virology* **362**, 109-119.

Cureton, D. K., Burdeinick-Kerr, R. & Whelan, S. P. (2012). Genetic inactivation of COPI coatomer separately inhibits vesicular stomatitis virus entry and gene expression. *J Virol* **86**, 655-666.

Cureton, D. K., Massol, R. H., Saffarian, S., Kirchhausen, T. L. & Whelan, S. P. (2009). Vesicular stomatitis virus enters cells through vesicles incompletely coated with clathrin that depend upon actin for internalization. *PLoS Pathog* **5**, e1000394.

Dal Canto, M. C., Rabinowitz, S. G. & Johnson, T. C. (1979). Virus-induced demyelination. Production by a viral temperature-sensitive mutant. *J Neurol Sci* **42**, 155-168.

Das, S. C., Nayak, D., Zhou, Y. & Pattnaik, A. K. (2006). Visualization of intracellular transport of vesicular stomatitis virus nucleocapsids in living cells. *J Virol* **80**, 6368-6377.

Das, S. C. & Pattnaik, A. K. (2005). Role of the hypervariable hinge region of phosphoprotein P of vesicular stomatitis virus in viral RNA synthesis and assembly of infectious virus particles. *J Virol* **79**, 8101-8112.

Dietzgen, R. G., Calisher, C. H., Kurath, G., Kuzman, I. V., Rodriguez, L. L., Stone, D. M., Tesh, R. B., Tordo, N., Walker, P. J., Wetzel, T. & Whitfield, A. E. (2011). Family – Rhabdoviridae. *Virus Taxonomy Ninth Report of the International Committee on Taxonomy of Viruses*, 686–713.

Dinh, P. X., Beura, L. K., Das, P. B., Panda, D., Das, A. & Pattnaik, A. K. (2013a). Induction of stress granule-like structures in vesicular stomatitis virus-infected cells. *J Virol* **87**, 372-383.

Dinh, P. X., Beura, L. K., Panda, D., Das, A. & Pattnaik, A. K. (2011). Antagonistic effects of cellular poly(C) binding proteins on vesicular stomatitis virus gene expression. *J Virol* **85**, 9459-9471.

Dinh, P. X., Das, A., Franco, R. & Pattnaik, A. K. (2013b). hnRNP K Supports Vesicular Stomatitis Virus Replication by Regulating Cell Survival and Cellular Gene Expression. *J Virol*.

Dionne, K. R., Leser, J. S., Lorenzen, K. A., Beckham, J. D. & Tyler, K. L. (2011). A brain slice culture model of viral encephalitis reveals an innate CNS cytokine response profile and the therapeutic potential of caspase inhibition. *Exp Neurol* **228**, 222-231.

Duprex, W. P., Collins, F. M. & Rima, B. K. (2002). Modulating the function of the measles virus RNA-dependent RNA polymerase by insertion of green fluorescent protein into the open reading frame. *J Virol* **76**, 7322-7328.

Easton, A. J. & Pringle, C. R. (2011). Order – Mononegavirales. In *Virus Taxonomy Ninth Report of the International Committee on Taxonomy of Viruses* pp. 653–657. Edited by Andrew M.Q. King, Elliot Lefkowitz, M. J. Adams & E. B. Carstens. London: Elsevier Inc.

Engelthaler, D. M., Mosley, D. G., Cheek, J. E., Levy, C. E., Komatsu, K. K., Ettestad, P., Davis, T., Tanda, D. T., Miller, L., Frampton, J. W., Porter, R. & Bryan, R. T. (1999). Climatic and environmental patterns associated with hantavirus pulmonary syndrome, Four Corners region, United States. *Emerg Infect Dis* **5**, 87-94.

Fazakerley, J. K. (2004). Semliki forest virus infection of laboratory mice: a model to study the pathogenesis of viral encephalitis. *Arch Virol Suppl*, 179-190.

Fazakerley, J. K., Pathak, S., Scallan, M., Amor, S. & Dyson, H. (1993). Replication of the A7(74) strain of Semliki Forest virus is restricted in neurons. *Virology* **195**, 627-637.

Fazakerley, J. K. & Walker, R. (2003). Virus demyelination. *J Neurovirol* **9**, 148-164.

Finkelshtein, D., Werman, A., Novick, D., Barak, S. & Rubinstein, M. (2013). LDL receptor and its family members serve as the cellular receptors for vesicular stomatitis virus. *Proc Natl Acad Sci U S A* **110**, 7306-7311.

Fontenille, D., Traore-Lamizana, M., Trouillet, J., Leclerc, A., Mondo, M., Ba, Y., Digoutte, J. P. & Zeller, H. G. (1994). First isolations of arboviruses from phlebotomine sand flies in West Africa. *Am J Trop Med Hyg* **50**, 570-574.

Friedl, G., Hofer, M., Auber, B., Sauder, C., Hausmann, J., Staeheli, P. & Pagenstecher, A. (2004). Borna disease virus multiplication in mouse organotypic slice cultures is site-specifically inhibited by gamma interferon but not by interleukin-12. *J Virol* **78**, 1212-1218.

Gaddy, D. F. & Lyles, D. S. (2005). Vesicular stomatitis viruses expressing wild-type or mutant M proteins activate apoptosis through distinct pathways. *J Virol* **79**, 4170-4179.

Gadkari, D. A. & Pringle, C. R. (1980). Temperature-sensitive mutants of Chandipura virus. II. Phenotypic characteristics of the six complementation groups. *J Virol* **33**, 107-114.

Garten, R. J., Davis, C. T., Russell, C. A., Shu, B., Lindstrom, S., Balish, A., Sessions, W. M., Xu, X., Skepner, E., Deyde, V., Okomo-Adhiambo, M., Gubareva, L., Barnes, J., Smith, C. B., Emery, S. L., Hillman, M. J., Rivailler, P., Smagala, J., de Graaf, M., Burke, D. F., Fouchier, R. A., Pappas, C., Alpuche-Aranda, C. M., Lopez-Gatell, H., Olivera, H., Lopez, I., Myers, C. A., Faix, D., Blair, P. J., Yu, C., Keene, K. M., Dotson, P. D., Jr., Boxrud, D., Sambol, A. R., Abid, S. H., St George, K., Bannerman, T., Moore, A. L., Stringer, D. J., Blevins, P., Demmler-Harrison, G. J., Ginsberg, M., Kriner, P., Waterman, S., Smole, S., Guevara, H. F., Belongia, E. A., Clark, P. A., Beatrice, S. T., Donis, R., Katz, J., Finelli, L., Bridges, C. B., Shaw, M., Jernigan, D. B., Uyeki, T. M., Smith, D. J., Klimov, A. I. & Cox, N. J. (2009). Antigenic and genetic characteristics of swine-origin 2009 A(H1N1) influenza viruses circulating in humans. *Science* **325**, 197-201.

Gaudier, M., Gaudin, Y. & Knossow, M. (2002). Crystal structure of vesicular stomatitis virus matrix protein. *EMBO J* **21**, 2886-2892.

Geevarghese, G., Arankalle, V. A., Jadi, R., Kanojia, P. C., Joshi, M. V. & Mishra, A. C. (2005). Detection of chandipura virus from sand flies in the genus Sergentomyia (Diptera: Phlebotomidae) at Karimnagar District, Andhra Pradesh, India. *J Med Entomol* **42**, 495-496.

Ghosh, S., Dutta, K. & Basu, A. (2013). Chandipura virus induces neuronal death through Fas-mediated extrinsic apoptotic pathway. *J Virol* **87**, 12398-12406.

Graham, R. L., Donaldson, E. F. & Baric, R. S. (2013). A decade after SARS: strategies for controlling emerging coronaviruses. *Nat Rev Microbiol* **11**, 836-848.

Grard, G., Fair, J. N., Lee, D., Slikas, E., Steffen, I., Muyembe, J. J., Sittler, T., Veeraraghavan, N., Ruby, J. G., Wang, C., Makuwa, M., Mulembakani, P., Tesh, R. B., Mazet, J., Rimoin, A. W., Taylor, T., Schneider, B. S., Simmons, G., Delwart, E., Wolfe, N. D., Chiu, C. Y. & Leroy, E. M. (2012). A novel rhabdovirus associated with acute hemorrhagic fever in central Africa. *PLoS Pathog* **8**, e1002924.

Grdzelishvili, V. Z., Smallwood, S., Tower, D., Hall, R. L., Hunt, D. M. & Moyer, S. A. (2005). A single amino acid change in the L-polymerase protein of vesicular stomatitis virus completely abolishes viral mRNA cap methylation. *J Virol* **79**, 7327-7337.

Grdzelishvili, V. Z., Smallwood, S., Tower, D., Hall, R. L., Hunt, D. M. & Moyer, S. A. (2006). Identification of a new region in the vesicular stomatitis virus L polymerase protein which is essential for mRNA cap methylation. *Virology* **350**, 394-405.

Green, T. J. & Luo, M. (2006). Resolution improvement of X-ray diffraction data of crystals of a vesicular stomatitis virus nucleocapsid protein oligomer complexed with RNA. *Acta Crystallogr D Biol Crystallogr* **62**, 498-504.

Green, T. J. & Luo, M. (2009). Structure of the vesicular stomatitis virus nucleocapsid in complex with the nucleocapsid-binding domain of the small polymerase cofactor, P. *Proc Natl Acad Sci U S A* **106**, 11713-11718.

Griffin, D. E. (2010). Emergence and re-emergence of viral diseases of the central nervous system. *Prog Neurobiol* **91**, 95-101.

Gross, H., Hennard, C., Masouris, I., Cassel, C., Barth, S., Stober-Grasser, U., Mamiani, A., Moritz, B., Ostareck, D., Ostareck-Lederer, A., Neuenkirchen, N., Fischer, U., Deng, W., Leonhardt, H., Noessner, E., Kremmer, E. & Grasser, F. A. (2012). Binding of the heterogeneous ribonucleoprotein K (hnRNP K) to the Epstein-Barr virus nuclear antigen 2 (EBNA2) enhances viral LMP2A expression. *PLoS One* **7**, e42106.

Gubler, D. J. (2007). The continuing spread of West Nile virus in the western hemisphere. *Clin Infect Dis* **45**, 1039-1046.

Gupta, A. K., Drazba, J. A. & Banerjee, A. K. (1998a). Specific interaction of heterogeneous nuclear ribonucleoprotein particle U with the leader RNA sequence of vesicular stomatitis virus. *J Virol* **72**, 8532-8540.

Gupta, S., De, B. P., Drazba, J. A. & Banerjee, A. K. (1998b). Involvement of actin microfilaments in the replication of human parainfluenza virus type 3. *J Virol* **72**, 2655-2662.

Gurav, Y. K., Tandale, B. V., Jadi, R. S., Gunjikar, R. S., Tikute, S. S., Jamgaonkar, A. V., Khadse, R. K., Jalgaonkar, S. V., Arankalle, V. A. & Mishra, A. C. (2010). Chandipura virus encephalitis outbreak among children in Nagpur division, Maharashtra, 2007. *Indian J Med Res* **132**, 395-399.

Halpin, K., Young, P. L., Field, H. E. & Mackenzie, J. S. (2000). Isolation of Hendra virus from pteropid bats: a natural reservoir of Hendra virus. *J Gen Virol* **81**, 1927-1932.

Harty, R. N., Paragas, J., Sudol, M. & Palese, P. (1999). A proline-rich motif within the matrix protein of vesicular stomatitis virus and rabies virus interacts with WW domains of cellular proteins: implications for viral budding. *J Virol* **73**, 2921-2929.

Heinrich, B. S., Cureton, D. K., Rahmeh, A. A. & Whelan, S. P. (2010). Protein expression redirects vesicular stomatitis virus RNA synthesis to cytoplasmic inclusions. *PLoS Pathog* **6**, e1000958.

Her, L. S., Lund, E. & Dahlberg, J. E. (1997). Inhibition of Ran guanosine triphosphatase-dependent nuclear transport by the matrix protein of vesicular stomatitis virus. *Science* **276**, 1845-1848.

Hercyk, N., Horikami, S. M. & Moyer, S. A. (1988). The vesicular stomatitis virus L protein possesses the mRNA methyltransferase activities. *Virology* **163**, 222-225.

Hino, K., Sato, H., Sugai, A., Kato, M., Yoneda, M. & Kai, C. (2013). Downregulation of Nipah virus N mRNA occurs through interaction between its 3' untranslated region and hnRNP D. *J Virol* **87**, 6582-6588.

Honer, B., Shoeman, R. L. & Traub, P. (1991). Human immunodeficiency virus type 1 protease microinjected into cultured human skin fibroblasts cleaves vimentin and affects cytoskeletal and nuclear architecture. *J Cell Sci* **100 (Pt 4)**, 799-807.

Horikami, S. M. & Moyer, S. A. (1982). Host range mutants of vesicular stomatitis virus defective in in vitro RNA methylation. *Proc Natl Acad Sci U S A* **79**, 7694-7698.

Hsieh, T. Y., Matsumoto, M., Chou, H. C., Schneider, R., Hwang, S. B., Lee, A. S. & Lai, M. M. (1998). Hepatitis C virus core protein interacts with heterogeneous nuclear ribonucleoprotein K. *J Biol Chem* **273**, 17651-17659.

Igarashi, A. (1978). Isolation of a Singh's Aedes albopictus cell clone sensitive to Dengue and Chikungunya viruses. *J Gen Virol* **40**, 531-544.

Irie, T., Liu, Y., Drolet, B. S., Carnero, E., Garcia-Sastre, A. & Harty, R. N. (2012). Cytopathogenesis of vesicular stomatitis virus is regulated by the PSAP motif of M protein in a species-dependent manner. *Viruses* **4**, 1605-1618.

Jadi, R. S., Sudeep, A. B., Kumar, S., Arankalle, V. A. & Mishra, A. C. (2010). Chandipura virus growth kinetics in vertebrate cell lines, insect cell lines & embryonated eggs. *Indian J Med Res* **132**, 155-159.

Jayakar, H. R., Murti, K. G. & Whitt, M. A. (2000). Mutations in the PPPY motif of vesicular stomatitis virus matrix protein reduce virus budding by inhibiting a late step in virion release. *J Virol* **74**, 9818-9827.

Johannsdottir, H. K., Mancini, R., Kartenbeck, J., Amato, L. & Helenius, A. (2009). Host cell factors and functions involved in vesicular stomatitis virus entry. *J Virol* **83**, 440-453.

John, T. (2010). Chandipura virus - what we know & do not know. *Indian J Med Res* **132**, 125-127.

Jortner, B. S., Bhatt, P. N. & Solitare, G. B. (1973). Experimental Chandipura virus infection in mice. I. Virus assay and light microscopic studies with emphasis on neuropathologic observations. *Acta Neuropathol* **23**, 320-325.

Joshi, M. V., Patil, D. R., Tupe, C. D., Umarani, U. B., Ayachit, V. M., Geevarghese, G. & Mishra, A. C. (2005). Incidence of neutralizing antibodies to Chandipura virus in domestic animals from Karimnagar and Warangal Districts of Andhra Pradesh, India. *Acta Virol* **49**, 69-71.

Joshi, R., Kalantri, S. P., Reingold, A. & Colford, J. M., Jr. (2012). Changing landscape of acute encephalitis syndrome in India: a systematic review. *Natl Med J India* **25**, 212-220.

Kim, M. Y., Ma, Y., Zhang, Y., Li, J., Shu, Y. & Oglesbee, M. (2013). hsp70-Dependent Antiviral Immunity against Cytopathic Neuronal Infection by Vesicular Stomatitis Virus. *J Virol* **87**, 10668-10678.

Kurilla, M. G. & Keene, J. D. (1983). The leader RNA of vesicular stomatitis virus is bound by a cellular protein reactive with anti-La lupus antibodies. *Cell* **34**, 837-845.

Le Blanc, I., Luyet, P. P., Pons, V., Ferguson, C., Emans, N., Petiot, A., Mayran, N., Demaurex, N., Faure, J., Sadoul, R., Parton, R. G. & Gruenberg, J. (2005). Endosome-to-cytosol transport of viral nucleocapsids. *Nat Cell Biol* **7**, 653-664.

Leroy, E. M., Kumulungui, B., Pourrut, X., Rouquet, P., Hassanin, A., Yaba, P., Delicat, A., Paweska, J. T., Gonzalez, J. P. & Swanepoel, R. (2005). Fruit bats as reservoirs of Ebola virus. *Nature* **438**, 575-576.

Leyrat, C., Schneider, R., Ribeiro, E. A., Jr., Yabukarski, F., Yao, M., Gerard, F. C., Jensen, M. R., Ruigrok, R. W., Blackledge, M. & Jamin, M. (2012). Ensemble structure of the modular and flexible full-length vesicular stomatitis virus phosphoprotein. *J Mol Biol* **423**, 182-197.

Li, F., Li, W., Farzan, M. & Harrison, S. C. (2005a). Structure of SARS coronavirus spike receptor-binding domain complexed with receptor. *Science* **309**, 1864-1868.

Li, G., Zhang, J., Tong, X., Liu, W. & Ye, X. (2011). Heat shock protein 70 inhibits the activity of Influenza A virus ribonucleoprotein and blocks the replication of virus in vitro and in vivo. *PLoS One* **6**, e16546.

Li, J., Rahmeh, A., Brusic, V. & Whelan, S. P. (2009). Opposing effects of inhibiting cap addition and cap methylation on polyadenylation during vesicular stomatitis virus mRNA synthesis. *J Virol* **83**, 1930-1940.

Li, J., Rahmeh, A., Morelli, M. & Whelan, S. P. (2008). A conserved motif in region v of the large polymerase proteins of nonsegmented negative-sense RNA viruses that is essential for mRNA capping. *J Virol* **82**, 775-784.

Li, J., Wang, J. T. & Whelan, S. P. (2006). A unique strategy for mRNA cap methylation used by vesicular stomatitis virus. *Proc Natl Acad Sci U S A* **103**, 8493-8498.

Li, W., Shi, Z., Yu, M., Ren, W., Smith, C., Epstein, J. H., Wang, H., Crameri, G., Hu, Z., Zhang, H., Zhang, J., McEachern, J., Field, H., Daszak, P., Eaton, B. T., Zhang, S. & Wang, L. F. (2005b). Bats are natural reservoirs of SARS-like coronaviruses. *Science* **310**, 676-679.

Lokensgard, J. R., Cheeran, M. C., Hu, S., Gekker, G. & Peterson, P. K. (2002). Glial cell responses to herpesvirus infections: role in defense and immunopathogenesis. *J Infect Dis* **186 Suppl 2**, S171-179.

Lopez-Manriquez, E., Vashist, S., Urena, L., Goodfellow, I., Chavez, P., Mora-Heredia, J. E., Cancio-Lonches, C., Garrido, E. & Gutierrez-Escolano, A. L. (2013). Norovirus genome circularization and efficient replication are facilitated by binding of PCBP2 and hnRNP A1. *J Virol* **87**, 11371-11387.

Lyles, D. S. & McKenzie, M. O. (1997). Activity of vesicular stomatitis virus M protein mutants in cell rounding is correlated with the ability to inhibit host gene expression and is not correlated with virus assembly function. *Virology* **229**, 77-89.

Lyles, D. S., Puddington, L. & McCreedy, B. J., Jr. (1988). Vesicular stomatitis virus M protein in the nuclei of infected cells. *J Virol* **62**, 4387-4392.

Mackenzie, J. S. & Jeggo, M. (2013). Reservoirs and vectors of emerging viruses. *Curr Opin Virol* **3**, 170-179.

Macneil, A., Nichol, S. T. & Spiropoulou, C. F. (2011). Hantavirus pulmonary syndrome. *Virus Res* **162**, 138-147.

MacNeil, A. & Rollin, P. E. (2012). Ebola and Marburg hemorrhagic fevers: neglected tropical diseases? *PLoS Negl Trop Dis* **6**, e1546.

Majumdar, A., Bhattacharya, R., Basak, S., Shaila, M. S., Chattopadhyay, D. & Roy, S. (2004). P-protein of Chandipura virus is an N-protein-specific chaperone that acts at the nucleation stage. *Biochemistry* **43**, 2863-2870.

Marriott, A. C. (2005). Complete genome sequences of Chandipura and Isfahan vesiculoviruses. *Arch Virol* **150**, 671-680.

Marriott, A. C. & Hornsey, C. A. (2011). Reverse genetics system for Chandipura virus: tagging the viral matrix protein with green fluorescent protein. *Virus Res* **160**, 166-172.

Masters, P. S., Bhella, R. S., Butcher, M., Patel, B., Ghosh, H. P. & Banerjee, A. K. (1989). Structure and expression of the glycoprotein gene of Chandipura virus. *Virology* **171**, 285-290.

Mavale, M. S., Fulmali, P. V., Geevarghese, G., Arankalle, V. A., Ghodke, Y. S., Kanojia, P. C. & Mishra, A. C. (2006). Venereal transmission of Chandipura virus by Phlebotomus papatasi (Scopoli). *Am J Trop Med Hyg* **75**, 1151-1152.

Mavale, M. S., Fulmali, P. V., Ghodke, Y. S., Mishra, A. C., Kanojia, P. & Geevarghese, G. (2007). Experimental transmission of Chandipura virus by Phlebotomus argentipes (diptera: psychodidae). *Am J Trop Med Hyg* **76**, 307-309.

Mavale, M. S., Geevarghese, G., Ghodke, Y. S., Fulmali, P. V., Singh, A. & Mishra, A. C. (2005). Vertical and venereal transmission of Chandipura virus (Rhabdoviridae) by Aedes aegypti (Diptera: Culicidae). *J Med Entomol* **42**, 909-911.

Melki, R., Gaudin, Y. & Blondel, D. (1994). Interaction between tubulin and the viral matrix protein of vesicular stomatitis virus: possible implications in the viral cytopathic effect. *Virology* **202**, 339-347.

Miller, M. S. & Hertel, L. (2009). Onset of human cytomegalovirus replication in fibroblasts requires the presence of an intact vimentin cytoskeleton. *J Virol* **83**, 7015-7028.

Misra, U. K. & Kalita, J. (2010). Overview: Japanese encephalitis. *Prog Neurobiol* **91**, 108-120.

Momose, F., Naito, T., Yano, K., Sugimoto, S., Morikawa, Y. & Nagata, K. (2002). Identification of Hsp90 as a stimulatory host factor involved in influenza virus RNA synthesis. *J Biol Chem* **277**, 45306-45314.

Moncorge, O., Long, J. S., Cauldwell, A. V., Zhou, H., Lycett, S. J. & Barclay, W. S. (2013). Investigation of influenza virus polymerase activity in pig cells. *J Virol* **87**, 384-394.

Mondal, A., Bhattacharya, R., Ganguly, T., Mukhopadhyay, S., Basu, A., Basak, S. & Chattopadhyay, D. (2010). Elucidation of functional domains of Chandipura virus Nucleocapsid protein involved in oligomerization and RNA binding: implication in viral genome encapsidation. *Virology* **407**, 33-42.

Mondal, A., Roy, A., Sarkar, S., Mukherjee, J., Ganguly, T. & Chattopadhyay, D. (2012). Interaction of chandipura virus N and P proteins: identification of

two mutually exclusive domains of N involved in interaction with P. *PLoS One* **7**, e34623.

Morin, B., Rahmeh, A. A. & Whelan, S. P. (2012). Mechanism of RNA synthesis initiation by the vesicular stomatitis virus polymerase. *EMBO J* **31**, 1320-1329.

Moyer, S. A., Baker, S. C. & Lessard, J. L. (1986). Tubulin: a factor necessary for the synthesis of both Sendai virus and vesicular stomatitis virus RNAs. *Proc Natl Acad Sci U S A* **83**, 5405-5409.

Mukhopadhyay, S., Maity, S. S., Roy, A., Chattopadhyay, D., Ghosh, K. S., Dasgupta, S. & Ghosh, S. (2010). Characterization of the structure of the phosphoprotein of Chandipura virus, a negative stranded RNA virus probing intratryptophan energy transfer using single and double tryptophan mutants. *Biochimie* **92**, 136-146.

Muller, R., Poch, O., Delarue, M., Bishop, D. H. & Bouloy, M. (1994). Rift Valley fever virus L segment: correction of the sequence and possible functional role of newly identified regions conserved in RNA-dependent polymerases. *J Gen Virol* **75 (Pt 6)**, 1345-1352.

Nedergaard, M., Ransom, B. & Goldman, S. A. (2003). New roles for astrocytes: redefining the functional architecture of the brain. *Trends Neurosci* **26**, 523-530.

Newcomb, W. W. & Brown, J. C. (1981). Role of the vesicular stomatitis virus matrix protein in maintaining the viral nucleocapsid in the condensed form found in native virions. *J Virol* **39**, 295-299.

Ogden, J. R., Pal, R. & Wagner, R. R. (1986). Mapping regions of the matrix protein of vesicular stomatitis virus which bind to ribonucleocapsids, liposomes, and monoclonal antibodies. *J Virol* **58**, 860-868.

Ogino, T. & Banerjee, A. K. (2007). Unconventional mechanism of mRNA capping by the RNA-dependent RNA polymerase of vesicular stomatitis virus. *Mol Cell* **25**, 85-97.

Ogino, T. & Banerjee, A. K. (2010). The HR motif in the RNA-dependent RNA polymerase L protein of Chandipura virus is required for unconventional mRNA-capping activity. *J Gen Virol* **91**, 1311-1314.

Ogino, T., Yadav, S. P. & Banerjee, A. K. (2010). Histidine-mediated RNA transfer to GDP for unique mRNA capping by vesicular stomatitis virus RNA polymerase. *Proc Natl Acad Sci U S A* **107**, 3463-3468.

Oliver, K. R. & Fazakerley, J. K. (1998). Transneuronal spread of Semliki Forest virus in the developing mouse olfactory system is determined by neuronal maturity. *Neuroscience* **82**, 867-877.

Paek, K. Y., Kim, C. S., Park, S. M., Kim, J. H. & Jang, S. K. (2008). RNA-binding protein hnRNP D modulates internal ribosome entry site-dependent translation of hepatitis C virus RNA. *J Virol* **82**, 12082-12093.

Panda, D., Das, A., Dinh, P. X., Subramaniam, S., Nayak, D., Barrows, N. J., Pearson, J. L., Thompson, J., Kelly, D. L., Ladunga, I. & Pattnaik, A. K. (2011). RNAi screening reveals requirement for host cell secretory pathway in infection by diverse families of negative-strand RNA viruses. *Proc Natl Acad Sci U S A* **108**, 19036-19041.

Peiris, J. S., Dittus, W. P. & Ratnayake, C. B. (1993). Seroepidemiology of dengue and other arboviruses in a natural population of toque macaques (Macaca sinica) at Polonnaruwa, Sri Lanka. *J Med Primatol* **22**, 240-245.

Perez, A. M., Pauszek, S. J., Jimenez, D., Kelley, W. N., Whedbee, Z. & Rodriguez, L. L. (2010). Spatial and phylogenetic analysis of vesicular stomatitis virus over-wintering in the United States. *Prev Vet Med* **93**, 258-264.

Petersen, J. M., Her, L. S. & Dahlberg, J. E. (2001). Multiple vesiculoviral matrix proteins inhibit both nuclear export and import. *Proc Natl Acad Sci U S A* **98**, 8590-8595.

Pettit Kneller, E. L., Connor, J. H. & Lyles, D. S. (2009). hnRNPs Relocalize to the cytoplasm following infection with vesicular stomatitis virus. *J Virol* **83**, 770-780.

Poch, O., Blumberg, B. M., Bougueleret, L. & Tordo, N. (1990). Sequence comparison of five polymerases (L proteins) of unsegmented negative-strand RNA viruses: theoretical assignment of functional domains. *J Gen Virol* **71 (Pt 5)**, 1153-1162.

Potharaju, N. R. & Potharaju, A. K. (2006). Is Chandipura virus an emerging human pathogen? *Arch Dis Child* **91**, 279-280.

Pringle, C. R. (1978). The tdCE and hrCE phenotypes: host range mutants of vesicular stomatitis virus in which polymerase function is affected. *Cell* **15**, 597-606.

Rahmeh, A. A., Li, J., Kranzusch, P. J. & Whelan, S. P. (2009). Ribose 2'-O methylation of the vesicular stomatitis virus mRNA cap precedes and facilitates subsequent guanine-N-7 methylation by the large polymerase protein. *J Virol* **83**, 11043-11050.

Rahmeh, A. A., Morin, B., Schenk, A. D., Liang, B., Heinrich, B. S., Brusic, V., Walz, T. & Whelan, S. P. (2012). Critical phosphoprotein elements that regulate polymerase architecture and function in vesicular stomatitis virus. *Proc Natl Acad Sci U S A* **109**, 14628-14633.

Rahmeh, A. A., Schenk, A. D., Danek, E. I., Kranzusch, P. J., Liang, B., Walz, T. & Whelan, S. P. (2010). Molecular architecture of the vesicular stomatitis virus RNA polymerase. *Proc Natl Acad Sci U S A* **107**, 20075-20080.

Rainwater-Lovett, K., Pauszek, S. J., Kelley, W. N. & Rodriguez, L. L. (2007). Molecular epidemiology of vesicular stomatitis New Jersey virus from the 2004-2005 US outbreak indicates a common origin with Mexican strains. *J Gen Virol* **88**, 2042-2051.

Rajani, K. R., Pettit Kneller, E. L., McKenzie, M. O., Horita, D. A., Chou, J. W. & Lyles, D. S. (2012). Complexes of vesicular stomatitis virus matrix protein with host Rae1 and Nup98 involved in inhibition of host transcription. *PLoS Pathog* **8**, e1002929.

Rao, B. L., Basu, A., Wairagkar, N. S., Gore, M. M., Arankalle, V. A., Thakare, J. P., Jadi, R. S., Rao, K. A. & Mishra, A. C. (2004). A large outbreak of acute encephalitis with high fatality rate in children in Andhra Pradesh, India, in 2003, associated with Chandipura virus. *Lancet* **364**, 869-874.

Rasool, N. & Pringle, C. R. (1986). In vitro transcriptase deficiency of temperature-dependent host range mutants of Chandipura virus. *J Gen Virol* **67 (Pt 5)**, 851-862.

Raux, H., Obiang, L., Richard, N., Harper, F., Blondel, D. & Gaudin, Y. (2010). The matrix protein of vesicular stomatitis virus binds dynamin for efficient viral assembly. *J Virol* **84**, 12609-12618.

Renukaradhya, G. J., Khan, M. A., Shaji, D. & Brutkiewicz, R. R. (2008). Vesicular stomatitis virus matrix protein impairs CD1d-mediated antigen presentation through activation of the p38 MAPK pathway. *J Virol* **82**, 12535-12542.

Robison, C. S. & Whitt, M. A. (2000). The membrane-proximal stem region of vesicular stomatitis virus G protein confers efficient virus assembly. *J Virol* **74**, 2239-2246.

Roche, S., Albertini, A. A., Lepault, J., Bressanelli, S. & Gaudin, Y. (2008). Structures of vesicular stomatitis virus glycoprotein: membrane fusion revisited. *Cell Mol Life Sci* **65**, 1716-1728.

Roche, S., Bressanelli, S., Rey, F. A. & Gaudin, Y. (2006). Crystal structure of the low-pH form of the vesicular stomatitis virus glycoprotein G. *Science* **313**, 187-191.

Rodrigues, J. J., Singh, P. B., Dave, D. S., Prasan, R., Ayachit, V., Shaikh, B. H. & Pavri, K. M. (1983). Isolation of Chandipura virus from the blood in acute encephalopathy syndrome. *Indian J Med Res* **77**, 303-307.

Rodriguez, L. L. (2002). Emergence and re-emergence of vesicular stomatitis in the United States. *Virus Res* **85**, 211-219.

Rolls, M. M., Webster, P., Balba, N. H. & Rose, J. K. (1994). Novel infectious particles generated by expression of the vesicular stomatitis virus glycoprotein from a self-replicating RNA. *Cell* **79**, 497-506.

Rose, J. K. & Gallione, C. J. (1981). Nucleotide sequences of the mRNA's encoding the vesicular stomatitis virus G and M proteins determined from cDNA clones containing the complete coding regions. *J Virol* **39**, 519-528.

Ruedas, J. B. & Perrault, J. (2009). Insertion of enhanced green fluorescent protein in a hinge region of vesicular stomatitis virus L polymerase protein creates a temperature-sensitive virus that displays no virion-associated polymerase activity in vitro. *J Virol* **83**, 12241-12252.

Simpson, R. W. & Obijeski, J. F. (1974). Conditional lethal mutants of vesicular stomatitis virus. I. Phenotypic characterization of single and double mutants exhibiting host restriction and temperature sensitivity. *Virology* **57**, 357-368.

Sleat, D. E. & Banerjee, A. K. (1993). Transcriptional activity and mutational analysis of recombinant vesicular stomatitis virus RNA polymerase. *J Virol* **67**, 1334-1339.

Sokhei, C. & Obukhova, V. R. (1984). [Susceptibility of laboratory animals to the Chandipura and Isfahan viruses]. *Vopr Virusol* **29**, 290-294.

Solomon, T., Michael, B. D., Smith, P. E., Sanderson, F., Davies, N. W., Hart, I. J., Holland, M., Easton, A., Buckley, C., Kneen, R. & Beeching, N. J. (2012). Management of suspected viral encephalitis in adults--Association of British Neurologists and British Infection Association National Guidelines. *J Infect* **64**, 347-373.

Solomon, T., Ni, H., Beasley, D. W., Ekkelenkamp, M., Cardosa, M. J. & Barrett, A. D. (2003). Origin and evolution of Japanese encephalitis virus in southeast Asia. *J Virol* **77**, 3091-3098.

Stefanovic, S., Windsor, M., Nagata, K. I., Inagaki, M. & Wileman, T. (2005). Vimentin rearrangement during African swine fever virus infection involves retrograde transport along microtubules and phosphorylation of vimentin by calcium calmodulin kinase II. *J Virol* **79**, 11766-11775.

Szilagyi, J. F. & Pringle, C. R. (1975). Virion trascriptase activity differences in host range mutants of vesicular stomatitis virus. *J Virol* **16**, 927-936.

Szilagyi, J. F., Pringle, C. R. & Macpherson, T. M. (1977). Temperature-dependent host range mutation in vesicular stomatitis virus affecting polypeptide L. *J Virol* **22**, 381-388.

Tandale, B. V., Tikute, S. S., Arankalle, V. A., Sathe, P. S., Joshi, M. V., Ranadive, S. N., Kanojia, P. C., Eshwarachary, D., Kumarswamy, M. & Mishra, A. C. (2008). Chandipura virus: a major cause of acute encephalitis in children in North Telangana, Andhra Pradesh, India. *J Med Virol* **80**, 118-124.

Taylor, A., Easton, A. J. & Marriott, A. C. (1999). Matrix protein of Chandipura virus inhibits transcription from an RNA polymerase II promoter. *Virus Genes* **19**, 223-228.

Tesh, R., Saidi, S., Javadian, E., Loh, P. & Nadim, A. (1977). Isfahan virus, a new vesiculovirus infecting humans, gerbils, and sandflies in Iran. *Am J Trop Med Hyg* **26**, 299-306.

Tesh, R. B. & Modi, G. B. (1983). Growth and transovarial transmission of Chandipura virus (Rhabdoviridae: Vesiculovirus) in phlebotomus papatasi. *Am J Trop Med Hyg* **32**, 621-623.

Thornton, G. B., Kopchick, J. J., Stacey, D. W. & Banerjee, A. K. (1983). Microinjection of vesicular stomatitis virus ribonucleoprotein into animal cells yields infectious virus. *Biochem Biophys Res Commun* **116**, 1160-1167.

Towner, J. S., Pourrut, X., Albarino, C. G., Nkogue, C. N., Bird, B. H., Grard, G., Ksiazek, T. G., Gonzalez, J. P., Nichol, S. T. & Leroy, E. M. (2007). Marburg virus infection detected in a common African bat. *PLoS One* **2**, e764.

Traore-Lamizana, M., Fontenille, D., Diallo, M., Ba, Y., Zeller, H. G., Mondo, M., Adam, F., Thonon, J. & Maiga, A. (2001). Arbovirus surveillance from 1990 to 1995 in the Barkedji area (Ferlo) of Senegal, a possible natural focus of Rift Valley fever virus. *J Med Entomol* **38**, 480-492.

Tsetsarkin, K. A., Vanlandingham, D. L., McGee, C. E. & Higgs, S. (2007). A single mutation in chikungunya virus affects vector specificity and epidemic potential. *PLoS Pathog* **3**, e201.

Tsutsui, Y., Kawasaki, H. & Kosugi, I. (2002). Reactivation of latent cytomegalovirus infection in mouse brain cells detected after transfer to brain slice cultures. *J Virol* **76**, 7247-7254.

van Doremalen, N., Shelton, H., Roberts, K. L., Jones, I. M., Pickles, R. J., Thompson, C. I. & Barclay, W. S. (2011). A single amino acid in the HA of pH1N1 2009 influenza virus affects cell tropism in human airway epithelium, but not transmission in ferrets. *PLoS One* **6**, e25755.

Van Ranst, M. (2004). Chandipura virus: an emerging human pathogen? *Lancet* **364**, 821-822.

Vasilakis, N., Widen, S., Mayer, S. V., Seymour, R., Wood, T. G., Popov, V., Guzman, H., Travassos da Rosa, A. P., Ghedin, E., Holmes, E. C., Walker, P. J. & Tesh, R. B. (2013a). Niakha virus: A novel member of the family Rhabdoviridae isolated from phlebotomine sandflies in Senegal. *Virology*.

Vasilakis, N., Widen, S., Travassos da Rosa, A. P., Wood, T. G., Walker, P. J., Holmes, E. C. & Tesh, R. B. (2013b). Malpais spring virus is a new species in the genus vesiculovirus. *Virol J* **10**, 69.

von Kobbe, C., van Deursen, J. M., Rodrigues, J. P., Sitterlin, D., Bachi, A., Wu, X., Wilm, M., Carmo-Fonseca, M. & Izaurralde, E. (2000). Vesicular stomatitis virus matrix protein inhibits host cell gene expression by targeting the nucleoporin Nup98. *Mol Cell* **6**, 1243-1252.

Walker, P. J., Dietzgen, R. G., Joubert, D. A. & Blasdell, K. R. (2011). Rhabdovirus accessory genes. *Virus Res* **162**, 110-125.

Wang, T., Gong, N., Liu, J., Kadiu, I., Kraft-Terry, S. D., Schlautman, J. D., Ciborowski, P., Volsky, D. J. & Gendelman, H. E. (2008). HIV-1-infected astrocytes and the microglial proteome. *J Neuroimmune Pharmacol* **3**, 173-186.

Weidner, J. M., Jiang, D., Pan, X. B., Chang, J., Block, T. M. & Guo, J. T. (2010). Interferon-induced cell membrane proteins, IFITM3 and tetherin, inhibit vesicular stomatitis virus infection via distinct mechanisms. *J Virol* **84**, 12646-12657.

Whitley, R. J. & Gnann, J. W. (2002). Viral encephalitis: familiar infections and emerging pathogens. *Lancet* **359**, 507-513.

Yao, Y., Ghosh, K., Epand, R. F., Epand, R. M. & Ghosh, H. P. (2003). Membrane fusion activity of vesicular stomatitis virus glycoprotein G is induced by low pH but not by heat or denaturant. *Virology* **310**, 319-332.

Ye, J., Chen, Z., Zhang, B., Miao, H., Zohaib, A., Xu, Q., Chen, H. & Cao, S. (2013). Heat shock protein 70 is associated with replicase complex of Japanese encephalitis virus and positively regulates viral genome replication. *PLoS One* **8**, e75188.

Zaki, A. M., van Boheemen, S., Bestebroer, T. M., Osterhaus, A. D. & Fouchier, R. A. (2012). Isolation of a novel coronavirus from a man with pneumonia in Saudi Arabia. *N Engl J Med* **367**, 1814-1820.

Zhong, Q., An, X., Yang, Y. X., Hu, H. D., Ren, H. & Hu, P. (2013). Keratin 8 is involved in hepatitis B virus replication. *J Med Virol*.

APPENDIX 1

Appendix 1: Primer sequences

Sequences of primers used in this investigation and their corresponding nucleotide positions in the CHPV genome (shown in brackets). Point mutations within mutagenic primers are shown in bold.

* CH112 C5760U R also contains the C_{5691}→U point mutation but this change was not made in the resultant product

Name	Primer sequence (5'-3')	Use
N1F	ATGGTACCACGAAGAAAAACAAACC AATTAAAC (1-25 from nt 9 of primer)	To generate PCR product 1
P8R	ATTGGATCGGAAGCAGGTGA (1901-1882)	To generate PCR product 1
P7F	CTGAGTGCTCTCCAACTTCT (1741-1760)	To generate PCR product 2
G7R	TAACTCAATCTGCAAGTTCGA (3780-3760)	To generate PCR product 2
G2F	GAATTCATGACTTCTTCAGTGACAAT TAG (3052-3075 from nt6 of primer)	To generate PCR product 3
L32R	CGCTGATCTAAGACAATGAAG (5400-5380)	To generate PCR product 3
L16F	GTTGTACTCAAAGCATGGCA (5050-5069)	To generate PCR product 4
L4R	AGTCTGCAGATTGCATRGTCTCATC (7044-7025 from nt6 of primer)	To generate PCR product 4
L10F	GAGTTGAGACAAGCCCTGAACCAAA T (6926-6951)	To generate PCR product 5
L34R	GCAACACTTCTCCTGTGGATC (9000-8980)	To generate PCR product 5
L20F	AGGGAAGGACGTCCATTTAG (8686-8705)	To generate PCR product 6
L27R	ATTGCAAAGTCTCTCACCTC (10038-10019)	To generate PCR product 6
L26F	GCTGGGACCCTACAAGCTC (9411-9429)	To generate PCR product 7
L35R	ATG GGC CCA CGA AGA AAA CAA AAC CAG TTA TA (11119-11096 from nt9 of primer)	To generate PCR product 7
CH112 C5691U F	CAG GAG ACA TAT TGA AT**T** GAC TGT AGA TGA ACT GAG TGC G (5674-5713)	Mutagenic forward primer to generate C_{5691} → U
CH112 C5691U R	CGC ACT CAG TTC ATC TAC AGT C**A**A TTC AAT ATG TCT CCT G (5713-5674)	Mutagenic reverse primer to generate C_{5691} → U
CH112 C5760U F	GTG CGA AGA CTC CAT TGA TCA GAG AAT TAT TCT CAC TGA TTG ATA CTT CTC **T**TA ATG TAG (5709-5768)	Mutagenic forward primer to generate C_{5760} → U
CH112 C5760U R*	TGA GAA TAA TTC TCT GAT CAA TGG AGT CTT CGC ACT CAG TTC ATC	Mutagenic reverse primer to generate C_{5760} → U

	TAC AGT C**A**A TTC AAT (5743-5684)	
CH112 C7217T F	GTG GCA CAT TTT GAT GTA CAC **T**CA TTG AAT GCA ATG ATT C (7196-7235)	Mutagenic forward primer to generate C_{7217} → U
CH112 C7217T R	GAA TCA TTG CAT TCA ATG **A**GT GTA CAT CAA AAT GTG CCA C (7235-7196)	Mutagenic reverse primer to generate C_{7217} → U
CH157 G9735U F	TAC AGG GAT GCA CTG TGT G**T**G GGT GAT GGA TCA GGA GGT A (9755-9716)	Mutagenic forward primer to generate G_{9735} → U
CH157 G9735U R	TAC CTC CTG ATC CAT CAC CC**A** CAC ACA GTG CAT CCC TGT A (9716-9755)	Mutagenic reverse primer to generate G_{9735} → U
CH256 G7694A F	GGA ATC AGA TAG TCA AAG AC**A** CCG TAT ACT ACA TAC ACT C (7674-7713)	Mutagenic forward primer to generate U_{4034} → C
CH256 G7694A R	GAG TGT ATG TAG TAT ACG G**T**G TCT TTG ACT ATC TGA TTC C (7713-7674)	Mutagenic reverse primer to generate U_{4034} → C
CH112 U3941C F	GGGCTCAAGTCTTGACC**C**CAGAGATT CAGAGGATTTTGG (3924-3962)	Mutagenic forward primer to generate U_{3941} → C
CH112 U3941C R	CCAAAATCCTCTGAATCTCTG**G**GGTC AAGACTTGAGCCCC (3962-3924)	Mutagenic reverse primer to generate U_{3941} → C
CH256 U4034 C F	GTCTCCATTGGATCTAAGC**C**ATTTGG CATCTAAATCTCCG (4015-4054)	Mutagenic forward primer to generate U_{4034} → C
CH256 U4034 C R	CGGAGATTTAGATGCCAAAT**G**GCTT AGATCCAATGGAGAC (4054-4015)	Mutagenic reverse primer to generate U_{4034} → C
Sal1 F	AGTTTGGAATTCCAAAA**GTCGACT**T ATCACTTAAGTTTGA	Insertion of a *Sal*1 restriction site in pT7CV at nucleotide 9502
Sal1 R	TCAAACTTAAGTGATA**AGTCGAC**TT TTGGAATTCCAAACT	Insertion of a *Sal*1 restriction site in pT7CV at nucleotide 9502
L F	TAT TAC ATC TCA AAT CCT AGT ATG TAA TGA GGA AAT CAG	Insertion of C-terminus Flag tag to L
LFlag R	ATATCATTA**CTTGTCATCGTCGTCC TTGTAGTC**ATCTACCCAATGCTCAG	Insertion of C-terminus Flag tag to L
LFlag F	GTAGAT**GACTACAAGGACGACGAT GACAAG**TAATGATATGAAAAAAACT AAGGGTG	Insertion of C-terminus Flag tag to L
L R	CATCCGAGTGGACGACGTCCTCCTTC GGATGCCCAGGTC	Insertion of C-terminus Flag tag to L
MGFPF	CCA ATC CTC AAC CCG GTC AAT TTC	Sequence eGFP insert in CVeGFP
GGFPR	CTT GTA ACC CTG GTT CTA GAA ACC	Sequence eGFP insert in CVeGFP

APPENDIX 2

Appendix 2: Plasmid maps

T7CHPV (full length genome clone)

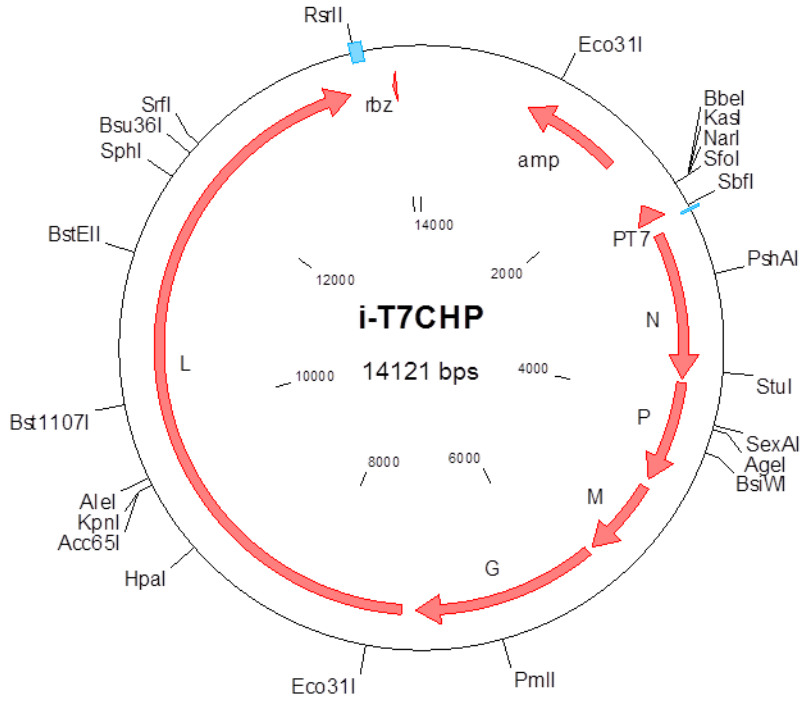

T7CVeGFP

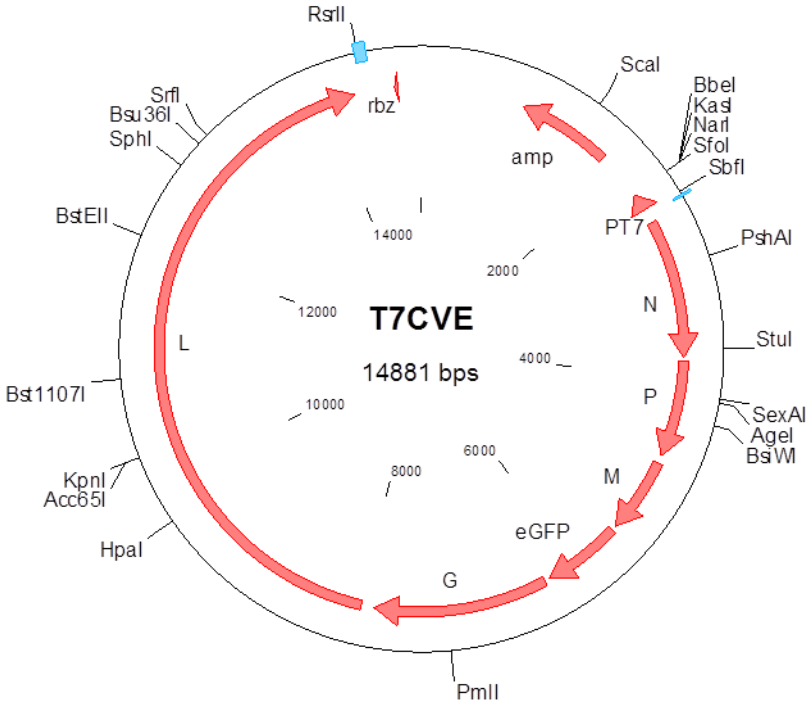

T7CVP/RFP

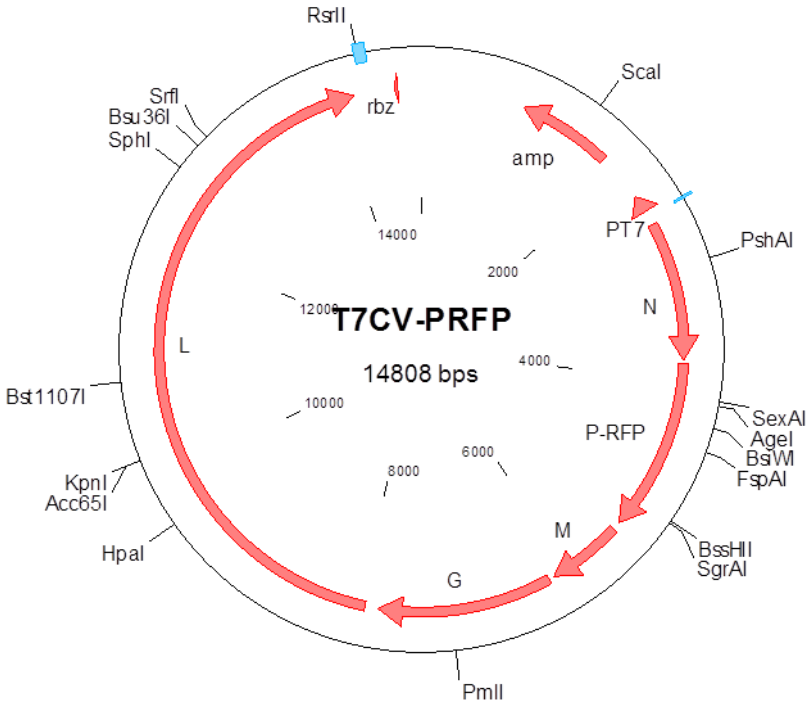

pT7N

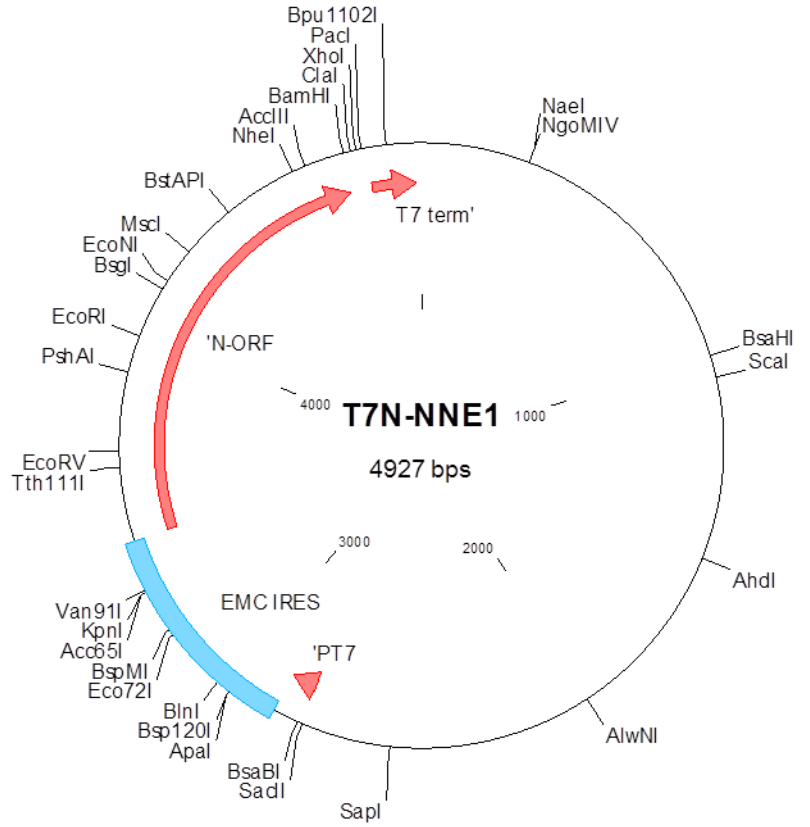

pT7P

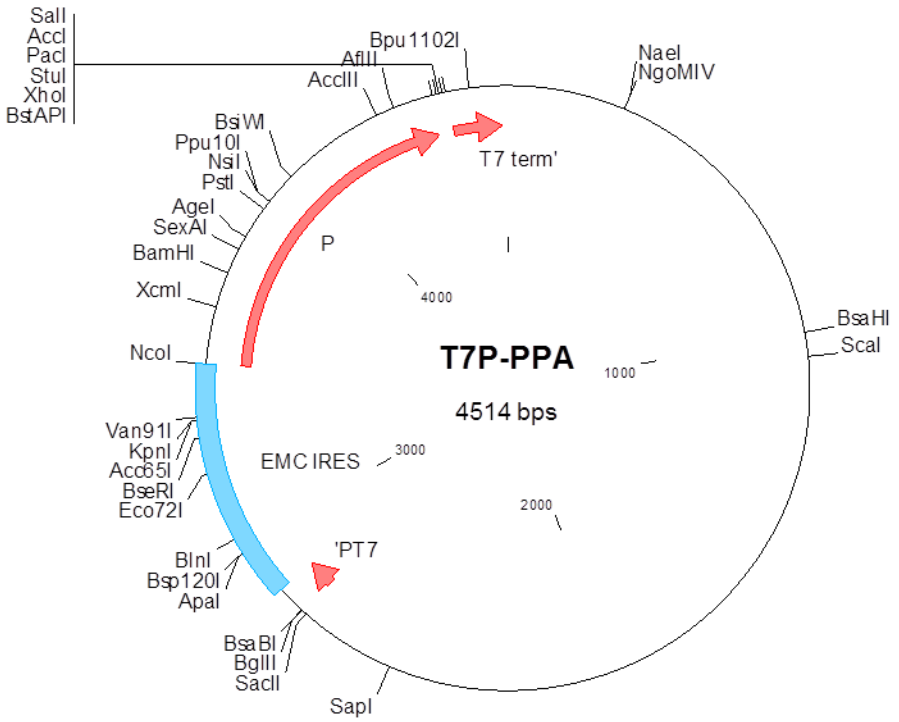
SalI
AccI
PacI
StuI
XhoI
BstAPI
Bpu1102I
AflII
AccIII
NaeI
NgoMIV
BsiWI
Ppu10I
NsiI
PstI
AgeI
SexAI
BamHI
XcmI
NcoI
Van91I
KpnI
Acc65I
BseRI
Eco72I
BlnI
Bsp120I
ApaI
BsaBI
BglII
SacII
SapI
BsaHI
ScaI
T7 term'
P
I
4000
T7P-PPA
1000
4514 bps
EMC IRES
3000
2000
'PT7

pT7L

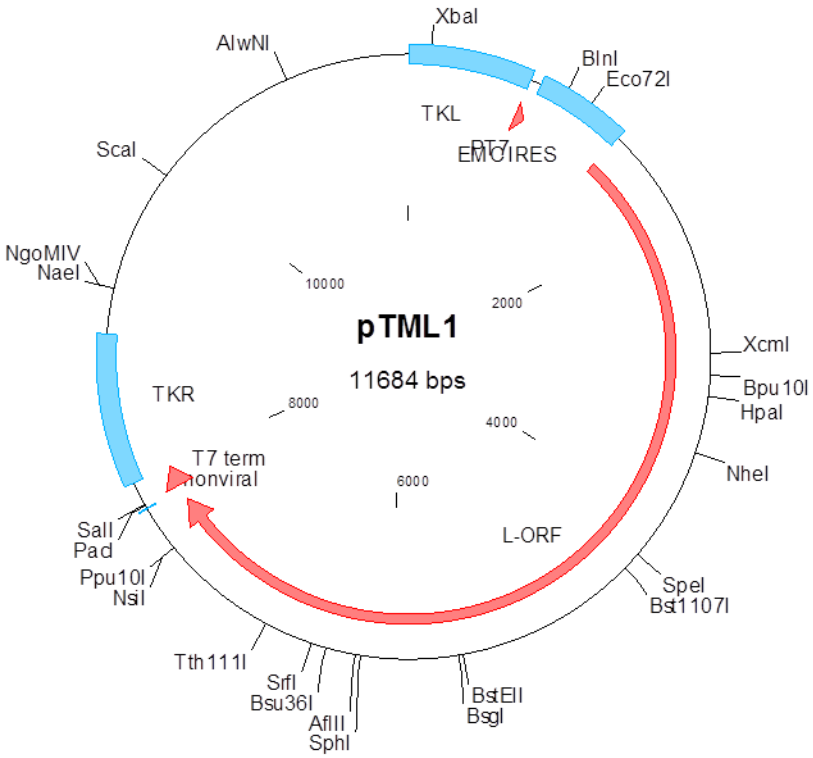
XbaI
AlwNI
BlnI
Eco72I
TKL
PT7
EMC IRES
ScaI
NgoMIV
NaeI
I
10000
2000
pTML1
11684 bps
XcmI
Bpu10I
HpaI
TKR
8000
4000
T7 term
nonviral
6000
NheI
SalI
PacI
L-ORF
Ppu10I
NsiI
SpeI
Bst1107I
Tth111I
SrfI
Bsu36I
AflII
SphI
BstEII
BsgI

Minigenome MGeGFP